Active tectonics of Mongolia : Characterizing active faulting processes in regions undergoing transpression and transtension

Battogtokh Davaasambuu

THÈSE POUR OBTENIR LE GRADE DE DOCTEUR DE L'UNIVERSITÉ DE MONTPELLIER

En Sciences de la Terre

École doctorale GAIA

Unité de recherche Géosciences Montpellier

Active tectonics of Mongolia: Characterizing active faulting processes in regions undergoing transpression and transtension

Présentée par Battogtokh DAVAASAMBUU

Le 2 décembre 2022

Sous la direction de Matthieu FERRY et Jean-François RITZ

Devant le jury composé de

Carole PETIT, Professeur, GéoAzur, Université de Nice	Rapportrice
Jérôme Van der Woerd, Chargé de Recherche, ITES, CNRS	Rapporteur
Laurent BOLLINGER, Directeur de Recherches, LDG, CEA	Examinateur
Stéphane MAZZOTTI, Professeur, Géosciences Montpellier, Université de Montpellier	Président
Matthieu FERRY, Maitre de Conférence, Géosciences Montpellier, Université de Montpellier	Directeur
Jean-François RITZ, Directeur de Recherche, Géosciences Montpellier, CNRS	Co-Directeur

UNIVERSITÉ DE MONTPELLIER

To my wife Naraa, with love.

... Сүмбэр уулыг дов байхад

Сүн далайг шалбааг байхад ...

Эртний Монгол домогт өгүүлснээр

ABSTRACT

The vast territory of Mongolia is under the influence of two different geodynamic environment in terms of active tectonics: the Altai and Gobi-Altai Mountains are under transpressive regimes associated with the Indo-Eurasia collision, whereas the Sayan and Khentii Mountains are influenced by the extension of the Baikal-Khövsgöl rift. Moreover, most of the territory of Central Mongolia is in a transtensional regime possibly related to the movement of the North China block (locally Amur micro-block) to the east.

My research was performed in areas located in different regions of tectonics and geographical boundaries as well as weather and topography/relief: the Khovd fault in the Altai Mountains, the Khövsgöl fault in the Sayan Mountains, and the Möngönmorit fault in the Khentii Mountains, that are hundreds of kilometers apart.

In this study, the following methods for studies of active faults were used. These include fault mapping based on satellite images and field routes, paleoseismological investigation to determine the ages and recurrence period of large earthquakes along the faults.

The Ar-Khötöl surface rupture is the central part of the main Khovd fault that is the longest strike-slip fault of the 5 major faults in the Altai Mountain Range. In this sense, it can be reckoned that the Ar-Khötöl surface rupture is the most prominent representation of the modern kinematics in the Altai Mountains.

I mapped the Ar-Khötöl surface rupture using satellite data such as Sentinel-2, TanDEM, Google Earth, and Pleiades with the resolutions of 0.5 – 15 m. The rupture itself exhibits a length of 238.5 ± 0.5 km and displays well defined changes in strike, faulting style and complexity generally associated with relay zones that may play a role in the propagation of the rupture. Considering general scaling relationships established by Wells & Coppersmith (1994) for strike-slip faults (with a = 5.16 ± 0.13 and b = 1.12 ± 0.08), we may derive a moment magnitude of 7.8 ± 0.3.

The paleoseismological study conducted in the Marmot Creek trench identified the large earthquake on the Ar-Khötöl fault between 1280 and 1640 CE.

The magnitude 6.7 Khankh earthquake of January 12, 2021 demonstrated a paramount representation on understanding the modern kinematic processes of the Khövsgöl rift. The location, azimuth, dip and depth of this earthquake defined by moment tensor solutions calculated by the international seismological centers and analysis of InSAR interferograms and field observations. The projected intersections of the east-dipping nodal planes with the surface for GCMT, JAJ and IPGP focal mechanism solutions correlate relatively well with the mapped strike and location of the old tectonic scarp of the Khövsgöl fault although we have not discovered any primary co-seismic surface rupture. Apparently, Khövsgöl fault is a transtensional fault with combined right-lateral strike-slip and normal components. The moderate earthquake of magnitude 6.7 can produce a surface rupture up to ~25 km long, but the considerable surface rupture is not detected on the ground surface, indicating that on the one hand, the main surface rupture is likely to be under Lake, and on the other hand, the deformation displayed in the InSAR interferogram may have spread over a large area without producing a surface rupture.

The Möngönmorit active fault is located at southern edge of the Khentii Dôme, in north-eastern Mongolia, 100 km eastward the capital city of Ulaanbaatar. From the point of view of paleoseismology, our investigations allow characterizing the occurrence of two surface-rupturing events since 8.4 ka. If we extend the time window of our observations, it seems that at least one stronger event occurred not long after 18 ka. The paleoseismological data concerning the last two events suggest a mean recurrence period of surface rupturing earthquakes occurring between 3000 and 5000 years. The latest earthquake along the fault having occurred 5 ka ago, yields an elapsed time equal to the maximum bound of the recurrence interval. Although this statement is based only on the 2 past events, and despite the fact that a possible earlier event at ~18ka increases the recurrence time (~10 ka), the question of the seismic hazard associated to the Möngönmorit fault is clearly posed.

RESUME

La Mongolie est le siège de séismes de très forte magnitude mais qui se produisent rarement. Avec un influencé par la lointaine collision Inde-Eurasie et la proche extension du Baïkal, les régimes tectoniques rencontrés sont variés et semblent changer rapidement dans l'espace. Dans cette thèse, j'explore quatre exemples-clés situés dans le quart nord-ouest du pays afin de mettre en évidence les différences de cinématique, de magnitude, de récurrence induits par la complexe distribution de contraintes et les structures pré-existantes.

LA RUPTURE DE SURFACE AR-HÖTÖL LE LONG DE LA FAILLE DE KHOVD (ALTAÏ MONGOL)

Nous présentons une carte à l'échelle 1/200 000 de la rupture de surface Ar-Hötöl le long de la faille de Khovd dans l'Altaï mongol. Cette carte couvre une superficie d'environ 900 km² avec des altitudes allant d'environ 1120 m (lac Khar Us Nuur) à 4204 m (mont Mönkh Khaikhan) et englobe les principales failles de la chaîne de l'Altay. Ce travail documente les preuves et le style de déformation active le long de la section centrale de la faille de Khovd orientée N140° (entre les latitudes 46°30' et 48°25'), avec un accent particulier sur la plus récente rupture de surface. Cela a des implications pour la tectonique (par exemple, l'influence de l'héritage structural sur la localisation de la sismicité actuelle), la géodynamique régionale (par exemple, le régime et la distribution de la déformation) et le risque sismique pour la ville en développement de Khovd.

La géologie fondamentale de l'Altay est composée de trois terrains de base qui correspondent à un prisme d'accrétion, des bassins d'arrière-arc et d'avant-arc et un arc insulaire qui ont fusionné au cours du Paléozoïque (Berkey et Morris, 1927 ; Cunningham et al., 1996 ; Cunningham, 1998 ; Badarch et al., 2002) et sont délimités par des zones de cisaillement majeures. Il y a peu de preuves de déformation régionale au cours du Mésozoïque, qui est considéré comme tectoniquement calme comme le suggère le développement d'une surface d'érosion régionale au sommet des grès argileux rouges de l'Oligocène (Devyatkin, 1974, 1975 ; Devyatkin et al., 1990; Kozhevnikov et al., 1970 ; Tikhonov, 1974 ; Baljinnyam et al., 1993). L'apparition de sédiments plus grossiers du Néogène (molasse conglomératique) le long des marges de l'aire de répartition et dans les bassins intramontagneux indique une nouvelle érosion régionale induite par le soulèvement qui a probablement commencé à la fin de l'Oligocène ou au début du Miocène (Devyatkin, 1974; 1975). Cet épisode de déformation se poursuit aujourd'hui comme l'attestent les enregistrements sédimentaires Oligocène-Holocène exposés dans les bassins

orientaux (Howard, 2004) et les dépôts du Pliocène précoce dans le bassin d'Ikh Nuuryn Khotgor (Devyatkin, 1975 ; Devyatkin et al., 1980 ; Baljinnyam et al., 1993). Cette réactivation cénozoïque tardive de la chaîne de l'Altay a été interprétée comme un effet lointain de la collision Inde-Eurasie (Molnar et Tapponnier, 1975 ; Tapponnier et Molnar, 1979).

Actuellement, la chaîne de l'Altay est un système transpressif majeur qui absorbe ~ 4 mm/an de déplacement latéral dextre avec un soulèvement mineur le long d'un système de failles orientées ~ N140 réparties sur une largeur de 150 à 300 km (Calais et al., 2003). D'ouest en est, la faille de Fu-Yun, de Tolbo Nuur, d' Ölgiy, de Khovd et de Khar Uus Nuur constituent les principales structures et sources potentielles de séismes destructeurs (e.g. Khilko et al., 1985; Baljinnyam et al., 1993 ; Walker et al., 2006 ; Frankel et al., 2010 ; Gregory et al., 2014).

Les documents historiques de l'Altay sont rares, incomplets et rarement accessibles. L'événement documenté le plus ancien est le grand tremblement de terre mongol de 1761 CE qui a fortement affecté les avant-postes militaires russes et les cantons dans les régions qui appartiennent maintenant au sud de la Sibérie et au Kazakhstan (Mushketov et Orlov, 1893). Des descriptions détaillées relatives à l'intensité et à la durée des secousses ont été analysées par Zhalkovsky et Muchnaya (1975) qui ont conclu qu'un tremblement de terre majeur s'est produit le 9 décembre 1761 dans la région de l'Altaï sensu largo. Khilko et al. (1985) ont complété cette analyse avec des contes folkloriques non publiés recueillis auprès d'anciens nomades et ont conclu que l'épicentre était situé le long de la faille de Khovd et que la magnitude associée atteignait probablement Mw 8.

Les premières observations de terrain le long de la faille (Trifonov, 1983 et Khilko et al., 1985) ont révélé de nombreuses ruptures de surface déplaçant des ruisseaux et des sépultures anciennes avec des quantités variables. Quelques mesures au mètre-ruban (~ 5) ont donné un décalage latéral dextre maximum de 4,5 m affectant une tombe au col d'Ar-Hötöl (Khilko et al., 1985). Baljinnyam et al. (1993) se sont appuyés sur cet effort et quelques points de données, parmi lesquels une mesure de « 7 m » au nord de Buyant Gol, près de la terminaison nord de la rupture. Dans l'ensemble, on sait peu de choses sur l'activité quaternaire tardive de la faille de Khovd, en particulier par rapport à des structures de taille similaire présentant des ruptures de surface historiques dans la région. Par conséquent, la caractérisation de la faille de Khovd nécessite un nouvel effort avec un ensemble de données dense et fiable qui permettra de mieux évaluer son comportement de rupture et son étendue ainsi que son ampleur potentielle. Dans ce qui suit, nous présentons une cartographie détaillée systématique et une quantification de la

déformation récente le long de l'Ar-Hötöl rupture de surface à l'aide d'approches robustes à haute résolution.

Nos observations de télédétection et de terrain donnent une longueur totale de rupture de surface (SRL) de 238,5 ± 0,5 km pour l'expression de surface la plus récente de la faille de Khovd. En considérant les relations d'échelle générales établies par Wells & Coppersmith (1994) pour les failles décrochantes (avec a = 5,16 ± 0,13 et b = 1,12 ± 0,08), nous pouvons dériver une magnitude de moment de 7,8 ± 0,3. Le dernier déplacement cosismique maximal (MD) identifié au centre de la distribution de glissement atteint 4,8 ± 0,5 m. La relation d'échelle associée (avec a = 6,81 ± 0,05 et b = 0,78 ± 0,06) donne une magnitude de moment de 7,3 ± 0,1. Des travaux antérieurs mentionnent une valeur plus élevée du déplacement maximal atteignant 7 m (Baljinnyam et al., 1993) sur la rive nord de la rivière Buyant. Ceci est documenté à environ 20 km de l'extrémité la plus au nord de la rupture de surface (Fig. 13 dans Baljinnyam et al., 1993) à un endroit où nous n'avons trouvé que quelques marqueurs qui enregistraient un glissement cosismique beaucoup plus faible (~ 2 m). Les auteurs mentionnent également une certaine incertitude dans l'interprétation de l'offset. Étant donné que nos résultats sont plus cohérents avec l'enveloppe de glissement locale (Fig. 4) et avec les faibles valeurs généralement associées aux pointes de rupture, nous considérons que la valeur d'origine est probablement cumulative et l'écartons de notre analyse.

Dans l'ensemble, nos observations sur le terrain documentent des éléments relativement "nouveaux" avec des escarpements marqués et des dépôts post-sismiques apparemment récents, ce qui pourrait indiquer un événement récent tel que le tremblement de terre de 1761 CE (Mushketov et Orlov, 1893). Cependant, à la lumière des très faibles taux d'érosion et de dépôt à l'œuvre en Mongolie, cela pourrait être une inférence très trompeuse (voir Walker et al., 2017 pour un exemple frappant sur la faille d'Egiin Davaa). Une étude paléosismologique complète de la rupture apporterait une contrainte bien nécessaire sur l'activité récente de la faille de Khovd.

L'écart apparent entre les grandeurs de moment dérivées de SRL et MD est en fait une observation générale documentée par Wells & Coppersmith (1994, Figure 12) qui rapportent MD allant de ~ 3 m à ~ 10 m pour un SRL donné de 240 km. Étant donné que le SRL reflète l'ensemble de la rupture alors que la MD peut être influencée par les conditions locales, nous nous appuyons sur l'estimation associée de Mw 7,8 ± 0,3 pour caractériser le séisme de rupture de surface le plus récent sur la section centrale de la faille de Khovd.

Dans l'ensemble, nous combinons la télédétection et les données de terrain à différentes échelles pour produire une carte détaillée de la rupture Ar-Hötöl longue de 238 km le long de la faille Khovd dans l'Altaï mongol. Les images orthorectifiées haute résolution et les DEM ont conduit à la quantification robuste du glissement co-sismique et cumulatif et à l'identification de six segments principaux organisés autour de changements majeurs dans la direction, la cinématique et la lithologie. Nous avons collecté plus de 100 valeurs de décalage, dont 67 co-sismiques pour confirmer l'estimation de magnitude originale de Mw ~ 7,8. Ces travaux serviront de données de base pour réaliser des études paléosismiques le long de la faille et contribueront à la caractériser pour la géodynamique et l'aléa sismique.

LE SEISME DE 2021 A KHANKH (M_W 6.7) DANS LE RIFT DE KHUVSGUL

Dans ce travail, nous présentons les mécanismes au foyer du tremblement de terre de Khankh Mw 6,7 et discutons de ses relations avec la faille sous-jacente de Khuvsgul, à travers l'analyse d'images satellites, de données InSAR et de caractéristiques de rupture de surface co-sismiques révélées par des études de terrain.

Les bassins de Khuvsgul (aussi écrit Hövsgöl), Darkhad et Busiin Gol sont considérés comme la terminaison sud-ouest du système de rift du Baïkal. Le rift du Baïkal est défini par un alignement de bassins allongés orientés nord-est s'étendant de la Mongolie à la Russie sur près de 1800 km. La zone de rift se compose de nombreux bassins, dont Busiin Gol, Darkhad, Khuvsgul, Tunka, Baïkal, Angara, Muya et Khara, du prolongement le plus au sud-ouest de la Mongolie jusqu'à la pointe la plus au nord-est de la Russie. Plusieurs hypothèses et modèles sur l'origine et l'évolution du rifting ont été proposés (comme Florensov, 1969 ; Molnar et Tapponnier, 1975 ; Zonenshain et Savostin, 1981 ; Logatchev et al., 1993 ; Ivanov, 2004 ; Petit et Deverchère, 2006). Molnar et Tapponnier (1975) ont interprété que la zone de rift du Baïkal est une manifestation de la collision Inde-Eurasie. Logatchev (1993) et Logatchev et al. (1983) ont fait valoir que l'initiation et le développement du rift sont une structure indépendante associée aux processus thermiques locaux dans le manteau sans aucune relation directe avec la collision des plaques indo-eurasiennes. Des études récentes de Petit et Deverchère (2006) ont pu confirmer les découvertes antérieures de Tapponnier et Molnar.

Plusieurs enquêtes (Calais et al., 2003 ; San'kov et al., 2000 ; Ritz et al., 2018) ont été menées pour estimer les taux et les quantités d'ouverture du rift du Baïkal à partir des mesures GPS et des taux de glissement le long du failles délimitant le bassin à partir d'observations géologiques. Les mesures GPS suggèrent une extension crustale d'environ 4 mm/an sur la partie principale

du rift du Baïkal (Calais et al., 2003). Le bassin central du Baïkal est délimité par la plate-forme sibérienne à l'ouest. Zonenshain et Savostin (1981) et plus récemment Barth et Wenzel (2010) ont montré que le système de rift du Baïkal est une limite de la plaque Amour. Les bassins de Khuvsgul, Darkhad et Busiin Gol sur le territoire mongol qui définissent la limite sud-ouest du système de rift ont des azimuts orientés N-S, tandis que le centre du Baïkal et d'autres bassins sur le territoire russe ont des directions principalement orientées SW-NE.

Le fort tremblement de terre a frappé après que la surface du lac Khuvsgul ait été complètement gelée. Chaque année, le lac est recouvert de glace de la mi-décembre à la mi-juin. L'épaisseur moyenne de la glace est de 40 à 70 cm. Le séisme de magnitude 6,7 n'a provoqué ni rupture majeure de la surface, ni rupture de la glace.

Aucune onde de seiche suffisante pour briser la glace dans l'eau du lac n'a été observée, ce qui est peut-être le résultat de (i) des ondes à haute fréquence (des ondes à plus longue période traversant le sol créent des seiches) ont été générées parce que l'épicentre sismique était trop proche sous le fond du lac et (ii) la couverture de glace du lac a pu bloquer une première oscillation pour produire des seiches malgré le fait que la couverture de glace est mince par rapport à l'épaisseur d'eau et en plus (iii) la cinématique en faille normale du tremblement de terre de Khankh de 2021 est probablement moins favorable générer des tsunamis et des seiches par rapport aux événements en compression (Seattle, 2014).

Le tremblement de terre a néanmoins produit de fortes secousses ressenties à une distance d'environ 600 km au 8ème étage d'un immeuble d'appartements de la ville d'Oulan-Bator (domicile de Battogtokh) avec le sentiment d'être poussé par le bas. Selon un entretien avec les éleveurs locaux Ulziibat, Ukhnaa et Sodkhuu qui vivent dans la zone épicentre du Doloon Uul (Fig. 2), ils ont tous dit qu'il y avait un bruit monstrueux pendant le tremblement de terre et c'était comme s'ils étaient jetés avec leurs maisons. Cela dit, les dégâts réels ont été relativement modestes, peut-être parce que les maisons sont généralement construites en rondins de bois plutôt qu'en pierre ou en béton. Selon l'éleveur Ulziibat, la vague du premier fort tremblement de terre semblait être dirigée du sud vers le nord, et la seconde semblait être dirigée le long de la latitude. L'emplacement de sa maison est orienté NNO-SSE. De plus, une jeep russe (UAZ-469) qui était garée devant sa maison a été projetée dans ~30 cm et est revenue à sa place. Le berger nous a montré les motifs des roues sur neige fraîche. Il y eut une forte secousse autour de la maison d'un berger Rinchen. Son étable à bétail s'est effondrée et 1 à 2 bûches de sa maison en rondins ont été arrachées d'environ 5 cm comme les maisons des autres familles d'éleveurs.

Près de sa maison et de sa grange, il y avait des fissures chaotiques avec de l'eau sablonneuse. Nous avons découvert une petite faille normale avec composante décrochante latérale gauche.

Nous avons commandé une imagerie satellite KOMPSAT-3 avec une résolution au sol de 0,7 m via le Laboratoire de tectonique active de l'Institut coréen des géosciences et des ressources minérales (KIGAM) et avons effectué une reconnaissance dessus, mais nous n'avons découvert aucune rupture de surface majeure qui pourrait être associé à l'événement co-sismique. Nos collègues américains, français, turcs et coréens ont obtenu des interférogrammes InSAR en utilisant les données Sentinel-1 pour caractériser la déformation co-sismique de ce séisme. Les données InSAR n'étaient pas disponibles jusqu'à ce que nous ayons presque terminé le travail de terrain dans la zone de l'épicentre. L'interférogramme InSAR (Fig. 8), révèle des franges le long du côté ouest du lac impliquant une déformation à la surface où dans la zone basse de Khodon et Mungarag entre la péninsule de Doloon Uul et la chaîne occidentale ainsi que dans la place Artsatiin Khash dans l'Ouest. Intervalle. Bien que nous ayons déjà effectué une reco nnaissance de terrain et traversé la zone à fort impact entre le Doloon Uul et la Western Range sur la base de l'enregistrement de nos traces GPS (Fig. 2 et Fig. 8), nous n'avons pas vu de ruptures de surface à l'exception d'un rupture d'une longueur d'environ 45 m et des micro-fissures que nous avons mentionnées ci-dessus. Nous n'avons pas réussi à visiter le site où InSAR indique très probablement une rupture de surface primaire en raison des conditions météorologiques hivernales. Mais nous avons vérifié provisoirement que les franges nettes dans les montagnes de l'Ouest pourraient également être des effets locaux. Nous avons demandé à un berger qui vit à cet endroit de vérifier s'il y avait des fissures de surface visibles autour de cette zone. Il a informé qu'il y avait des fissures interrompues d'une largeur d'environ 10 cm dans la zone appelée Artsatiin Khash (Fig. 2 et 6). Il est prévu de vérifier la zone et d'effectuer d'autres investigations géologiques au cours de l'été prochain.

Cependant, il y a des effets nets et des franges dans l'InSAR (Fig. 8) le long des rives ouest du lac. Les franges disparaissent dès qu'il émerge de la rive du lac. Le modèle de frange InSAR implique qu'une grande partie de la rupture pourrait se trouver sous le lac. Des escarpements tectoniques préexistants continus et des déplacements cumulatifs latéraux droits sont visibles autour de la vallée de la rivière Khongor Buush (autour de 51˚35′05″ N, 100˚09′11″ E) au sud-ouest de la montagne Emeel (Fig. 2) sur Landsat 8, Google Earth et Bing Map. Aucune rupture de surface fraîche n'a été découverte le long de ce segment sur l'imagerie KOMPSAT en temps réel acquise après le tremblement de terre. Cependant, les mécanismes focaux de l'IAG, de

l'USGS, du GCMT, de l'IPGP et du JAJ sont déterminés comme un décrochement dextre avec une composante normale à tendance NNW qui décrit bien les structures anciennes.

Un tremblement de terre de Mw 6,7 a de fortes chances de produire une rupture de surface avec un décalage co-sismique d'environ 0,5 m et une longueur d'environ 25 km d'apres les relations empiriques de la magnitude de Wells et Coppersmith (1994). En revanche, il y a peu de chance qu'il y ait autant de rupture en surface d'après notre visite sur le terrain, les traversées des éleveurs locaux et même lors de la reconnaissance sur les images satellites KOMPSAT-3 en temps réel. En parallèle, l'escarpement de faille associé au tremblement de terre pourrait avoir été produit sur le fond du lac Khuvsgul le long de la côte ouest. Dans ce cas, nous supposons que la pointe la plus au nord de la rupture est la grande fissure à 51˚19′37″ N, 100˚15′55″ E où nous voyons l'escarpement de faille normale le plus proéminent au bord du lac malgré le fait qu'il se termine à une distance de à seulement ~45 m du rivage. Le compartiment ouest de l'escarpement de la faille s'est déplacé de 25 à 30 cm par rapport au compartiment Est. De plus, la localisation et la cinématique de cette fracture de petite longueur sont relativement compatibles avec les solutions de plan de faille qui ont été calculées par JAJ, GFZ et IPGP. Bien qu'il existe une quantité considérable de petites fissures allongées avec des azimuts chaotiques et une largeur de 1 à 5 cm dans le delta de Khodon entre la péninsule de Doloon Uul et la chaîne occidentale, ces fissures sont clairement des effets de site associés au fort tremblement de terre. Par conséquent, toutes sortes de caractéristiques de la cinématique telles que les micro-chevauchements, les failles micro-failles normales avec composante latérale gauche et les micro-fissures de tension en échelon dextre reflètent les failles de décrochement sénestres découvertes dans cette zone.

LA FAILLE D'OULAN BATOR

La capitale de la Mongolie, Oulan-Bator (ci-après abrégé UB), est située dans la vallée de la rivière Tuul, dans la région montagneuse du Khentii, qui est relativement élevée au-dessus du niveau de la mer. En termes d'activité sismique, le territoire de la Mongolie se situe dans les conditions géodynamiques de la collision indo-eurasienne et de l'extension du rift Baïkal (Molnar et Tapponnier, 1975 ; Zonenshain et Savostin, 1981). Calais et Amarjargal (2000) ont conclu de la mesure GPS continue que la croûte où se trouve Oulan-Bator se déplace relativement vers le sud-est avec un taux de 6,4 ± 1,6 mm/an par rapport à l'Eurasie.

Dans la région, plusieurs failles actives ont été reconnues et cartographiées telles que les failles de Mungunmorit, Deren, Agit, Khustai, Sharkhai, Avdar, Emeelt, Gunj et Oulan Bator ainsi

que des failles régionales telles que Terelj, Khui, Khurkhree, Chuluut-Turkhurkh, Deendei, Yuden, Barkh et Nalaikh dans les environs d'Oulan-Bator et des villes voisines. Les failles régionales se trouvent généralement le long des limites des formations géologiques orientées NE-SO. Les failles actives coexistent avec les failles régionales mésozoïques et sont contrôlées par leur structure générale.

Des recherches ont noté que les roches paléozoïques d'Oulan-Bator et de sa banlieue sont originaires de la fermeture de la mer Mongol-Okhotsk et ont formé des plis anticlinaux et synclinaux avec des axes de pli nord-est sous l'influence des forces dirigées vers le nord-ouest. Des failles systématiques orientées nord-est contrôlent les grands massifs mésozoïques. La faille Deendei est un décrochement dextre orienté nord-est et a une influence sur la formation du massif granitique de Bogd-Uul. Les failles orientées nord-est et nord-ouest sont généralement associées à des structures profondes, tandis que les failles nord-sud et est-ouest sont considérées comme superficielles et n'affectent que la partie supérieure de la croûte (Unudelger et Banzragch, 1993).

Suite à nos travaux de terrain, nous avons conclu que la faille d'Oulan Bator présente les caractéristiques suivantes :

- L'apparition de la gouge implique au moins une première étape de déformation compressive intense et localisée. Le fait que la gouge soit plissée et translatée sur des dépôts plus jeunes implique une deuxième étape de déformation (également en compression).
- Le fait que la séquence sédimentaire (par exemple, ensemble d'unités argileuses, riches en oxyde de fer, contenant des colluvions granitiques du mont Bogd Khan) montre une augmentation de la quantité de clastes, et une augmentation de leur taille vers le SW, ainsi comme une sédimentation en forme d'éventail loin de la zone de gouge (U200 et U210), suggère fortement qu'un épisode de sédimentation syn-tectonique s'est produit entre les 2 stades de compression mentionnés ci-dessus.

Par conséquent, l'interprétation est qu'au moins 2 épisodes principaux de déformation se sont produits :

- Compression post-grés-alevrolite (Paléozoïque) mettant en contact le grès-alevrolite avec le granite de la montagne Bogd Khan le long de la zone de faille antérieure UB (Takeuchi et al., 2012). La gouge de faille observée dans la tranchée est soit héritée de

cet épisode, soit d'un épisode plus ancien (La gouge de faille correspond à un élément tectonique secondaire au sein d'une zone de faille UB plus large).

- Extension cénozoïque ou cénozoïque tardive avec réactivation des anciens contacts de la zone de faille UB sous la forme d'une faille normale à pendage NE conduisant à la formation d'une gouttière détritique syn-tectonique le long de la faille UB (la principale faille qui contrôle cette sédimentation syn-tectonique n'est pas observé dans la tranchée).

Une question importante est de savoir si des mouvements récents (Quaternaire) se sont produits le long de la faille UB, et/ou si la faille pourrait être réactivée à nouveau. En d'autres termes, la zone de faille UB est-elle potentiellement active?

Cependant, aucune observation historique de la région d'Oulan-Bator n'est disponible pour étayer ou réfuter cette hypothèse. Il n'y a pas de séismes historiques connus le long de la faille UB.

La faille UB suit la zone de faille ancienne. En d'autres termes, il se situe aux limites des différentes formations géologiques (Takeuchi et al., 2012).

Suzuki et al (2021) ont cartographié la faille UB entre le sud-est de la montagne Bogd Khan et le nord-ouest du mont Tolgoit sur environ 56 km. La section autour des montagnes Bayankhoshuu et Tolgoit ainsi que la section à l'est et au nord-est de la montagne Bogd Khan, ont des escarpements linéaires qui sont clairement visibles du fait de l'aménagement de la zone urbaine de UB. Cependant, les escarpements de faille dans la partie centrale de la ville ne sont pas visibles. Ainsi, ils ont provisoirement relié les segments de la montagne Bogd Khan et du mont Tolgoit et marqués par les lignes pointillées.

La plupart des escarpements de faille sont cartographiés le long des anciennes limites géologiques entre les différentes formations rocheuses, ainsi les taux d'érosion différentiels peuvent avoir influencé les expositions des escarpements de faille cartographiés.

D'après les forages, les substratums rocheux des blocs nord et sud du plan de faille dans la tranchée de Khurel Togoot sont deux types de roches différents avec des compositions et des origines différentes. Par conséquent, il est clair que le plan de faille est la limite entre deux types de roches différents.

Dans les parois de la tranchée, l'unité de gouges noires épaisses (U200 et U210) avec la structure plissée anticlinale recouvrant l'unité grés-alevrolite décomposée et déformée (U300) est observée chevauchant les séquences sédimentaires (U10 à U190) vers le sud-ouest. En

regardant l'épaississement des couches sédimentaires devant la gouge de faille noire vers le flanc de la montagne Bogd Khan, les couches sédimentaires sont susceptibles d'être tournées entre les deux failles (faille non détectée dans les parois de la tranchée non loin au sud de la tranchée).

Toutes les couches sédimentaires multicolores sont déformées et certaines d'entre elles ont été déplacées par les failles. Donc logiquement, cela signifie que la dernière activité tectonique s'y est déroulée depuis le dépôt des couches les plus jeunes. Nous avons documenté le fait que les couches U30 et U40 ont été déplacées par les derniers événements. Selon les études paléosismologiques de la tranchée de Khurel Togoot, le dernier fort tremblement de terre dans la faille UB pourrait s'être produit au Pléistocène supérieur, il y a environ ~ 15 800 ans, tandis que le plus ancien a été daté a ~ 40 500 ans.

Compte tenu de la longueur de la faille d'environ 50 km, un tremblement de terre de magnitude 7 est susceptible de se produire sur la faille d'Oulan-Bator. Cependant, les autres excavations le long de la faille d'Oulan-Bator ne fournissent pas de preuves d'activité sismique Holocène ou Pléistocène supérieur. Par conséquent, la faille d'Oulan-Bator doit faire l'objet d'une enquête plus approfondie.

CINEMATIQUE ET PALEOSISMICITE DE LA FAILLE DE MUNGUNMORIT (DOME DE HENTII)

La tectonique actuelle en Mongolie est contrôlée par deux processus géodynamiques : la collision SSW-NNE Inde-Eurasie et l'extension WNW-ESE du système de rift du Baïkal (e.g. Larroque et al., 2001 ; Calais et al., 2003 ; Ritz, 2003 ; Arjannikova et al., 2004 ; Vassallo, 2006 ; Lukhnev et al., 2010 ; Ritz et al., 2018). En raison de la collision SSW-NNE, des déformations transpressives sont observées dans l'ouest de la Mongolie dans les chaînes de montagnes de l'Altay et du Gobi-Altay, qui sont respectivement caractérisées par des failles décrochantes dextres et sénestres à grande échelle, toutes deux associées à des failles inverses secondaires. En raison de l'extension WNW-ESE du système de rift du Baïkal, des déformations transtensives sont observées dans les régions de Darkhad et du lac Khuvsgul, toutes deux caractérisées par des failles normales obliques le long des systèmes de failles ~NS associées à des mouvements latéraux droits. Ces déformations transtensives sont également observées plus au sud-est dans les parties centrales ouest-centrale et sud-est du dôme de Khangai et de Khentii, respectivement, où des failles normales ou des failles décrochantes combinées à des failles normales sont observées le long des structures NE-SW. (par exemple, Walker et al., 2007 ; 2008 ; Al Ashkar, 2015, Al Ashkar et al., 2022 ; Walker et al., 2015).

Ces deux régimes de déformation sont cohérents avec les mesures GPS, qui montrent que l'ouest de la Mongolie est soumis à une compression nord-nord-est à un taux de 5 mm/an, qui est accommodée par de grandes failles décrochantes latérales droites NW-SE associées à les failles inverses secondaires et la rotation dans le sens inverse des aiguilles d'une montre des blocs crustaux entre ces failles, tandis que le sud, le centre et l'est de la Mongolie se déplacent vers l'est-sud-est avec un taux moyen d'environ 4 mm/an par rapport au rift du Baïkal (par exemple, Calais & Amarjargal, 2000 ; Calais et al., 2003). Par rapport à l'ouest de la Mongolie, l'est de la Mongolie correspond à une région à faible activité sismique. Ce n'est que récemment que des failles actives telles que les failles de Mungunmorit, Avdar, Sharkhai ou Khustai ont été décrites à partir d'études morphologiques et paléosismologiques (par exemple, Imaev et al., 2012 ; Smekalin et al., 2016 ; Al Ashkar, 2022) . Actuellement, la faille de Mungunmorit est considérée comme la faille active la plus orientale de Mongolie. Au-delà de la faille, vers l'est, les reliefs diminuent rejoignant la Grande Steppe et le Plateau de Dornod.

La faille de Mungunmorit est située dans la région sud-ouest de Khentii, dans le centre-nord de la Mongolie, et est considérée comme une faille active capable de produire des ruptures de surface. Située à 100 km à l'est d'Oulan Bator, elle représente donc un aléa sismique potentiel pour la capitale mongole avec 6 autres failles situées à proximité (i.e. situées dans un rayon de 100 km autour de la ville ; Figure 1). La faille de Mungunmorit est la plus éloignée de UB (100 km) parmi les failles d'Avdar (42 km), de Sharkhai (42 km), de Khustai (35 km), d'Emeelt (23 km), de Gunj (12 km) et d'Oulan Bator (1,6 km), mais c'est la plus longue (80 km). Avdar et Sharkhai correspondent à des failles orientées NE-SW et sont situées à environ 40 km au sud-ouest d'Oulan-Bator, avec des longueurs de 47 km et 40 km, respectivement (Al Ashkar, 2015, Al Ashkar et al., 2022). Ces failles ont été définies comme des failles décrochantes sénestres avec une composante normale. La faille de Khustay a la même orientation (NE-SW) et est située sur les contreforts sud des monts Khustay, à l'ouest d'Oulan-Bator. Elle se caractérise également par un sens de mouvement sénestre avec une composante normale (Ferry et al., 2010). La faille d'Emeelt d'orientation NS, située au NW est décrite comme essentiellement une faille normale (Dujardin et al., 2014 ; Ulziibat et al., 2015). Ces quatre failles et leur cinématique sont cohérentes avec le champ de vitesse GPS dans la zone, qui - bien qu'encore mal défini - montre que la région se déforme sous un régime de transtension E-W (Calais et al., 2003).

Cependant, d'autres études sur d'autres failles dans la même région suggèrent au contraire que la région est caractérisée par une déformation transpressive. Par exemple, Imaev et al. (2012) ont décrit la faille Gunj orientée NE-SW située au nord d'Oulan Bator comme correspondant à

une faille décrochante dextre avec une composante inverse. Récemment, Suzuki et al., (2021) ont décrit la faille Bogd orientée NW-SE, une structure traversant la ville d'Oulan Bator et héritée de l'orogenèse paléozoïque, comme une faille inverse sénestre. Concernant la faille de Mungunmorit, Smekalin et al. (2016) ont conclu qu'elle correspondait à une faille inverse NNE-SSW à partir d'investigations paléosismologiques.

Dans cet article, sur la base de nouvelles observations issues à la fois des investigations morphotectoniques et paléosismologiques, nous déterminons les caractéristiques sismotectoniques de la faille de Mungunmorit (géométrie, longueur, segmentation, cinématique, magnitude potentielle et intervalles de récurrence des événements passés). Nous discutons ensuite sa signification dans le cadre de la géodynamique régionale Mongolie-Baïkal.

Notre étude morphotectonique et paléosismologique le long de la faille de Mungunmorit montre qu'elle correspond à une faille normale active à faible pendage vers l'est, au moins en sub-surface. De ce point de vue cinématique, ce résultat confirme que la région du sud-ouest de Khentii subit un régime de déformation extensive active, ce qui est cohérent avec le régime de transtension E-W observé dans la région d'Oulan-Bator immédiatement au sud-ouest. Ce régime transtensif/extensif semble être corrélé au régime de déformation du rift du Baïkal, et serait contrôlé par le soulèvement de l'asthénosphère dans la région. Du point de vue de la paléosismologie, nos investigations permettent de caractériser la survenue de deux événements de rupture de surface depuis 8,4 ka. Si nous étendons la fenêtre temporelle de nos observations, il semble qu'au moins un autre événement fort se soit produit peu de temps après 18 ka.

Les données paléosismologiques concernant les deux derniers événements suggèrent une période moyenne de récurrence des événements de rupture de surface comprise entre 3000 et 5000 ans. Le dernier séisme le long de la faille ayant eu lieu il y a 5 ka, donne un temps écoulé égal à la borne maximale de l'intervalle de récurrence. Bien que cette affirmation ne soit basée que sur les 2 événements passés, et malgré le fait qu'un éventuel événement antérieur à ~18ka augmente le temps de récurrence (~10 ka), la question de l'aléa sismique associé à la faille de Mungunmorit se pose clairement.

De plus, bien que le glissement co-sismique associé aux différents événements observés dans les tranchées n'ait pas pu être déterminé (caractéristique co-sismique observée correspondant principalement à des failles ou fissures normales secondaires à petite échelle), d'autres caractéristiques comme le décalage vertical minimal observé dans la morphologie (soit 0,5 m, voir section 3), associés au très faible pendage (~20°) de la faille, sa longueur totale (~160 km) et la longueur de ses différents segments (30 – 90 km) montrent la possibilité de les événements

de rupture de surface atteignant facilement Mw 7 après les fonctions d'échelle de Wells et Coppersmith (1994), reliant le glissement co-sismique, la longueur de rupture et la magnitude du moment.

En conclusion, la faille de Mungunmorit représente un aléa sismique non négligeable pour la région sud du Khentii notamment pour le village de Mungunmorit et ses ~3000 habitants, ainsi que pour la ville de Baganuur où vivent ~30 000 personnes. Même pour Oulan-Bator, située à ~100 km à l'ouest, la faille de Mungunmorit représente un aléa sismique dont il faut tenir compte compte tenu des ~1,6 million de citoyens qui vivent dans la capitale mongole.

ACKNOWLEDGEMENTS

First of all, I would like to thank Matthieu Ferry and Jeff Ritz, the two professors who led this PhD project from whom I learned a great knowledge. Since December 12, 2016, when I started my PhD study at Geosciences Montpellier, we have met hundreds of times, discussed research work, worked together for several months in the field campaigns and exchanged thousands of business letters. I have appreciated their patience and hard work.

I am grateful for the Ministry of Education and Science of Mongolia and the Embassy of France for funding my PhD research project between 2016 and 2018.

In addition, I would like to acknowledge the Institute of Astronomy and Geophysics of the Mongolian Academy of Sciences, Director Demberel, Scientific Secretary Odonbaatar, and Head of the Seismology Sector Ölziibat. The administration of the Institute supported this PhD project in all aspects.

Serge Lallemand, the former director of Geosciences Montpellier provided much-appreciated support. Also, many thanks to Pauline, Anne, Fabrice, Bernadette Marie and Helene for their help with the administrative assistance during my stay in Montpellier.

The scientists Amgalan Bayasgalan, Richard Walker, Steve Wesnousky, Takashi Nakata, Yasuhiro Suzuki, Yann Klinger, Jin-Hyuck Choi, Cengiz Zabci in Active Tectonics Field all made important contributions to my research.

I would like to thank the researchers who are Batsaikhan, Adiya Mönkhsaikhan, Battulga, Narantsetseg, Ankhtsetseg, Buyantogtokh, Nyambayar, Erdenezul, Möngönsüren, Amarsanaa Mönkhsaikhan, Ganzorig, Oyun-Erdene, Amarmend, and other colleagues of the earthquake research sector of the Institute. As well, I would like to express my gratitude to Mönkhöö, Bayaraa, Dugarmaa, and Adiya, senior researchers of the Institute.

The heads of the seismic network stations of the Institute in Gobi-Altai, Khovd, Bayan-Ölgii provinces: Batjargal, Zagdsüren, and Khos-Bürged, the researchers Batbayar, Diimaa, Janbolat, Serikjan, the drivers Enkhtüvshin, Zolboot, Tsagaansükh, Narantsogt, and Pürevsüren have all contributed to the success of our field work. Many thanks.

The assistance provided by the French cooperants at the Institute was very important for the French language administration. In addition, Narantuya of UB Tower 1001 office, graciously

facilitated for providing a comfortable office during the 3 months sabbatical leave from the Institute to finish up writing my PhD thesis. Thank you.

I want to thank my high school classmate IT engineer Ochirvaani for taking care of the reliable service of my computer. Geologist Nürzed Mönkhsaikhan taught me how to draw geological maps on GIS software and helped us to find a drilling machine to drill the UB fault. Many thanks for your contributions.

Thank you to Manlai, Mönkhgerel, Önörjargal, Otgonjargal, and Dölgöön, who were selected for the Mongolian-French government scholarship program and studied in various fields at the same time in all corners of France. We kept in touch and helped each other.

I am very greatful for the contributions of my international friends in Montpellier for providing a social life during my years of study. In particular, I would like to extend a special thanks to B. J. Shaw and Kenneth Berkman. Bee, for introducing me to Canadian culture. Our many dinners and games of Barbu, and interesting conversations with people from around the world, will be remembered forever. Ken has been a great friend. Thanks to his little green car I was able to travel with my wife and kids around Montpellier and its environs as well as take my parents to the Alps. In addition, his subsequent participation in my field research in the Altai Mountains in Mongolia was a pleasure.

Thanks to my fellow PhD students who are Audrey, Sven, Dowchu, Anita, Ben, Oswald, Anneka, Manar, Enora, Elenora and everybody at the Geosciences Montpellier. Special thanks to my dear friend Robin. I will never forget the time we lived together under the same roof in Aiguelongue. His kindness, many wonderful friends, and trips to visit his family in the mountains are happy memories. I look forward to working together again in the future.

I wish to thank my friend Oyun-Erdene in Paris who helped facilitate trips between France and Mongolia and my uncle Ganbold and his wife Oyuntülkhüür who made me feel very much at home in Germany.

Thanks to my mother Ichinkhorloo, my father Davaasambuu, my wife's mother Tsendjav, and father Oyungerel who have taken such good care of my family while I was away.

Finally and most important of all, I would like to express my sincere gratitude to my wife Narantsetseg and sons Bartanbaatar and Michidbaatar. Without the selfless support of my family over many years, this thesis could never been completed. Thank you from the bottom of my heart.

CONTENTS

LIST OF FIGURES

LIST OF TABLES

CHAPTER 1

1. INTRODUCTION

1.1 General tectonics of Mongolia

Mongolia is located on the Central Asian Plateau, has an area of ~1.5 million square kilometers. It has a common border with Russia in the north and China in the south. The total length of the border line is 8158 km. Mongolia has a population of 3.5 million. Half of the population is concentrated in the capital city of Ulaanbaatar, and the other half are scattered in the other provincial settlements and rural areas. Mongolia has a dry cool climate with four extreme seasons, the average annual precipitation in the northern part of the country is 200-350 mm, whereas it is 100-200 mm in the southern part (Gobi). Most of the main rivers flow through Lake Baikal into the Arctic Ocean, while the Kherlen river flows eastward through Lake Dalai to the Pacific Ocean. In term of orography, the mountains in Mongolia consist of the Gobi-Altai, Mongolian Altai, and Sayan Mountain Ranges in the southwest, west, and northwest, the Khangai and Khentii Mountains in the center, and the Dornod Plateau in the east (Figure 1).

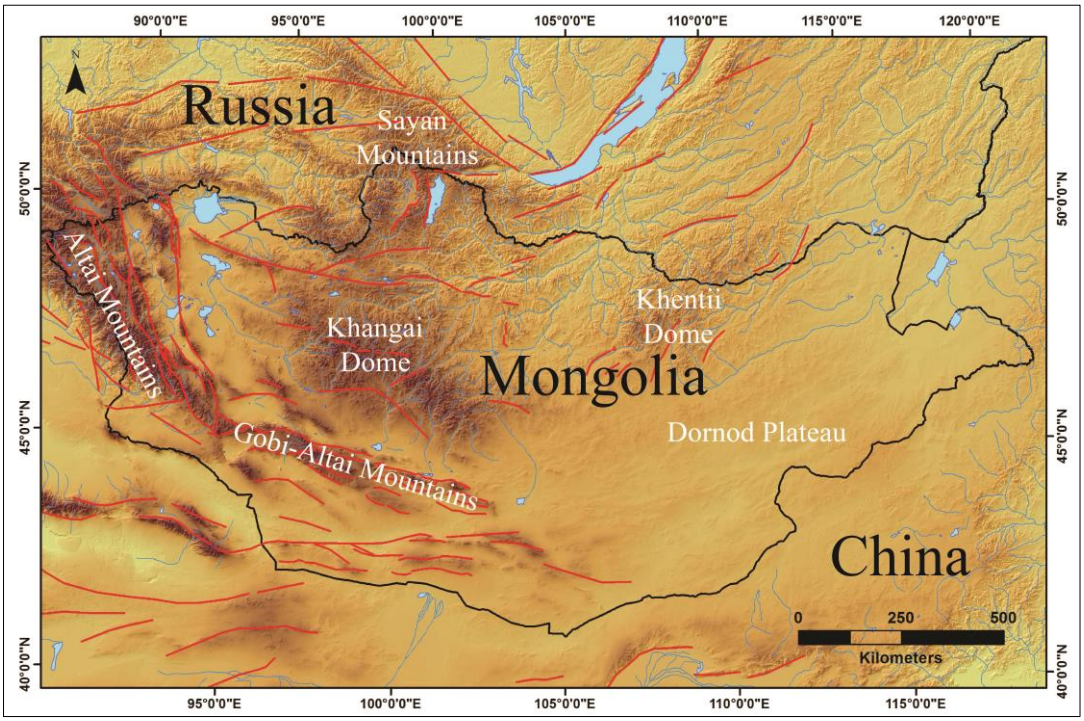

Figure 1. The Main Mountain Ranges and Major Active Faults in Mongolia.

The vast territory of Mongolia is situated in the Central Asian fold belt which is located between the ancient cratons of Siberia in the north and China in the south (Badarch et al., 2002). Richthofen (1841) noted that the territory of Central Asia, especially Mongolia, is partly covered with sand, clay, and volcanic lava accumulated in an enormous endorheic basin called the Khankhai where it is located in the center, and called it as the East Asian Plateau.

When Mongolia was a large peneplain, and the relief and topography were raised gradually. There were the accretion and collision zones before that (Badarch et al., 2002 (see Figure 2); Tumurtogoo, 2003; Windley et al., 2007). It can be seen in the geological maps with the rocks of the various origins, ages, and compositions (Tumurtogoo et al., 1998; Tumurtogoo, 2002; Tumurtogoo, 2003). After an ancient uplift of the peneplain, the tectonic process of the Cenozoic era acted and created the current topography. As a result of the movement of the tectonic plates, the India plate collided with the Eurasia plate 50 million years ago, the Himalayas were formed, and the continuation of the compressional forces deformed the region 2000-2500 km away to the far north, forming the Tien Shan, Altai and Gobi-Altai Mountains (Molnar & Tapponnier, 1975).

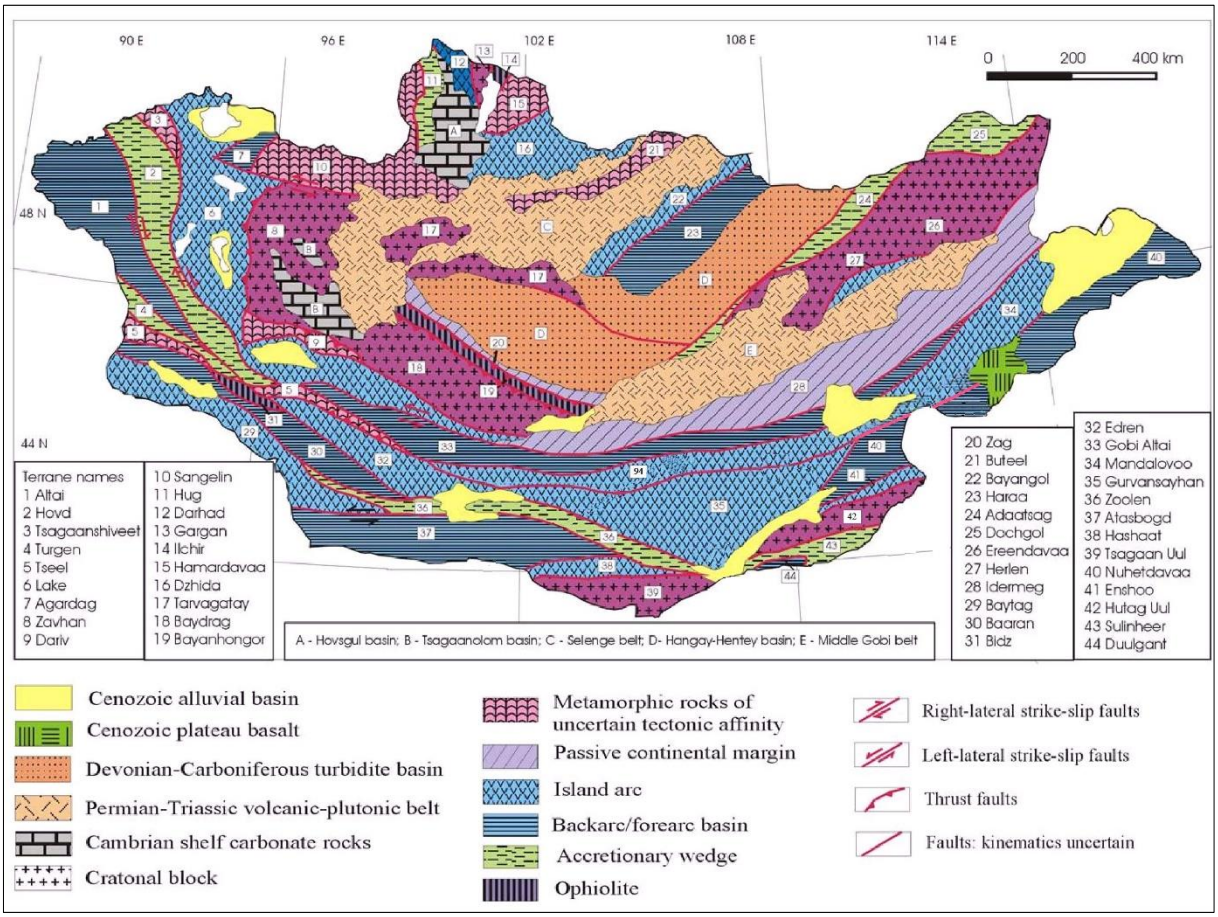

Figure 2. Tectonostratigraphic terrane map of Mongolia. After Badarch et al. (2002).

This process is still ongoing. In addition, Baikal and Khövsgöl lakes were formed as a result of active rifting processes, and basins of lakes are gradually expanding in long term. According to the fact that the deformation force of the collision of the India and Eurasia plates dissipates from the front to the rear, the mountains of the deep Central Asia were formed later than the Himalayas. For instance, the Himalayas began to form approximately 50 million years ago, whereas the Kunlun Shan Mountains formed 40-30 million years ago, the Tien Shan Mountains 15-10 million years ago, the Altai Mountains 8-2 million years ago, and the Sayan Mountains ~1 million year ago (Figure 3) and the mountain-building process still continues (Vassalo et al., 2007).

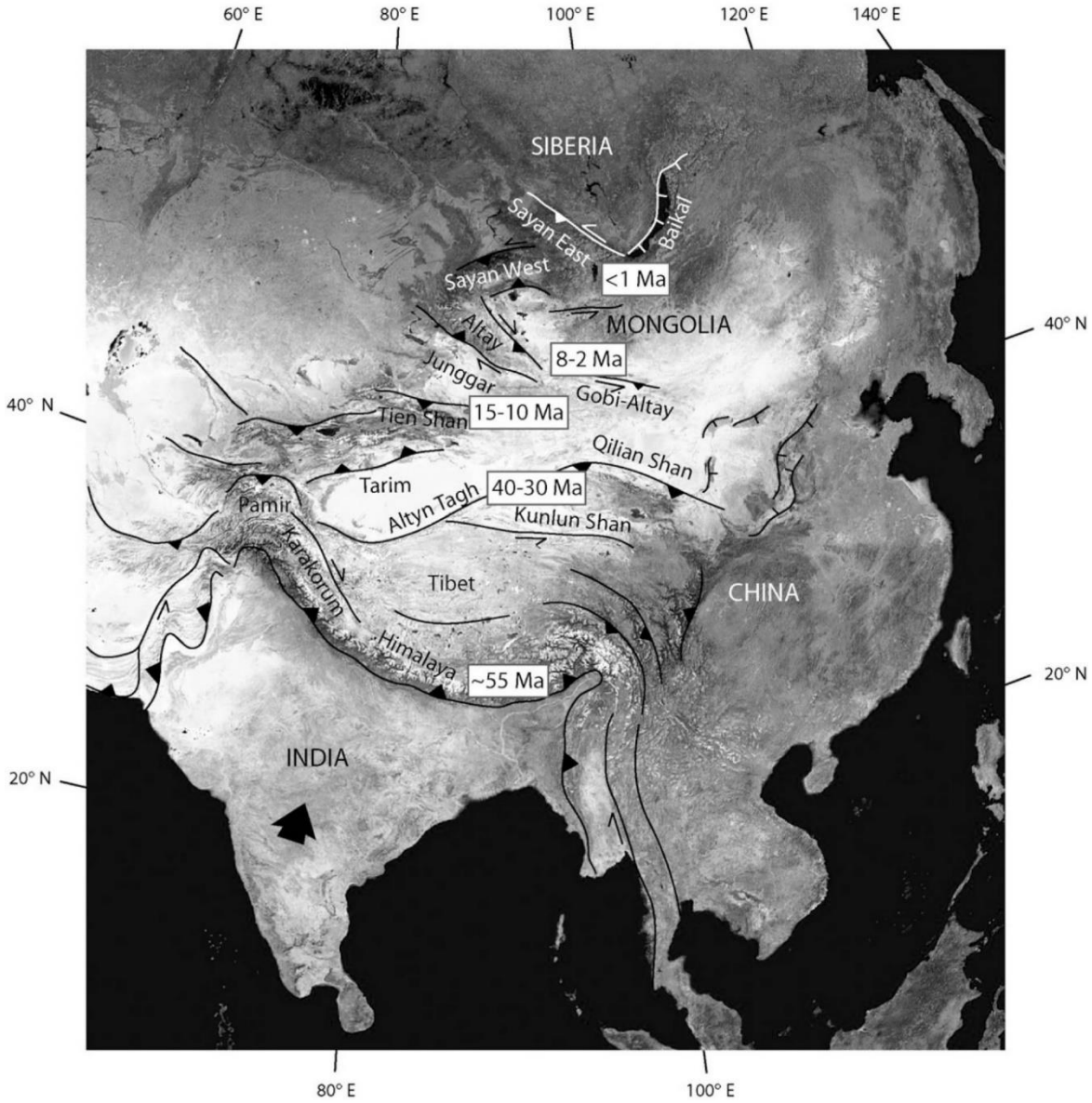

Figure 3. Simplified tectonic map of Central Asia. After Vassallo et al., 2007

Despite the fact that the India-Eurasia continental collision and the Baikal extension result from different kinematics (crustal shortening and asthenospheric upwelling), they may have started at the same time (Molnar & Tapponnier, 1975; Logatchev, 1993). However, crustal collision gradually penetrated deep into the territory of Central Asia, covering a huge area.

The Baikal rifting process may have started during the Paleocene (Logatchev, 1993; Ivanov, 2004), anyhow it was definitely started in the early Oligocene (Logatchev, 1993; Ivanov, 2004). This is confirmed by the dating of 4 km thick sediments under the Tunka basin where it is located between Khövsgöl and Baikal. In the Oligocene, the water of Lake Baikal spread in the Tunka basin. If the compressional force of the Indo-Eurasia collision had not reached the Baikal rifting zone, the Tunka basin would not have been elevated and would be still lake.

As seen on the DEM at broad scale (Figure 1), the Altai and Gobi-Altai Mountains are prominent structures (elongated and localized), whereas the Khangai and Khentii Mountains have the smooth domed topography. This implies different tectonic processes.

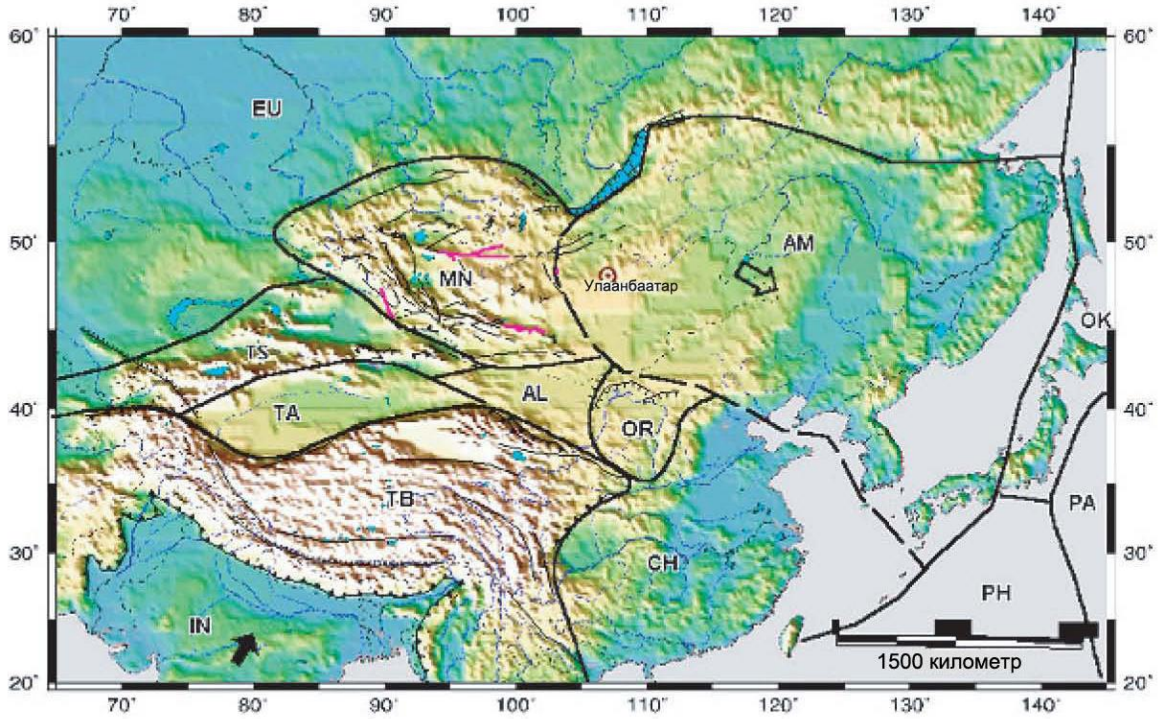

Figure 4. The micro-plates in Central Asia. Names of plates and microplates: EU – Eurasia, AM – Amuria, TS – Tien Shan, MN – Mongol, AL – Alashan, OR – Ordos, CH – China, TA – Tarim, TB – Tibet, IN – India, OK – Okhotsk, PH Philippine, and PA – Pacific. After Dugarmaa et al, 2006.

The territory of Mongolia comprises two distinct micro-plates with two different geodynamics environments in Central Asia (Figure 4). Western Mongolia is under the influence of SW-NE directed transpressional areas and it is considered as a seismically active region. On the other

hand, Eastern Mongolia belongs to the southeastern extensional force and its activity is less than Western Mongolia (Zonenshain, 1981; Bird, 2003; Barth & Wenzel, 2010).

Earthquakes occur mainly along the active faults along the boundaries of the micro-blocks, and the frequencies of the large earthquakes are low – their return periods are long (estimated as several thousand years) (e.g. Ritz et al., 2003; Rizza et al., 2015; Kurtz, 2017).

Thus, the research works have confirmed that the lithosphere of Mongolia is moving to the southeast due to the Indo-Eurasian compression and the Baikal-Khövsgöl extension (Figure 5). According to the results of detailed studies using data from the GPS stations, it was revealed that the Altai region is moving at a rate of ~5 mm/year, the Bulnai fault at 2.6±1.0 mm/year, and Central Mongolia at a rate of 6.4±1.6 mm/year with respect to Eurasia (Calais & Amarjargal, 2000; Calais et al., 2002; Calais et al., 2003).

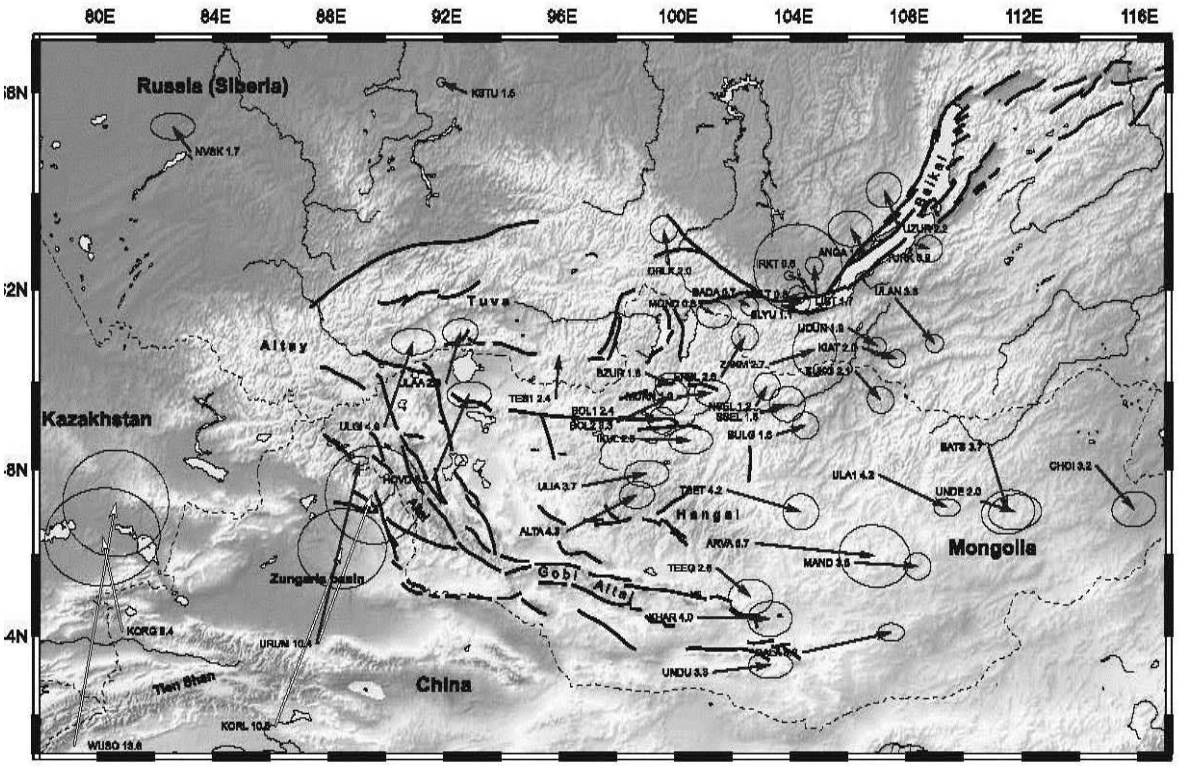

Figure 5. GPS velocities in Mongolia. Numbers with the site names are velocities with respect to Eurasia in mm/year. (After Calais et al., 2003.)

1.1.1 The Altai Mountain Range

The Mongolian Altai is the highest standing mountainous area in Mongolia. It occupies a large territories of western Mongolia and is topographically connected to the Sayan Range in southern Russia and to the Chinese Altai along western border of Mongolia (Figure 1).

Generally the entire range consists of NW-trending aggregated mountains that were sandwiched with elongated basins. It has an average elevation of ~2000-2500 m and a large number of summits exceeding 3500 m.

The fundamental geology of the Altai is composed of 3 basic terranes with distinctive geologic history. These terranes are following as an accretionary wedge, a backarc and a forearc basins and an island arc that are accreted and collided during Phanerozoic (Cunningham, 1996; Cunningham, 1998; Badarch et al., 2002). The boundaries of the terranes are controlled by neotectonically reactivated faults during the late Cenozoic.

It has been reported that the basement geology of the Altai was consolidated by the end of the Paleozoic era. During the Mesozoic era, the Altai was tectonically calm (Devyatkin, 1974, 1975; Devyatkin and Shuvalov, 1990; Kozhevnikov and others, 1970; Tikhonov, 1974; Baljinnyam et al., 1993).

Devyatkin (1974; 1975; 1981), and Howard (2004) noted that Oligocene-Holocene sedimentary rocks are deposited in the margins of the range and intermontane basins which indicates that Cenozoic rejuvenation of the Mongolian Altai began in the Oligocene and continues today.

The Altai has been formed in the late Cenozoic as a distant strain of the India-Eurasia collision (Molnar and Tapponnier, 1975; Tapponnier and Molnar, 1979).

Construction of the Altai seems to occur within regions including mechanically weak Paleozoic units. The region was sandwiched between the Khangai and the Junggar blocks and the North China Craton (Sengor and Natal'in, 1996; Cunningham, 1998).

It has been suggested that there is a fundamental connection between the Cenozoic fault trends and the older basement strike trends. The Cenozoic deformation regimes appear to be dictated by the angular relationship between preexisting basement structural trends and the prevailing NE directed compressive stress (Cunningham, 1998; Cunningham, 2005). In other words, the major active faults follow the structural faults and geological boundaries identically or roughly. A number of researchers have documented that the old fault zones host the active young faults (e.g. King et al., 1985; Vallage et al., 2016; Choi et al., 2018).

Previous researchers noted that thrust faulting and crustal thickening are associated with strike-slip faulting in the Altai (e.g. Tapponnier and Molnar, 1979; Baljinnyam et al., 1993).

Cunningham (1996; 1998) showed that coalescence of flower structures rooted into the major right-lateral strike-slip faults are influential for the mountain building in the Altai.

A number of the mountains in the Altai have flat summits. Researchers have suggested that those flat summits must be a result of uplift and preserved remnants of an ancient erosion surface since (Berkey and Morris, 1927). They interpreted the mountain chains with flat summits as sandwiched elongated basins due to block faulting (Berkey and Morris, 1927; Tapponnier and Molnar, 1979).

Afterwards, Cunningham et al. (2005) demonstrated the geometry and evolution of the uplifted flat areas and base mountains in the Altai as standpoint of the fault kinematics and restraining bend. And the idea is that the restraining bends are fundamentally influenced by the initial width of the stepover zone and then the initial area can be uplifted and preserved gradually with its width by next seismic events.

Over the long run, the right-lateral strike-slip faults seem to play an essential role in the development of orogeny in the Altai although they are not responsible for their uplift.

There are the active faults such as the Fu-Yun, Dayan-Nuur, Tsagaan-Gol, Sagsai, Bor-Burgas, Tsengel-Khairkhan, Khökh-Serkh, Ölgii, Tolbo-Nuur, Mönkh-Khairkhan, Khovd, Ar-Khötöl, Jid, and Khar-Us-Nuur in the Altai (Walker et al., 2006; Nissen et al., 2009; Gregory, 2012; Gregory et al., 2014; Odonbaatar et al., 2017; Battogtokh et al., 2022).

On average, the major strike-slip fault systems are separated by 25 ± 5 km and intervening areas appear tectonically inactive at the surface (Cunningham, 2005).

Total NE-SW shortening across central and southern Mongolian Altai is estimated to be on the order of 20-30 km (Cunningham, 2005).

GPS measurements show that 10-15% of the Indo-Eurasian collision is accommodated in the Altai region (Calais et al., 2003; Frankel et al., 2010).

The following researchers have estimated the geological slip-rates along the major active faults based on the displaced alluvial fan sediments. The right-lateral slip-rate of the Khovd fault (Vassallo et al., 2006) is > 0.5 mm/yr and > 1.2 mm/yr, the Har-Us-Nuur fault (Nissen et al., 2009) is 2.4 ± 0.4 mm/yr, the Höh Serh-Tsagaan-Salaa fault (Frankel et al., 2010) is 0.9 +0.2/-

0.1 mm/yr, the northern section of the Ulgii fault (Gregory et al., 2014) is 0.3-1.3 mm/yr respectively.

Approximately 2-8 km of cumulative right-lateral displacement is measured in 3 large river valleys along the Khovd and Ar-Khötöl faults that are the main representative structure controlling deformation in the Altai region (Trifonov, 1983; Khilko and others, 1985; Baljinnyam et al., 1993; Ulziibat, 2006; Battogtokh et al., 2022). Correlating the average slip-rate of ~1 mm/year and the average cumulative displacement of ~5 km, the Khovd fault began to move ~5 million years ago.

Finally, it is clear that the Altai is a tectonically active mountain range in an intraplate setting far away from prominent plate tectonic boundaries. The dominant style of faulting in the Altai is right-lateral strike-slip faulting.

1.1.2 The Gobi-Altai Mountain Range

The Gobi-Altai mountain range is located in the south and southwest part of the territory of Mongolia, between ~94˚-105˚ longitude, and most of it is between ~43˚-46˚ latitude, stretching latitudinally (Figure 1).

The researchers believe that the Gobi-Altai mountain range, like the Altai mountain range and many other mountains in Central Asia, was formed by the Indo-Eurasian convergence (Molnar & Tapponnier, 1975; Baljinnyam et al., 1993; Cunningham et al., 1996, 1998; Ritz et al., 2006; Vassallo et al., 2007). The Gobi-Altai Mountains attracted the attention of the world earthquake researchers with the ~270 km long Bogd fault that broke during the magnitude 8.1 earthquake of December 4, 1957 (Bobrov et al., 1959; Florensov & Solonenko, 1963; Khilko et al., 1985; Baljinnyam et al., 1993; Ritz et al., 1995; Kurushin et al., 1997; Choi et al., 2012).

The Gobi-Altai range is different compared to the Altai range for landform, geometry and kinematics. The mountains in the Altai are mostly northwest-southeast oriented, whereas the mountains in the Gobi-Altai have almost E-W orientation. While the shortening of the crust in the Altai range took place on a wide area of ~300-500 km covering several aggregated parallel mountains separated by large depressions, shortening in the Gobi-Altai range took place at the scale of a few isolated parallel mountains. Also, the landform of the Gobi-Altai Mountains is more rugged and young compared to the relatively smooth landform of the Altai Mountains. The main difference is the kinematics of the active faults. The Ranges in the Altai are bounded by right-lateral oblique-slip faults, while the Ranges in the Gobi-Altai are controlled by left-

lateral oblique-slip faults. However, the Gobi-Altai and Altai Mountain Ranges show similarities, including restraining bends, flat summits, and elongated basins connecting them. Baljinnyam et al (1993) proposed that the Gobi-Altai may be similar to the earlier stage of the mountain building processes in the Altai.

The Gobi-Altai Mountains mainly consist of restraining bends with reverse component due to the step geometry of the left-lateral strike-slip faults. For instance, the summit plateau of the Great Bogd Mountain with a broad area of ~7 km (the widest flat top) x 20 km (the length) implies that the initial step of the bounding faults were much broader (Figure 6). In other words, the plateau was a Jurassic erosional surface (Florensov & Solonenko, 1963) and then it has been uplifted ~2000 m relative to its surrounding lowland keeping up with the size that was occupied by the initial step (Figure 6). The horizontal level of the summit plateau is still almost parallel to the ground surface, which means that the vertical slip-rate of the structurally controlling reverse faults in the south and north flank of the Great Bogd Mountain was the same for a long time (Ritz et al., 2003). Jolivet et al (2007), based on the extraordinary preservation of the plateau, points out that there was no any tectonic process in the area from the Jurassic period to the onset of the Cenozoic, and climate of the area during the mountain building was incredibly arid over millions of years in order to preserve the summit plateau from ersosion. Vassallo et al (2007) determined that the Great Bogd and Baga Bogd mountains started to raise since 5±3 million years.

The slip-rate of the Great Bogd fault is 0.5-1.2 mm/year (Ritz et al., 1995; Ritz et al., 2003; Vassallo et al., 2007). Kurtz et al (2018) determined that the slip-rate along the West Bogd fault is 0.7±0.2 mm/year and the slip-rate along the Valley of Lake fault is 0.5±0.1 mm/year.

Ritz et al (2006) estimated that a similar event to the 1957 earthquake could occur every 3000-4000 years with a slip-rate of ~1 mm/year along the Great Bogd fault.

The active faults in the Gobi-Altai Mountain Range include the Great Bogd, West Bogd, Valley of Lake, Sharga, Tsagaan Gol, Zarman, Budargana, Argalant, Khavtsgait, Arts Bogd, Bulagtai, Gurvan Saikhan, Buuriin Khyar, Tsetsii (Khilko et al., 1985; Baljinnyam et al., 1993; Ritz et al., 1995; Kurushin et al., 1997; Odonbaatar et al., 2017; Kurtz, 2017).

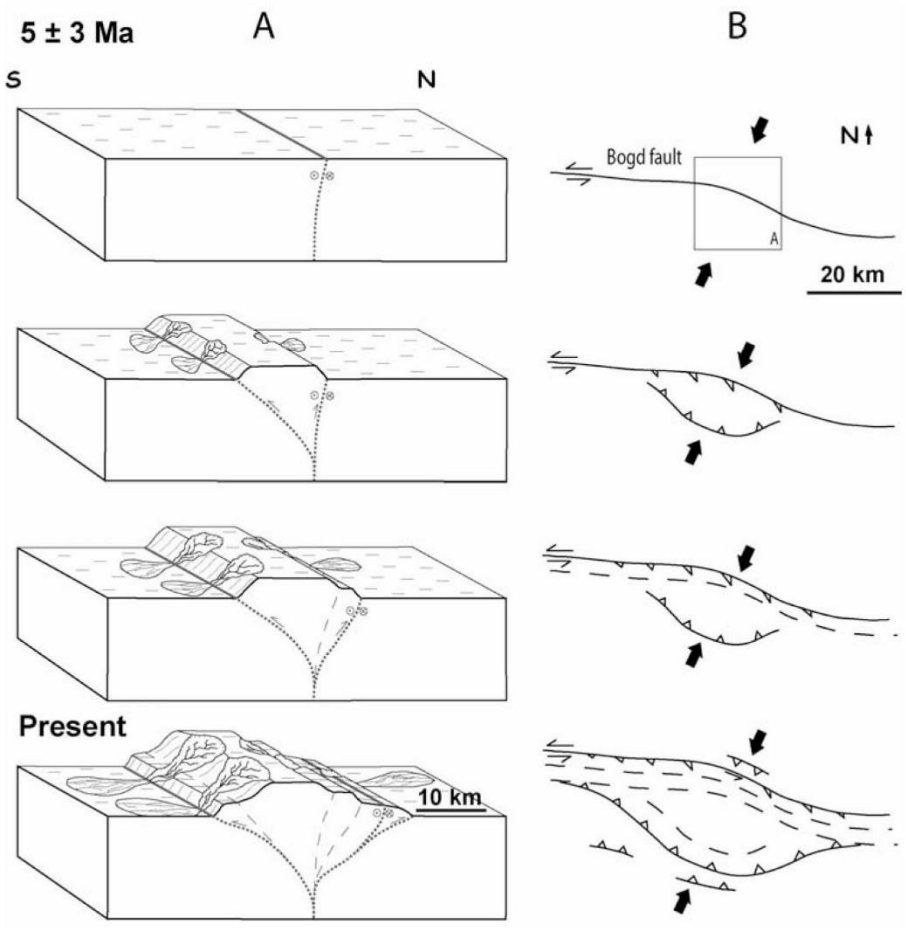

Figure 6. The growth of the Ikh Bogd massif. After Vassallo et al., 2007.

1.1.3 The Mountains around Khövsgöl basin (Sayan Range)

The surrounding mountains of Khövsgöl lake basin are the Bayan Mountain Range (3193 m), the Khoridol Saridag Mountains (3093 m), the Ulaan Taiga Range (3351 m) to the west, the Sayan Mountains (3491 m) to the north, and the Sant Range (2367 m) to the east. The mountains on the west and north have a rugged topography controlled by active faults, while the Sant Range and the mountains on the east side have smooth and dome-shaped summits.

It is believed that the Siberian craton has not been affected by tectonic processes since the Paleozoic. However, the Sayan Range and the mountains around the Khövsgöl basin (Figure 1) are elevated compared to the Siberian platform, where relief and topography have developed. Logatchev (1993) noted that the cause of the broad domal uplift is associated with mantle upwelling, while Molnar and Tapponnier (1975) suggested that it is the far field effects of the India-Eurasia collision.

Khövsgöl-Sayan orogenic belt is made up of accreted island arc, accretionary wedge and metamorphic terranes that are dominantly composed of rocks of various types such as basalt, andesite, gneiss, schist, gabbro, ophiolite, pillow lava, and shelf carbonate rocks with Neoproterozoic ages and intruded by post-collisional Paleozoic granites (Melnikov et al., 1994; Badarch et al., 2002).

Jolivet et al (2012) assumed that the surface of the Sayan may have formed as an elevated plateau built up during the Mesozoic orogeny and preserved from erosion since that time.

The domal uplift is disturbed by the Baikal rift valleys filled with continental sediments of the Paleogene, Neogene and Quaternary (Logatchev, 1993).

The Baikal rift system is defined by an alignment of north-south and north-east trending elongated basins extending from Mongolia to Russia connected by strike-slip faults. The north-south oriented Khövsgöl (~1645 m), Darkhad (~1550 m), and Büsiin Gol (~1300 m) basins in Mongolian territory are considered to be the south-west termination of the Baikal rift system.

Active faults in the vicinity of the Khövsgöl-Sayan region have been studied by a number of researchers (e.g. Molnar & Tapponnier, 1975; Zonenshain & Savostin, 1981; Khilko et al., 1985; Sankov et al., 2003; Arjannikova et al., 2004; Byamba et al., 2009; Ritz et al., 2018).

1.1.4 The Khangai Dome

The Khangai Dome is located between the Bulnai left-lateral strike-slip fault to the north and the Gobi-Altai left-lateral strike-slip fault to the south (Figure 1). The origin of the Khangai Dome and the Cenozoic tectonic regime are still not fully understood.

The dome-shaped Khangai Mountains rise up to 4021 m above sea level (at Mount Otgontenger) coeval with the late Cretaceous erosional surfaces. There is no reliable evidence for the timing of this uplift, however, basins surrounding the Khangai Mountains exhibit widespread coarse sedimentary formations of Middle Oligocene age (Yanshin, 1975).

Tertiary and Quaternary effusive rocks are widespread throughout the Khangai Mountains (Filippov et al., 1976; Ionov, 2007; Barry et al., 2003; Yarmolyuk et al., 2008; Hunt et al., 2012). Based on the distribution of the Late Cenozoic volcanic rocks, the Khangai Dome is thought to have been formed by hot mantle intrusion (Windley and Allen, 1993). Hence, it has been proposed that low-activity mantle upwelling may have accumulated under the lower part of the crust in response to the collision of India and Eurasia (Petit et al., 2002).

Two distinct populations of active faults have been described in this region. On the one hand, the South Khangai, Songino-Martgats, and Khag Nuur left-lateral exhibit strike-slip kinematics and are associated to the Indo-Eurasian compression (Walker et al., 2007; 2008). On the other hand, the Terkhiin Tsagaan, Khökh Davaa, Egiin Davaa, Bat-Ölziit, and Khujirt faults are normal, which is more consistent with regional uplift in connection with a rising lithosphere (Walker et al., 2015; Odonbaatar et al., 2017).

1.1.5 The Khentii Dome

The Khentii Mountains cover the north-eastern part of the country (Ikh and Baga Khentii). They display a northeast-southwest elongation and reach elevations of 2800 m (at Mount Asralt Khairkhan).

The general landform of the Khentii Mountains are dominantly dome-shaped tops. Unlike the Altai and Khangai, there are no modern glaciers, however, the smooth and gentle landscape in the high-elevated mountains indicates the paleo-peneplain.

To the east of Ulaanbaatar city, the river valleys are dominantly northeast-southwest oriented and may be inherited paleo-valleys. The NNE-SSW trending Möngönmorit fault is a normal. The Khustai fault is a transtensional due to the Baikal rift.

Research works associated to neotectonics are rare in the Khentii Dome and its tributary mountains.

According to the instrumental seismicity recordings in Mongolia, 4-5 strong earthquakes with intensities VI-VII took place in the northwestern part of the Khentii Mountains.

Several active faults such as the Khustai, Emeelt, Sharkhai, Avdar, Bayantsagaan, Gunj, Asralt Khairkhan, Möngönmorit, Bayandelger, and Dayant were surveyed and documented (Odonbaatar et al., 2015).

1.1.6 Eastern Mongolia

According to the physical geography of Mongolia, Eastern Mongolia belongs to the Dornod plateau region. The Dornod plateau is bordered by the Khangai Mountains, the Valley of Lakes, the Gobi-Altai Mountains to the west, the Khentii Mountains to the north, and the Khyangan Mountains to the south (Figure 1). This vast plain gradually slopes from the west to the east,

and its lowest altitude reaches 560 m near the Khökh Nuur in the north-eastern part of the country. That is the lowest point in the entire territory of Mongolia.

In terms of surface morphology, it is a plateau with an average altitude of 1000-1100 m above sea level and it consists of flat or dome-shaped small hills and lowlands. The highest points are Mount Delgerkhangai (1913 m), Mount Mönkh Khan (1606 m), and Mount Lkhachinvandad (1233 m) and so on (The National Atlas of Mongolia by Sodnom et al., 1990).

During the Cenozoic period, the territory of the eastern part of Mongolia has been a quiet platform-like region without any tectonic activity. The fact that no active faults are known or studied means that there is almost no deformation and folding process caused by recent plate movements.

Although this indicates that the Quaternary tectonic activity in the region is absent or slow, several microearthquakes with magnitude 2.5-3.5 were recorded and located with the international and local seismic stations (Barth & Wenzel, 2010; Odonbaatar et al., 2017).

Many active faults have been discovered and studied in the western, central, and northern parts of Mongolia, and dozens of scientific articles have been published associated with them, but in the region east of 108˚ longitude, where the Möngönmorit fault is located, no active fault has been mapped, and scientific articles associated with local active tectonics have hardly been published.

The Möngönmorit fault is considered to be the easternmost active fault in Mongolia. Beyond the fault to the east, the mountainous relief of Mongolian territory decreases, joining the Great Steppe and the Dornod plateau and becomes more flat.

According to GPS velocities, the displacement of the crust in the south-west, west, north-west, and central parts of Mongolia move to the east and south-east with a clearly visible vectors, and lowers in eastern part of Mongolia and northern China (Calais et al., 2003; Calais et al., 2006; Vergnolle et al., 2007). These velocities become progressively smaller in the east and south-east of the territory where there is no evidence for active tectonics in terms of seismicity and morphotectonics. The deformation might be accommodated within Khangai and Khentii Mountains.

1.2 Seismicity

1.2.1 Historical seismicity

Since ancient times, human beings have been interested in the causes of earthquakes. They were trying to find out from which direction earthquake waves were coming, and to record the time of earthquakes. The first instrument to detect ground motion was invented by Chinese astronomer Zhang Heng in 132 CE. It is a device depicted by eight dragons facing the 4 cardinal directions and the 4 intercardinal directions with balls in their mouths. When the ground moves strongly, the balls in the mouth of one of the dragons roll out and fall into the mouth of a gaping frog (Figure 7).

Figure 7. Chinese Astronomer Zhang Heng's seismoscope.

Mongolia is a country with an ancient history, but it has a nomadic civilization. Therefore, there is almost no written information about earthquakes. There are many stories and legends about ancient earthquakes passed down from the ancestors, but their descriptions are not precise enough to yield reliable and usable information. Neighboring countries with sedentary societies, such as China and Russia, may hold detailed written records of events that have occurred in Mongolia, provided they are strong enough to be felt far away (Mushketov & Orlov, 1893; Gu et al., 1989).

Mushketov & Orlov (1893) noted that a large earthquake was felt by the inhabitants of the Ob and the Black Irtysh river basins of the Russian Empire in December 1761. Kondorskaya et al. (1977) found new macroseismic data from the State Archives of the Russian Altai Territory and combined it with the macroseismic data of Mushketov & Orlov and calculated that the earthquake occurred on December 9, 1761 at 17:20 in the Mongolian Altai Mountains.

Senior researchers of IAG conducted an interview among the elderly people in Khovd province and were told of old stories transmitted by oral tradition. Those old people say that in the ancient times, there was a strong earthquake in the Mongolian Altai Mountains that caused a large amount of rocks to fall down from the mountains, and courtyards were crushed and destroyed.

Khovd city was first established on the banks of the Khovd River in 1685 as a military fortification and agricultural settlement. In 1762, it was moved to its current location on the banks of the Buyant River and turned into a real civil city (Gongor, 1964). The Khovd River is the largest river in the Mongolian Altai Mountains, and originates from the Altai Tavan Bogd Mountains, ~320 km northwest of Khar-Us Lake, a tributary of the Khovd River. The Buyant River flows into Khar-Us Lake, which originates from the Khökh Serkh Mountain Range, just to the west of Khovd city. It is said through word of mouth that a great flood affected the displacement of Khovd city.

1.2.2 Instrumental seismicity

The oldest instrumental earthquakes that occurred on the territory of Mongolia are the 1903 Üüreg Nuur earthquake and the 1905 Tsetserleg and Bulnai earthquakes, which were strong enough to be recorded by stations worldwide (e.g. Schlupp & Cisternas, 2007).

The first seismic stations were established in Mongolia in 1957 (Adiya, 2021) and upgraded in 1994 when a new digital, high sensitivities, telemetered seismic stations were installed.

From 1900 until now, there have been 4 destructive earthquakes of magnitude 8-8.3, 4 large earthquakes of magnitude 7-7.5, and 11 moderate earthquakes of magnitude 6-6.9. A total of 19 earthquakes with a magnitude of 6-8.3 occurred on the territory of Mongolia and the neighboring countries near the border of Mongolia (Table 1).

Among them, 4 earthquakes (Fu-Yun, Achit Nuur, Üüreg Nuur, and Mönkh Khairkhan) occurred in the Altai Mountains, 5 earthquakes (Takhiin Shar, Bayan Tsagaan, Ünegtei, Buuriin Khyar, and Great Bogd) occured in the Gobi-Altai Mountain Range, 4 earthquakes (Mondy, Büsiin Gol, Chuya, and Khankh) were located in the Sayan Range, 3 earthquakes (Tsetserleg, Bulnai, and Mogod) took place in the Khangai Mountains, 2 earthquakes (in Büteel and Saikhan) were located in the Büren-Büteel Range, the Erdene Khan earthquake was recorded in the Khentii Mountains.

Table 1. Large M>6 Earthquakes in Mongolia.

Name of earthquake	Date	Magnitude	Type of fault[1]	Length of fault (km)	Reference
Ünegtei	01/02/1903	7.5	-	4-20	Khilko[2]
Tsetserleg	09/07/1905	8.0	LL	130	Khilko[2], Choi[3]
Bulnai	23/07/1905	8.3	LL	388	Khilko[2], Choi[3]
Fu-Yun	10/08/1931	8.0	RL	180	Khilko[2]
Achit Nuur	19/10/1938	6.9	-	-	Khilko[2]
Mondy	04/04/1950	6.9	LL	-	Delouis[4], Ritz[5]
Erdene Khan	01/01/1951	6.1	-	-	Khilko[2]
Büteel	06/02/1957	6.4	-	-	Khilko[2]
Gobi-Altai	04/12/1957	8.1	LL	270	Khilko[2],Kurushin[6],Choi[7]
Bayan Tsagaan	07/04/1958	6.9	LL	7	Khilko[2]
Saikhan	23/06/1958	6.2	-	-	Khilko[2]
Buuriin Khyar	03/12/1960	6.7	R	18	Khilko[2]
Mogod	05/01/1967	7.1	RL / R	45	Khilko[2], Baysgalan[8]
Üüreg Nuur	15/05/1970	7.0	RL / R	6-8	Khilko[2]
Takhiin Shar	04/07/1974	6.9	LL	17	Khilko[2]
Mönkh Khairkhan	31/03/1975	6.0	RL	-	Khilko[2]
Büsiin Gol	27/12/1991	6.3	RL / N	-	Bayasgalan[9]
Chuya	27/09/2003	7.3	RL	~60	Ulziibat[10]
Khankh	12/01/2021	6.7	RL / N	~25	Battogtokh[11]

Note: [1]LL – left lateral, RL – right lateral, R – reverse, N – normal. [2]Khilko et al., 1985; [3]Choi et al., 2018; [4]Delouis et al., 2002; [5]Ritz et al., 2018; [6]Kurushin et al., 1997; [7]Choi et al., 2012; [8]Bayasgalan & Jackson, 1999; [9]Bayasgalan et al., 2005; [10]Ulziibat, 2006; [11]Battogtokh et al., 2021.

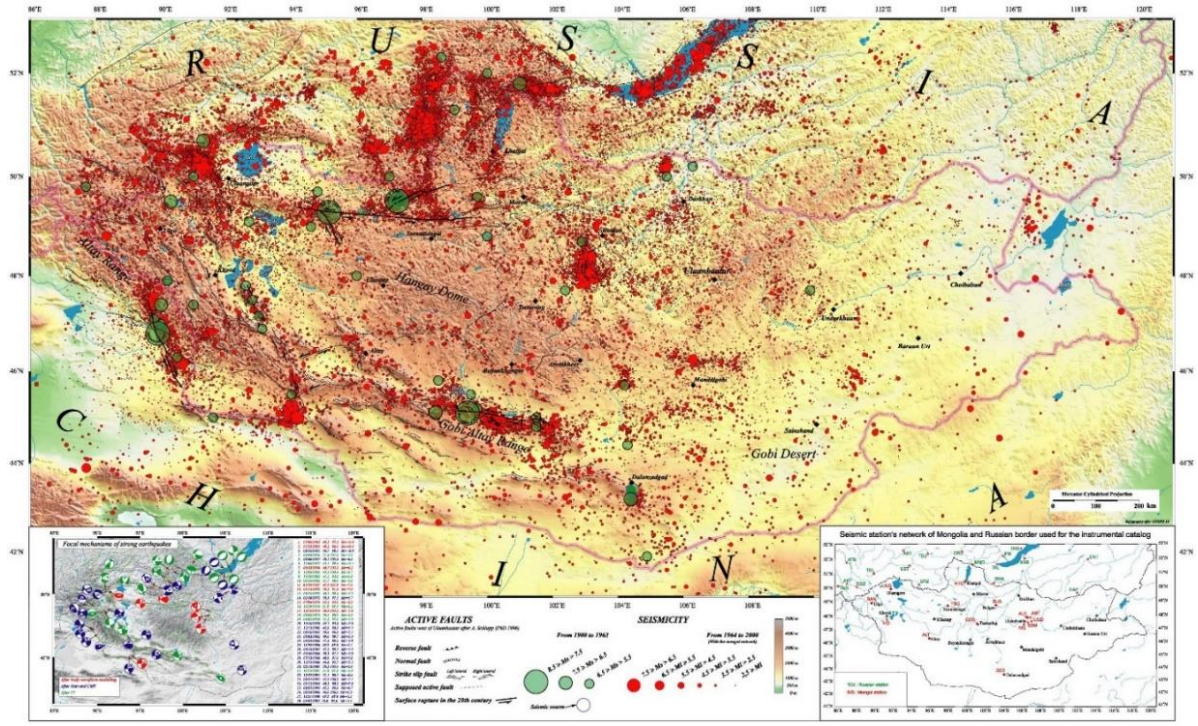

Figure 8. One Century of Seismicity in Mongolia. After Dugarmaa et al., 2002.

In addition, hundreds of magnitude 3-5 earthquakes occurred on the territory of Mongolia (Figure 8). Thus, Mongolia is considered to be in active seismic zone.

1.3 Methods

1.3.1 Mapping active faults

Geomorphology - *The study of landforms and surface processes*. Active Tectonics by Edward A. Keller.

Geomorphology – *The investigation of the earth's landforms; specifically the study of the nature, origin, and development of present landforms, their relationships to underlying structures, and of the history of geologic changes as recorded by these surface features.* The Geology of Earthquakes by Robert S. Yeats.

As mentioned in the definitions above, geomorphology is the study of the shape of the earth's surface. Naturally, the physical activities such as sun, wind, and water, and in addition, biological activities of animals and plants affect the changes in the shape of the earth's surface. Moreover, the internal activities under the earth's crust, such as tectonic processes, would greatly affect the surface of the earth. If a researcher is going to deal with geomorphology, the researcher had better look at the sediments on the surface, determine what geological processes took place there in the past and present, and map the modern surface.

I performed the detailed map of the Ar-Khötöl surface rupture on the Pleiades satellite images with 0.5 m resolution. Also, the images were used to identify the specific geomorphological features (such as gullies, stream risers and terraces) along the fault, and to distinguish the segmentation and kinematics of the fault. Another notable research that was executed using Pleiades images was the measurements of the co-seismic offsets and short-term cumulative displacements (a few meters to a few tens of meters) along the Ar-Khötöl surface rupture. Using these values, I produced the graphics of slip-distribution and slip-envelope. In addition, the Pleiades images were widely used in the field works, planning the geological routes, selecting paleoseismological research sites etc.

High-resolution topography has been one of the key components of fault mapping, deformation quantification and planning of field campaigns. Our main objective was to use the DEM to identify the expression of the Khovd fault and the Ar-Khötöl surface rupture on the earth's landforms such as Late Pleistocene glacial moraines, fluvial terraces and alluvial fans. The high accuracy of the product allowed to quantify the cumulative deformation recorded by landforms over time. Even though the Khovd fault is dominantly strike-slip, it also displays a slight compressive component. Furthermore, horizontal offset of sloping surfaces (e.g. edges of

alluvial fans or moraines) produces apparent vertical displacement (that may amplify or reduce the local tectonic component). Hence, scarps with height ranging from a few meters to tens of meters frequently mark the location of the fault.

Detailed fault mapping on the 12-m-DEM was performed by identifying and mapping landforms associated to recent surface processes at play along the fault using a geomorphological approach. Geomorphometric indices (slope, slope distribution, curvature, and terrain ruggedness) already established for coarser DEM data (SRTM 1 and ASTER GDEM) were adapted to TanDEM data. Semi-oriented classification based on these indices were tested to automatically identify the various landforms and accelerate the mapping process. Quantification of cumulative deformation affecting landforms relied on direct measurements on the DEM for the horizontal offsets and extraction of topographic profiles to derive the vertical component. For recent landforms and associated relatively small amounts of deformation, we complemented and refined our observations with 0.5-m-resolution Pleiades data.

In this study, the UAV (unmanned aerial vehicle) survey was used to map a morphology of the land surface. By mapping the morphology of the surface in detail with UAV survey, the possibilities have been opened for mapping the fault scarps, measuring vertical and horizontal offsets of the faults, and studying the long-term surface processes.

The Ar-Khötöl surface rupture has clearly visible scarps on the ground surface, and the traces left by the latest earthquake are relatively well visible, but in some parts, the remnants of the rupture were washed away by erosion. We conducted UAV and terrestrial laser scanner surveys in order to measure the displacements of temporary and permanent drainages and clarify the geomorphological features along the fault.

For example, the UAV survey shown in the point D in Main Map of the chapter 2 was filmed at a place called the Baga-Ulaan Davaa and the Urtiin Gol where it is located in the territory of Möst sum, Khovd province. At this point, a total of 81 photos taken coincidentally by a drone were processed by computer and combined to obtain the Digital Surface Model (DSM) and the orthophotograph of the area. The resolution of the DSM is 5 cm and the resolution of the orthophotograph is 3 cm. This is a good enough resolution with a potential to measure displacements and to map geomorphological features. It is clearly visible on the figure that the surface rupture that was produced by the earthquake depicted en echelon extensional depressions and compressional pop-ups on the thick sediments. The extensional depressions

have en echelon expressions and left-stepping structure. The left-stepping structure is a typical feature of a right-lateral strike-slip fault although any displacement is unmeasurable at the site.

1.3.1.1 Satellite images

1.3.1.1.1 Why satellite images

The development of mankind let them enter to space with the use of high-tech airplanes, rockets, and satellites. Hence, aerial and satellite images of various features and purposes are taken from space, and used for geology, geography, geodesy, biology, ecology, agriculture, mining, and resource management etc. For instance, researchers use periodic satellite images to prove that snow cover, ice caps and glaciers are retreating rapidly due to global warming. The percentage of evergreen forest in Mongolia can be easily determined by satellite images taken in the cold winter season.

It should be emphasized that satellite imageries have been the most powerful tool in my research. It is unimaginable to study the mountain ranges, faults, geological and geomorphological objects in the vast territory of Mongolia without the use of satellite images. I used many types of satellite images such as Landsat 8, TanDEM, Pleiades, Sentinel 2, Google Earth, Bing Map, and Global Mapper default during this project.

1.3.1.1.2 Spatial and spectral resolution

When working on satellite imageries, the concept of spatial resolution comes out. In simple words, the spatial resolutions of 30 m, 5 m, and 0.5 m can be defined as squares of that size. In space imagery, that square can be thought of as a pixel. The pixel is the smallest unit of dots that make up an image on the screen. In other words, spatial resolution is the size of one pixel of the satellite imagery on the actual ground surface. For example, Landsat 8 satellite imagery has 30 meter spatial resolution which means the single pixel of the imagery represents an area on the ground that is 30 meters side to side (Figure 9). However, they can be pansharpened using a high-resolution panchromatic band to produce a final 15-m-resolution color image.

The advantage of mapping on medium-resolution imagery is to see the faults in a large area of several tens of kilometers, to identify the main faults that control the structures, and to recognize some geomorphological features, for example, to discover the large alluvial fans that were displaced by faults, to see the general mountain buildings, and to get very first ideas about the relationship between mountains and faults.

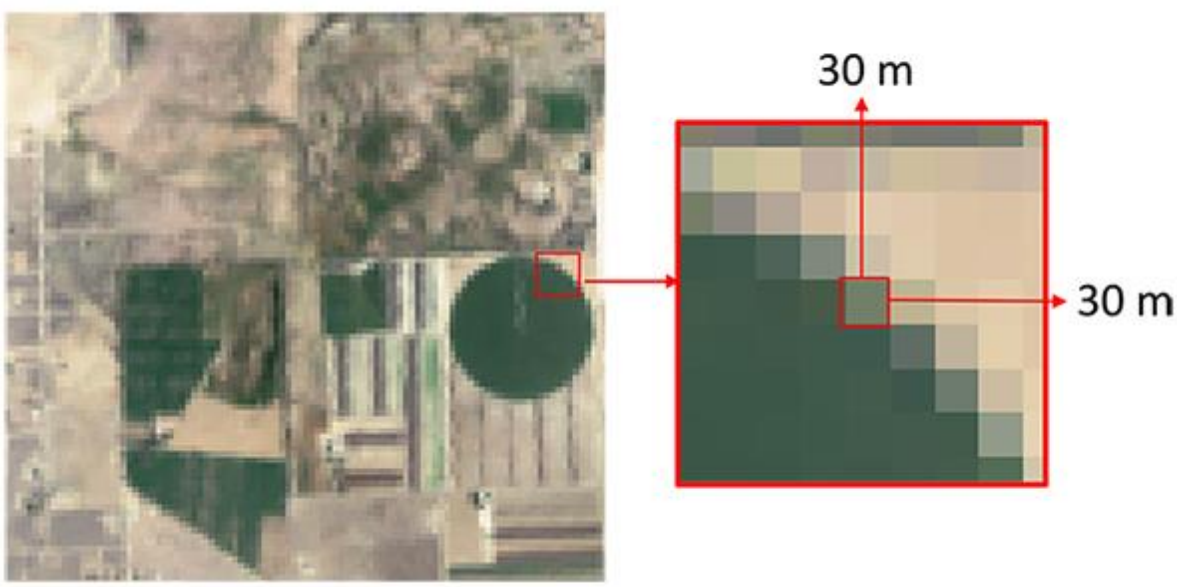

Figure 9. The spatial resolution of Landsat 8 satellite image.

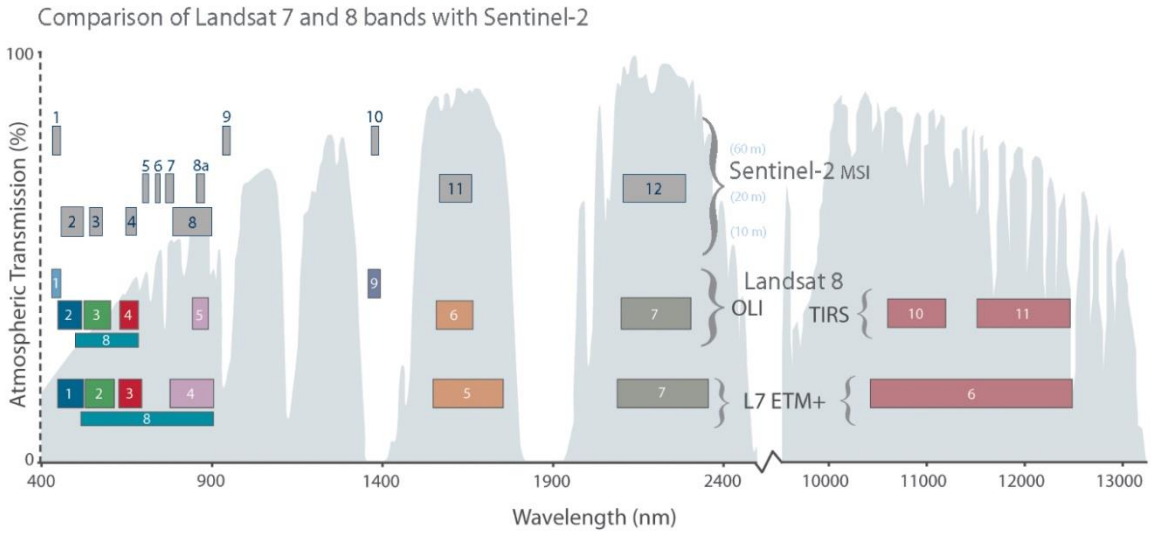

Figure 10. Comparison of spectral bands provided by Sentinel-2, Landsat-8 and Landsat-7 satellites. Pleiades satellites provide color bands equivalent to Landsat-8 bands 2, 3, 4 and 5 at 2 m resolution.

1.3.1.1.3 Landsat 8

Landsat 8 is an American Earth observation satellite launched in 2013 in the frame of the collaboration between the National Aeronautics and Space Administration (NASA) and the United States Geological Survey (USGS). The main goal of the mission is to provide medium-resolution imagery of the Earth's land surface for the public for free. Landsat 8 has got two sensors that are the Operational Land Imager (OLI) and the Thermal InfraRed Sensor (TIRS) to collect image data of 9 shortwave bands and 2 longwave thermal bands (Figure 10).

I prepared a seamless mosaic of Landsat-8 images to cover the whole Mongolian Altai Mountain Range at medium resolution. From the USGS website (www.earthexplorer.usgs.gov) I selected images acquired during the summer season (July to September), in the daytime, with cloud cover inferior to 10%. The raw imageries were processed using the Spectral Discovery for Landsat 8 Imagery software on a high-performance super PC (40 cores, 128 GB RAM) at the Remote Sensing lab of Geosciences Montpellier. The images were created as pansharpened true color compositions with a spatial resolution of 15 m.

Additionally, I prepared false color combinations using bands B4-B3-B2 (Red/Green/Blue) using ENVI software. Those false color images were compared with the false color images of Sentinel 2B and used to map the geology along the Khovd and Ar-Khötöl fault.

1.3.1.1.4 Pleiades

Pleiades is a satellite constellation launched by CNES (the French space agency) in 2011 (Pleiades 1A) and 2012 (Pleiades 1B) to obtain high-resolution satellite images of commercial and strategic interest. These two satellites go around the earth at an altitude of 694 km in the same orbit and take images of the earth's surface with a resolution of 50 cm. Pleiades imagery is used for both civil and military usages for remote sensing applications. In 2021, two upgraded satellite (Pleiades Neo 3 and 4) joined the constellation with the capacity to deliver 30-cm-resolution images. At this moment, this new generation is available for commercial tasking but not yet for the academic community (through the Dinamis program).

Our project was supported by CNES and Equipex GEOSUD to program and acquire a tri-stereo coverage of the Ar-Khötöl surface rupture.

1.3.1.1.5 Google Earth

"Google Earth" has become a convenient tool for surveying where satellite images are not readily available. As it combines online streaming to sources of medium to high-resolution images and global elevation from SRTM, it is a versatile tool to map faults and associated features and prepare supplementary acquisitions (Pleiades images, UAV surveys, field works).

Google Earth's base imagery is provided by Landsat-8 data pansharpened at 15 m resolution which is currently being phased out and replaced by SPOT images at 2.5 m resolution. Most urban areas and part of rural areas are also covered by high-resolution images provided by the original Keyhole dataset and updated images from Maxar and CNES (Pleiades).

Locally, Google Earth images may contain unacceptable cloud or snow cover. More generally, processing is very basic and further improvements (e.g. band combinations, histogram stretching) are rendered impossible due to the high compression JPEG format used to limit bandwidth usage.

1.3.1.1.6 Bing Map

After field observations revealed that the southernmost rupture of the Ar-Khötöl segment extends further south than was previously thought, we completed our VHR satellite coverage with "Bing Map" satellite images (neither Pleiades nor Google Earth were available there). "Bing Map" is a satellite imaging search service released by Microsoft in 2009 that provides high-quality and high-resolution satellite images in some parts of the earth including from the "Bird's Eye" satellite.

Overall, I used a combination of medium-resolution satellite images to map regional features and large geomorphological landforms and very-high resolution images to identify and characterize small-scale features. I systematically explored the various providers to obtain the best images available over my area of interest.

1.3.1.2 Digital Elevation Models

Through its TanDEM program, the German Space Agency (DLR) has produced a global DEM by InSAR with a spatial resolution of 12 m. Although the product is distributed commercially, specific project calls are open to academics to obtain limited coverage free of charge. This project was awarded 11 tiles that cover the eastern border of the Mongolian Altai and most of the Khovd fault.

1.3.1.3 UAV

UAV means an unmanned aerial vehicle which is commonly known as a drone. Ground-controlled, unmanned aerial vehicles were first used and developed for military purposes in the 20th century, and in the 21st century, they have been used for civilian usages. Nowadays, UAV surveys are widely used for aerial mappings, deliveries of goods, monitoring of agriculture and forestry, peacekeeping activities, multidisciplinary scientific research etc.

For our purpose, UAV are used as a tool for remote sensing surveys with images reaching a ground resolution of ~ 5 cm, which lets us explore and characterize features previously

identified in satellite data. We deployed a commercial ready-to-use DJI Phantom 4 Pro equipped with a 20 Mpix camera and capable of performing accurate geolocation by differential GPS with respect to a fixed remote unit (Figure 11). Flight plans were prepared with the Pix4Dcapture application by defining standard grids or double grids with 70 % inline and crossline overlap and non-nadir incidence angle (typically 75-80°). This setup provides the best data to produce a high-resolution low-distortion photogrammetric DEM at half resolution and a seamless orthophoto at native resolution. Specifically, the non-nadir incidence angle is designed to counteract the well-known "doming effect" (or barrel effect) that affects photogrammetry surveys without ground control points (James & Robson, 2014).

In this project, we processed projects of several hundred images using Agisoft Metashape to derive DEMs with resolutions of 5-20 cm and orthophotos with half that resolution.

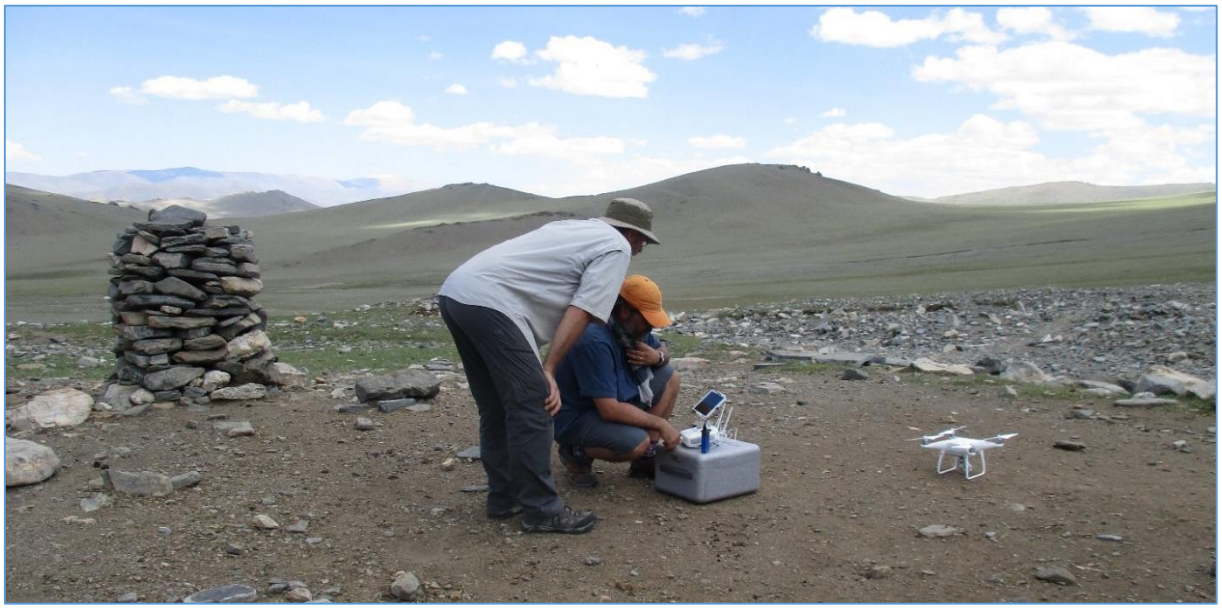

Figure 11. Setting up the DJI Phantom 4 Pro before a flight along the Khovd fault.

1.3.1.4 Terrestrial laser scanner

To survey small geomorphological features with steep slopes that cannot be properly images by UAV, we relied on a terrestrial laser scanner. The instrument used here (FARO X330, see Figure 12) is composed of a powerful green laser with a maximum range of 330 m that is distributed by a rotating mirror to scan a vertical plane. Simultaneously, the instrument rotates around its vertical axis to scan -almost- the whole sphere around it with an accuracy of a few mm at 10 m distance. The achievable resolution surpasses what is necessary for our study and is generally set to 3 mm at 10 m distance to limit survey time and data storage space. It also includes a GPS for rough geolocation, a compass, an inclinometer and an altimeter. The data

are processed via the proprietary FARO Scene software (conversion, registration and generation of point clouds), CloudCompare software (editing and filtering) and Golden Software Surfer (gridding) to produce point clouds and DEMs.

Figure 12. On the left, a photograph of "FARO Focus 3D X330" terrestrial laser scanner. On the right, a procedure of scanning a displaced gully in Davst Lake valley along the Ar-Khötöl surface rupture in July 2017.

1.3.1.5 Identification and quantification of activity

The study of landforms formed by tectonic processes played an important role in the research work. The 3 main types of faults that are strike-slip, normal, and reverse faults create their own unique landforms on the earth's surface. Nevertheless, oblique-slip faults, a combination of them, are common in nature. Therefore, their appearance on the surface can be uniform.

Strike-slip faults are mostly vertical dips and linearly elongated, thus they form landforms such as linear valleys, shutter ridges, and deflected drainages (Figure 13).

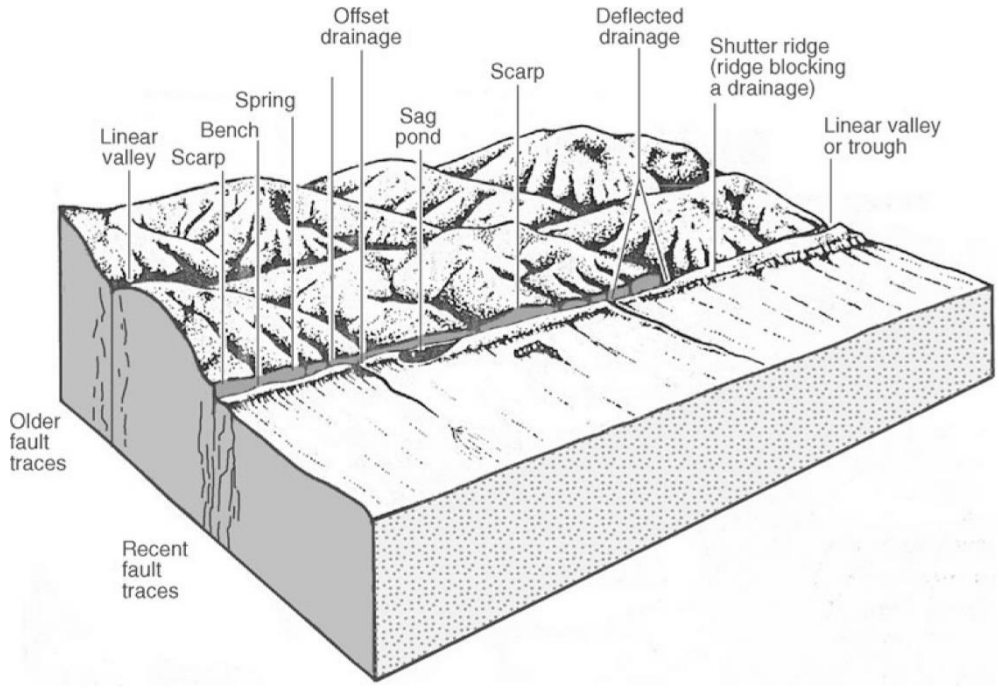

Figure 13. Assemblage of landforms associated with active strike-slip faulting. After Hengesh & Lettis, 2004.

Normal faults are produced by crustal extension. Normal faults create large rift valleys at regional scale, while at local scale they create small basins. The assemblage of landforms associated with normal faults are triangular facets of mountain fronts, horsts, and grabens. Reverse faultings are characterized by compression, thus they are responsible for crustal thickening and folding.

In my research work, I concentrated in:

- Mapping the fault scarp
- Identifying and mapping mole-tracks & tension-gashes[1]
- Defining a style of faulting
- Measuring the uplift and sink of the block on both sides of the fault scarp
- Mapping and identifying the boundaries of restraining bends and extensional basins
- Measuring the displacements of drainage networks displaced by fault
- Compiling a graphics of slip distribution and envelope (Chapter: JOM paper)
- Identifying fault junctions and segmentation
- Mapping the alluvial deposits based on origins, ages, and compositions
- Mapping moraines

[1] The morphological expressions that are called mole-tracks and tension-gashes are left behind when strike-slip faults pass through large valleys or plains with thick sedimentary deposits. Mole-tracks and tension-gashes formed by a single rupture are small, and mole-tracks and tension-gashes formed by multiple earthquakes are larger.

- Classifying the terraces formed by paleo and modern fluvial activities
- Selecting the sites of the paleoseismological investigations
- Other features associated with co-seismic and aseismic processes (Chapter: Khankh paper)

The geomorphological studies have been widely used for the research works as mentioned above.

1.3.2 InSAR interferometry

Interferometric Synthetic Aperture Radar (abbreviated as InSAR) is a methodology of remote sensing geodesy. It is based on its capacity to detect minute changes in the topography between two observations by comparing the phases of radar waves reflected by the ground surface.

Since the first use of InSAR to study the Landers earthquake in California in 1992, the technique has been used widely in earthquake research around the world to quantify co-seismic deformation fields as well as interseismic loading patterns over large regions.

In this project, InSAR was used to study the Mw 6.7 Khankh earthquake that occurred in northern Mongolia on January 12, 2021 (see Chapter 4 and Battogtokh et al., 2021).

1.3.3 Drilling

Drilling is the preferred way in order to explore the deep structure of the geological units below the ground surface. In order to figure out the deep continuities of the sedimentary layers exposed in the walls of the trench excavated in the Ulaanbaatar fault, to find out the thickness of sedimentary deposits trapped by the fault scarp, to discover the location and structure of the bedrock, and to determine the location of the fault plane at the depth, we drilled two boreholes at a vertical angle of 90˚ and an inclination of 70˚ with a total of 50 m length.

1.3.3.1 Setup

The drilling was carried out by a high-capacity SANDVIK drilling machine that is manufactured in Australia. The drilling diameter was selected as HQ standard (Borehole diameter was 75 mm).

1.3.4 Paleoseismology

Broadly speaking, Paleoseismology is the discipline that aims at characterizing the source parameters of an earthquake from its expression in the landscape. Hence, it combines i) aspects of tectonic geomorphology to determine the location, co-seismic displacement, segmentation and length of the rupture and derive the coordinates of the epicenter (or epicentral zone), its kinematics and magnitude and ii) excavation logging (hereafter referred to as trenching) to derive the age of recent surface-rupturing events.

The first aspects have been described under "Mapping active faults"; here I will focus on excavation works. The basic approach is to describe in detail the stratigraphy, faulting and folding and resulting abutting relationships to build a chronological context for faulting events. For each event, the youngest deformed strata and the oldest undeformed strata are sampled for datation to determine an age bracket for the occurrence of the earthquake.

Logically, the paleoseismological approach requires that the earthquake to be characterized left permanent traces at the surface and in the stratigraphy. Worldwide databases suggest surface rupture is generally achieved for earthquakes with Mw > 5.5-6.0 (Khilko et al., 1985; Wells & Coppersmith, 1994) but this can be modulated considering the local geology (e.g. thickness of the crust, topography). Additionally, in the time between large earthquakes, sufficient sediments must have accumulated to provide a distinct stratigraphic record, and those sedimentary layers affected by the fault should not have been washed away.

Previous studies of active faults in Mongolia suggest the recurrence period of surface-rupturing earthquakes is several thousands of years along major faults (e.g., Prentice et al., 2002; Rizza et al., 2015; Walker et al., 2015; Kurtz, 2017) and reach several tens of thousands of years along shorter structures (Bollinger et al., 2021).

1.3.4.1 Site analysis and selection

To select a site for paleoseismological investigation, several criteria should be followed. They include:

- The surface displacement should be well expressed. Hence, one would favor the central third of segments where deformation is maximum. A detailed map should also evidence sections where deformation is localized. To robustly associate a rupture with co-seismic displacement, the trench site should also be located near a deformed marker.

- Sedimentation should be adequate. Sedimentation should provide adequate stratigraphy where grain-size is significantly smaller than unit thickness, and sedimentation rates are expected to help preserve deformation without burying it too deeply. Erosional features should be identified and avoided as they may lead to the removal of deformed layers and the formation of unexpectedly large hiatuses. Hence, favorable sites for sedimentation correspond to small depressions, ponds or lakes.

As part of this thesis, we included investigations of 3 trenches such as Marmot Creek, Yellow Lake, and Broken Boulder along the Ar-Khötöl fault and 3 trenches along the Möngönmorit fault and 1 trench along the Ulaanbaatar fault. All the trenches were excavated perpendicular to the faults. Also, most of these trenches were excavated near sedimentary deposits and drainage networks where cumulative displacements were identified.

1.3.4.2 Trenching and event analysis

In order to construct the stratigraphic section of a trench wall, strata are first distinguished on the basis of their color, composition, structure, and texture. In addition, it is important to determine relationship of units, position, and stratigraphic order. Additionally, the origin of clasts that constitute units with respect to the geology of the watershed basin and evidence of weathering (e.g. carbonate coating, oxide patina) should be described.

Generally, trench exposures in Mongolia reveal some type of local bedrock (here, note that any pre-Quaternary rock may be considered as bedrock), a succession of alluvial and/or colluvial deposits and a deep brown topsoil unit, usually 10-20 cm thick.

To easily connect trench observations with the surrounding geomorphology, trench wall should be as close to a vertical wall as possible. Ideally, excavation with a backhoe or by hand should produce flat straight walls. Then, detailed cleaning with specialized tools should remove any trace of the excavation phase and reveal the stratigraphy. Oftentimes, a final step using fine brushes helps remove the finer silt and outline coarse silt and gravel layers.

At this stage, it is recommended to install grid nodes (steel nails) with a spacing of 0.5-1 m, depending on stratigraphy and planned scale for drawing. Thorough photographing of walls following a high overlap path should be carried out keeping in mind large bumps and depressions require more orientation. It is best to proceed with photographing walls before installing grid strings as they will introduce noise in the 3D model. The photographic set will be processed at the lab to produce a textured 3D model as well as an orthomosaic of the whole

trench walls. Doing so will strongly reduce geometric issues and distortions from the original photographs by projecting the 3D model onto a perfect vertical plane. To some extent, the orthomosaic may also compensate for a poorly executed wall.

Since field work conditions in Mongolia are usually somehow rough, it is generally impossible to process a photogrammetric project and produce an orthomosaic in the field. Logging is then usually performed on millimeter paper at a scale of 1:10 to 1:20.

1.3.4.3 Datation

During cleaning and logging, any material a priori suitable for datation is flagged. Once surface-rupturing events are identified in the stratigraphy and reported onto the log, layers are identified that would adequately pre-date and post-date each event and associated materials are sampled for analysis. Each sample is retrieved following a protocol specific to the datation method, wrapped, photographed and reported onto the log with its exact location within the stratigraphic section.

Large parts of Mongolia display a semi-arid climate with very limited vegetation cover and a thin organic soil. Although charcoal fragments for radiocarbon dating often preferred by paleoseismologists are rare, favorable sedimentary conditions may yield thin peat layers and paleosols (e.g. at Marmot Creek and Yellow Lake). Alternatively, bulk sediments may be sampled in search for micro-charcoals. Fine-grained stratigraphy will also be sampled for Optically-Stimulated Luminescence in case the extraction of organic matter does not yield sufficient 14C for AMS measurements. Here, sampling is performed by excavating a 20-cm-wide cube of sediment and wrapping it in aluminum foil and plastic to protect it from the light and preserve its water content and shape. The outer part will be discarded in the lab and be used for dose rate assessment.

1.4 Analysis

Most active faults in Mongolia are located along ancient structures that correspond to the boundaries of micro-blocks, far from the boundaries of the large tectonic plates. Faulting along those micro-blocks is reactivated by the distant Indo-Eurasian collision or the extension of Lake Baikal, as confirmed by multidisciplinary studies in geology and geophysics. Striking examples are the large active faults that produced Mw 7.5+ earthquakes in the last centuries, such as the Ar-Khötöl fault (Mw ~7.8 possibly in 1761) in the Mongolian Altai Mountain Range, the Ikh-

Bogd fault (Mw 8.1 in 1957) in the Gobi-Altai Mountain Range and the Bulnai fault (Mw 8.3 in 1905). The same context is also capable of activating smaller structures such as the Mogod fault (Mw 7.1 in 1967) in the Khangai Mountains.

In this work, I will analyze systematic offset measurements, slip variations along strike and timing of surface-rupturing earthquakes following a now standard and robust paradigm that combines scaling laws, structural long-term segmentation, slip distribution (short-term) segmentation and recurrence patterns described hereafter.

1.4.1 Scaling laws

A number of studies have reported that co-seismic offsets along a fault depend on the length of the fault (e.g. Khilko et al., 1985; Wells & Coppersmith, 1994; Willemse, 1997; Kurushin et al., 1997; Burbank & Anderson, 2001; Kim & Sanderson, 2005; Kondo et al., 2010; Choi et al., 2018) and argue that longer faults tend to produce larger co-seismic offsets.

Table 2. Relations between magnitude, rupture length and co-seismic offset.

Counrty	**Earthquake**	**Year**	**Type**	**Magnitude**	**Rupture Length (km)**	**Maximum Offset (m)**	**Average Offset (m)**	**Reference**
Mongolia	Ar-Hötöl	1761	RL[1]	7.8 (Mw)	238	4.8 ± 0.5		This study
Japan	Nobi	1891	LL[2]	8.0	80	**8.0**	**5.04**	Wells
Mongolia	Bulnai	1905	LL	8.2	388	**~6.5**	**6.3±0.9**	Choi
USA	San Francisco	1906	RL	7.8	432	**6.1**	**3.3**	Wells
USA	Imperial Valley	1940	RL	7.2	60	**5.9**	**1.5**	Wells
Turkey	Bolu-Gerede	1944	RL	7.4	180	**6**		Kondo
Mongolia	Gobi-Altai	1957	LL	8.1	270	**5-7**	**3 - 4**	Kurushin
Mongolia	Mogod	1967	RL R[3]	7.1	45	**2.5**	**1.5**	Khilko Bayasgalan
Iran	Dasht-e-Bayaz	1968	LL	7.1	80	**5.2**	**2.3**	Wells
Algeria	El Asnam	1980	R	7.3	31.2	**6.5**	**1.54**	Wells
New Zealand	Edgecumbe	1987	N[4]	6.6	18	**2.9**	**1.7**	Wells
USA	Landers	1992	RL	7.6	71	**6.0**	**2.95**	Wells
References: Wells – Wells & Coppersmith, 1994; Kondo – Kondo et al., 2010; Kurushin – Kurushin et al., 2012; Khilko – Khilko et al., 1985; Bayasgalan – Bayasgalan & Jackson, 1999.								

[1]RL – Right lateral strike-slip fault
[2]LL – Left lateral strike-slip fault
[3]R – Reverse
[4]N – Normal

A co-seismic offset is the amount of slip observed at the surface when two blocks separated by a fault move relative to each other during an earthquake on that fault. The amount of slip depends on the magnitude of the earthquake and the kinematics of the fault (see Table 2 for examples and Wells & Coppersmith, 1994 for more details).

1.4.2 Structural segmentation

General observations reflected by scaling laws suggest that the total length of a surface rupture is also dependent on the magnitude of the causative earthquake. At various scales, the surface rupture may appear variously segmented, i.e. discontinuous, and formed by several - possibly many - apparently individual segments separated by geometrical complexities such as changes in azimuth and/or dip and step-overs (e.g. jogs, bends and pull-apart basins). Over time, stable complexities may grow in size and form major markers in the landscape such as cross-cutting drainages.

The sizes of restraining and releasing steps between segments (Wesnousky, 1988; Harris & Day, 1993; Du & Aydin, 1995; Wesnousky, 2006; Choi et al., 2012; Finzi & Langer, 2012) and deviation angles between fault segments (Klinger, 2010; Biasi & Wesnousky, 2017) may have a significant effect on the fault propagation and termination. Considering the length of a rupture is an important parameter to assess the likely magnitude of associated earthquakes, characterizing compressional and extensional steps may have a crucial impact on seismic hazard assessment.

For instance, Kurtz et al (2018) divided the 270 km of surface rupture that was produced by the Mw 8.1 earthquake in 1957 Great Bogd fault into 15 distinct segments. More generally, Klinger (2010) suggests that the average length of segments is 17.9 km ± 5.2 km and the maximum length is ~25 km for continental strike-slip earthquakes, which may reflect the thickness of the seismogenic crust. However, it should be noted that lengths of segmentations are not absolutely fixed as Klinger (2010). The Bulnai surface rupture of 388 km long, which was formed by the 1905 Mw 8.3 earthquake, displays segments over 50 km long (Choi et al., 2018). Similarly, I show here that the Ar-Khötöl surface rupture also displays segments of as long as 51 km, which are preserved across multiple earthquakes (recording the multiple envelopes).

At a wider scale, the Ar-Khötöl segment is part of the ~ 600-km-long Khovd fault that is itself comprised of several faults susceptible to produce major to great earthquakes. Over time, such faults may also interact with each other and modulate a neighboring fault's internal clock.

Similarly, the main southern strand of the East Anatolian fault system (Duman & Emre, 2013) is 580 km long between Karliova and Antakya. It consists of 11 discrete faults that ruptured in historical and instrumental times (Figure 14). In addition, the North Anatolian fault system (Kondo et al., 2010) extends ~1200 km and consists of more than 10 discrete faults (Figure 15). Those faults also consist of many segments in them.

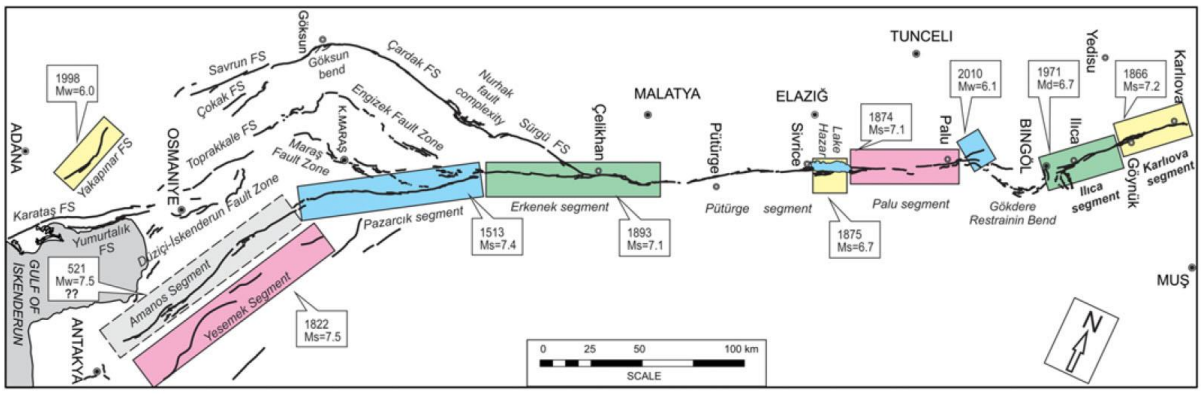

Figure 14. Distinct surface ruptures that produced by large earthquakes during the XIXth-XXth centuries along the East Anatolian Fault. Ruptured faults are highlighted by colored rectangles. After Duman & Emre (2013).

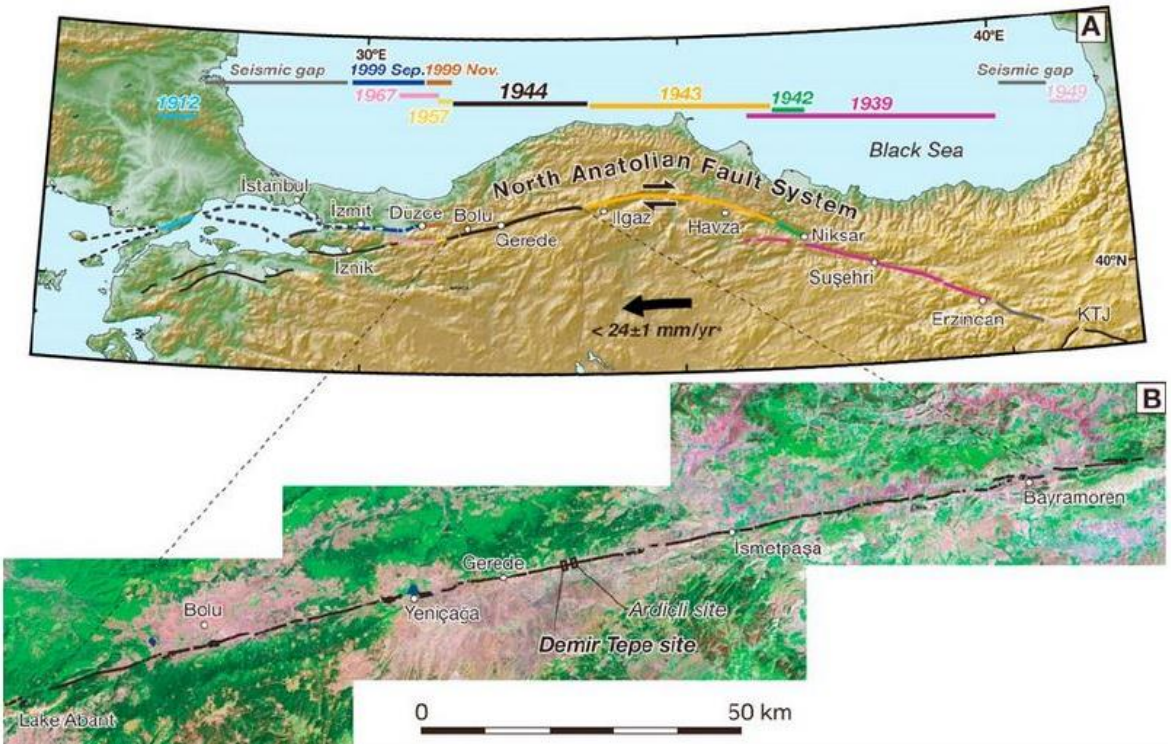

Figure 15. Spatial and temporal distribution of large earthquakes in the XXth century along the North Anatolian fault system and the 1944 Bolu-Gerede earthquake rupture. After Kondo et al (2010).

The Ar-Khötöl surface rupture may be the key to unlock the Khovd fault. If the 1761 earthquake had not occurred, the Khovd fault could be divided into an unresolved number of distinct faults. Moreover, it would be uncertain how extended a single-event surface rupture could be. Once

the trace of the Ar-Khötöl surface rupture is clear, it is possible to map the other parts of the other faults that consist of the Khovd fault, continuing from the southern and northern ends of the Ar-Khötöl surface rupture.

1.4.3 Rupture process and segmentation

1.4.4 Slip distribution

Considering the ideal and simplified case of an elliptical rupture intersecting the surface, coseismic slip would be expected to be zero at the tip of fault, while the maximum value is around the center of fault as illustrated by Kim & Sanderson (2005) in Figure 16. The overall surface slip distribution would displays a roughly elliptical shape as well.

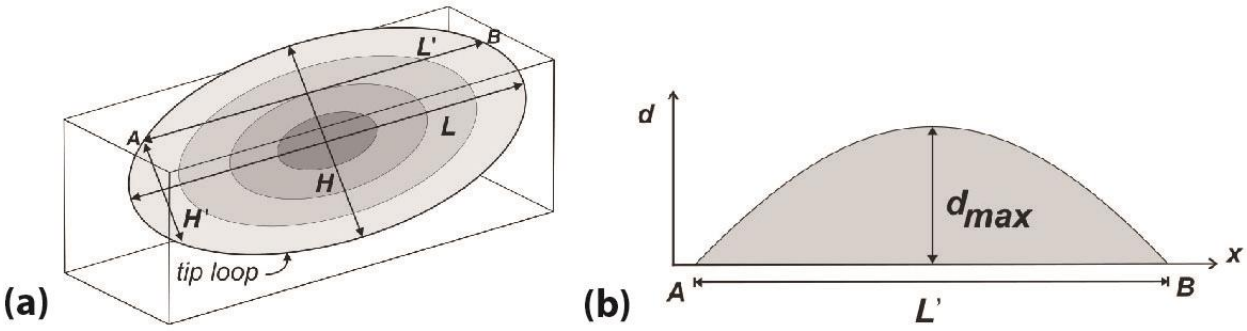

Figure 16. (a) Diagram to illustrate displacement distribution on an elliptical fault surface of length (L) and height (H); density of shading increasing with increasing displacement towards center of fault. The fault intersects the upper surface of the block along line A-B. (b) Displacement (d)-distance (x) plot of fault trace along line A-B. After Kim & Sanderson, 2005.

Unsurprisingly, natural observations somehow differ, especially where ruptures exhibit complexity. For example, Willemse (1997) documented the displacement patterns of 7 short fault segments (~100 m long) found in the Bishop Tuff (Figure 17). The outermost segments are asymmetric, and the maximum displacement is towards the center of the fault. The central 3 segments show a more symmetrical slip distribution. The maximum displacement is at the central segment while the minimum displacement is at the outer ends of the marginal segments, thus suggesting interaction between the different segments and synchronous breaking into a composite rupture.

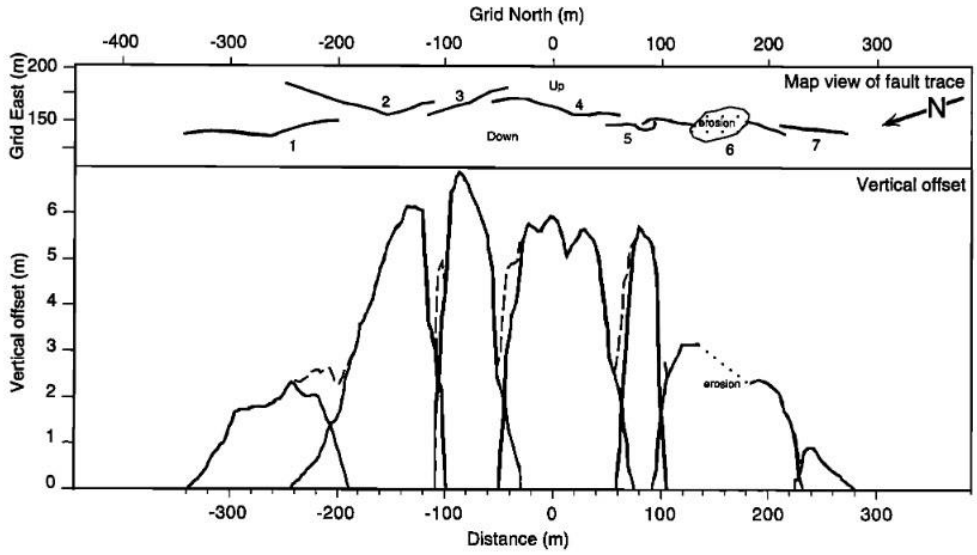

Figure 17. The 2-D slip distributions along segmented normal fault in the Bishop Tuff, California. Numbers on the fault trace map identify the seven segments. The distribution of vertical offset along the various segments is asymmetric on the distal segments and more symmetric on the central segments. The slip-to-length ratio is greatest on the central segments. Dashed line indicate aggregate of all segments but does not include the extra offset accommodated by rotation of bedding in the relay zones. After Willemse (1997).

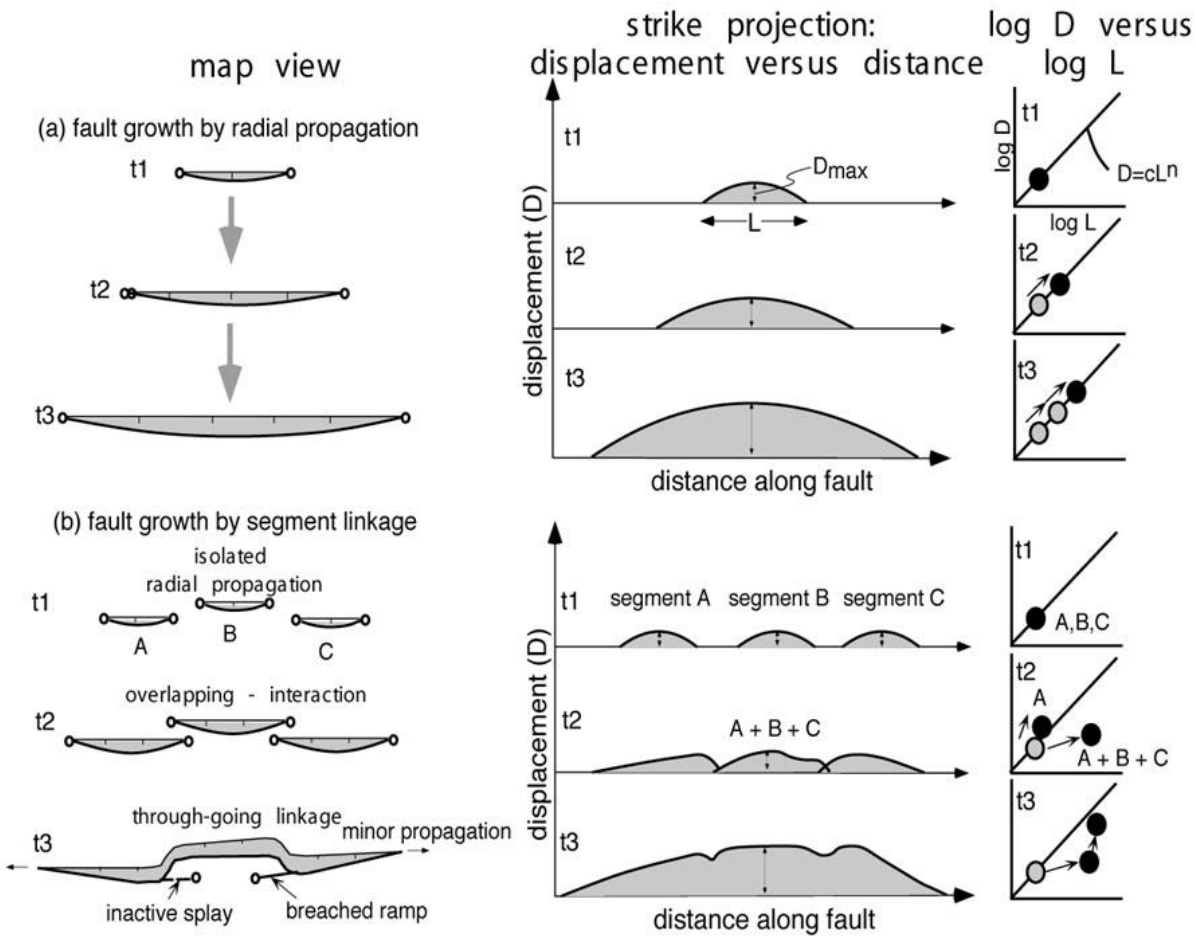

Figure 18. The two models for fault evolution. After Burbank & Anderson (2001).

A fault may extend in a straight line or a fault may extend as a segment. Burbank & Anderson (2001) showed that in the long term, the length of fault due to multiple earthquakes can increase displacement of fault (Figure 18). When the fault extends in a straight line, displacements of fault and length of fault are linearly related, but when fault extends in a segmental manner, displacements of fault are the same at time t1 and t2, and becomes larger at time t3 when fault segments start to connect to each other.

This type of case is observed on the slip distribution graphics of the Ar-Khötöl surface rupture. For example, segments S1, S2, S3 of the northern margin and S9, S10, S11 of the southern margin, which are divided based on the fault geometry, are divided into single segments as northernmost and southernmost segments based on the slip envelope.

1.4.5 Event recurrence

Active fault could produce large earthquakes at regular intervals if constant stress acts on fault.

The earthquake recurrence between historic or prehistoric events may be regular or greatly regular over several seismic cycles (Dolan et al. 2007; Goes 1996; Schwartz and Coppersmith 1984; Sieh et al. 1989; Thatcher 1984; Thatcher 1990; Weldon et al. 2004).

In recent years, there has been a increasing number of publications focusing on paleoseismological investigations on active faults in Mongolia (Prentice et al., 2002; Walker et al., 2006; Imaev et al., 2012; Rogozin et al., 2013; Rizza et al., 2015; Walker et al., 2015; Al-Ashkar, 2015; Smekalin et al., 2016; Kurtz, 2017; Suzuki et al., 2021; Bollinger et al., 2021; Al-Ashkar et al., 2022) but only few works have reported precisely defined recurrence periods.

Ritz et al (2003) determined the recurrence interval of the Ikh Bogd fault, the main representative fault in the Gobi-Altai Mountain Range, to be 3.7±1.3 kyr based on the age of the alluvial sediments displaced by the fault.

Kurtz (2017) noted that the active structure of the western part of the Gobi-Altai Range is more complex than the eastern part. The deformation in this area is concentrated on two major left-lateral strike-slip faults that are the West Bogd fault and the Valley of Lake fault. It has been concluded that earthquakes of magnitude Mw7.6-8 are likely to occur on these two faults every 3000-4000 years.

Rizza et al (2015), based on paleoseismological study, estimated the recurrence interval of two large earthquakes preceding the 1905 magnitude 8.3 earthquake on the Bulnai fault to be ~2700-4000 years.

Summing up the results of the above research works, the recurrence period of active faults on the territory of Mongolia is 3000-5000 years. GPS velocity (Calais & Amarjargal, 2000; Calais et al., 2006; Vergnolle et al., 2007) shows that the crustal deformation in the Mongolian Altai and Gobi-Altai Mountains are faster in comparison with the Khangai and Khentii Domes.

1.5 References

Adiya, M. (2021). The Earthquake. Book (in Mongolian), 112 p.

Al-Ashkar, A. (2015). Active tectonics of the Ulaanbaatar region, Mongolia. Morphotectonic and paleoseismological analysis of the active faults of Sharkhai and Avdar. PhD thesis. *University of Strasbourg.*

Al-Ashkar, A., Schlupp, A., Ferry, M., & Munkhuu, U. (2022). Tectonic Geomorphology and Paleoseismology of the Sharkhai fault: a new source of seismic hazard for Ulaanbaatar (Mongolia). *Solid Earth, 13*, 761-777. https://doi.org/10.5194/se-13-761-2022

Arjannikova, A., Larroque, C., Ritz, J.-F., Deverchere, J., Stephan, J. F., Arjannikov, S., & San'kov, V. (2004). Geometry and kinematics of recent deformation in the Mondy-Tunka area (south-westernmost Baikal rift zone, Mongolia-Siberia). *Terra Nova, 16*, 265-272. https://doi:10.1111/j.1365-3121.2004.00565.x

Badarch, G., Cunningham, W. D., & Windley, B. F. (2002). A new terrane subdivision for Mongolia: implications for the Phanerozoic crustal growth of Central Asia. *Journal of Asian Earth Sciences, 21*, 87-110. https://doi.org/10.1016/S1367-9120(02)00017-2

Baljinnyam, I., Bayasgalan, A., Borisov, B. A., Cisternas, A., Dem'yanovich, M. G., Ganbaatar, L., … Vashchilov, Yu. Ya. (1993). Ruptures of major earthquakes and active deformation in Mongolia and its surroundings. *Geological Society of America*.

Barry, T. L., Saunders, A. D., Kempton, P. D., Windley, B. F., Pringle, M. S., Dorjnamjaa, D., & Saandar, S. (2003). Petrogenesis of Cenozoic Basalts from Mongolia: Evidence for the role of Asthenospheric versus Metasomatized Lithospheric Mantle Sources. *Journal of Petrology*, *44*(1), 55-91.

Barth, A., & Wenzel, F. (2010). New constraints on the intraplate stress field of the Amurian plate deduced from light earthquake focal mechanisms. *Tectonophysics*, *482*(2010), 160-169. https://doi.org/10.1016/j.tecto.2009.01.029

Battogtokh, D., Bayasgalan, A., Wang., K., Ganzorig, D., & Bayaraa, J. (2021). The 2021 Mw 6.7 Khankh earthquake in the Khuvsgul rift, Mongolia. https://doi.org/10.5564/mgs.v26i52.1361

Battogtokh, D., Ferry, M., Ritz, J.-F., & Munkhuu, U. (2022). The Ar-Hötöl surface rupture along the Khovd fault (Mongolian Altay). *Journal of Maps.* https://doi.org/10.1080/17445647.2022.2132884

Bayasgalan, A., & Jackson, J. A. (1999). A re-assessment of the faulting in the 1967 Mogod earthquakes in Mongolia. *Geophysical Journal International, 138*, 784-800.

Bayasgalan, A., Jackson, J., & McKenzie, D. (2005). Lithosphere rheology and active tectonics in Mongolia: relations between earthquake source parameters, gravity and GPS measurements. *Geophysical Journal International, 163*(3), 1151-1179. https://doi.org/10.1111/j.1365-246X.2005.02764.x

Berkey, C. P., & Morris, F. K. (1927). Geology of Mongolia, in Natural History of Central Asia. *American Central Asiatic Expedition*. New York.

Biasi, G. P., & Wesnousky, S. G. (2017). Bends and Ends of Surface Ruptures. *Bulletin of the Seismological Society of America, 107*(6), 2543-2560. https://doi:10.1785/0120160292

Bird, P. (2003). An updated digital model of plate boundaries. *Geochemistry, Geophysics, Geosystems, 4*, 1-52. https://doi.org/10.1029/2001GC000252

Bobrov, B. A., Baldan, O., & Marinov, N. A. (1959). The Earthquake that occurred in Gobi-Altay Mountains (in Russian and Mongolian). 147 p.

Bollinger, L., Klinger, Y., Forman, S. L., Chimed, O., Bayasgalan, A., Munkhuu, U., … Sodnomsambuu, D. (2021). 25,000 Years long seismic cycle in a slow deforming continental region of Mongolia. *Scientific Reports.* https://doi.org/10.1038/s41598-021-97167-w

Burbank, D. W., & Anderson, R. S. (2001). Tectonic Geomorphology. Blackwell Publishing. 274 p.

Byamba, J. (2009). Geology and Mineral Resources of Mongolia. Lithospheric Plate tectonics, IV, 495 p.

Calais, E., & Amarjargal, S. (2000). New constraints on current deformation in Asia from continuous GPS measurements at Ulan Baatar, Mongolia. *Geophysical Research Letter, 27*(10). https://doi.org/10.1029/1999GL005444

Calais, E., Vergnolle, M., Deverchere, J., San'kov, V., Lukhnev, A., & Amarjargal, S. (2002). Are post-seismic effects of the M=8.4 Bolnay earthquake (1905 July 23) still influencing GPS velocities in the Mongolia-Baikal area? *Geophysical Journal International, 149*, 157-168.

Calais, E., Vergnolle, M., San'kov, V., Lukhnev, A., Miroshnitchenko, A., Amarjargal, S., & Deverchere, J. (2003). GPS measurements of crustal deformation in the Baikal-Mongolia area (1994-2002): Implications for current kinematics of Asia. *Journal of Geophysical Research, 108*(B10), 2501. https://doi.org/10.1029/2002JB002373

Choi, J. H., Jin, K., Enkhbayar, D., Davaasambuu, B., Bayasgalan, A., & Kim, Y. S. (2012). Ruptures propagation inferred from damage patterns, slip distribution, and segmentation of the 1957 M_w8.1 Gobi-Altay earthquake rupture along the Bogd fault, Mongolia. *Journal of Geophysical Research, 117*, B12401. https://doi:10.1029/2011JB008676

Choi, J. H., Klinger, Y., Ferry, M., Ritz, J. F., Kurtz, R., Rizza, M., & Demberel, S. (2018). Geologic inheritance and earthquake rupture processes: The 1905 M≥8 Tsetserleg-Bulnay strike-slip earthquake sequence, Mongolia. *Journal of Geophysical Research: Solid Earth, 123.* https://doi.org/10.1002/2017JB013962

Cunningham, W. D. (1998). Lithospheric controls on late Cenozoic construction of the Mongolian Altai. *Tectonics, 17*, 891-902.

Cunningham, W. D. (2005). Active intracontinental transpressional mountain building in the Mongolian Altai: Defining a new class of orogen. *Earth and Planetary Science Letters*, 436-444.

Cunningham, W. D., Windley, B. F., Dorjnamjaa, D., Badamgarav, G., & Saandar, M. (1996). A structural transect across the Mongolian Western Altai: Active transpressional mountain building in central Asia. *Tectonics, 15*, 142-156.

Delouis, B., Deverchere, J., Melnikova, V., Radziminovitch, N., Loncke, L., Larroque, C., & San'kov, V. (2002). A reappraisal of the 1950 (Mw 6.9) Mondy earthquake, Siberia, and its relationship to the strain pattern at the south-western end of the Baikal rift zone. *Terra Nova, 14*, 491-500.

Devyatkin, E. V. (1974). Structures and formational complexes of the Cenozoic activated stage (in Russian), in Tectonics of the Mongolian People's Republic. *Nauka*, 182-195. Moscow.

Devyatkin, E. V. (1975). Neotectonic structures of western Mongolia (in Russian), in Mesozoic and Cenozoic tectonics and Magmatism of Mongolia. *Nauka*, 264-282. Moscow.

Devyatkin, E. V. (1981). Cenozoic of Inner Asia (Stratigraphy, Geochronology, Correlation). *Nauka*, Moscow, 196. (In Russian)

Devyatkin, E. V., & Shuvalov, V. F. (1990). The continental Mesozoic and Cenozoic of Mongolia (stratigraphy, geochronology and paleogeography). *Nauka*, 165-177. Moscow.

Dolan, J. F., Bowman, D. D., & Sammis, C. G. (2007). Long-range and long-term fault interactions in Southern California. *Geology, 35*(9), 855-858. https://doi:10.1130/G23789A.1

Du, Y., & Aydin, A. (1995). Shear fracture patterns and connectivity at geometric complexities along strike-slip faults. *Journal of Geophysical Research, 100*(B9), 18,093-18,102.

Dugarmaa, T., Schlupp, A., Adiya, M., Ankhtsetseg, D., Baasanbat, T., Bayar, G., … Urtnasan, Kh. (2002). One Century of Seismicity in Mongolia (1900-2000). *RCAG-DASE*.

Dugarmaa, T., Schluppe, A., Adiya, M., Baasanbat, Ts., Battulga, B., Batsaikhan, Ts., … Bayasgalan, A. (2006). Seismic Hazard Assessment of Ulaanbaatar, capital of Mongolia. Seismic micro zoning map. Research Center of Astronomy and Geophysics of Mongolian Academy of Sciences.

Duman, T. Y., & Emre, Ö. (2013). The East Anatolian Fault: geometry, segmentation and jog characteristics. *Geological Society, London, Special Publications, 372*, 495-529. http://dx.doi.org/10.1144/SP372.14

Florensov, N. A., & Solonenko, V. P. (1963). The Gobi Altai earthquake (book).

Filippov, L. V., Lipovskiy, Y. O., & Kapitonova, T. A. (1976). Central Mongolian potassic basaltoids and abyssal magma formation. *Geochemistry International, 13*, 106-118.

Finzi, Y., & Langer, S. (2012). Damage in step-overs may enable large cascading earthquakes. *Geophysical Research Letter, 39*(L16303). https://doi:10.1029/2012GL052436

Frankel, K. L., Wegmann, K. W., Bayasgalan, A., Carson, R. J., Bader, N. E., Adiya, Ts., … & Gregory, L. (2010). Late Pleistocene slip rate of the Höh Serh-Tsagaan Salaa fault

system, Mongolian Altai and intracontinental deformation in central Asia. *Geophysical Journal International, 183*, 1134-1150. https://doi:10.1111/j.1365-246X.2010.04826.x

Goes, D. B. (1996). Irregular recurrence of large earthquakes: An analysis of historic and paleoseismic catalogs. *Journal of Geophysical Research*. https://doi.org/10.1029/95jB03044

Gongor, D. (1964). The History of the Khovd. The Institute of History of the Mongolian Academy of Sciences. (In Mongolian)

Gregory, L. C. (2012). Active Faulting and Deformation of the Mongolian Altay Mountains. PhD thesis. *University of Oxford*.

Gregory, L. C., Thomas, A. L., Walker, R. T., Garland, R., Mac Niocaill, C., Fenton, C. R., … West, A. J. (2014). Combined uranium series and ^{10}Be cosmogenic exposure dating of surface abandonment: A case study from the Ölgiy strike-slip fault in western Mongolia. *Quaternary Geochronolgy*, *24*, 27-43. https://dx.doi.org/10.1016/j.quageo.2014.07.005

Gu, G., Lin, T., Shi, Z., Li, Q., Lu, S., Chen, H., … Wang, S. (1989). Catalogue of Chinese Earthquakes (1831 B.C.-1969 A.D.). *Science Press, Beijing*, China.

Harris, R. A., & Day, S. M. (1993). Dynamics of Fault Interaction: Parallel Strike-Slip Faults. *Journal of Geophysical Research, 98*(B3), 4461-4472.

Hengesh, J. V., & Lettis, W. R. (2004). Characterization of surface rupture hazards for BTC pipeline fault crossings, Turkey. Active Tectonic Environments and Seismic Hazards. 220-263 p.

Howard, J. P. (2004). A multi-disciplined field-based study of sedimentary basin evolution along seismically active transpressional fault systems in the Mongolian Altai. (PhD thesis), *University of Leicester, Leicester (UK)*.

Hunt, A. C., Parkinson, I. J., Harris, N. B. W., Barry, T. L., Rogers, N. W., & Yondon, M. (2012). Cenozoic volcanism on the Hangai Dome, Central Mongolia: Geochemical evidence for changing melt sources and implications for mechanism of melting. *Journal of Petrology, 53*, 1913-1942. https://doi:10.1093/petrology/egs038

Imaev, V. S., Smekalin, O. P., Strom, A. L., Chipizubov, A. V., & Syas'ko, A. A. (2012). Seismic-hazard assessment for Ulaanbaatar (Mongolia) on the basis of seismogeological studies. *Russian Geology and Geophysics, 53*(2012), 906-915.

Ionov, D. A. (2007). Compositional variations and heterogeneity in fertile lithospheric mantle: peridotite xenoliths in basalts from Tariat, Mongolia. *Contributions to Mineralogy and Petrology, 154*, 455-477.

Ivanov, A. V. (2004). One rift, two models. *Science First Hand, 1*, 50-62.

James, M. R., & Robson, S. (2014). Sequential digital elevation models of active lava flows from ground-based stereo time-lapse imagery. *ISPRS Journal of Phogrammetry and Remote Sensing, 97*, 160-170. https://doi.org/10.1016/j.isprsjprs.2014.08.011

Jolivet, M., Arzhannikov, S., Chauvet, A., Arzhannikova, A., Vassallo, R., Kulagina, N., & Akulova, V. (2012). Accommodating large-scale intracontinental extension and compression in a single stress-field: A key example from the Baikal Rift System. *Gondwana Research*, GR-00891. http://dx.doi.org/10.1016/j.gr.2012.07.017

Jolivet, M., Ritz, J.-F., Vassallo, R., Larroque, C., Braucher, R., Todbileg, M., … Arzhanikov, S. (2007). Mongolian summits: An uplifted, flat, old but still preserved erosion surface. *Geology, 35*(10), 871-874. http://doi:10.1130/G23758A.1

Keller, E. A., & Pinter, N. (2002). Active Tectonics (Earthquakes, Uplift, and Landscape). Second Edition. Prentice Hall Earth Science Series, Upper Saddle River, New Jersey 07458. 362 p.

Khil'ko, S. D., Kurushin, R. A., Kochetkov, V. M., Baljinnyam, I., & Munkhuu, D. (1985). Strong earthquakes, paleoseismogeological and macroseismic data, in earthquakes and the bases for seismic zoning of Mongolia. The joint Soviet-Mongolian scientific geological research expedition. *Nauka*, Moscow.

Kim, Y.-S., & Sanderson, D. J. (2005). The relationship between displacement and length of faults: a review. *Earth-Science Reviews, 68*, 317-334. https://doi:10.1016/j.earscirev.2004.06.003

King, G. C., Nabelek, J. (1985). The role of fault bends in the initiation and termination of earthquake rupture. *Science, 228*, 984-987. https://doi.org/10.1126/science.228.4702.984

Klinger, Y. (2010). Relation between continental strike-slip earthquake segmentation and thickness of the crust. *Journal of Geophysical Research, 115*(B07306). https://doi:10.1029/2009JB006550

Kondorskaya, N. B., Shebalin, N. B., & Khrometskaya, E. A. (1977). New Catalogue of Large Earthquakes in USSR, *Nauka* (In Russian).

Kondo, H., Özaksoy, V., & Yildirim, C. (2010). Slip history of the 1944 Bolu-Gerede earthquake rupture along the North Anatolian fault system: Implications for recurrence behavior of multisegment earthquakes. *Journal of Geophysical Research, 115*(B04316). http://doi:10.1029/2009JB006413

Kozhevnikov, A. V., Savin, V. E., & Uflyand, A. K. (1970). The history of development of the Hangay upland in the Mesozoic and Cenozoic (in Russian), in Geology of the Mesozoic and Cenozoic of western Mongolia. *Nauka*, 151-169. Moscow.

Kurtz, R. (2017). Late-Pleistocene to Holocene spatio-temporal evolution of the seismic deformations in the Gobi-Altay mountain range, Mongolia: morphotectonical and paleoseismological approaches. PhD Thesis. The Geosciences Montpellier of the University of Montpellier.

Kurtz, R., Klinger, Y., Ferry, M., & Ritz, J-F. (2018). Horizontal surface-slip distribution through several seismic cycles: the Eastern Bogd fault, Gobi-Altai, Mongolia. *Tectonophysics*. https://doi:10.1016/j.tecto.2018.03.011

Kurushin, R. A., Bayasgalan, A., Ölziybat, M., Enhtuvshin, B., Molnar, P., Bayarsayhan, Ch., … Lin, J. (1997). The Surface Rupture of the 1957 Gobi-Altay, Mongolia, Earthquake. The Geological Society of America. *Special Paper, 320*.

Logatchev, N. A. (1993). History and geodynamics of the lake Baikal rift in the context of the eastern Siberia rift system: A review. *Bulletin – Centres de Recherches Exploration – Production Elf – Aquitaine, 17*(2), 353-370.

Melnikov, A. I., Mazukabkzov, A. M., Sklyarov, E. V., & Vasiljev, E. P. (1994). Baikal rift basement: Structure and tectonic evolution. *Bulletin du Centre de Recherches Exploration-Production Elf Aquitaine, 18*(1), 99-122.

Molnar, P., & Tapponnier, P. (1975). Cenozoic tectonics of Asia: Effects of a continental collision. *Science, 189*(4201), 419-426. https://doi.org/10.1126/science.189.4201.419

Munkhuu, U. (2006). The 2003 Chuya sequence (North Altay range): tectonic context and seismological study. PhD Thesis. Universite De Nice-Sophia Antipolis – UFR Sciences.

Mushketov, I., & Orlov, A. (1893). The Catalogue of the Earthquakes in the Russian Empire (in Russian). Saint Petersburg. 599 p.

Nissen, E., Walker, R., Bayasgalan, A., Carter, A., Fattahi, M., Molor, E., … Xu, S. (2009). The late Quaternary slip-rate of the Har-Us-Nuur fault (Mongolian Altai) from cosmogenic ^{10}Be and luminescence dating. *Earth and Planetary Science Letters, EPSL-09924*, 12 p. https://doi:10.1016/j.epsl.2009.06.048

Odonbaatar, Ch., Ulziibat, M., Battogtokh, D., … Dugarmaa, T. 2015. Micro-zoning map (1:10,000 scale) of Ulaanbaatar city and its satellite districts (in Mongolian). The Institute of Astronomy and Geophysics of Mongolian Academy of Sciences. Ulaanbaatar.

Odonbaatar, Ch., Ulziibat, M., Battogtokh, D., Baatarsuren, G., Bayasgalan, A., Mungunsuren, D., … Janbolat, M. (2017). Engineering-geological, hydrogeological, seismic, and technical research aimed at mapping the seismic micro-zoning of provinces, districts, and settlements, and determining the seismic hazard assessment (in Mongolian). The Institute of Astronomy & Geophysics of Mongolian Academy of Sciences. Ulaanbaatar.

Petit, C., Deverchere, J., Calais, E., San'kov, V., & Fairhead, D. (2002). Deep structure and mechanical behavior of the lithosphere in the Hangai-Hövsgöl region, Mongolia: new constraints from gravity modeling. *Earth and Planetary Science Letters, 197*, 133-149.

Prentice, C. S., Kendrick, K., Berryman, K., Bayasgalan, A., Ritz., & Spencer, J. Q. (2002). Prehistoric ruptures of the Gurvan Bulag fault, Gobi Altay, Mongolia. *Journal of Geophysical Research, 107*, B12, 2321. https://doi.org/10.1029/2001JB000803

Ritz, J.-F., Arzhannikova, A., Vassallo, R., Arzhannikov, S., Larroque, C., Michelot, J.-L., Massault, M. (2018). Characterizing the present-day activity of the Tunka and Sayan faults within their relay zone (western Baikal rift system, Russia). *Tectonics, 37*, 1376-1392. https://doi.org/10.1002/2017TC004691

Ritz, J.-F., Bourles, D., Brown, E. T., Carretier, S., Chery, J., Enhtuvshin, B., … Yiou, F. (2003). Late Pleistocene to Holocene slip rates for the Gurvan Bulag thrust fault (Gobi-Altay, Mongolia) estimated with ^{10}Be dates. *Journal of Geophysical Research, 108*(B3), 2162. http://doi:10.1029/2001JB000553

Ritz, J. F., Brown, E. T., Bourles, D. L., Philip, H., Schlupp, A., Raisbeck, G. M., … Enkhtuvshin, B. (1995). Slip rates along active faults estimated with cosmic-ray-exposure dates: Application to the Bogd fault, Gobi-Altai, Mongolia. *Geology, 23*(11), 1019-1022.

Ritz, J.-F., Vassallo, R., Braucher, R., Brown, E. T., Carretier, S., & Bourles, D. L. (2006). Using in situ-produced ^{10}Be to quantify active tectonics in the Gurvan Bogd mountain range (Gobi-Altay, Mongolia). *Geological Society of America, Special Paper, 415*, 87-110. http://doi:10.1130/2006.2415(06)

Rizza, M., Ritz, J.-F., Prentice, C., Vassallo, R., Braucher, R., Larroque, C., & ASTER Team. (2015). Earthquake Geology of the Bulnay Fault (Mongolia). *Bulletin of the Seismological Society of America, 105*(1). https://doi:10.1785/0120140119

Rogozin, E. A., Lar'kov, A. S., Demberel, S., & Battulga, B. (2013). Recurrence of Strong Earthquakes in the Active Hovd Fault Zone, Mongolian Altay. *Geotectonics, 47*(5), 340-350.

Sankov, V. A., Parfeevets, A. V., Miroshnitchenko, A. I., Lukhnev, A. V., & Arzhannikova, A. V. (2003). Cenozoic dynamics of Baikal and Khubsugul basins. *International Symposium – Speciation in Ancient Lakes*, SIAL III – Irkutsk, September 2-7, 2002.

Schlupp, A., & Cisternas, A. (2007). Source history of the 1905 great Mongolian earthquakes (Tsetserleg, Bolnay). *Geophysical Journal International, 169*(3), 1115-1131. https://doi:10.1111/j.1365-246X.2007.03323.x

Schwartz, D. P., & Coppersmith, K. J. (1984). Fault Behavior and Characteristic Earthquakes: Examples From the Wasatch and San Andreas Fault Zones. *Journal of Geophysical Research, 89*(B7), 5681-5698.

Sengor, A. M. C., & Natal'in, B. A. (1996). Paleotectonics of Asia: Fragments of a synthesis, in the Tectonic Evolution of Asia. *Cambridge University Press, 486-640*. New York.

Sieh, K., Stuiver, M., & Brillinger, D. (1989). A more precise chronology of earthquakes produced by the San Andreas Fault in southern California. *Journal of Geophysical Research, 94*(B1), 603-623. https://doi.org/10.1029/jB094iB01p00603

Smekalin, O. P., Chipizubov, A. V., & Imaev, V. S. (2016). Seismogeology of Verkhnekerulen basin (Khentei, Northern Mongolia). *Geodynamics & Tectonophysics, 7*(1), 39-57. http://dx.doi.org/10.5800/GT-2016-7-1-0196

Sodnom, N., Yanshin, A.L., Tsegmid, Sh., Vorobiev, V.V., and others. 1990. The National Atlas of the Mongolian People's Republic. USSR, Minsk.

Suzuki, Y., Nakata, T., Watanabe, M., Battulga, S., Enkhtaivan, D., Demberel, S., … Badral, T. (2021). Discovery of Ulaanbaatar Fault: A New Earthquake Threat to the Capital of Mongolia. *Seismological Research Letters, 92*, 437-447. http://doi:10.1785/0220200109

Tapponnier, P., & Molnar, P. (1979). Active faulting and Cenozoic tectonics of the Tien Shan, Mongolia, and Baykal regions. *Journal of Geophysical Research, 84*, 3425-3459.

Thatcher, W. (1984). The earthquake deformation cycle, recurrence, and the time-predictable model. *Journal of Geophysical Research, 89*(B7), 5674-5680. https://doi.org/10.1029/jB089iB07p05674

Thatcher, W. (1990). Order and diversity in the modes of Circum-Pacific Earthquake recurrence. *Journal of Geophysical Research, 95*(B3), 2609-2623. https://doi.org/10.1029/jB095iB03p02609

Tikhonov, V. I. (1974). Faults (in Russian), in Tectonics of the Mongolian People's Republic. *Nauka*, 196-209. Moscow.

Trifonov, V. G. (1983). Late Quaternary Tectogenesis. Moscow: Nauka.

Tumurtogoo, O. (2002). Tectonics of Mongolia. *Institute of Geology and Mineral Resources of Mongolian Academy of Sciences*. 42 p.

Tumurtogoo, O. (2003). Tectonic setting of Mongolia (in Mongolian). *The Institute of Geology and Mineralogy of Mongolian Academy of Sciences*, 37 p.

Tumurtogoo, O., Byamba, J., Badarch, G., Minjin, Ch., Orolmaa, D., Khosbayar., … Bat-Ireedui, Ya. (1998). Geological Map of Mongolia. Geological Survey of Mineral Resources Authority of Mongolia & Institute of Geology and Mineral Resources of Mongolian Academy of Sciences, Ulaanbaatar, 44 p.

Ulziibat, M. (2006). The 2003 Chuya sequence (North Altay range): tectonic context and seismological study. PhD thesis. University of Nice Sophia Antipolis.

Vallage, A., Klinger, Y., Lacassin, R., Delorme, A., & Pierrot-Deseilligny, M. (2016). Geological structures control on earthquake ruptures: The Mw7.7, 2013, Balochistan earthquake, Pakistan. *Geophysical Research Letters, 43*, 10155-10163. https://doi.org/10.1002/2016GL070418

Vassallo, R., Jolivet, M., Ritz, J.-F., Braucher, R., Larroque, C., Sue, C., … Javkhlanbold, D. (2007). Uplift age and rates of the Gurvan Bogd system (Gobi-Altay) by apatite fission track analysis. *Earth and Planetary Science Letters, 259*, 333-346. https://doi:10.1016/j.epsl.2007.04.047

Vassallo, R., Ritz, J.-F., Braucher, R., Jolivet, M., Carretier, S., Larroque, C., … Arzhannikov, S. (2007). Transpressional tectonics and stream terraces of the Gobi-Altay, Mongolia. Tectonics, 26(TC5013). http://doi:10.1029/2006TC002081

Vergnolle, M., Calais, E., & Dong, L. (2007). Dynamics of continental deformation in Asia. *Journal of Geophysical Research, 112*, B11403. https://doi:10.1029/2006JB004807

Walker, R. T., Bayasgalan, A., Carson, R., Hazlett, R., McCarthy, L., Mischler, J., … Tsolmon, G. (2006). Geomorphology and structure of the Jid right-lateral strike-slip fault in the Mongolian Altay mountains. *Journal of Structural Geology, 28*, 1607-1622. https://doi:10.10106/j.jsg.2006.04.007

Walker, R. T., Molor, E., Fox, M., & Bayasgalan, A. (2008). Active tectonics of an apparently aseismic region: distributed active strike-slip faulting in the Hangay Mountains of central Mongolia. *Geophysical Journal International*. https://doi:10.1111/j.1365-246X.2008.03874.x

Walker, R. T., Nissen, E., Molor, E., & Bayasgalan, A. (2007). Reinterpretation of the active faulting in central Mongolia. *Geology, 35*(8), 759-762. https://doi:10.1130/G23716A.1

Walker, R. T., Wegmann, K. W., Bayasgalan, A., Carson, R. J., Elliot, J., Fox, M., … Wright, E. (2015). The Egiin Davaa prehistoric rupture, central Mongolia: a large magnitude normal faulting earthquake on a reactivated fault with little cumulative slip located in a slowly deforming intraplate setting. *The Geological Society of London, Special Publications, 432*. http://doi.org/10.1144/SP432.4

Weldon, R., Fumal, T., & Biasi, G. (2004). Wrightwood and the earthquake cycle: What a long recurrence record tells us about how faults work. GSA Today, 14(9).

Wells, D. L., & Coppersmith, K. J. (1994). New empirical relationships among magnitude, rupture length, rupture width, rupture area, and surface displacement. *Bulletin of the Seismological Society of America, 84*(4), 974-1002.

Wesnousky, S. G. (1988). Seismological and structural evolution of strike-slip faults. *Nature, 335*, 340-343.

Wesnousky, S. G. (2006). Predicting the endpoints of earthquake ruptures. *Nature, 444*, 358-360. https://doi:10.1038/nature05275

Willemse, J. M. (1997). Segmented normal faults: Correspondence between three-dimensional mechanical models and field data. Journal of Gephysical Research. https://doi.org/10.1029/96jB01651

Windley, B. F., Alexeiev, D., Xiao, W., Kroner, A., & Badarch, G. (2007). Tectonic models for accretion of the Central Asian Orogenic Belt. *Journal of the Geological Society, London, 164*, 31-47.

Windley, B., & Allen, M. (1993). Mongolian plateau: Evidence for a late Cenozoic mantle plume under central Asia. *Geology, 21*, 295-298.

Yanshin, A. L. (1975). Mesozoic and Cenozoic Tectonics and the Magmatism of Mongolia (in Russian). Joint Soviet-Mongolian Scientific Research Geological Expedition.

Yarmolyuk, V. V., Kudryashova, E. A., Kozlovsky, A. M., & Lebedev, V. A. (2008). Late Cenozoic volcanism of Khangai (Central Mongolia): Evidence for recent orogeny in Central Asia. *Doklady Earth Sciences, 422*, 1032-1036. https://doi:10.1134/S1028334X08070064

Yeats, R. S., Sieh, K., & Allen, C. R. (1997). The Geology of Earthquakes. Oxford University Press. 568 p.

Zonenshain, L. P. (1972). The geosynclinal theory and its application to Central Asia's orogenic belt (in Russian), Moscow, *Nedra*, 240 p.

Zonenshain, L. P., & Savostin, L. A. (1981). Geodynamics of the Baikal rift zone and plate tectonics of Asia. *Tectonophysics, 76*(1981), 1-45.

JOURNAL OF MAPS
https://doi.org/10.1080/17445647.2022.2132884

The Ar-Hötöl surface rupture along the Khovd fault (Mongolian Altay)

Battogtokh Davaasambuu [a,b], Matthieu Ferry [a], Jean-Francois Ritz [a] and Ulziibat Munkhuu [b]

[a]Géosciences Montpellier, University of Montpellier, CNRS, Montpellier, France; [b]Institute of Astronomy and Geophysics, Mongolian Academy of Sciences, Ulan Bator, Mongolia

ABSTRACT

We present a 1:200,000 scale map of the Ar-Hötöl surface rupture along the Khovd fault (Mongolian Altay), presumed to be the expression of the 1761 CE Mw ~ 7.8 Great Mongol earthquake. The detailed mapping combines airborne and terrestrial imaging and topographic techniques (Sentinel-2, Pleiades, TanDEM-X, UAV and TLS) to quantify right-lateral and vertical offsets ranging from ~ 1 m to ~ 4 km over a length of 238 km. The smaller offsets document the deformation associated with the last surface-rupturing earthquake that affects several Bronze to Iron Age burial mounds. Their analysis yields a robust segmentation model comprising 6 segments of 20 to 51 km in length, a maximum co-seismic slip value of 4.8 m ± 0.5 m located near the center of the rupture. Our observations precise the varying kinematics along strike, bring new evidence of repeated faulting and confirm a Mw of 7.8 ± 0.3.

ARTICLE HISTORY
Received 22 February 2022
Revised 22 June 2022
Accepted 22 September 2022

KEYWORDS
Active fault; surface rupture; Altay Range

1. Introduction

We present a 1:200,000 scale map of the Ar-Hötöl surface rupture along the Khovd fault in the Mongolian Altay. This map covers an area of ~900 km² with elevations ranging from ~1120 m (Khar Us Nuur Lake) to 4204 m (Mönkh Khaikhan Mountain) and encompasses the main faults of the Altay Range. This work documents evidence and style of active deformation along the central section of the N140°-trending Khovd fault (between latitudes 46°30' and 48°25'), with special emphasis on the most recent earthquake surface rupture. It has implications for tectonics (e.g. influence of structural heritage on the localization of present seismicity), regional geodynamics (e.g. deformation regime and distribution) and seismic hazard to the developing Khovd city.

The fundamental geology of the Altay is composed of three basic terranes that correspond to an accretionary wedge, backarc and forearc basins and an island arc that have amalgamated during the Paleozoic (Badarch et al., 2002; Berkey & Morris, 1927; Cunningham, 1998; Cunningham et al., 1996) and are bounded by major shear zones (Figure 1). There is little evidence of regional deformation during the Mesozoic, which is considered tectonically calm as suggested by the development of a regional erosion surface at the top of red argillaceous sandstones from the Oligocene (Baljinnyam et al., 1993; Devyatkin, 1974, 1975; Devyatkin & Shuvalov, 1980; Kozhevnikov et al., 1970; Tikhonov, 1974). The onset of Neogene coarser sediments (conglomeratic molasses) along the margins of the range and within intramontaineous basins indicates renewed regional uplift-driven erosion likely started at the end of the Oligocene or the beginning of the Miocene (Devyatkin, 1974, 1975). This deformation episode continues today as attested by Oligocene-Holocene sedimentary records exposed within the eastern basins (Howard, 2004) and early Pliocene deposits in the Ikh Nuuryn Khotgor basin (Baljinnyam et al., 1993; Devyatkin, 1975; Devyatkin et al., 1980). This late Cenozoic reactivation of the Altay Range has been interpreted as a distant effect of the India-Eurasia collision (Molnar & Tapponnier, 1975; Tapponnier & Molnar, 1979).

Presently, the Altay Range is a major transpressive system that accommodates ~4 mm/yr of right-lateral displacement with minor uplift along a system of ~N140-oriented faults distributed over its width of 150–300 km after GPS measurements (Calais et al., 2003). From west to east, the Fu-Yun fault, the Tolbo Nuur fault, the Ölgiy fault, the Khovd fault and the Khar Uus Nuur fault constitute the main structures and potential sources of destructive earthquakes (e.g. Baljinnyam et al., 1993; Frankel et al., 2010; Gregory et al., 2014; Khilko et al., 1985; Walker et al., 2006). Seismicity in Central and Western Mongolia is dominated by rare and powerful earthquakes as illustrated by the extensively studied twentieth

CONTACT Matthieu Ferry matthieu.ferry@umontpellier.fr Géosciences Montpellier, Université de Montpellier, 5 place E. Bataillon, 34095 Montpellier, France

Supplemental map for this article is available online at https://doi.org/10.1080/17445647.2022.2132884.

CHAPTER 2

2. THE AR-HÖTÖL SURFACE RUPTURE ALONG THE KHOVD FAULT (MONGOLIAN ALTAY)

Davaasambuu Battogtokh[1,2], Matthieu Ferry[1], Jean-Francois Ritz[1] and Ulziibat Munkhuu[2]

1. Géosciences Montpellier, University of Montpellier, CNRS, France
2. Institute of Astronomy and Geophysics, Mongolian Academy of Sciences, Mongolia

2.1 Abstract

We present a 1:200,000 scale map of the Ar-Hötöl surface rupture along the Khovd fault in the Mongolian Altay, presumed to be the surface expression of a Mw ~ 7.8 earthquake that was felt regionally in 1761 CE. The detailed mapping is based on a multi-scale approach combining a range of airborne and terrestrial imaging and topographic techniques: Sentinel-2, Pleiades, TanDEM-X, UAV, and terrestrial laser scanning. This effort led to the detailed quantification of right-lateral and vertical offsets ranging from ~ 1 m to ~ 4 km over a continuous rupture length of 238 km. The distribution of the smaller offsets documents the deformation associated with the last surface-rupturing earthquake that affects several Bronze to Iron Age burial mounds. Its analysis yields a robust segmentation model comprising 6 segments of 20 to 51 km in length, a maximum co-seismic slip value of 4.8 m ± 0.5 m located near the center of the rupture. Our detailed remote sensing and field observations precise the varying kinematics along strike, bring new evidence of repeated faulting and confirm a moment magnitude of 7.8 ± 0.3.

Keywords: active fault, surface rupture, Altay Range

2.2 Introduction

We present a 1:200,000 scale map of the Ar-Hötöl surface rupture along the Khovd fault in the Mongolian Altay. This map covers an area of ~ 900 km² with elevations ranging from ~ 1120 m (Khar Us Nuur Lake) to 4204 m (Mönkh Khaikhan Mountain) and encompasses the main

faults of the Altay Range. This work documents evidence and style of active deformation along the central section of the N140°-trending Khovd fault (between latitudes 46°30' and 48°25'), with special emphasis on the most recent earthquake surface rupture. It has implications for tectonics (e.g. influence of structural heritage on the localization of present seismicity), regional geodynamics (e.g. deformation regime and distribution) and seismic hazard to the developing Khovd city.

The fundamental geology of the Altay is composed of three basic terranes that correspond to an accretionary wedge, backarc and forearc basins and an island arc that have amalgamated during the Paleozoic (Berkey and Morris, 1927; Cunningham et al., 1996; Cunningham, 1998; Badarch et al., 2002) and are bounded by major shear zones (Figure 20). There is little evidence of regional deformation during the Mesozoic, which is considered tectonically calm as suggested by the development of a regional erosion surface at the top of red argillaceous sandstones from the Oligocene (Devyatkin, 1974, 1975; Devyatkin et al., 1990; Kozhevnikov et al., 1970; Tikhonov, 1974; Baljinnyam et al., 1993). The onset of Neogene coarser sediments (conglomeratic molasses) along the margins of the range and within intramontaineous basins indicates renewed regional uplift-driven erosion likely started at the end of the Oligocene or the beginning of the Miocene (Devyatkin, 1974; 1975). This deformation episode continues today as attested by Oligocene-Holocene sedimentary records exposed within the eastern basins (Howard, 2004) and early Pliocene deposits in the Ikh Nuuryn Khotgor basin (Devyatkin, 1975; Devyatkin et al., 1980; Baljinnyam et al., 1993). This late Cenozoic reactivation of the Altay Range has been interpreted as a distant effect of the India-Eurasia collision (Molnar and Tapponnier, 1975; Tapponnier and Molnar, 1979).

Presently, the Altay Range is a major transpressive system that accommodates ~ 4 mm/yr of right-lateral displacement with minor uplift along a system of ~ N140-oriented faults distributed over its width of 150-300 km after GPS measurements (Calais et al., 2003). From west to east, the Fu-Yun fault, the Tolbo Nuur fault, the Ölgii fault, the Khovd fault and the Khar Uus Nuur fault constitute the main structures and potential sources of destructive earthquakes (e.g. Khilko et al., 1985; Baljinnyam et al., 1993; Walker et al., 2006; Frankel et al., 2010; Gregory et al., 2014). Seismicity in Central and Western Mongolia is dominated by rare and powerful earthquakes as illustrated by the extensively studied 20th century sequence: 1905 (Mw 8.1 Tsetserleg and Mw 8.4 Bulnay), 1931 (Mw 8.0 Fu-Yun), 1957 (Mw 8.1 Bogd) and 1967 (Mw 7.6 Mogod). Paleoseismological investigations -where available- suggest such events have an

average recurrence period of ~ 3500 yr (Prentice et al., 2002; Rizza et al., 2011; Rizza et al., 2015).

Historical records in the Altay are scarce, incomplete and rarely accessible. The oldest documented event is the Great Mongol Earthquake of 1761 CE that strongly affected Russian military outposts and townships in regions that now belong to southern Siberia and Kazakhstan (Mushketov and Orlov, 1893). Detailed descriptions pertaining to shaking intensity and duration were analyzed by Zhalkovsky (1982) who concluded that a major earthquake occurred on 9 December 1761 within the Altay region *sensu largo*. Khilko et al. (1985) augmented this analysis with unpublished folk tales collected from nomad elders and concluded that the epicenter was located along the Khovd fault and the associated magnitude likely reached Mw 8.

First field observations along the fault (Trifonov, 1983 and Khilko et al., 1985) revealed numerous surface breaks displacing streams and ancient graves with various amounts. A few tape measurements (~ 5) yielded a maximum 4.5 m right-lateral offset affecting a Turkic grave at the Ar-Hötöl pass (Khilko et al., 1985). Baljinnyam et al. (1993) built on this effort and some data points, among which a "7 m" measurement north of Buyant River, near the northern termination of the rupture. Overall, little is known about the late Quaternary activity of the Khovd fault, especially compared to similarly large structures exhibiting historical surface ruptures in the region. Hence, the characterization of the Khovd fault requires a new effort with a dense reliable dataset that shall help better assess its rupture behavior and extent as well as its potential magnitude. In the following, we present systematic detailed mapping and quantification of the recent deformation along the Ar-Hötöl surface rupture using robust high-resolution approaches.

2.3 Results

2.3.1 Identification of faulting and quantification of deformation

Within the limits of our map, the northernmost expression of the Khovd fault bounds the SW flank of the Tsambagarav Massif (Main Map) interpreted as a restraining bend by Cunningham (2005). Such features observed elsewhere are likely to act as major barriers to earthquake rupture propagation (Wesnousky, 2008). There, the fault trace is sealed by superficial unconsolidated slope deposits, which suggests the last surface rupture is relatively ancient.

Immediately south of the Khongo River at a site called Yellow Lake, interrupted markers are suggestive of deformation and let us measure four different offsets. Previous studies (Khilko et al., 1985; Baljinnyam et al. 1993) did not report observations of deformation visible in the field there, which can be explained by the fact that the surface rupture veers to the W by ~ 20° with respect to its local average strike to follow the piedmont of the range. To the south, the Shurag River displays a right-lateral deflection of ~ 3 km. Considering the drainage is strongly controlled by the edge of a massif downstream of the fault, we interpret this value as an upper bound for the true cumulative displacement. Southward, the fault's orientation changes relatively gradually from N135 to N155 then N165 at the Shiver River. Along this section, the surface rupture follows the contact between Late Devonian intrusive, Late-Cambrian-to-Early Ordovician metamorphic and Early-Middle Ordovician rocks.

Between the Burgast and Buyant rivers, we document numerous well-expressed offsets affecting gullies, stream risers and mounds. Furthermore, widespread accumulation of stream sediments against the fault suggests ponding promoted by uplift of the eastern block. A few kilometers south of the Buyant River, we identifiy a 60-m-wide and 270-m-long sag pond that forms a local depression, which diverts upstream drainages into a sediment trap. There, the rupture roughly follows the boundary between Paleozoic intrusive rocks and Late-Ordovician deposits (limestone and marine formations). About 10 km south of that sag pond, the Shiver River displays a clear ~ 4 km deflection. Considering the stream trajectory is well constrained by its deeply incised valley, we interpret this deflection as a cumulative offset.

A few kilometers south of the Shiver River the fault changes strike from ~ N165 to ~ N150 and forms a 1-km-wide 5-km-long relay zone that we identify as a potential barrier to rupture propagation. Afterwards, the fault follows a straight trace and reaches the Ar-Hötöl Pass where it affects several man-made rock mounds. The mounds are made of blocks of local pink granite, circular in shape and composed of a central mound ~ 10 m in diameter within a ~ 20-m-diameter enclosure. These constructions are typical khirigsuurs (burial mounds) found throughout Central Asia and dated Late Bronze to Early Iron Age (3200-2300 BP) in the Mongolian Altay (Allard & Erdenebaatar, 2005; Wright, 2007). Two such khirigsuurs were documented by earlier researchers (Khilko et al., 1985 and Baljinnyam et al., 1993) who proposed right-lateral offsets reaching 5.5 ± 1 m and ~ 3 m. We re-measured these points using Pleiades satellite images and a terrestrial laser scanner and found slightly lower values of 4.5 ± 0.5 and 2.5 ± 0.3 m, respectively (see insert A in Main Map). The vast majority of large offset values observed along the Ar-Hötöl rupture are located within a few 10s of kilometers of the Ar-Hötöl Pass

(Khilko et al., 1985; Baljinnyam et al., 1993 and this study). On the southern side of the pass, the Tsagaan Burgast River displays a very sharp right-lateral deflection of ~ 2.7 km that is probably mostly due to cumulative displacement along the Khovd fault.

Between the Khoid Tsenkher and Dund Tsenkher rivers, the fault splits into two branches. The northern branch follows the piedmont of the Altay Range formed by the contact between Ordivician limestones (north) and a Paleozoic intrusion (south) (Figure 20). This section exhibits little deformation affecting Quaternary landforms as illustrated by the relatively small cumulative offsets affecting the valleys of the Dund Tsenkher and Urd Tsenkher rivers and is considered to correspond to the geological Khovd Fault (Main Map). The western branch follows the southern edge of the Paleozoic intrusion, delimits the northern tip of the Goo Mountains and exhibits recent deformation considered part of the Ar-Hötöl rupture (Khilko et al., 1985; Baljinnyam et al., 1993 and this study). At this junction, the fault trace changes direction abruptly from ~ N150 to ~ N165 over ~ 18 km then veers back progressively to ~ N150 over ~ 25 km until it reaches the southern tip of the Goo Mountains. This local elongated feature (~ 50 x 10 km) is interpreted as a thrust fault-bounded pop-up structure by Cunningham (2005) and is likely to influence the expression of the rupture (in terms of kinematics, amplitude and geometry). Our measurements show relatively lower horizontal offsets and significant vertical displacements along that section, which confirms the locally changing kinematics. South of Urd Tsenkher, the fault displaces a local stream as well as a khirigsuur (point B and corresponding insert in Main Map). The poorly preserved geometry of the latter does not allow any reconstruction and offset estimation. However, a recent terrace riser within the stream exhibits a clear right-lateral offset of 2.5 ± 0.5 m. Nearby, the Lunch Creek stream is affected by a well-expressed moletrack line and exhibits a cumulative offset of 13.8 ± 1.5 m (point C and corresponding insert in Main Map). There, numerous shallow rills are similarly right-laterally offset by as little as ~ 1 m and vertically by up to 1.5 m with the NE side up.

Along the SE flank of the Goo Mountains, subtle deformation visible in Pleiades images was confirmed by field observations and suggests a short section produced slip recently. Strikingly, this section does not follow any clear geological contact and rather cuts through Ordovician and Paleozoic units (Figure 20). At the southern tip of the massif, both branches merge into a linear trace (point 4 in Main Map) over ~ 6 km before splitting again. This section is geometrically complex with widely distributed deformation illustrated by the two parallel strands visible in Pleiades images (Figure 21) and in the field (points 3, 4, 5 and corresponding photographs in Main Map). We documented relay zones at various scales, among which the Ulaan Bulagt pull-

apart structure where the two main strands connect (point D and corresponding insert in Main Map and Figure 21). Hence, we collected four offset measurements ranging from 2.75 ± 0.25 m to 10.25 ± 1.75 m that may only reflect partial horizontal slip estimates.

As the rupture reaches Mount Höh Öndör, it propagates along both flanks of the massif (south of point 7 in Main Map and Figure 22). Along the northern flank, field observations revealed fresh-looking cracks over a few kilometers only while the geological fault runs along the contact between Devonian formations and Paleozoic intrusive rocks then Ordovician limestone over at least 50 km along a N150 direction (Main Map, Fig. 1 and Fig. 3a). Along the southern flank of the massif, the rupture is well expressed and follows the contact between Devonian and Paleozoic formations along a N170 - N180 direction. There, it exhibits spectacular morphology with exceptionally large en-echelon tension gashes (up to 20 m in length, 5 m in width and more than 3 m in depth) affecting thick alluvium (point E and corresponding insert in Main Map). These features reflect locally transtensional kinematics consistent with a significant change of strike along a right-lateral strike-slip fault. Further south, similarly large tension gashes were observed at the Baga Ulaan Davaa. Along strike, fresh-looking deformation features die out a few kilometers to the south. The southernmost expression of recent surface rupture was found at the Broken Boulder site (point 9 and corresponding field picture in Main Map). There, the fault makes a step to the left (going southward) and forms a 3-km-long linear counter-slope scarp that affects a well-defined boulder field interpreted as a remnant of a rock glacier. A simple correlation to the extent of glaciers publised by Lehmkuhl et al. (2011) suggests this rock glacier is of late Pleistocene age, possibly from the Last Glacial Maximum. Considering that i) the scarp is well expressed but does not look as pristine as the rest of our observations and ii) the step-over is wide enough (~ 2 km, see Wesnousky, 2006) to act as a barrier to the propagation of the rupture, we cannot conclude positively that deformation at the Broken Boulder site is part of the Ar-Khötöl rupture. This, however, does not affect the overall length of the rupture.

2.3.2 Segmentation

Co-seismic slip distribution and associated segmentation have long been recognized as robust criteria to assess fault maturity and rupture behavior (see Burbank & Anderson, 2001 for a review). Using a combined approach based on remote sensing at cm to 10-m scales supplemented with detailed field observations, we mapped the most recent expression of

surface deformation along the Khovd fault over a length of 238.5 ± 0.5 km (Main Map). The surface rupture exhibits various changes in strike, faulting style and complexity generally associated with relay zones that may play a role in the propagation of the rupture (e.g. Harris & Day, 1993; Oglesby, 2005; Wesnousky, 2008; Choi et al., 2018). On that basis, we propose a structural segmentation model that separates the fault into 11 segments (S1 to S11 in Figure 23) displaying homogeneous characteristics. The central segments S7 and S8 reach lengths of ~ 50 km while the remaining segments reach lengths ranging from 7 km (S5) to 23 km (S3). In parallel, we represent all slip measurements smaller than 10 m (central value, excluding uncertainties) as this threshold would most certainly encompass all values associated with the last major surface-rupturing earthquake. Considering the lowest values encountered along strike should reflect the most recent co-seismic slip, we derive the co-seismic slip distribution as well as two cumulative curves (Fig. 4). The co-seismic slip curve displays a series of slip envelopes consistent with individual segments and suggests a broader model with only 6 well-defined segments. It should be noted that the boundaries of the segments determined from the slip envelopes correspond to boundaries of segments determined by mapping. The Northernmost segment (S1+S2+S3), the Khoid Tsenkher segment (S7), the Goo Mountains segment (S8) and the Southernmost segment (S9+S10+S11) reach lengths ranging from 45 km to 51 km. The Buyant segment (S4) and Ar-Hötöl segment (S5+S6) only reach 20 km and 23 km, respectively. This configuration indicates that only some structural features influence the distribution of slip at the surface. Finally, the central segment (Khoid Tsenkher) displays the largest co-seismic slip value (4.8 ± 0.5 m) as well as two well-defined cumulative curves that mimic the co-seismic distribution thus suggesting previous events were recorded at the same sites.

2.4 Discussions and Conclusions

Our remote sensing and field observations yield a total surface rupture length (SRL) of 238.5 ± 0.5 km for the most recent surface expression of the Khovd fault. Considering general scaling relationships established by Wells & Coppersmith (1994) for strike-slip faults (with a = 5.16 ± 0.13 and b = 1.12 ± 0.08), we may derive a moment magnitude of 7.8 ± 0.3. In parallel, the maximum last coseismic displacement (MD) identified at the center of the slip distribution reaches 4.8 ± 0.5 m. The associated scaling relationship (with a = 6.81 ± 0.05 and b = 0.78 ± 0.06) yields a moment magnitude of 7.3 ± 0.1. Previous works mention a higher value of maximum displacement reaching 7 m (Baljinnyam et al., 1993) on the northern bank of the Buyant River. This is documented about 20 km from the northernmost end of the surface rupture

(Fig. 13 in Baljinnyam et al., 1993) at a location where we found only a few markers that registered much lower coseismic slip (~ 2 m). Authors also mention some uncertainty in the interpretation of the offset. Since our findings are more consistent with the local slip envelope (Figure 23) and with the low values usually associated with rupture tips, we consider the original value likely cumulative and discard it from our analysis.

Overall, our field observations document relatively "fresh-looking" features with steep scarps and apparently recent post-seismic deposits, which could point to a recent event such as the AD 1761 earthquake (Mushketov and Orlov, 1893). However, in light of the very low erosion and deposition rates at work in Mongolia, this could be a very misleading inference (see Walker et al., 2015 for a striking example on the Egiin Davaa Fault). A comprehensive paleoseismological study of the rupture would bring much needed constraint on the recent activity of the Khovd Fault.

The apparent discrepancy between the moment magnitudes derived from SRL and MD is in fact a general observation documented by Wells & Coppersmith (1994, Figure 12) who report MD ranging from ~ 3 m to ~ 10 m for a given SRL of 240 km. Since the SRL reflects the whole rupture while MD may be influenced by local conditions, we rely on the associated estimate of Mw 7.8 ± 0.3 to characterize the most recent surface-rupturing earthquake on the central section of the Khovd fault.

Overall, we combine remote sensing and field data at various scales to produce a detailed map of the 238-km-long Ar-Hötöl rupture along the Khovd fault in the Mongolian Altay. High resolution orthorectified images and DEMs led to the robust quantification of co-seismic and cumulative slip and the identification of six main segments organized around major changes in strike, kinematics and lithology. We collected more than 100 offset values, 67 of which co-seismic to confirm the original magnitude estimate of Mw ~ 7.8. This work will serve as base data to carry out paleoseismic studies along the fault and help characterize it for geodynamics and seismic hazard.

DATA AVAILABILITY STATEMENT

The original dataset containing the detailed map in vector format as well as a table of offset data are available on the Zenodo platform (Battogtokh et al., 2022).

SOFTWARE

Processing of Sentinel-2 images was performed within ESA's SNAP software (available at http://step.esa.int/main/download/snap-download/) using the Sen2Cor plugin (available at http://step.esa.int/main/snap-supported-plugins/sen2cor/sen2cor_v2-8/). The basemap was produced by draping the Sentinel-2 mosaic over the TanDEM-X DEM using Global Mapper v18. Photogrammetric DSM were calculated from tri-stereo Pleiades images with Erdas Imagine Photogrammetry 2014. UAV photogrammetry was performed with Agisoft Metashape Pro v1.7 (https://www.agisoft.com/features/professional-edition/) and laserscanner data were processed with Faro Scene (https://www.faro.com/en/Products/Software/SCENE-Software) and CloudCompare (https://www.cloudcompare.org/). All remote sensing measurements were performed within ArcGIS (https://desktop.arcgis.com/), which was subsequently used to prepare maps before final editing in Adobe Illustrator (https://www.adobe.com/products/illustrator.html).

ACKNOWLEDGEMENTS

Equipex GEOSUD (https://ids.equipex-geosud.fr/) granted early access to tasking for Pleiades data. Pleiades data are provided by CNES. Authors also greatly benefited from Copernicus Sentinel-2 data provided by ESA (European Space Agency) and TanDEM-X data provided by DLR (Deutsches Zentrum für Luft- und Raumfahrt, proposal DEM_GEOL1629). Authors wish to thank the many Mongol colleagues from the Institute of Astronomy and Geophysics (Mongolian Academy of Sciences) who directly participated in, or facilitated, fieldwork, especially at the Khovd and Olgii seismological stations.

Authors also wish to acknowledge the careful review of Jorien van der Wal, Chris Orton and Ochirbat Batkhishig that significantly improved the quality of the manuscript.

DISCLOSURE STATEMENT

The authors declare no conflict of interest.

FUNDING

Financial support was provided by CNRS (Centre National de la Recherche Scientifique, PICS SEISMONG), the French Embassy in Mongolia and the Ministry of Education, Culture, Sciences and Sports of Mongolia (B.D.'s PhD fellowship). This work was also supported by CNES (Centre National d'Etudes Spatiales). It is based on observations with Pleiades.

2.5 References

Adiri, Z., Lhissou, R., El Harti, A., Jellouli, A., & Chakouri, M. (2020). Recent advances in the use of public domain satellite imagery for mineral exploration: A review of Landsat-8 and Sentinel-2 applications. *Ore Geology Reviews, 117*, 103332. https://doi.org/10.1016/j.oregeorev.2020.103332

Allard, F., & Erdenebaatar, D. (2005). Khirigsuurs, ritual and mobility in the Bronze Age of Mongolia. *Antiquity, 79*(305), 547-563. https://doi:10.1017/S0003598X00114498

Badarch, G., Cunningham, D. W., & Windley, B. F. (2002). A new terrane subdivision for Mongolia: implications for the Phanerozoic crustal growth of Central Asia. *Journal of Asian Earth Sciences, 21*(1), 87-110.

Baljinnyam, I., Bayasgalan, A., Borisov, B. A., Cisternas, A., Dem'yanovich, M. G., Ganbaatar, L., . . . Vashchilov, Y. (1993). Ruptures of major earthquakes and active deformation in Mongolia and its surroundings (Vol. 181). Boulder, Colorado: Geological Society of America.

Berkey, C. P., & Morris, F. K. (1927). Geology of Mongolia. New York: American Museum of Natural History.

Bollinger, L., Klinger, Y., Forman, S. L., Chimed, O., Bayasgalan, A., Munkhuu, U., … Sodnomsambuu, D. (2021). 25,000 years long seismic cycle in a slow deforming continental region of Mongolia. *Scientific Reports, 11*, 17855. https://doi.org/10.1038/s41598-021-97167-w

Burbank, D. W., & Anderson, R. S. (2001). Tectonic Geomorphology. Malden, MA, USA: Blackwell Science.

Calais, E., Vergnolle, M., San'kov, V., Lukhnev, A., Miroshnitchenko, A., Amarjargal, S., & Déverchère, J. (2003). GPS measurements of crustal deformation in the Baikal-Mongolia area (1994–2002): Implications for current kinematics of Asia. *Journal of Geophysical Research, 108*, 2501.

Choi, J.-H., Klinger, Y., Ferry, M., Ritz, J.-F., Kurtz, R., Rizza, M., . . . Demberel, S. (2018). Geologic Inheritance and Earthquake Rupture Processes: The 1905 M ≥ 8 Tsetserleg-Bulnay Strike-Slip Earthquake Sequence, Mongolia. Journal of Geophysical Research: Solid Earth. https://doi:10.1002/2017JB013962

Cunningham, W. D. (1998). Lithospheric controls on late Cenozoic construction of the Mongolian Altai. *Tectonics, 17*(6), 891-902. https://doi.org/10.1029/1998TC900001

Cunningham, W. D. (2005). Active intracontinental transpressional mountain building in the Mongolian Altai: Defining a new class of orogen. *Earth and Planetary Science Letters, 240*(2), 436-444.

Cunningham, W. D., Windley, B. F., Dorjnamjaa, D., Badamgarov, G., & Saandar, M. (1996). A structural transect across the Mongolian Western Altai: Active transpressional mountain building in central Asia. *Tectonics*, 15. https://doi:10.1029/95tc02354

Davaasambuu, B., Ferry, M., Ritz, J.-F., & Munkhuu, U. (2022). Map and offsets of the Ar-Hötöl surface rupture along the Khovd fault (Mongolian Altay) [Data Set]: Zenodo. https://doi.org/10.5281/zenodo.6089738.

Devyatkin, E. V. (1974). Structures and formational complexes of the Cenozoic activated stage (in Russian). Tectonics of the Mongolian People's Republic, 41, 182-195

Devyatkin, E. V. (1975). Neotectonic structures of western Mongolia (in Russian). Mesozoic and Cenozoic tectonics and Magmatism of Mongolia, 11, 264-282.

Devyatkin, E. V., Shuvalov, V. F., Zaitzev, N. S., & Kovalenko, V. I. (1980). Continental Mesozoic and Cenozoic of Mongolia (stratigraphy, geochronology, paleogeography) (in Russian). Evolution of Geological Processes and Metallogenesis of Mongolia, 165-176.

Ferry, M., Le Roux-Mallouf, R., Ritz, J.-F., Berthet, T., Peyret, M., Vernant, P., . . . Poujol, A. (2014). Tri-stereo Pleiades images-derived digital surface models for tectonic geomorphology studies. EGU General Assembly. Vienna.

Frankel, K. L., Wegmann, K. W., Bayasgalan, A., Carson, R. J., Bader, N. E., Adiya, T., . . . Gregory, L. (2010). Late Pleistocene slip rate of the Höh Serh–Tsagaan Salaa fault system, Mongolian Altai and intracontinental deformation in central Asia. *Geophysical Journal International, 183*(3), 1134-1150. https://doi:10.1111/j.1365-246X.2010.04826.x

Ge, W., Cheng, Q., Tang, Y., Jing, L., & Gao, C. (2018). Lithological Classification Using Sentinel-2A Data in the Shibanjing Ophiolite Complex in Inner Mongolia, China. *Remote Sensing, 10*(4), 638. https://doi:10.3390/rs10040638

Gregory, L. C., Thomas, A. L., Walker, R. T., Garland, R., Mac Niocaill, C., Fenton, C. R., . . . West, A. J. (2014). Combined uranium series and 10Be cosmogenic exposure dating of surface abandonment: A case study from the Ölgiy strike-slip fault in western Mongolia. *Quaternary Geochronology, 24*, 27-43. https://doi:10.1016/j.quageo.2014.07.005

Harris, R. A., & Day, S. M. (1993). Dynamics of fault interaction: parallel strike-slip faults. *Journal of Geophysical Research: Solid Earth, 98*(B3), 4461-4472. https://doi:10.1029/92JB02272

Howard, J. P. (2004). A multi-disciplined field-based study of sedimentary basin evolution along seismically active transpressional fault systems in the Mongolian Altai. (Ph.D thesis), University of Leicester, Leicester (UK).

Khilko, S., Kurushin, R., Kotchetkov, V., Misharina, L., Melnikova, V., Gileva, N., . . . Monhoo, D. (1985). Strong earthquakes, paleoseismogeological and macroseismic data (in Russian). Earthquakes and the Base for Seismic Zoning of Mongolia, 19-83.

Kozhevnikov, A. V., Savin, V. E., & Uflyand, A. K. (1970). The history of development of the Hangay upland in the Mesozoic and Cenozoic (in Russian). In Geology of the Mesozoic and Cenozoic of western Mongolia (pp. 151-169). Moscow: Nauka.

Kurtz, R., Klinger, Y., Ferry, M., & Ritz, J. F. (2018). Horizontal surface-slip distribution through several seismic cycles: The Eastern Bogd fault, Gobi-Altai, Mongolia. Tectonophysics. https://doi.org/10.1016/j.tecto.2018.03.011

Lehmkuhl, F., Klinge, M., & Stauch, G. (2011). Chapter 69 - The Extent and Timing of Late Pleistocene Glaciations in the Altai and Neighbouring Mountain Systems. In J. Ehlers, P. L. Gibbard & P. D. Hughes (Eds.), Developments in Quaternary Sciences (Vol. 15, pp. 967-979): Elsevier.

Molnar, P., & Tapponnier, P. (1975). Cenozoic Tectonics of Asia: Effects of a Continental Collision. *Science, 189*(4201), 419-426. https://doi:10.1126/science.189.4201.419

Mushketov, I. V., & Orlov, A. P. (1893). Katalog zemletryasenii Rossiiskoiimperii (An Earthquake Catalog of the Russian Empire),Volume 26, St. Petersburg: Imper. AN.

Oglesby, D. D. (2005). The Dynamics of Strike-Slip Step-Overs with Linking Dip-Slip Faults. *Bulletin of the Seismological Society of America, 95*(5), 1604-1622.

Prentice, C. S., Kendrick, K., Berryman, K., Bayasgalan, A., Ritz, J. F., & Spencer, J. Q. (2002). Prehistoric ruptures of the Gurvan Bulag fault, Gobi Altay, Mongolia. *Journal of Geophysical Research, 107*(B12), 2321. https://doi:10.1029/2001jb000803

Ritz, J. F., Brown, E. T., Bourlès, D. L., Philip, H., Schlupp, A., Raisbeck, G. M., . . . Enkhtuvshin, B. (1995). Slip rates along active faults estimated with cosmic-ray–exposure dates: Application to the Bogd fault, Gobi-Altaï, Mongolia. *Geology, 23*(11), 1019-1022. https://doi:10.1130/0091-7613

Rizza, M., Ritz, J. F., Prentice, C., Vassallo, R., Braucher, R., Larroque, C., . . . Team, A. (2015). Earthquake Geology of the Bulnay Fault (Mongolia). Bulletin of the Seismological Society of America, 105(1), 72-93. https://doi:10.1785/0120140119

Rizza, M., Ritz, J.-F., Braucher, R., Vassallo, R., Prentice, C., Mahan, S., . . . Bourlès, D. (2011). Slip rate and slip magnitudes of past earthquakes along the Bogd left-lateral strike-slip fault (Mongolia). *Geophysical Journal International, 186*(3), 897-927. https://doi:10.1111/j.1365-246X.2011.05075.x

Rupnik, E., Pierrot-Deseilligny, M., & Delorme, A. (2018). 3D reconstruction from multi-view VHR-satellite images in MicMac. *ISPRS Journal of Photogrammetry and Remote Sensing, 139*, 201-211. https://doi.org/10.1016/j.isprsjprs.2018.03.016

Tapponnier, P., & Molnar, P. (1979). Active faulting and Cenozoic tectonics of the Tien Shan, Mongolia, and Baykal regions. *Journal of Geophysical Research, 84*(B7), 3425-3459. https://doi.org/10.1029/JB084iB07p03425

Tumurtogoo, O., Takahashi, Y., Nakajima, T., Ichinnorov, N., Oyungerel, S., Minjin, Ch., Bayarmandal, Lh., Teraoka, Y., Kurimoto, Ch., Tungalag, F., Delgertsogt, B., Naito, K. (Cartographer). (1998). *Geological map of Mongolia*.

Tikhonov, V. I. (1974). Faults (in Russian). Tectonics of the Mongolian People's Republic, 196-209.

Trifonov, V. G. (1983). *Late Quaternary Tectogenesis*. Moscow: Nauka.

Vassallo, R., Ritz, J.-F., Braucher, R., & Carretier, S. (2005). Dating faulted alluvial fans with cosmogenic 10Be in the Gurvan Bogd mountain range (Gobi-Altay, Mongolia): climatic and tectonic implications. *Terra Nova*, 17(3), 278-285.

Walker, R. T., Bayasgalan, A., Carson, R., Hazlett, R., McCarthy, L., Mischler, J., . . . Tsolmon, G. (2006). Geomorphology and structure of the Jid right-lateral strike-slip fault in the Mongolian Altay mountains. *Journal of Structural Geology, 28*(9), 1607-1622.

Walker, R. T., Wegmann, K. W., Bayasgalan, A., Carson, R. J., Elliott, J., Fox, M., . . . Wright, E. (2015). The Egiin Davaa prehistoric rupture, central Mongolia: a large magnitude normal faulting earthquake on a reactivated fault with little cumulative slip located in a slowly deforming intraplate setting. *Geological Society, London, Special Publications, 432*(1), 187-212. https://doi:10.1144/sp432.4

Wells, D. L., & Coppersmith, K. J. (1994). New empirical relationships among magnitude, rupture length, rupture width, rupture area, and surface displacement. *Bulletin of the Seismological Society of America, 84*(4), 974-1002.

Wesnousky, S. G. (2006). Predicting the endpoints of earthquake ruptures. *Nature, 444*, 358-360. https://doi:10.1038/nature05275

Wesnousky, S. G. (2008). Displacement and Geometrical Characteristics of Earthquake Surface Ruptures: Issues and Implications for Seismic-Hazard Analysis and the Process

of Earthquake Rupture. *Bulletin of the Seismological Society of America, 98*(4), 1609-1632. https://doi:10.1785/0120070111

Wright, J. (2007). Organizational principles of Khirigsuur monuments in the lower Egiin Gol valley, Mongolia. *Journal of Anthropological Archaeology, 26*(3), 350-365. https://doi.org/10.1016/j.jaa.2007.04.001

Zhalkovsky, N. D. (1982). Altai and Sayany. In N. V. Kondorskaya & N. V. Shebalin (Eds.), *New catalog of strong earthquakes in the U.S.S.R. from Ancient Times through 1977* (Vol. SE-31). National Oceanic and Atmospheric Administration.

FIGURE CAPTIONS ALT TEXT

Main Map caption: Surface rupture associated with the last major earthquake along the Ar-Hötöl section of the Khovd fault, Mongolian Altay. Basemap is Sentinel-2 composite image (bands 12/8/2) draped over TanDEM-X DEM. Insets 1 to 9 show field observations of the fault trace and related offset landforms. Insets A to E show examples of deformed markers surveyed with terrestrial laserscanner (A), satellite photogrammetry (B and C) and UAV photogrammetry (D and E).

Main Map Alt Text: Map of the Hovd Fault drawn from satellite and UAV images completed by field observations. The fault offsets numerous streams and rivers in a right-lateral fashion and runs for more than 300 km. Insets show the general location of the fault in Western Mongolia as well as details from field observations.

Figure 1 caption: Simplified geological map of the Ar-Hötöl section of the Khovd fault and neighboring area modified from the Geological Map of Mongolia at a scale of 1:500 000 (Mineral Resources Authority of Mongolia, 1999). Quaternary faults are from Byamba et al. (2009). The Ar-Hötöl surface rupture is from this study. See main text for description.

Figure 1 Alt Text: A comparison between the geology (rock units and faults) and the Ar-Hötöl surface rupture show how they coincide in most places and diverge in some. This reflects the control of structural heritage over the active deformation.

Figure 2 caption: Fault zone complexity at the Ulaan Bulagt Mountain relay zone. (a) Pleiades panchromatic orthoimage. (b) Surface rupture map (red lines) along with documented offset markers (yellow dots). Circled numbers (3, 4 and 5) and letter (D) point to field pictures and a very high-resolution DEM visible in the Main Map. See Main Map for location.

Figure 2 Alt Text: An example of the complexity of the rupture at the Ulaan Bulagt Mountain relay zone where the fault splits into two branches that run along the flanks of the Mountain.

Figure 3 caption: Fault junction at Höh Öndör Mountain. (a) TanDEM-X shaded relief with resolution of 12 m. The red lines show the southernmost termination of the Ar-Hötöl surface rupture as it reaches Höh Öndör Mountain and runs along the west flank of the mountain. The eastern splay dies out a few kilometers SE of the junction. The orange lines represent Quaternary faults. The yellow dots are documented offsets. (b) Close-up of the junction on Pleiades images with 0.5 m of resolution showing the complexity and distribution of the deformation. See Main Map for location.

Figure 3 Alt Text: At the Höh Öndör Mountain the rupture splits into two branches; the eastern one quickly dies out while the western one keeps going over a dozen kilometers to the south.

Figure 4 caption: Segmentation from surface rupture map and dextral slip distribution of the Ar-Hötöl surface rupture. The color surface rupture map is divided into 11 segments (S1 to S11) based on changes in strike, deformation distribution and geometric complexity (see text for details). A second segmentation model (double-headed black arrows) comprises 6 segments and is based on our analysis of the slip distribution (lower panel). There, we retain slip values lower than 10 m of medium and high quality (red dots) and low quality (blue dots). We connect the lower individual values to build a slip envelope for the most recent event (dark grey) as well as cumulative slip envelopes that include the penultimate event (medium grey) and the antepenultimate event (light grey).

Figure 4 Alt Text: A chart showing how the surface rupture is divided into 11 segments based on changes in strike, deformation distribution and geometric complexity and only 6 segments based on slip distribution.

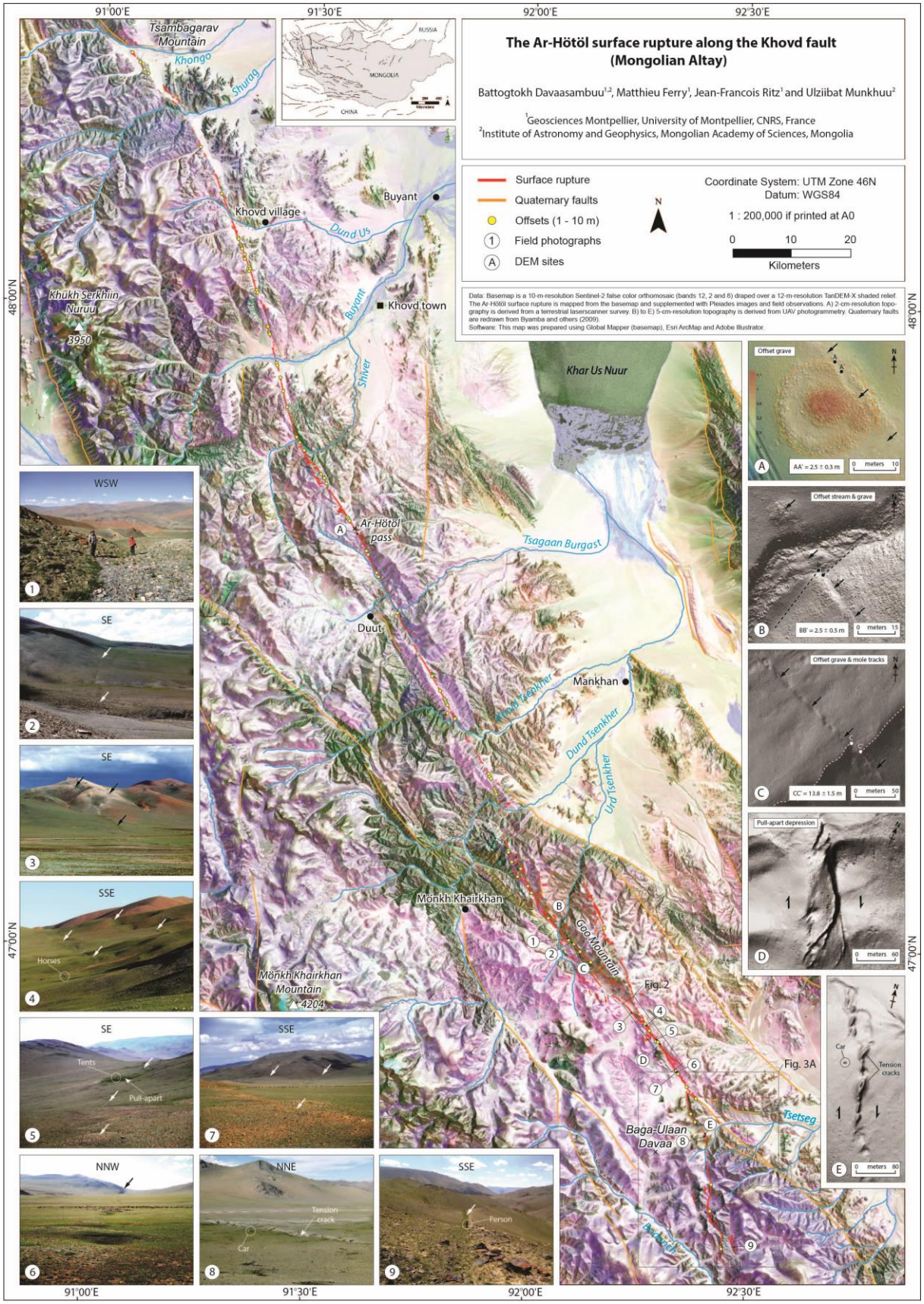

Figure 19. Main map of the Ar-Hötöl surface rupture.

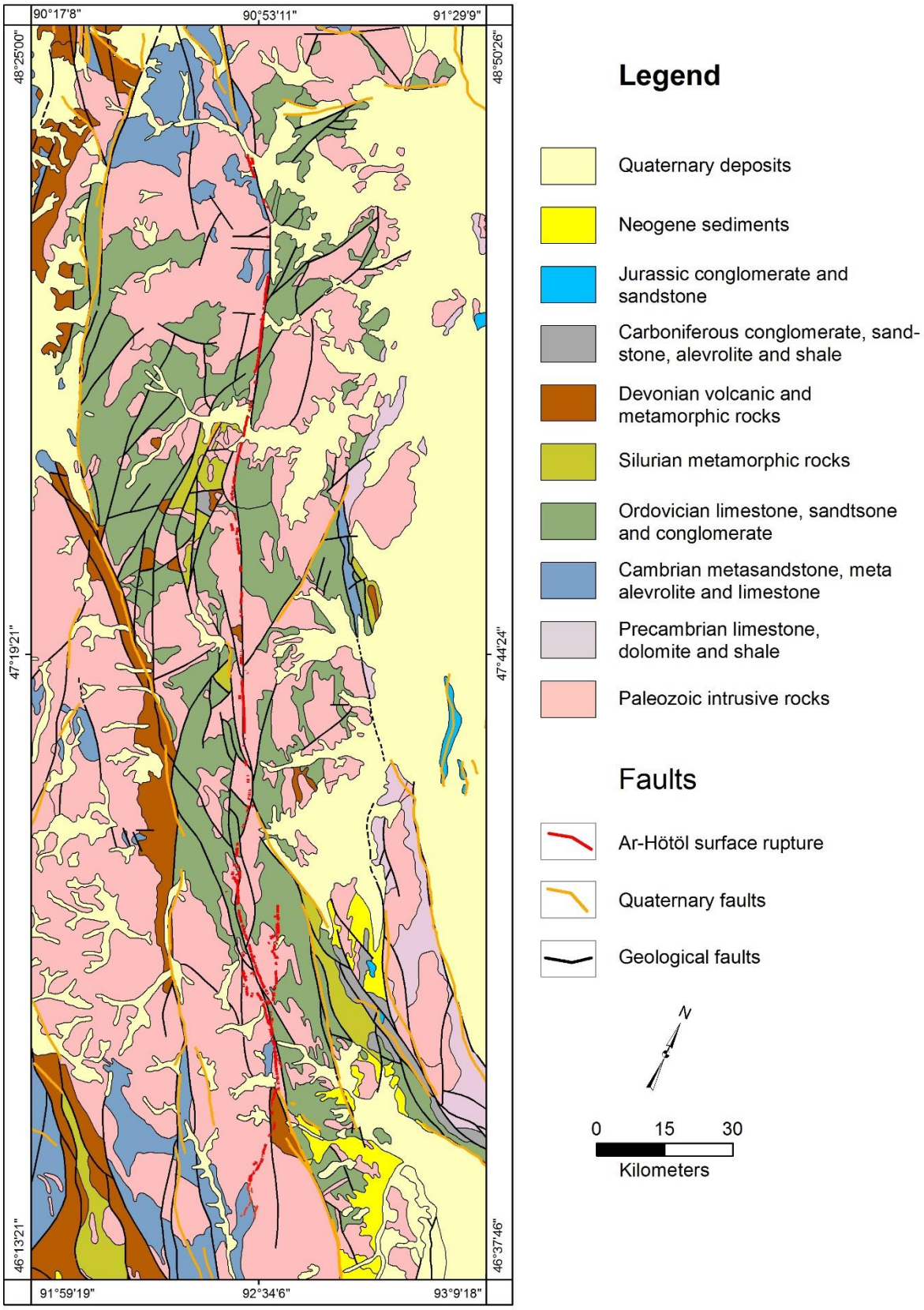

Figure 20. Simplified geological map of the Ar-Hötöl section of the Khovd fault and neighboring area modified from the Geological Map of Mongolia at a scale of 1:500 000 (Mineral Resources Authority of Mongolia, 1999). Quaternary faults are from Byamba et al. (2009). The Ar-Hötöl surface rupture is from this study. See main text for description.

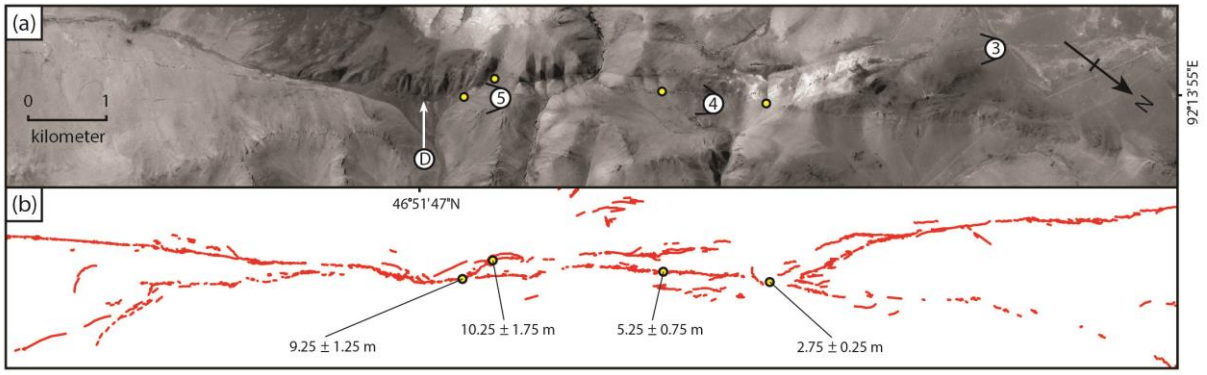

Figure 21. Fault zone complexity at Mount Ulaan Bulagt relay zone. (a) Pleiades panchromatic orthoimage. (b) Surface rupture map (red lines) along with documented offset markers (yellow dots). Circled numbers (3, 4 and 5) and letter (D) point to field pictures and a very high-resolution DEM visible in the Main Map. See Main Map for location.

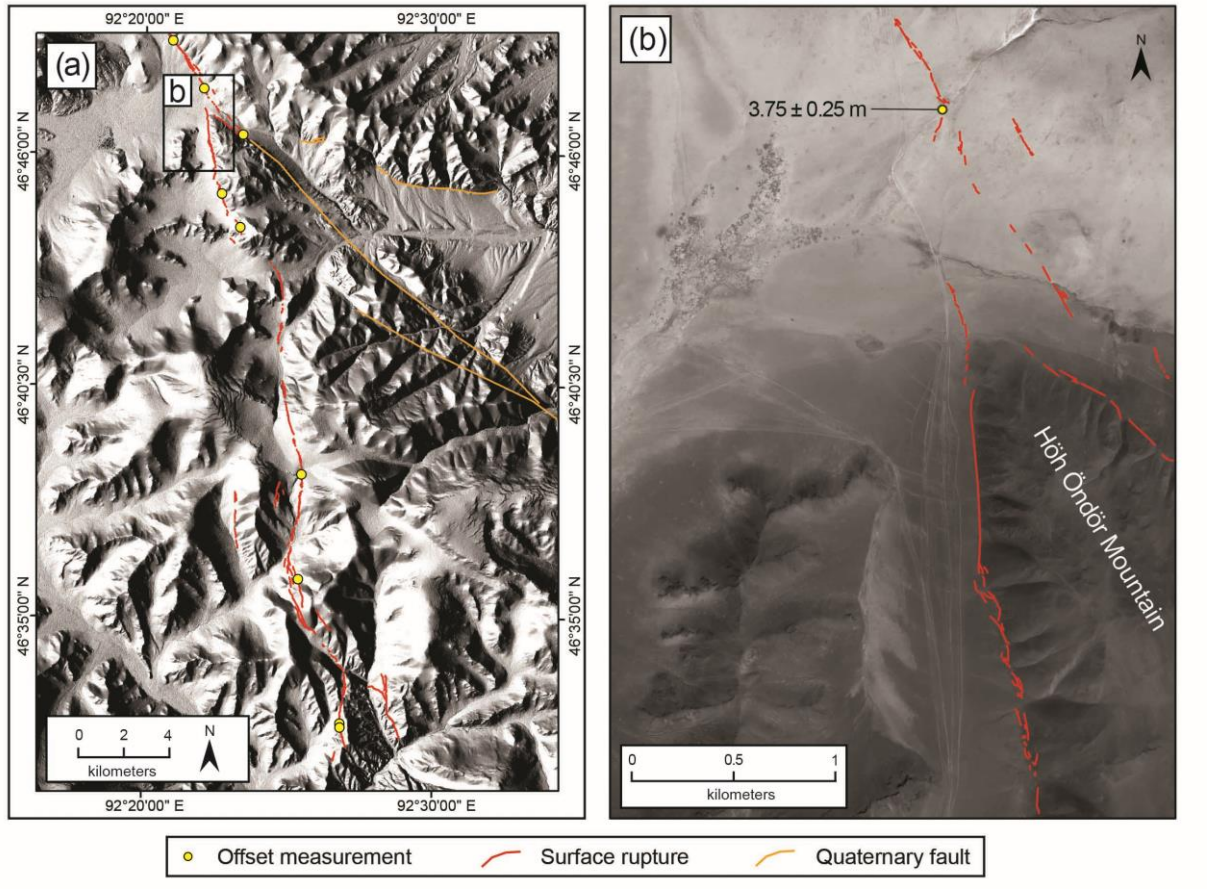

Figure 22. Fault junction at Höh Öndör Mountain. (a) TanDEM-X shaded relief with resolution of 12 m. The red lines show the southernmost termination of the Ar-Hötöl surface rupture as it reaches Höh Öndör Mountain and runs along the west flank of the mountain. The eastern splay dies out a few kilometers SE of the junction. The orange lines represent Quaternary faults. The yellow dots are documented offsets. (b) Close-up of the junction on Pleiades images with 0.5 m of resolution showing the complexity and distribution of the deformation. See Main Map for location.

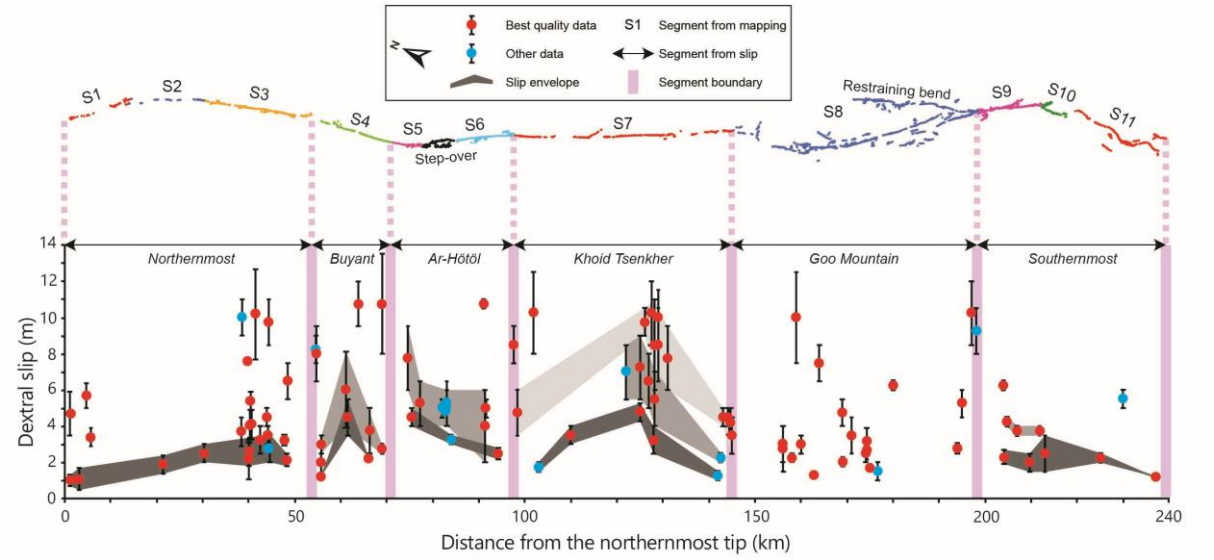

Figure 23. Segmentation from surface rupture map and dextral slip distribution of the Ar-Hötöl surface rupture. The color surface rupture map is divided into 11 segments (S1 to S11) based on changes in strike, deformation distribution and geometric complexity (see text for details). A second segmentation model (double-headed black arrows) comprises 6 segments and is based on our analysis of the slip distribution (lower panel). There, we retain slip values lower than 10 m of medium and high quality (red dots) and low quality (blue dots). We connect the lower individual values to build a slip envelope for the most recent event (dark grey) as well as cumulative slip envelopes that include the penultimate event (medium grey) and the antepenultimate event (light grey).

CHAPTER 3

3. PALEOSEISMOLOGICAL STUDY ALONG THE AR-KHÖTÖL SURFACE RUPTURE

In this interim chapter, paleoseismological studies of the Marmot Creek, Broken Boulder, and Yellow Lake trenches excavated in the Ar-Khötöl fault will be discussed. These 3 trenches are located at southern end (Broken Boulder), middle part (Marmot Creek), and northern end (Yellow Lake) of the Ar-Khötöl fault (Figure 24).

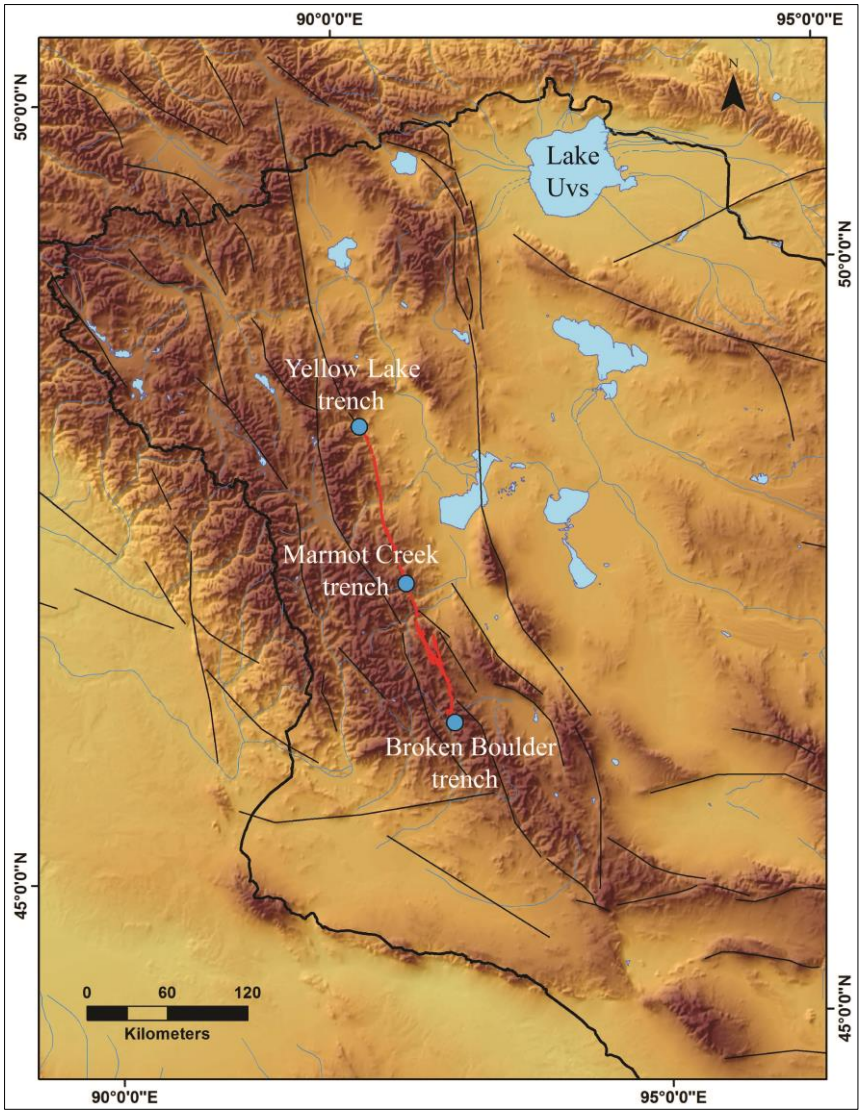

Figure 24. Locations of the Broken Boulder, Marmot Creek, and Yellow Lake trenches along the Ar-Khötöl fault in the Mongolian Altai Mountain Range. The Ar-Khötöl surface rupture is mapped in red and the trenches are indicated with blue circles. The black lines demonstrate the other active faults in the region.

3.1 Marmot Creek trench

The Marmot Creek site is located at the center of the Ar-Khötöl fault where the fault is well localized (Figure 24). At the Marmot Creek, short drainages flow across the fault and form against the main scarp (Figure 25). The paleoseismic trench reveals stratigraphy with numerous peat layers that developed over alluvial sands (Figure 26). The fault exhibits near vertical strands affecting pre-ponding units as well as a well-developed peat unit radiocarbon-dated AD 1440-1640. This unit likely corresponds to the sealing unit of the large earthquake. It is overlain with a sandy pond unit on top of which a second continuous peat unit developed after AD 1670-1945. According to OxCal modelling (Figure 27) of the whole stratigraphic sequence, the large event occurred between AD 1280 and AD 1640 with a favored time of occurrence at the end of the earlier peat development. The most recent earthquake occurred after 1690-1945 CE. This includes the 1761 historical event.

3.1.1 Field notes in the trench

The field notes are the following brief descriptions of the units.

- U10: Surface
- U20: Loose granules to small pebbles with a few large pebbles up to 3 cm. Grades up to coarse sand with a silty, peaty cap. Contains several peaty horizons (former ground surface).
- U30: Same as U20.
- U40: Loose, coarse sand and granules. Peat in place along upper contact and is everywhere dark along upper contact, indicating this is an old ground surface. Unit contains rip-up clasts of peat likely derived from ground surface that existed at the top of unit 50.
- U50: Brown, relatively stiff compared to unit 40, pebbly, coarse sand and granules in silty matrix. Rare cobbles. Cobbles increase towards the east. Older alluvial package that is scoured by unit 40.
- U70: Massive, unsorted, silt to large cobbles. Slope colluvium.
- U100: White CaCO3 and silty matrix with scattered pebbles to cobbles and boulders.

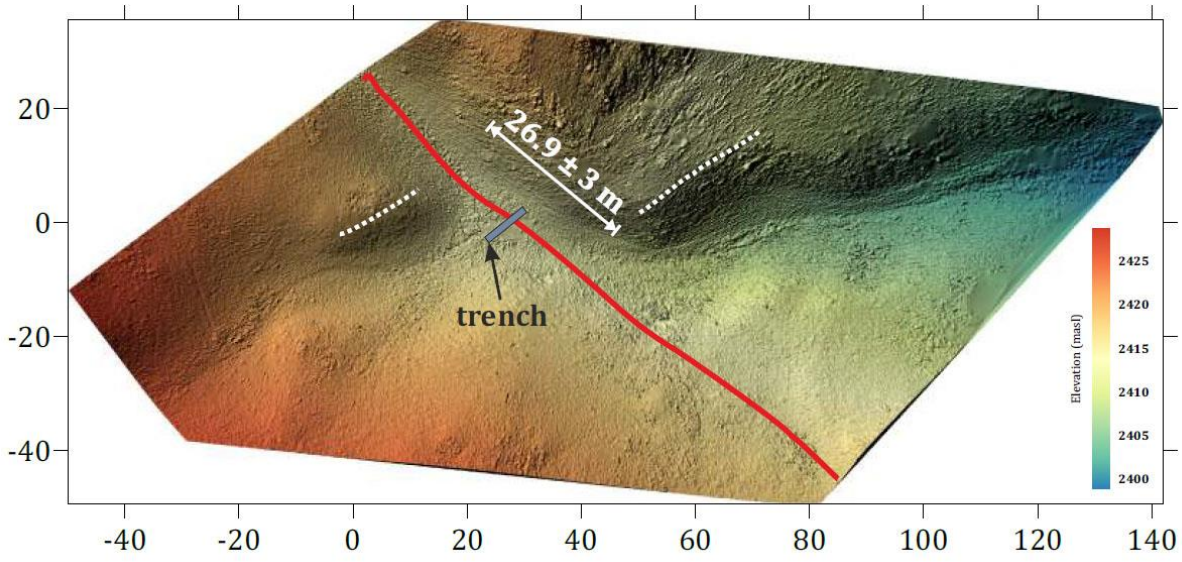

Figure 25. 3D scanner DEM of Marmot Creek site. Marmot Creek is right-laterally offset by ~27 m. A counter-slope scarp blocks the flow and forces deposition of sandy material. The geographical coordinate of the Marmot Creek trench is N47˚24'52.4", E91˚47'12.4".

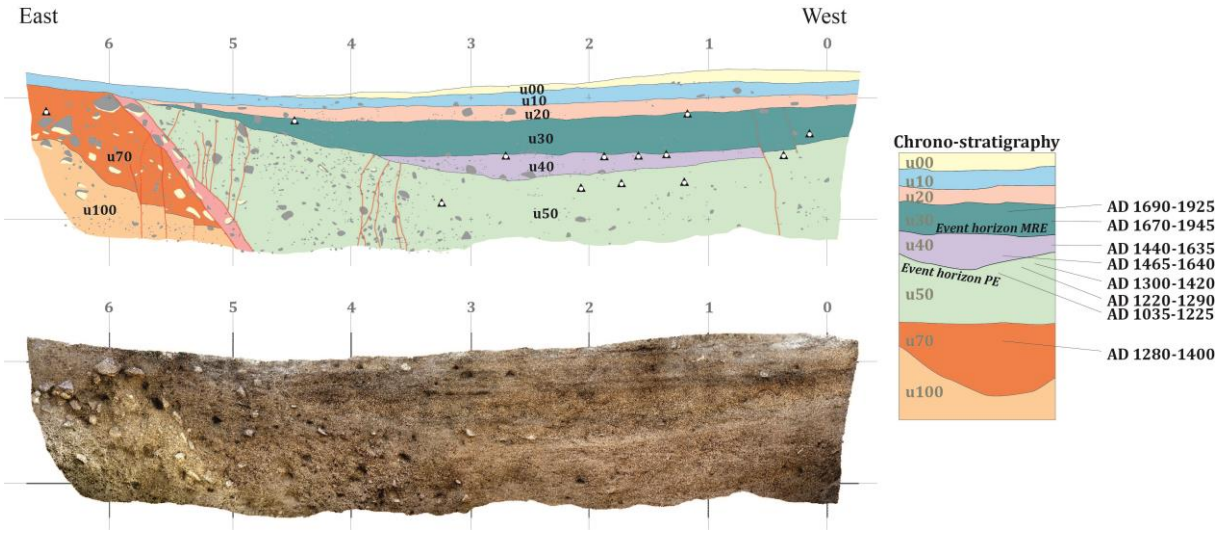

Figure 26. The Marmot Creek trench (south wall). A hand-dug trench exposure reveals a sequence of peat developments (soil) and sand units (alluvium fill). At least two surface-rupturing events may be identified.

Fault zone: There are many large clasts oriented along faults. Small offsets 0.1-0.5 cm.

Other note: $CaCO_3$ coating on base. Rocks along fault have $CaCO_3$ coating aligned along fault, not at bottom of the rocks. It implies that rocks along faults have been rotated – the $CaCO_3$ coating formed along the bottom of the rocks, then was rotated due to fault motion into alignment with the fault.

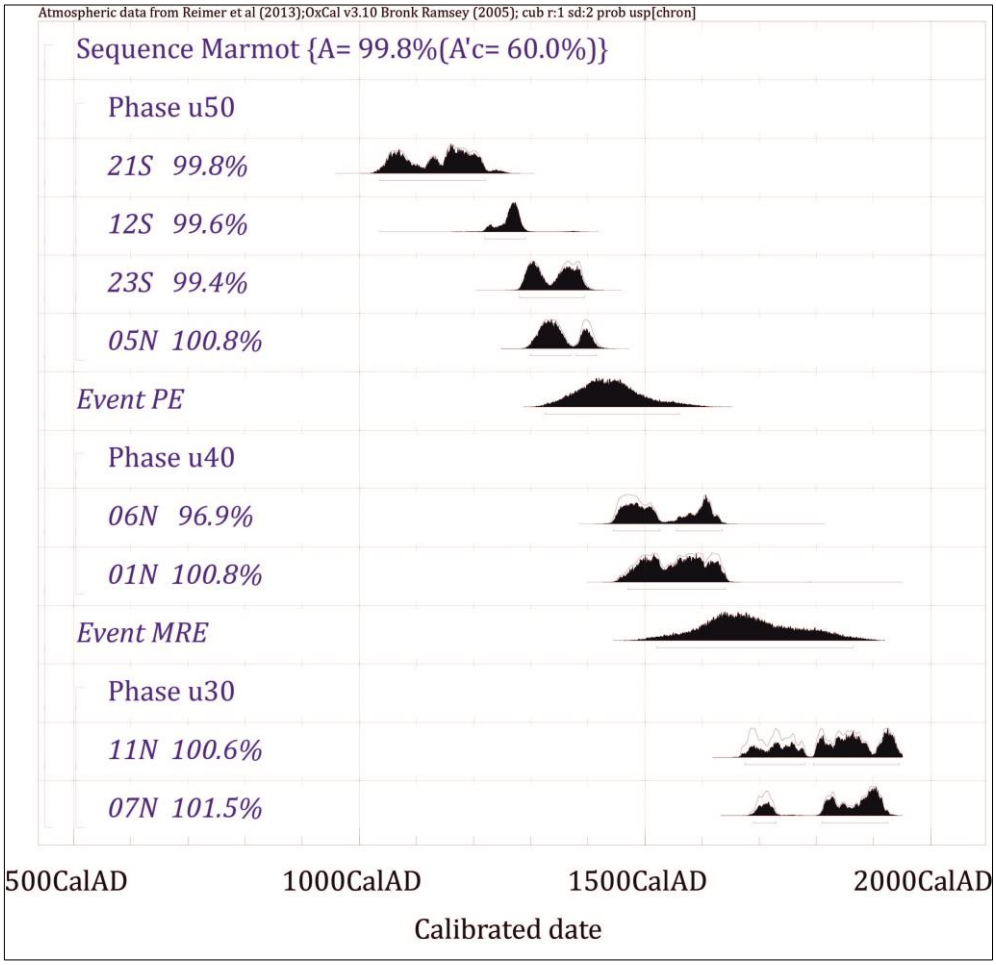

Figure 27. Radiocarbon OxCal model. The stratigraphic model indicates dates of occurrence for the last two events (Most Recent Earthquake MRE and Penultimate Earthquake PE).

3.2 Yellow Lake trench

Yellow Lake trench was excavated and studied at the northernmost tip of the Ar-Hötöl fault south of Mount Tsambagarav (Figure 24 and Figure 28).

Two large earthquakes are clearly visible in this trench. A detailed log was made on the south wall of the trench (Figure 29 and Figure 30). On the northeast side of the trench, Unit B and C are faulted and sealed by Unit A. The fault (F2) affecting the respective units appears as a big crack with a width of ~10-20 cm and filled with brown soil. Looking closely, the smaller

pebbles contained in the brown soil are vertically oriented along the fault. After that, Unit A layer is disturbed by fault (F1). The fault (F1) that cut Unit A also has brown earthy fill material with a gravelly matrix that fills ~10-30 cm wide fissure with characteristics similar to the fault that cut Unit B and C. In the middle part of the trench, the uppermost Unit A was disturbed by the faults (F1) representing the Most Recent Earthquake. At the south-west edge of the trench, Unit C1, E, and F layers were affected by the Penultimate Earthquake (F2), and ended under the sandy and gravelly layer at the bottom of Unit B layer.

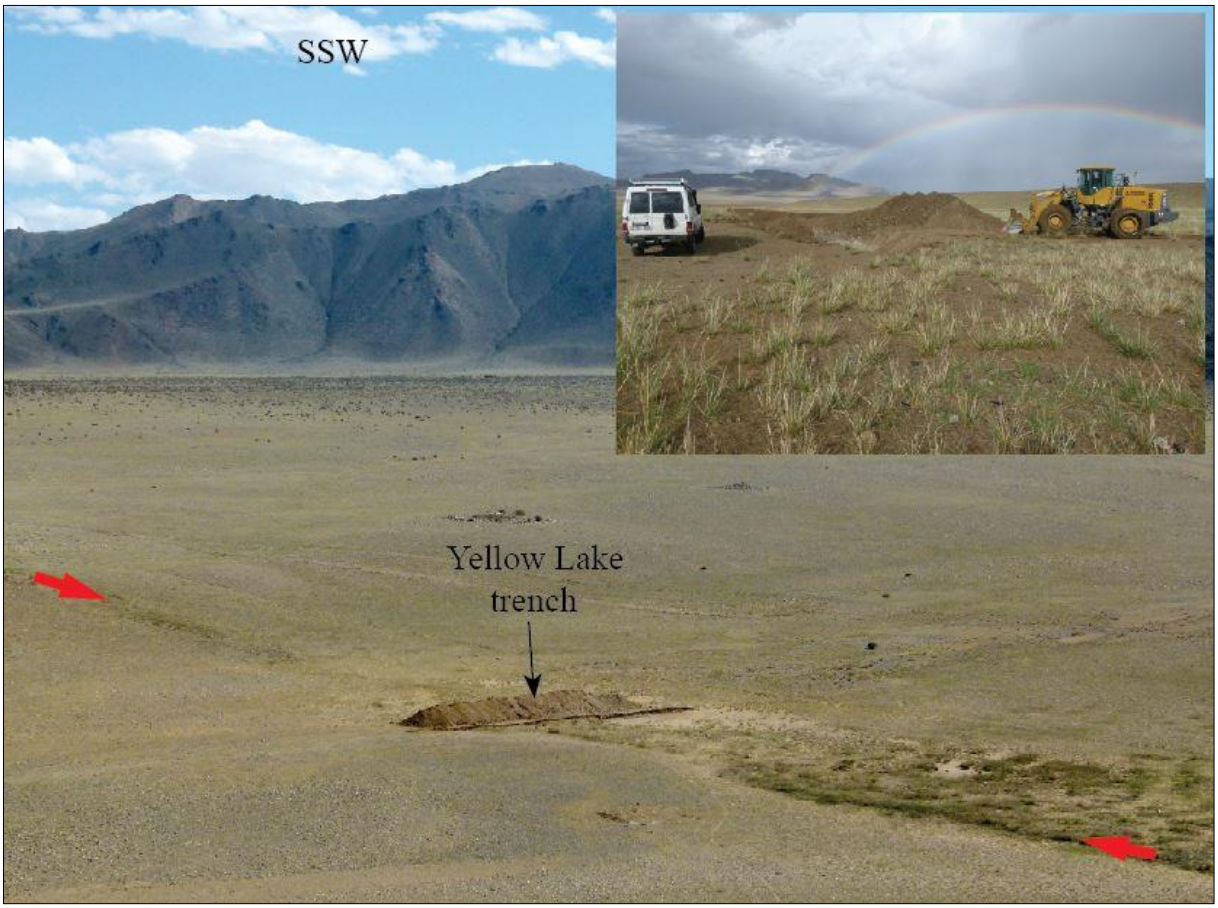

Figure 28. Yellow Lake trench. The red arrows are located along the fault. The inset map represents trenching process on August 2017. The geographical coordinate of Yellow Lake trench is N48˚23'4.01", E91˚3'31.18".

In Yellow Lake trench, stratification, sedimentary accumulation, and the faults that cross them are clearly observed. The units of the trench are described below.

Nevertheless, there were a lack of samples to determine the timing of the two large earthquakes detected in the trench. The 4 radiocarbon samples were taken from the trench. The samples were dated and analyzed in the Radiocarbon Dating Laboratory in Poznan, Poland. The dating results of those samples are 101.54±0.34 pMC (Sample name: MO17-15), 105±30 BP (MO17-14), 123.38±0.38 pMC (MO17-18), 2130±35 BP (MO17-16).

Samples MO17-15 and MO17-18 located within the Unit A lie in ~1 m thick of sediment deposit, but their modern age is less convincing. Modern materials may have been transported to the depths by activities of animals and plants. However, above these samples, the sample yielding the age of 2130 BP is noteworthy. The 2130 BP (350-49 calibrated BCE) age pre-dates the latest earthquake because the Unit A was affected by the seismic fault (F1).

3.2.1 Description of layers

- A – White yellowish clayey layer. This layer is partially bordered by a thin turf to ground surface.
- B – Rounded, unsorted, large and small pebbles dominated friable layer.
- C – Carbonaceous clay in the part bordering the faults, vertically oriented pebbles, orange and green-gray clay in the lower part. It contains gravels.
- C1 – Carbonate, scattered gravels bearing light colored sandy and clay unit. It is solid and contains small and large, angular and rounded pebbles.
- D – Rounded pebbles of maximum 8x10 cm and small sizes of angular and rounded pebbles containing clayey and gravelly layer. Dominant color of this layer is orange.
- E – Rounded gravels and boulders bearing unit. Matrix is fine-grained gravels. A red-brown layer with smoothed pebbles. Columns 19-29.
- F – Yellowish colored clay layer. It contains scattered gravels. Solid unit. The lowermost part of the trench extending westward from Column 21. Both walls of the trench have the same stratigraphy.
- M – Fine-grained gravelly unit.

Figure 29. Photomosaic of south wall of Yellow Lake trench. The faulted units were enlarged by the two zoom images (A & B).

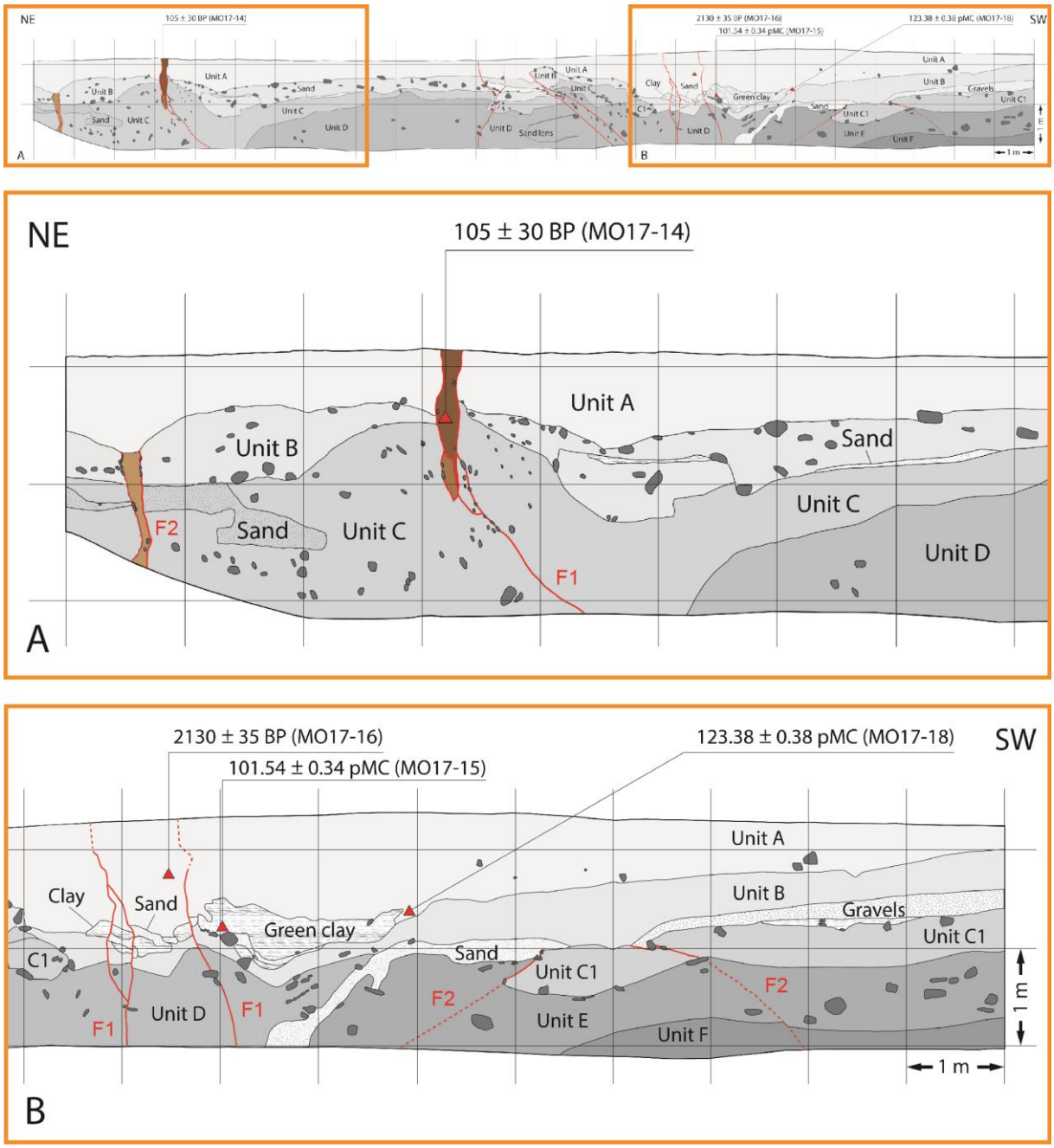

Figure 30. Log of south wall of Yellow Lake trench. The faulted layers are enlarged as the figures labeled by A & B.

3.3 Broken Boulder trench

The southernmost tip of the Ar-Hötöl fault terminates near the Bodonch River (see the main map of the Ar-Hötöl fault chapter). In that area, the fault splits and forms a typical horse-tale structure. The Broken Boulder trench was excavated on the eastern one of those branch faults (Figure 24).

In the trench site, large granite boulders transported by glaciers are abundant (Figure 31). During the route survey, we discovered that a granite boulder of ~3x7 m size located on the fault was partially broken into a tension-crack opened by the latest earthquake, and we dug a small trench under the boulder by hand and executed paleoseismological investigation in it. This paleoseismological study aimed to determine the most recent earthquake that occurred there.

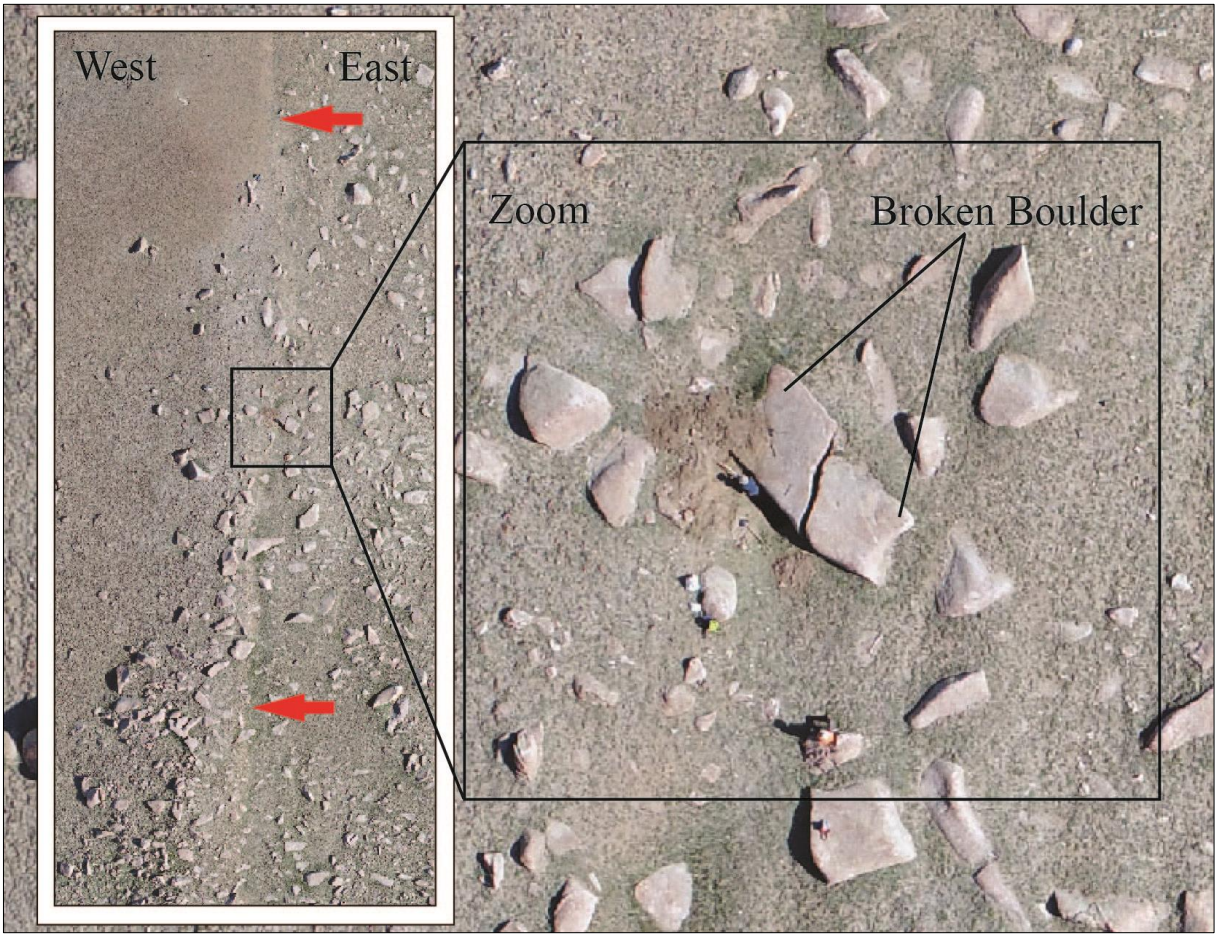

Figure 31. UAV photo of the Broken Boulder site. On the left side of the figure, the site is looked in a bigger area. The red arrows point out the fault scarps. On the right side, it is a closer zoom of the left. The Broken Boulder has a dimension of ~3x7 m. A man is shoveling a dirt for trenching next to the boulder. The geographical coordinate of the Broken Boulder trench is N46˚33'32.6", E92˚28'25.4".

The stratigraphy in the trench is relatively simple (Figure 32 and Figure 33). On the surface, or at the top, there is a giant boulder. Adjacent to it, a modern brown soil (U10) was deposited as a wedge. U21 and U20 layers are located below the giant boulder and the U10 layer. U21 and U20 layers are not disturbed by any faults. These layers have a brownish-yellow color and sandy to gravelly matrix, and irregularly scattered angular rock clasts, especially in the eastern part of the layer. The Unit 30 layer is located under the Unit 20. This layer is slightly darker than the top layer and has a dense texture. The faults are observed within the U30 layer. It is obvious that the brown soil layer (most likely lens) sampled in this layer had displaced by the fault. In addition, there is a black-brown fault gouge with a thickness of about 5 cm, which dips to the right. In this layer, there are a lot of irregularly positioned rocks, especially angular and unsorted rock clasts on the left side of the fault gouge.

The 4 bulk samples were collected from the trench. Those samples were analyzed in the Radiocarbon Laboratory in Poznan of Poland, and the samples yielded the laboratory ages of 1320±30 BP (Sample name: MO17-7), 2765±30 BP (MO17-8), 1435±30 BP (MO17-9), and 985±30 BP (MO17-10). These results of the laboratory give the ages of 653-767 calibrated CE, 993-834 calibrated BCE, 572-655 calibrated CE, and 991-1153 calibrated CE respectively.

The event horizon is located between the U20 and U30 layers. The faulted brown soil strata (lens) within the U30 gave the ages of 572-655 CE and 653-767 CE. However, the samples from the U20 yielded ages of 991-1153 CE and 993-834 BCE. When the samples are placed in stratigraphic sequence, the sample with the dating result of 993-834 BCE is significantly different from the depositional period of the samples above and below it. Therefore, this sample can be ignored. In this case, the latest earthquake at the Broken Boulder site is bracketed between 572 CE and 1153 CE.

Figure 32. Photomosaic of northern wall of the Broken Boulder trench.

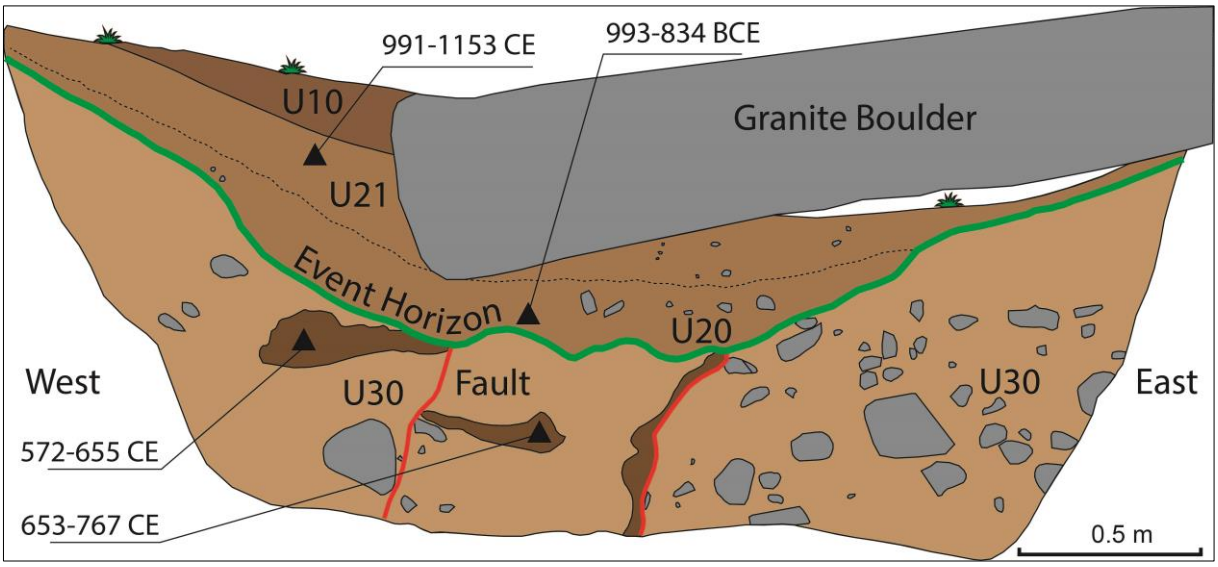

Figure 33. Log of northern wall of the Broken Boulder trench.

3.4 Conclusion

According to the paleoseismological studies, the most recent and penultimate earthquakes along the Ar-Khötöl fault are clearly visible in the Marmot Creek and Yellow Lake trenches.

In order to determine the most recent earthquakes along the fault, the values were given after 1690-1945 CE for the Marmot Creek site, after 350-49 BCE for Yellow Lake site, and between 572 CE and 1153 CE for the Broken Boulder site.

At the Marmot Creek site, the large earthquake rather than the most recent earthquake (the small) may have occurred between 1280 CE and 1640 CE. The small earthquake that was investigated in the Marmot Creek trench may be the farthest termination of the 1761 event which faulted another section along the Khovd master fault.

For the Marmot Creek trench, there were the sufficient radiocarbon samples for dating the layers, and the most recent earthquake was determined within a relatively short interval. For the Yellow Lake trench, the dating result of the latest earthquake after 350-49 BCE supports at least the periods (events) for the Marmot Creek and the Broken Boulder sites. The 991-1153 CE in the Broken Boulder trench is the only value of the one sample. The most recent earthquake at the site may have occurred at least after 572-767 CE because U30 is the pre-dating layer for the last earthquake.

Battogtokh et al, 2021. Mongolian Geoscientist 26 (52) 46-61
DOI: https://doi.org/10.5564/mgs.v26i52.1361

Mongolian Geoscientist

Original article

The 2021 M_w 6.7 Khankh earthquake in the Khuvsgul rift, Mongolia

Davaasambuu Battogtokh[1,2]*, Amgalan Bayasgalan[1], Kang Wang[3], Davaasuren Ganzorig[1], Jargalsaikhan Bayaraa[1]

[1]*Department of Earthquake Research, Institute of Astronomy and Geophysics, Mongolian Academy of Sciences, Ulaanbaatar 13341, Mongolia*
[2]*Geophysical and Satellite Imaging Team, Geosciences Montpellier, University of Montpellier, Montpellier 34095, France*
[3]*Department of Earth and Planetary Sciences, University of California, Berkeley 94720, USA*

**Corresponding author: Battogtokh@iag.ac.mn, ORCID: 0000-0003-3545-9383*

ARTICLE INFO

Article history:
Received 25 March, 2021
Accepted 29 May, 2021

ABSTRACT

A M_w 6.7 occurred at Lake Khuvsgul in northwestern Mongolia at 05:32:56 AM Ulaanbaatar time on the 12th of January 2021. The epicenter of the event was offshore south of the Doloon Uul peninsula around 30 km SSW of Khankh village. Shaking was felt within most of central and western Mongolia, including the capital city Ulaanbaatar ~600 km from the epicenter. The earthquake appears to have ruptured the Khuvsgul fault along the western coast of Lake Khuvsgul. The earthquake is the largest in Mongolia since the M_w 6.3 Busiin Gol earthquake in 1991. Our research team from the Institute of Astronomy and Geophysics, Mongolian Academy of Sciences visited the epicenter area for 5 days soon after the earthquake and installed four broad-band seismic stations and searched the area for geological evidence of the earthquake. The location, azimuth, dip and depth of this earthquake defined by moment tensor solutions calculated by the international seismological centers and analysis of InSAR interferograms and field observations. The projected intersections of the east-dipping nodal planes with the surface for solutions of the international seismological centers and researchers correlate relatively well with the mapped strike and location of the old tectonic scarp of the Khuvsgul fault although we have not discovered any primary co-seismic surface rupture. The InSAR interferogram demonstrates the sharp discontinuity and fringes in the area between the Western Range and Doloon Uul peninsula which implies surface deformation. Aftershocks that have continued during the three months subsequent to the earthquake define overall strike of the mainshock rupture.

Keywords: Basin, co-seismic, epicenter, fault and solutions

INTRODUCTION

In this paper, we present the fault plane solutions of the Khankh earthquake M_w 6.7 and discuss its relations with the underlying Khuvsgul fault, through analysis of satellite images, InSAR data and co-seismic surface rupture features revealed by the field visit.

The Khuvsgul (it is written as Hövsgöl according to Baljinnyam et al., 1993), Darkhad and Busiin Gol basins are considered to be the south-west termination of the Baikal rift system. The Baikal rift is defined by an alignment of north-east-trending elongated basins stretching from Mongolia to Russia for roughly 1700-1800

CHAPTER 4

4. THE 2021 M_W 6.7 KHANKH EARTHQUAKE IN THE KHUVSGUL RIFT, MONGOLIA

Davaasambuu Battogtokh[1,2]*, Amgalan Bayasgalan[1], Kang Wang[3],

Davaasuren Ganzorig[1], Jargalsaikhan Bayaraa[1]

[1]*Department of Earthquake Research, Institute of Astronomy and Geophysics, Mongolian Academy of Sciences, Ulaanbaatar 13341, Mongolia*

[2]*Geophysical and Satellite Imaging Team, Geosciences Montpellier, University of Montpellier, Montpellier 34095, France*

[3]*Department of Earth and Planetary Sciences, University of California, Berkeley 94720, USA*

**Corresponding author: Battogtokh@iag.ac.mn, ORCID: 0000-0003-3545-9383*

4.1 Abstract

The M_w 6.7 occurred at Lake Khuvsgul in northwestern Mongolia at 05:32:56 AM Ulaanbaatar time on the 12th of January 2021. The epicenter of the event was offshore south of the Doloon Uul peninsula around 30 km SSW of Khankh village. Shaking was felt within most of central and western Mongolia, including the capital city Ulaanbaatar ~600 km from the epicenter. The earthquake appears to have ruptured the Khuvsgul fault along the western coast of the Lake Khuvsgul. The earthquake is the largest in Mongolia since the M_w 6.3 Busiin Gol earthquake in 1991. Our research team from the Institute of Astronomy and Geophysics, Mongolian Academy of Sciences visited the epicenter area for 5 days soon after the earthquake and installed four broad-band seismic stations and searched the area for geological evidence of the earthquake. The location, azimuth, dip and depth of this earthquake defined by moment tensor solutions calculated by the international seismological centers and analysis of InSAR interferograms and field observations. The projected intersections of the east-dipping nodal planes with the surface for solutions of the international seismological centers and researchers correlate relatively well with the mapped strike and location of the old tectonic scarp of the Khuvsgul fault although we have not discovered any primary co-seismic surface rupture. The

InSAR interferogram demonstrates the sharp discontinuity and fringes in the area between the Western Range and Doloon Uul peninsula which implies surface deformations. Aftershocks that have continued during the three months subsequent to the earthquake define overall strike of the mainshock rupture.

4.2 Introduction

In this paper, we present the fault plane solutions of the Khankh earthquake M_w 6.7 and discuss its relations with the underlying Khuvsgul fault, through analysis of satellite images, InSAR data and co-seismic surface rupture features revealed by the field visit.

The Khuvsgul (it is written as Hövsgöl according to Baljinnyam et al., 1993), Darkhad and Busiin Gol basins are considered to be the south-west termination of the Baikal rift system. The Baikal rift is defined by an alignment of north-east-trending elongated basins stretching from Mongolia to Russia for roughly 1700-1800 km. The rift zone consists of numerous basins including Busiin Gol, Darkhad, Khuvsgul, Tunka, Baikal, Angara, Muya and Khara from the south-westernmost continuation in Mongolia to the north-easternmost tip in Russia.

The scientific study of Lake Baikal began from the 18th century geographic expeditions of the Russian Geographical Society. The first scientific realization of the Baikal basin in the frame of tectonic context was reported by Obruchev in 1938. In the literature, Lake Baikal is expected to fill out a graben formed by expansion of tectonic blocks. Pavlovsky (1948) revealed the similarity to the east African rift.

Several hypotheses and models on the origin and evolution of the rifting have been proposed (such as Florensov, 1969; Molnar and Tapponnier, 1975; Zonenshain and Savostin, 1981; Logatchev et al., 1993; Ivanov, 2004; Petit and Deverchere, 2006). Molnar and Tapponnier (1975) interpreted that the Baikal rift zone is a manifestation of the India-Eurasia collision. Logatchev et al. (1983) and Logatchev (1993) argued that the initiation and development of the rift is an independent structure associated with the local thermal processes in the mantle without any direct relation to the collision of India-Eurasian plates. Recent studies by Petit and Deverchere (2006) have been able to confirm earlier findings by Tapponnier and Molnar.

Several investigations (Calais et al., 2003; San'kov et al., 2000; Ritz et al., 2018) have been conducted to estimate the rates and amounts of opening of the Baikal rift from GPS measurements and slip-rates along the basin bounding faults from geological observations. GPS measurements suggests a crustal extension of ~4 mm/year across the main portion of the Baikal

rift (Calais et al., 2003). The central Baikal basin is bounded by the Siberian platform to the west. Zonenshain and Savostin (1981) and more recently Barth and Wenzel (2010) showed that the Baikal rift system is a boundary of the Amurian plate. Khuvsgul, Darkhad and Busiin Gol basins in the Mongolian territory which define the southwestern limit of the rift system have N-S trending azimuths, whereas the Central Baikal and other basins in the Russian territory has dominantly SW-NE oriented strikes (Figure 34).

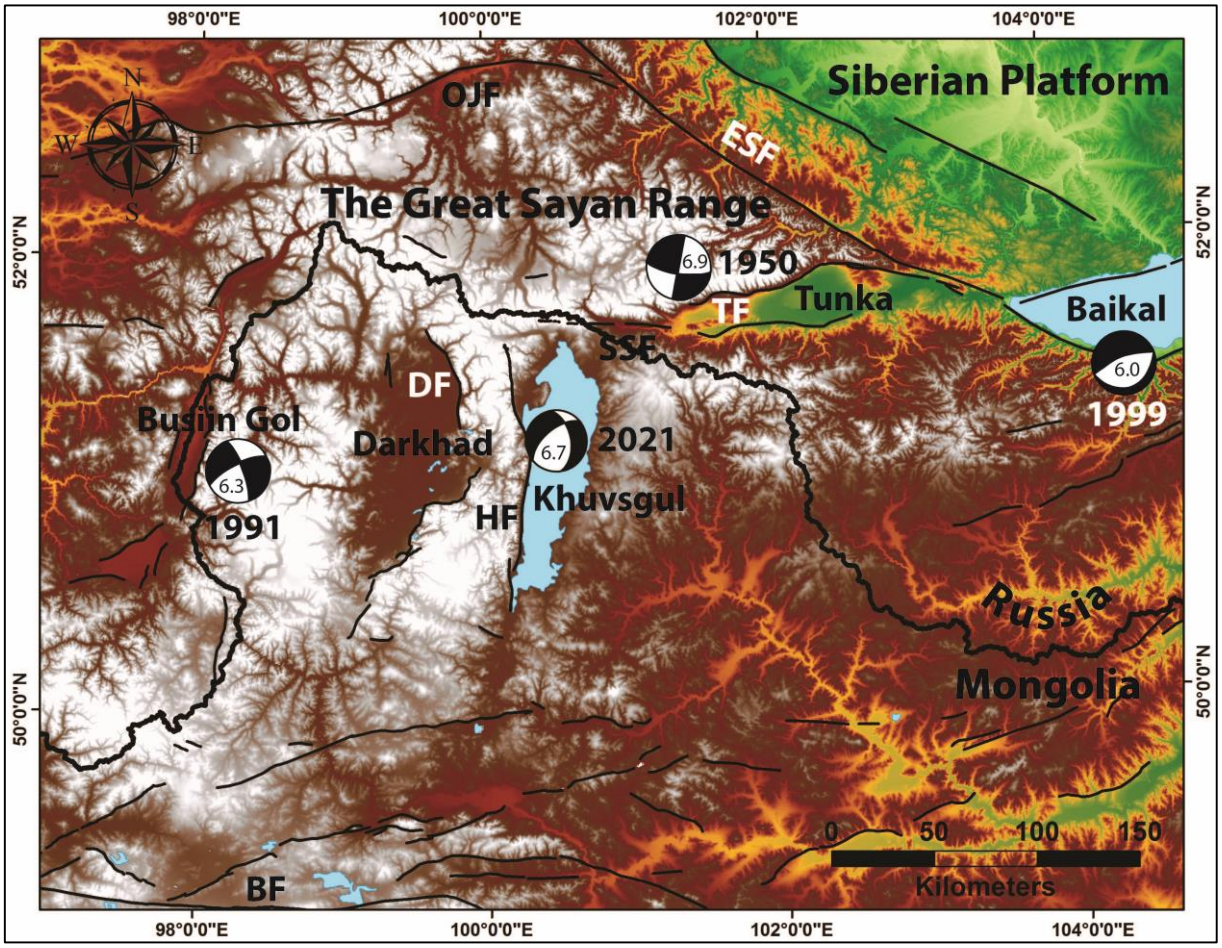

Figure 34. General map of the Busiin Gol, Darkhad, Khuvsgul, Tunka at south-western edge of the Baikal rift system. Focal mechanisms of earthquakes ($M_w \geq 6.0$) and active faults are plotted on Shuttle Radar Topography Mission (SRTM). Elevations are from ~500 (light-green) to ~3500 m (white). The thick curved black line is the border between Mongolia and Russia. The focal mechanism solutions for $M_w \geq 6.0$ events are from Bayasgalan et al. (2005) and Ritz et al. (2018). Black lines represent the active faults, including Khuvsgul fault (HF), South Sayan fault (SSF), Darkhad fault (DF), Busiin Gol fault, Oka-Jombolok fault (OJF), Eastern Sayan fault (ESF) and Bulnai fault.

4.3 Geology

The basement geology of the Busiin Gol, Darkhad and Khuvsgul rifts regions are accreted Neoproterozoic and Paleozoic accretionary wedge and island arc terranes (Badarch et al., 2002). It is composed of Neoproterozoic metamorphic, volcanic rocks and ophiolite. Some part of the basement rocks are covered by Neoproterozoic-Lower Cambrian shelf carbonate rocks of the Khuvsgul basin and intruded by post-collisional Ordovician, Devonian and Permian granites. The central section of the Baikal rifting initiated in Oligocene and other neighboring basins were developed during Miocene (Florensov, 1969; Logatchev, 1993). The rifting of Lake Khuvsgul began in the Late-Miocene and the Darkhad and Busiin Gol depressions initiated later in the Middle-Pliocene (Logatchev, 1993).

Late-Pleistocene moraines and post-glacial sediment deposits are widespread along the river valleys around the lake (Wegmann et al., 2011; Orkhonselenge et al., 2014).

4.4 The brief characteristics of the Khuvsgul basin

The Khuvsgul basin is bounded by the Khoridol Saridag (3093 m) and Ulaan Taiga Range (3193 m) to the west and the Sayan Range (Munkh Saridag 3491 m) to the north. The eastern mountains (the highest point is the Tsagaan Uul 2367 m) are relatively low and dome shaped comparing to the western and northern ranges. Lake Khuvsgul is 136 km long and 36.5 km wide at its widest section (Figure 34). Its depth reaches 267 m and areal expanse is 2620 km^2, with a total water volume of 381 km^3. The surface elevation of the lake is ~1645 m above sea level (Sodnom et al., 1990). A large number of permanent rivers flow into Lake Khuvsgul and the Khoroo river from the north-west is the largest among them. Only the Eg river flows out from the lake to join the Selenge river which flows into the world largest fresh water Lake Baikal.

4.5 Active faults in the Khuvsgul rift

The western side of Lake Khuvsgul is controlled by an active fault forming a half-graben structure. The half-graben is identified as the western block which features a linear and rugged topography as well as thickness of sediment deposits to the western coast by a seismic profile across the lake (Fedotov, 2007; Prokeponko and Kendall, 2008).

Active faults in the vicinity of the Khuvsgul rift have been mapped roughly by Molnar and Tapponnier (1975), relatively in detail by Zonenshain and Savostin (1981) and Khilko et al. (1985), in somewhat greater detail by Sankov et al. (2003); Arjannikova et al. (2004), Byamba (2009) and Ritz et al. (2018).

From its northern end near Khongor Buush river, the Khuvsgul fault strikes southward into Lake Khuvsgul. The NNW-trending northern segment in the surface is mapped tentatively as discontinuous and interrupted scarps from the lake margin around 51˚08′35″ N, 100˚19′15″ E the south of the Doloon Uul peninsula and northward to around 51˚36′39″ N, 100˚08′17″ E the south of the Khoroo river valley (Figure 35). Several river valleys and risers are displaced right-laterally along the fault to the north based on satellite images.

The Sayan active fault is located along the front of the Sayan Mountain Range at the north of Lake Khuvsgul. The rivers from the range are displaced left-laterally in tens of meters by the fault. Considering the triangular facets of the Sayan Mountain Range, it could be a normal fault with left-lateral strike-slip component. Ritz et al. (2018) estimated that the left-lateral slip rate along the Eastern Sayan fault is 1.3-3.9 mm/year.

There is no research work investigating the geological slip rate along the Khuvsgul fault.

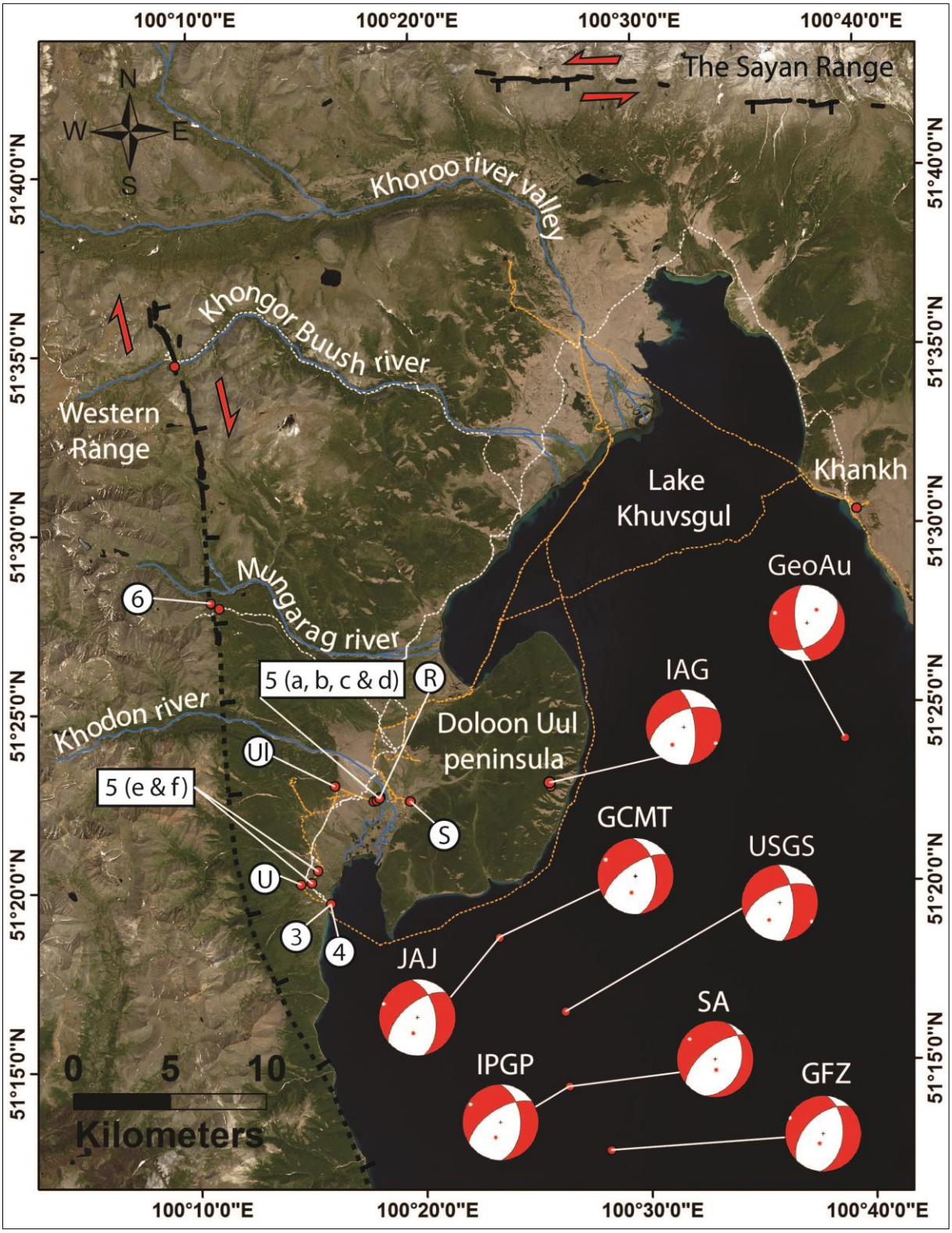

Figure 35. The epicenter area of the Doloon Uul peninsula. The Base Map is based on the Landsat 8 image. Tectonic scarps of Khuvsgul and Sayan faults are marked by the thick black lines. The dashed black line is the inferred Khuvsgul fault. Golden dashed lines are our tracks during the winter field research work. Note that I added my summer field route on this figure by the white dashed lines. Capital letters (U, Ul, R and S) represent the locations of the herder families who are Ukhnaa, Ulziibat, Rinchen and Sodkhuu where we collected the macro-data. Numbers of 3, 4, 5 and 6 express the locations of the field photographs for Figure 36 to Figure 39. Fault plane solutions are modified from the official websites and personal communications. See the Table 3 for the detailed information.

4.6 Fault plane solutions of the Khankh earthquake

We compare different fault plane solutions by different seismological centers and researchers around the world in Figure 35 and Fig. A2. The location, depth, strike, dip and rake of the event are summarized in Table 3. The locations of each are consistent with the event occurring on the down-dip projection of the east-dipping Khuvsgul normal fault (Figure 35 and Figure 40). The east-dipping nodal planes of each mechanisms are similarly consistent with normal displacement along the northerly striking Khuvsgul fault. The alignment of the estimated epicenters along a northwest trending line most likely is not tectonically significant but rather an artifact of different locations procedures and data used by the respective agencies.

The moment tensor and epicenter labeled IAG in Figure 35 and Fig. A2 are determined via local seismic network stations which belong to MNDC, IAG (Mongolian National Data Center, Institute of Astronomy and Geophysics). We define the earthquake moment tensor inversions as the estimation of the source depth (Z), the moment magnitude (M_w), and strike, dip and rake angles for the shear dislocation source (Herrmann et al., 2011; Herrmann, 2013). The moment tensor solutions in Figure 35 and Fig. A2 are determined with the broadband channels of the regional seismic networks for a rapid estimation of the source parameters with body waves except for Geoscience Australia (GeoAu) and Seismic Analysis (SA) which used W-phase and body wave source inversion data and methods.

Table 3. Moment tensor solutions for the Khankh earthquake.

Moment tensor solutions for the Khankh earthquake

Date	Lat (°N)	Lon (°E)	Depth (km)	M_w	Strike	Dip	Rake	Source
2021.01.11	51.380°	100.430°	12.0	6.65	353°	66°	-141°	IAG
21:32:59	51.281°	100.438°	8.0	6.65	356°	61°	-143°	USGS
(UTC)	51.21°	100.47°	18	6.7	4°	47°	-121°	GFZ
	51.40°	100.65°	18	6.7	172°	65°	-126°	GeoAu
2021.01.12	51.31°	100.39°	14.3	6.8	354°	45°	-143°	GCMT
05:32:56	51.24°	100.44°	13	6.8	358°	46°	-139°	IPGP
(UB time)	51.24°	100.44°	10	6.69	16°	32°	-121°	SA
	51.31°	100.39°	15	6.63	350°	50°	-138°	JAJ

Note: Date, latitude, longitude, depth, magnitude, strike, dip of the fault plane, rake of the slip vector and abbreviations of the international seismological centers and researchers. IAG – The Institute of Astronomy and Geophysics of Mongolian Academy of Sciences; USGS – The United States Geological Survey; GFZ – German Research Centre for Geosciences; GeoAu – Geoscience Australia; GCMT – The Global Centroid Moment Tensor; IPGP – Institut de Physique du Globe de Paris; SA – Seismic Analysis, Mohammad Raeesi; JAJ – Professor James Jackson, University of Cambridge, personal communications.

We show in Figure 40 the location of surface rupture that can be expected by propagating up dip along the fault plane and epicenter determined by each agency. The projected intersections of the nodal planes with the surface for GCMT, JAJ and IPGP solutions correlate relatively well with the mapped strike and location of the Khuvsgul fault. The projected locations of IAG, USGS and GeoAu are a few kilometers away to the east from the fault although their strikes are well directed. IPGP is focused on the right location of the big crack (Figure 36 and Figure 37). JAJ is perfectly fixed along the Khuvsgul fault. The waveforms of JAJ are presented in Appendix (Fig. A1).

The focal mechanism solutions are modified and plotted by Generic Mapping Tools (Wessel et al., 2013) and demonstrated in Fig. A2.

Thousands of aftershocks have been recorded after the mainshock of the 2021 M_w 6.7 Khankh earthquake. According to IAG news as of March 10, 2021, there have been ~40,000 aftershocks recorded by the seismic network, among which ~180 are magnitude 3.5 and above.

4.7 The field work report following the Khankh earthquake

The research team from the Institute of the Astronomy and Geophysics in Ulaanbaatar city set off after 3 days after the earthquake and arrived in the Khankh village at the northern coast of Lake Khuvsgul on 17th January. We worked for two days in the epicentral area in the vicinity of the Doloon Uul peninsula.

With the help of local herders, we located numerous cracks. The cracks with 1-5 cm of widths were seen in many places in the low area of the Mungarag and Khodon between the Doloon Uul peninsula and the Western Range (Figure 38). The length of the cracks are several hundreds of meters and even might reach up to several kilometers. The strikes of the cracks are chaotic. Some cracks are NW trending and some of them are NE oriented. Moreover there are cracks with azimuth along latitude. At 51˚20′12″ N, 100˚15′03″ E, we observed a linear structure with many sand volcanoes and linear liquefaction cracks (Figure 38-e-f). This structure extended continuously for approximately 700 m (the dashed track on Figure 35).

One possible mechanism of such phenomena is that during the earthquake soil particles are rearranged and compacted, forcing out water onto the surface, to create sand volcanoes, sand boils and surface cracking. Such kind of phenomena happened during the 2010 Canterbury Earthquakes in New Zealand (Royal.., 2010).

The central part of the low area was the most affected place where a herder's (Figure 35) food storage log cabin was nearly collapsed and the herdsman had to move to his summer house in a couple of kilometers to the south.

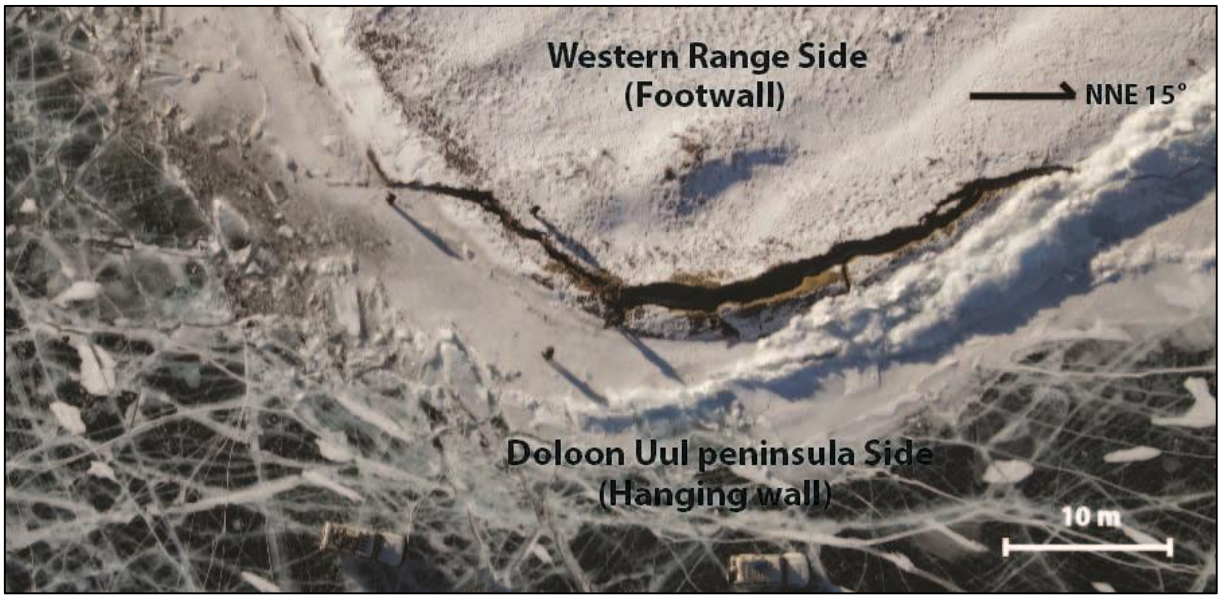

Figure 36. A drone image for the big crack. It is only site with considerable surface offset that is most likely associated with the earthquake during our field route. The western side (Footwall) moves upward relative to the eastern side (Hangingwall). The people and cars provide for scale. Image by Bayaraa.

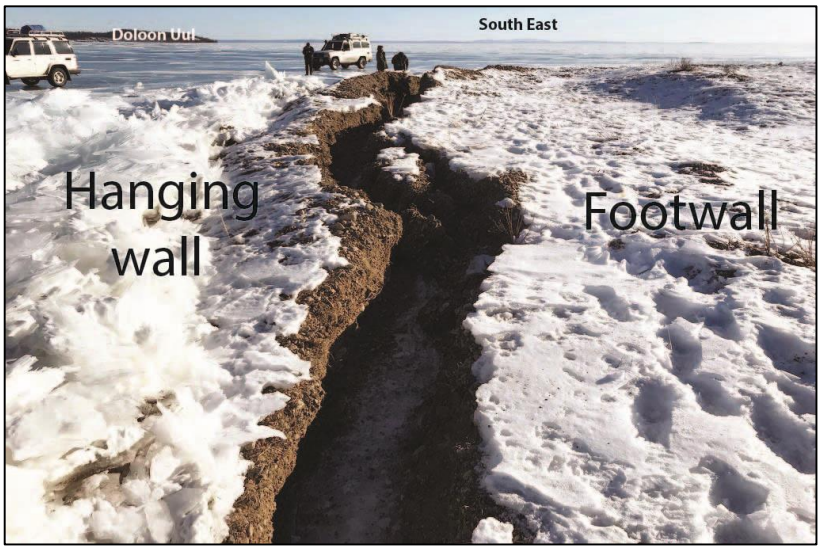

Figure 37. A photograph for the big crack. The width of the surface rupture is ~1.3 m. Photo by Bayasgalan.

This place was next to the river which has a permanent water flow due to many springs. At this site we found many cracks with a wide spread of orientation and all the offsets in this area were on the order of few centimeters (Figure 38-a, b, c and d) Some of the opening cracks produced a T-shaped structure. We also discovered a site with small amount (5-10 cm) of left-lateral offset at 51˚22′34.9″N, 100˚18′11.1″E (Figure 38-a). NNW 335˚ trending right-stepping cracks

are documented at 51˚22′29.1″ N, 100˚18′2.0″ E (Figure 38-b). We interpret these surface cracks to also be secondary fissures related with local uplift of watery horizon.

We could see only site with a considerable surface rupture is likely to be related with the earthquake that moved during the latest event (Figure 36 and Figure 37) This ~45 m rupture was found near the shore of the lake and had a strike of NNE 15˚, which was characterized by a ~1.3 m opening fissure with about 20-30 cm of vertical offset, with the east side being down.

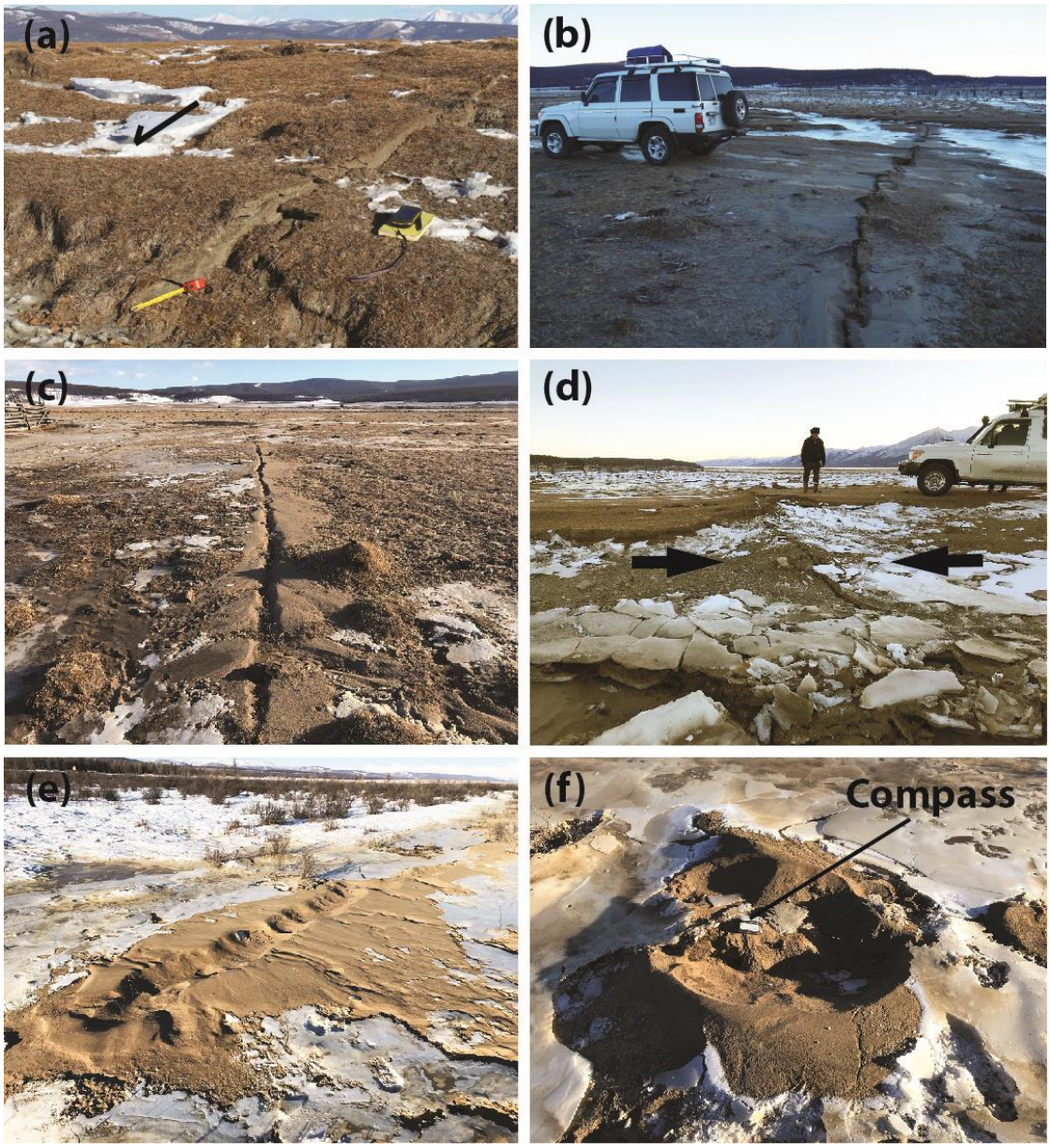

Figure 38. Micro-features related with the earthquake in the low area between the Doloon Uul peninsula and the Western Range. (a) photo shows a normal fault of ~10 cm with left-lateral strike-slip component of ~5 cm. The western side is up. (b) photograph expresses a right-stepping micro-tension-cracks that implies the left-lateral strike-slip fault. There are the linear cracks with sand liquefaction and sand volcanos on (c, e, f) photos. Photo (d) shows the small-thrust fault due to local micro-compression. Photos by Battogtokh and Bayasgalan.

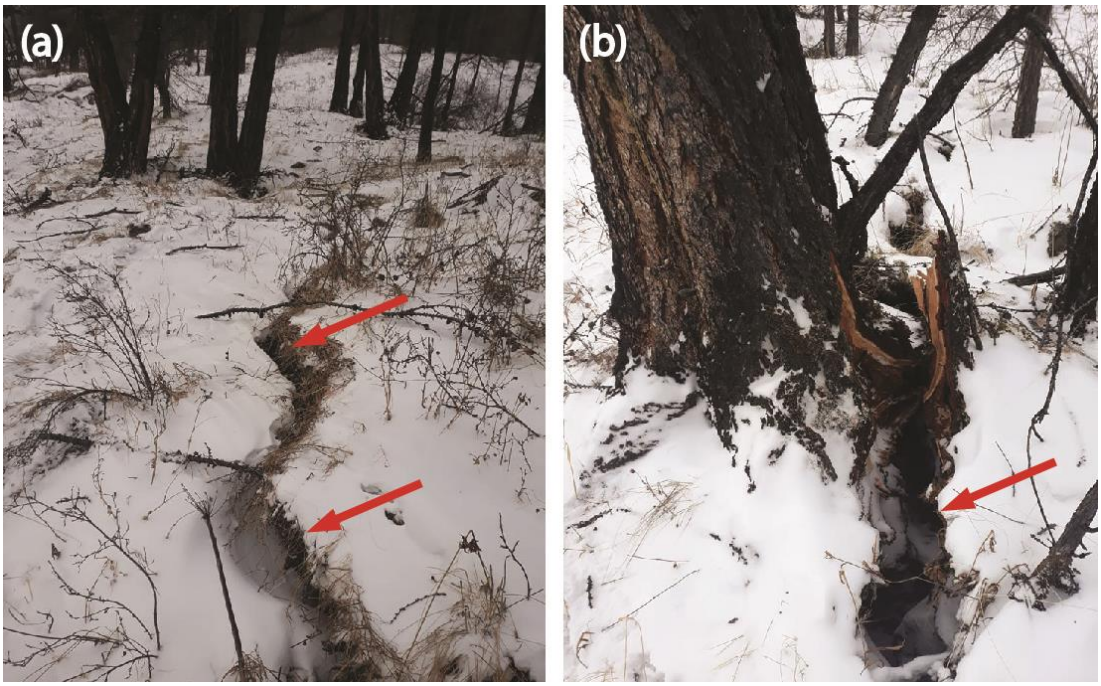

Figure 39. Cracks in the Western Range. (a) an elongated crack with width of ~10 cm is marked by the red arrows. (b) a big tree is broken by the co-seismic event. The local name of the location is the Artsatiin Khash. Photos by Batdelger.

4.8 Discussion

The strong earthquake struck after the surface of Lake Khuvsgul was completely frozen. Every year the lake is ice covered from middle of December to middle of June for ~6 months. The average thickness of ice is 40-70 cm. The magnitude 6.7 earthquake neither caused a major surface rupture, nor a break in the ice.

No seiche waves sufficient to break the ice in the lake water is perhaps the result of (i) high-frequency waves (longer-period waves traveling through the ground create seiches) were generated because the seismic epicenter was too close under the lake floor and (ii) the ice cover of the lake was able to barrier an initial oscillations to produce seisches despite the fact that ice cover is too thin compared to the lake water and in addition (iii) normal faulting of the 2021 Khankh earthquake is probably less favorable to generate tsunamis and seiches compared to thrust events (Seattle.., 2014).

The earthquake was nonetheless strong in shaking. It was felt on the 8th floor of an apartment building of Ulaanbaatar city (Battogtokh's home address) waking up with a feeling of being pushed from below at a distance of ~600 km away. According to interview with local herders Ulziibat, Ukhnaa and Sodkhuu who live in the epicenter area of the Doloon Uul (Figure 35), they all said that there was a monstrous noise during the earthquake and it was as if they were

thrown with their houses. That said the real damage was relatively modest, perhaps because homes are generally constructed from wooden logs rather than stone or concrete. According to herder Ulziibat, the wave of the first strong earthquake seemed to be directed from south to north, and the second one seemed to be directed along the latitude. They expected like that because their houses were shaken in those directions. The location of his house is NNW-SSE oriented. Moreover, a Russian Jeep (UAZ-469) which had been parked in front of his house was thrown in ~30 cm and returned to its place. The herdsman showed us the wheels patterns on fresh snow. There was a strong tremor around a herder Rinchen's house. His livestock barn was collapsed and 1-2 logs in his log house were pulled out about ~5 cm like other herder families' houses. Near his house and barn, there were chaotic cracks with sandy water. We discovered a micro-normal fault with left-lateral strike-slip component.

We ordered a real-time KOMPSAT-3 satellite imagery with a ground-resolution of 0.7 m via the Active Tectonics Laboratory of Korea Institute of Geoscience and Mineral Resources (KIGAM) and did reconnaissance on it but we did not discover any major surface rupture that might be associated with the co-seismic event.

Our colleagues from America, France, Turkey and Korea obtained InSAR interferograms in using Sentinel-1 data to characterize the co-seismic deformation of this earthquake. InSAR data were not available until we almost finished the field work in the epicenter area. The InSAR interferogram (Figure 41), reveals fringes along the western side of the lake implying deformation on the surface where in Khodon and Mungarag low area between the Doloon Uul peninsula and the Western Range as well as in the Artsatiin Khash place in the Western Range. Although we already did the field routes and traverses through the high-effected area between the Doloon Uul and the Western Range based on the record of our GPS tracks (Figure 35 and Figure 41), there were not any primary surface ruptures except the most prominent one with a length of ~45 m and micro-cracks we mentioned above. We could not manage to visit the site where InSAR most likely indicates a primary surface rupture because of the winter weather condition. But we verified tentatively that the sharp fringes in the Western Mountains might be local effects as well. We asked a herdsman who lives in the place to check if there were any noticeable surface cracks around this area. He informed that there were an interrupted cracks with width of ~10 cm in the area called Artsatiin Khash (Figure 35 and Figure 39). We had better check the area and execute more geological investigations in the upcoming summer.

However, there are the sharp effects and fringes in the InSAR (Figure 41) along the west shores of the lake. The fringes disappear as soon as it emerges the lake shore because it is connected

to the water. The InSAR fringe pattern implies that large portion of the rupture might be underneath the lake.

Continuous preexisting tectonic scarps and right-lateral cumulative displacements are visible around the Khongor Buush river valley (around at 51˚35′05″ N, 100˚09′11″ E) southwest of the Emeel Mountain (Figure 35) on Landsat 8, Google Earth and Bing Map. Any fresh surface rupture was not discovered along this segment on the real-time KOMPSAT imagery acquired after the earthquake. However, the focal mechanisms from IAG, USGS, GCMT, IPGP and JAJ are determined as the dextral strike-slip fault with normal component trending NNW that are consistent with the old dextral tectonic scarps on the satellite images. A large number of weak aftershocks have been recorded along this segment.

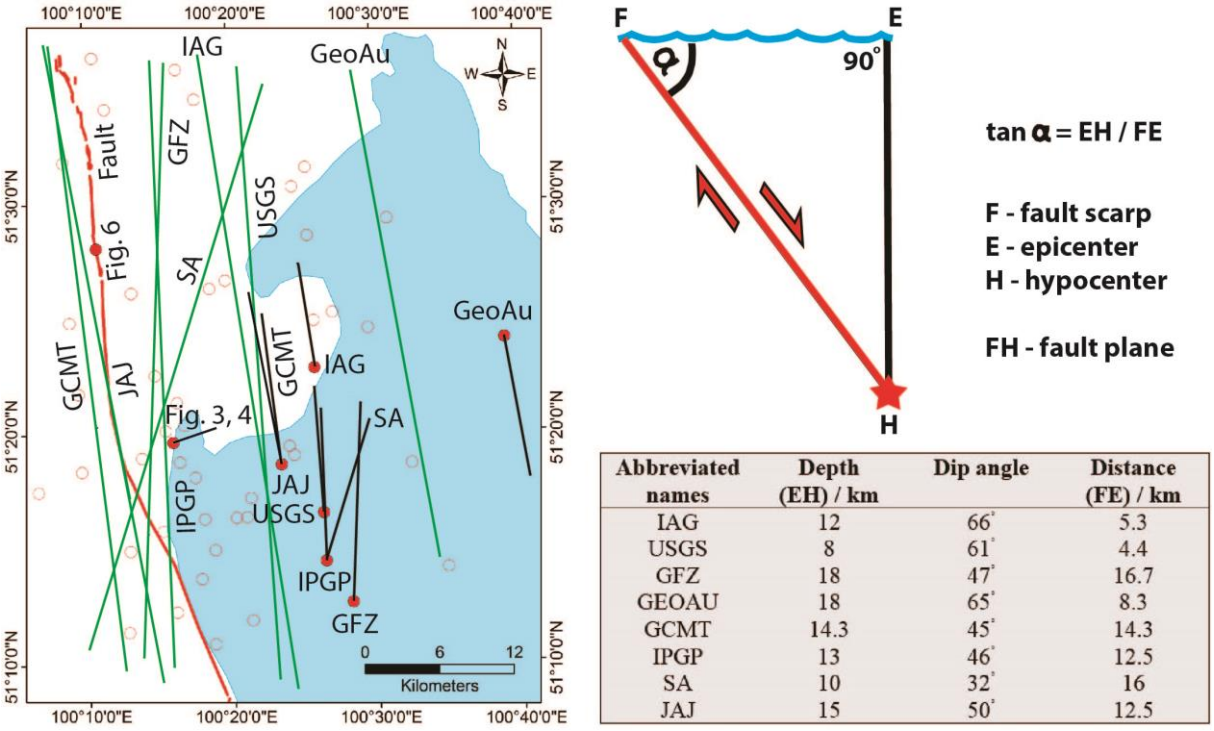

Abbreviated names	Depth (EH) / km	Dip angle	Distance (FE) / km
IAG	12	66˚	5.3
USGS	8	61˚	4.4
GFZ	18	47˚	16.7
GEOAU	18	65˚	8.3
GCMT	14.3	45˚	14.3
IPGP	13	46˚	12.5
SA	10	32˚	16
JAJ	15	50˚	12.5

Figure 40. Model of the projected fault scarps. The black lines show the strikes that were calculated by the seismological centers. The green lines are the projected (visualized) fault scarps based on information of the focal mechanisms (Figure 35, Fig. A2 and Table 3). The red circles except two circles (Figure 36 and Figure 38) are the epicenters of the focal mechanisms. Figure 36 to Figure 38 are the considerable surface rupture (See Figure 35) during the co-seismic process. The hollow red circles represent aftershocks between M_w 4.1 and M_w 5.4 from the open-source data of USGS. The table demonstrate the distances between the projected fault scarps and the epicenters.

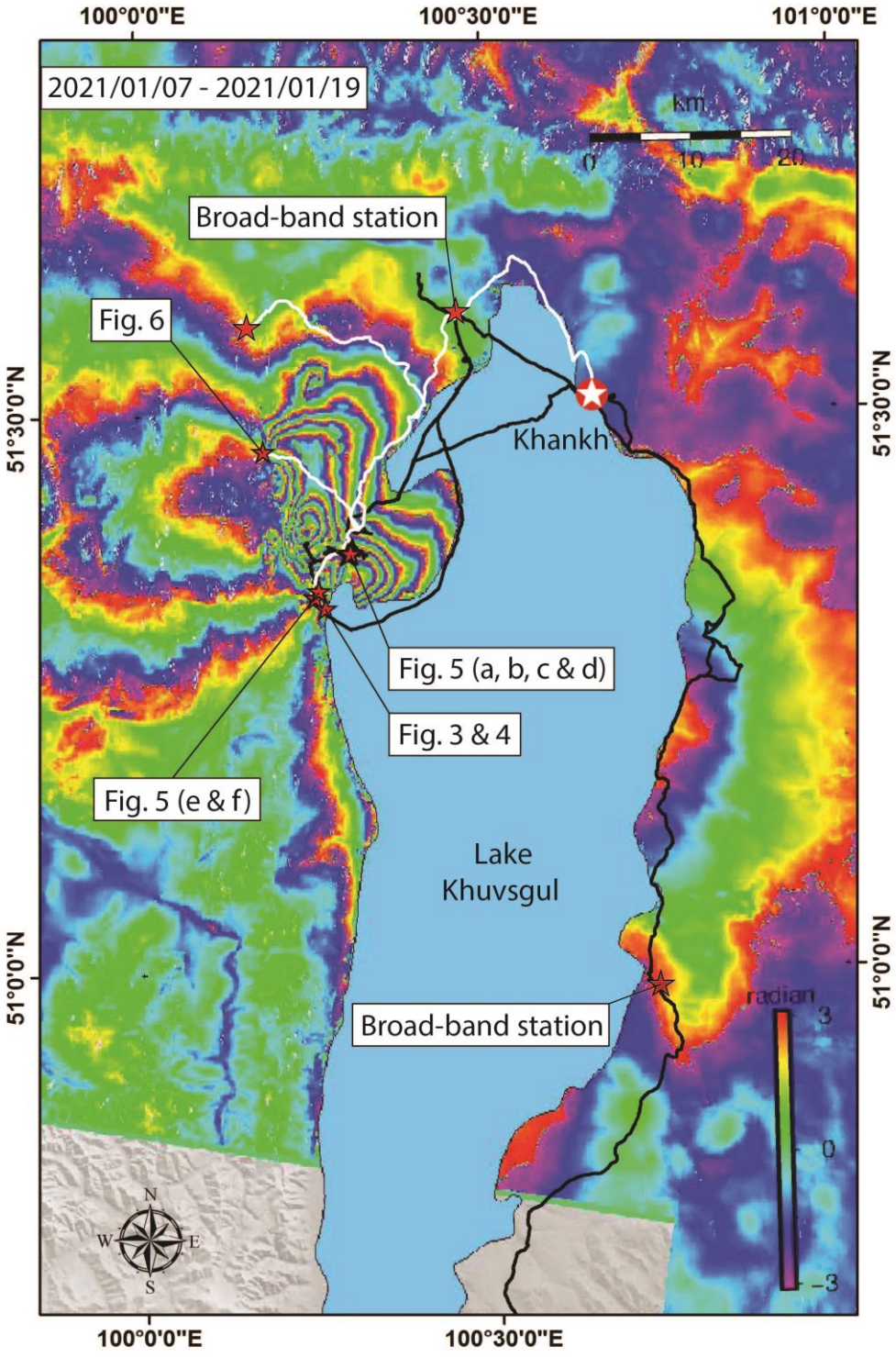

Figure 41. A Sentinel-1 InSAR interferogram from data of a descending track covering the Khankh earthquake M_w 6.7. The white star marks the Khankh village. The red stars represent the locations of Figure 36 to Figure 39 and also show the locations of the broad-band seismic stations those were installed by us in order to record aftershocks. The black curved traverses express our track during the winter field work. And the white curved traverses express our track during the summer field work. Note that I added my summer-field-work track on this figure. By the time the article was published, the summer field work did not take place. The results of the summer campaign were included in the general conclusion of the thesis.

4.9 Conclusions

M_w 6.7 earthquake has a high-chance to produce a surface rupture with a co-seismic offset of ~0.5 m and a length of ~25 km providing that we consider the empirical relations of the magnitude by Wells and Coppersmith (1994). In contrast with it, there is a little-chance to be that much rupture on the surface according to during our field visit, local herders' traverses and even during reconnaissance on the real time KOMPSAT-3 satellite images.

In parallel, the fault scarp associated with the earthquake might have been produced on the floor of Lake Khuvsgul along the western coast. In that case, we speculate that the northernmost tip of the rupture is the big crack at 51˚19′37″ N, 100˚15′55″ E where we see the most prominent normal fault scarp at the lake shore despite the fact that it terminates in a distance of only ~45 m from the shore. The western side of the fault scarp moved up for 25-30 cm compared with the eastern side. Moreover the location and kinematics of this tiny-length fracture is relatively convenient with the fault plane solutions which were calculated by JAJ, GFZ and IPGP.

Although there are a considerable amount of elongated small cracks with chaotic azimuths and width of 1-5 cm in the Khodon delta between the Doloon Uul peninsula and the Western Range those cracks are clearly site effects associated with the strong earthquake. Therefore all kind of features of kinematics such as micro-thrust, micro-normal faults with left-lateral component and micro-right-stepping tension-cracks to express left-lateral strike-slip faults are discovered in this area.

ACKNOWLEDGEMENTS

This work was supported by IAG, MAS. The authors thank James Jackson for his fruitful comments associated with fault plane solutions from the international seismological centers as well as for his produced focal mechanism. Jean-Francois Ritz, Yann Klinger, Munkhuu Ulziibat, Jin-Hyuck Choi and Takashi Nakata are regarded as their views and scientific conversations with us for this earthquake. We are very grateful to Steven G. Wesnousky for his detailed review and comments which greatly improved the manuscript. Local driver Batsukh Batsuuri is thanked for guiding us in the area of Doloon Uul peninsula. Local herder Banzai Batdelger is thanked for ground-checking and discovering some cracks related to the earthquakes in the high-mountains of the western range with his horse.

4.10 References

Arjannikova, A., Larroque, C., Ritz, J.-F., Deverchere, J., Stephan, J.F., Arjannikov, S., San'kov, V. 2004. Geometry and kinematics of recent deformation in the Mondy-Tunka area (south-westernmost Baikal rift zone, Mongolia-Siberia). Terra Nova, v. 16(5), p. 265-272. https://doi.org/10.1111/j.1365-3121.2004.00565.x

Badarch, G., Cunningham, W.D., Windley, B.F. 2002. A new terrane subdivision for Mongolia: implications for the Phanerozoic crustal growth of Central Asia. Journal of Asian Earth Sciences, v. 21(1), p. 87-110. https://doi.org/10.1016/S1367-9120(02)00017-2

Baljinnyam, I., Bayasgalan, A., Borisov, B.A., Armando Cisternas., Dem'yanovich, M.G., Ganbaatar, L., Kochetkov, V.M., Kurushin, R.A., Peter Molnar., Herve Philip., Vashchilov, Yu. Ya. 1993. Ruptures of major earthquakes and active deformation in Mongolia and its surroundings. The Geological Society of America. GSA Memoirs, v. 181. https://doi.org/10.1130/MEM181

Barth, A., Wenzel, F. 2010. New constraints on the intraplate stress field of the Amurian plate deduced from light earthquake focal mechanisms. Tectonophysics, v. 482(1-4), p. 160-169. https://doi.org/10.1016/j.tecto.2009.01.029

Bayasgalan, A., Jackson, J., McKenzie, D. 2005. Lithosphere rheology and active tectonics in Mongolia: relations between earthquake source parameters, gravity and GPS measurements. Geophysical Journal International, v. 163(3), p. 1151-1179. https://doi.org/10.1111/j.1365-246X.2005.02764.x

Byamba, J. (eds) 2009. Geology and Mineral Resources of Mongolia. Lithospheric Plate tectonics, v. IV, 495 p.

Calais, E., Vergnolle, M., San'kov, V., Lukhnev, A., Miroshnitchenko, A., Amarjargal, Sh., Deverchere, J. 2003. GPS measurements of crustal deformation in the Baikal-Mongolia area (1994-2002): Implications for current kinematics of Asia. Journal of Geophysical Research, v. 108(B10), 2501. https://doi.org/10.1029/2002JB002373

Fedotov, A.P. 2007. Structure and composition of sediment strata of the Khubsugul basin as a record of tectonic-climatic evolution of Northern Mongolia in Late Cenozoic. Doctor of Sciences Thesis, Kazan State University, 42 p (in Russian).

Florensov, N.A. 1969. Rifts of the Baikal mountain region. Tectonophysics, 8, 443-447, 451-456. https://doi.org/10.1016/0040-1951(69)90048-1

Herrmann, R. 2013. Computer programs in seismology: An evolving tools for instruction and research. Seismological Research Letters, v. 84(6), p. 1081-1088. https://doi.org/10.1785/0220110096

Herrmann, R.B., Benz, H., Ammon, C.J. 2011. Monitoring the earthquake source process in North America. Bulletin of the Seismological Society of America, v. 101(6), p. 2609-2625. https://doi.org/10.1785/0120110095

Ivanov, A.V. 2004. One rift, two models. Science First Hand.v. 1, p. 50-62.

Khilko, S.D., Kurushin, R.A., Kochetkov, V.M., Misharina, L.A., Melnikova, V.I., Gilyova, N.A., Lastochkin, S.V., Balzhinnyam, I., Monhoo, D. 1985. Earthquakes and the bases of the seismic zoning of Mongolia. The Joint Soviet-Mongolian Scientific-Research Geological Expedition. Nauka, Volume 41, 223 p.

Logatchev, N.A. 1993. History and geodynamics of the Lake Baikal rift in the context of the eastern Siberia rift system: A review. Bulletin - Centres de Recherches Exploration-Production Elf- Aquitaine, v. 17(2), 353-370.

Logatchev, N.A., Zorin, Y.A., Rogozhina, V.A. 1983. Baikal rift: Active or Passive? - Comparison of the Baikal and Kenya rift zones. Development in Geotectonics, 19, 223-240. https://doi.org/10.1016/B978-0-444-42198-2.50020-1

Molnar, P., Tapponnier, P. 1975. Cenozoic tectonics of Asia: Effects of a continental collision. Science, v. 189, p. 419-426. https://doi.org/10.1126/science.189.4201.419

Obruchev, V.A. 1938. Geology of Siberia. USSR. 1357 p.

Orkhonselenge, A., Krivonogov, S.K., Mino, K., Kashiwaya, K., Yamamoto, M., Nakamura, T. 2014. Holocene Landform Evolution of Lake Khuvsgul basin, Mongolia. Quaternary Geomorphology, v. 20(4), 343-354. https://doi.org/10.4000/geomorphologie.10781

Pavlovsky, E.V. 1948. Comparative tectonics of the Meso-Cenozoic structures of East Siberia and the Great rift of Africa and Arabia. USSR. Geology, 5, 25-38.

Petit, C., Deverchere, J. 2006. Structure and evolution of the Baikal rift: A synthesis. Geochemistry, Geophysics, Geosystems, v. 7(11), p. 1-26. https://doi.org/10.1029/2006GC001265

Prokopenko, A.A., Kendall, C. 2008. Seismic evidence for the Pleistocene depositional changes in Lake Hovsgol, Mongolia, and implications for the age model and the sediment grain size record of KDP-01 drill core. Journal of Paleolimnology, v. 40, p. 1185-1192. https://doi.org/10.1007/s10933-008-9219-1

Ritz, J.-F., Arzhannikova, A., Vassallo, R., Arzhannikov, S., Larroque, C., Michelot, J.-L., Massault, M. 2018. Characterizing the present-day activity of the Tunka and Sayan faults within their relay zone (western Baikal rift system, Russia). Tectonics, v. 37(5), p. 1376-1392. https://doi.org/10.1002/2017TC004691

Royal. 2010. https://royalsociety.org.nz/assets/documents/Information-paperThe-Canterbury-Earthquakes.pdf

San'kov, V., Deverchere, J., Gaudemer, Y., Houdry, F., Filippov, A. 2000. Geometry and rate of faulting in the North Baikal Rift, Siberia. Tectonics, v. 19(4), p. 707-722. https://doi.org/10.1029/2000TC900012

Sankov, V.A., Parfeevets, A.V., Miroshnitchenko, A.I., Lukhnev, A.V., Arzhannikova, A.V. 2003. Cenozoic dynamics of Baikal and Khubsugul basins. International Symposium - Speciation in Ancient Lakes, SIAL III - Irkutsk, September 2-7, 2002. Berliner Paläobiologische Abhandlungen, v. 4, p. 49-54.

Seattle.2014.https://www.seattle.gov/Documents/Departments/Emergency/PlansOEM/SHIVA/2014-04-23_TsunamiandSeiches.pdf

Sodnom, N., Yanshin, A.L., Tsegmid, Sh., Vorobiev, V.V., and others. 1990. The National Atlas of the Mongolian People's Republic. USSR, Minsk.

Wegmann, K.W., Tsolmon, A., Frankel, K.L., Dewet, A.P., Bayasgalan, A. 2011. Geologic, geomorphic, and environmental change at the northern termination of the lake Hövsgöl rift, Mongolia. Annual Keck Symposium in Geology, v. 24, p. 220-228.

Wells, D.L., Coppersmith, K.J. 1994. New empirical relations among magnitude, rupture length, rupture width, rupture area, and surface displacement. Bulletin of the Seismological Society of America, v. 84(4), p. 974-1002.

Wessel, P., Smith, W.H.F., Scharroo, R., Luis, J., Wobbe, F. 2013. Generic Mapping Tools: Improved Version Released. Eos, Transactions American Geophysical Union, v. 94(45) p. 409-410. https://doi.org/10.1002/2013EO450001

Zonenshain, L.P., Savostin, L.A. 1981. Geodynamics of the Baikal rift zone and plate tectonics of Asia. Tectonophysics, v. 76(1-2), p. 1-45. https://doi.org/10.1016/0040-1951(81)90251-1

4.11 Appendix

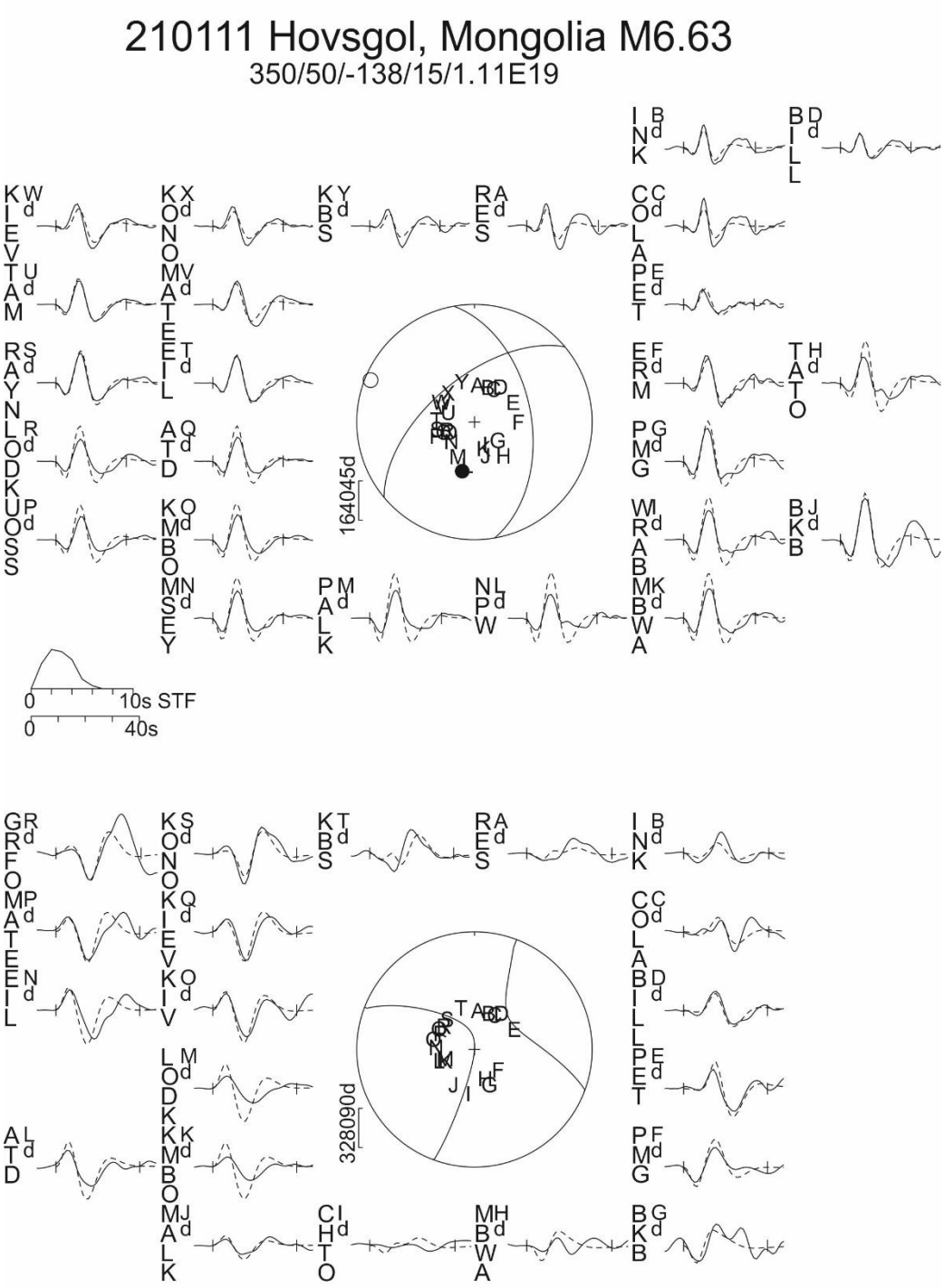

Fig. A1. P and SH waveforms for 210112 Khankh event. The event header shows the strike, dip, rake, centroid depth and scalar seismic moment of the minimum misfit solution. The upper focal sphere shows the lower hemisphere stereographic projection of the P waveform nodal planes, and the positions of the seismic stations used in the modelling routine. The lower focal sphere shows the SH nodal planes. Capital letters next to the station codes correspond to the position on the focal sphere. The solid lines are the observed waveforms, and the dashed lines are the synthetics.

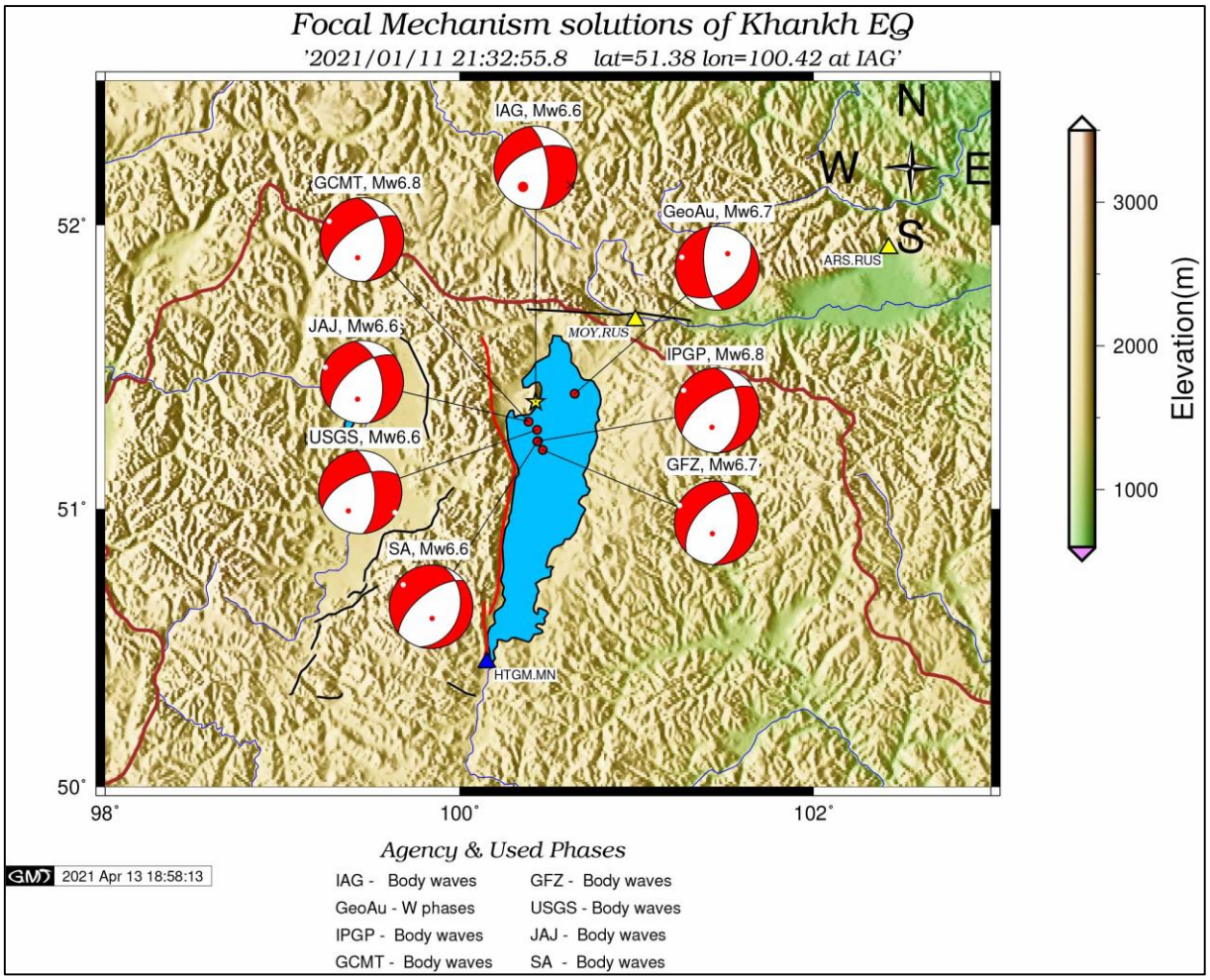

Fig. A2. The focal mechanism solutions are modified and plotted by Generic Mapping Tools (Wessel et al., 2013). The fault plane solutions of USGS, GCMT, GeoAu, IPGP and GFZ are from the web-based open-source data. JAJ and SA are from the personal communications. The fault plane solution of IAG was determined in the Mongolian National Data Center. All focal mechanisms were estimated with moment magnitude (M_w). The yellow triangles show the locations of the Russian local seismic stations. The blue triangle shows the location of the Mongolian local seismic station.

CHAPTER 5

5. THE ULAANBAATAR FAULT

This chapter provides the results of a paleoseismological study along the Ulaanbaatar fault carried out in the framework of the "Studying the seismic activities in the Ulaanbaatar and its surroundings" project which was financed by the Fund of Science and Technology of Mongolia between 2018 and 2022. In this project, I was specifically in charge of paleoseismology, which I carried out with the help and advice of my supervisor J-F Ritz. I am presenting here the revised version of the report I wrote for the National Emergency Agency of Mongolia. This chapter should make the object of an article in the near future.

5.1 Introduction

The capital of Mongolia, Ulaanbaatar, is located in the Tuul river valley within the Southwestern Khentii mountainous region (Figure 42 and Figure 43). In terms of seismic activity, the territory of Mongolia is situated under the geodynamics of the Indo-Eurasian collision and the NE-SW extension of the Baikal rift (Molnar and Tapponnier, 1975; Zonenshain and Savostin, 1981). (see the introduction chapter)

From GPS measurements the region of Ulaanbaatar is moving to the southeastern direction relatively to stable Eurasia with the rate of 6.4 ± 1.6 mm/yr (Calais and Amarjargal, 2000) (see Figure 5).

The region of Ulaanbaatar is affected by some active faulting showing both extensional and left-lateral movement along NE-SW faults, consistent with the GPS data (Al-Ashkar et al., 2022). There are active faults such as Möngönmorit, Deren, Agit, Khustai, Sharkhai, Avdar, Emeelt, Gunj, as well as regional faults such as Terelj, Khui, Khürkhree, Chuluut-Törkhurakh, Deendei, Yuden, Barkh, and Nalaikh in the vicinity of Ulaanbaatar and its neighboring settlements (Figure 42).

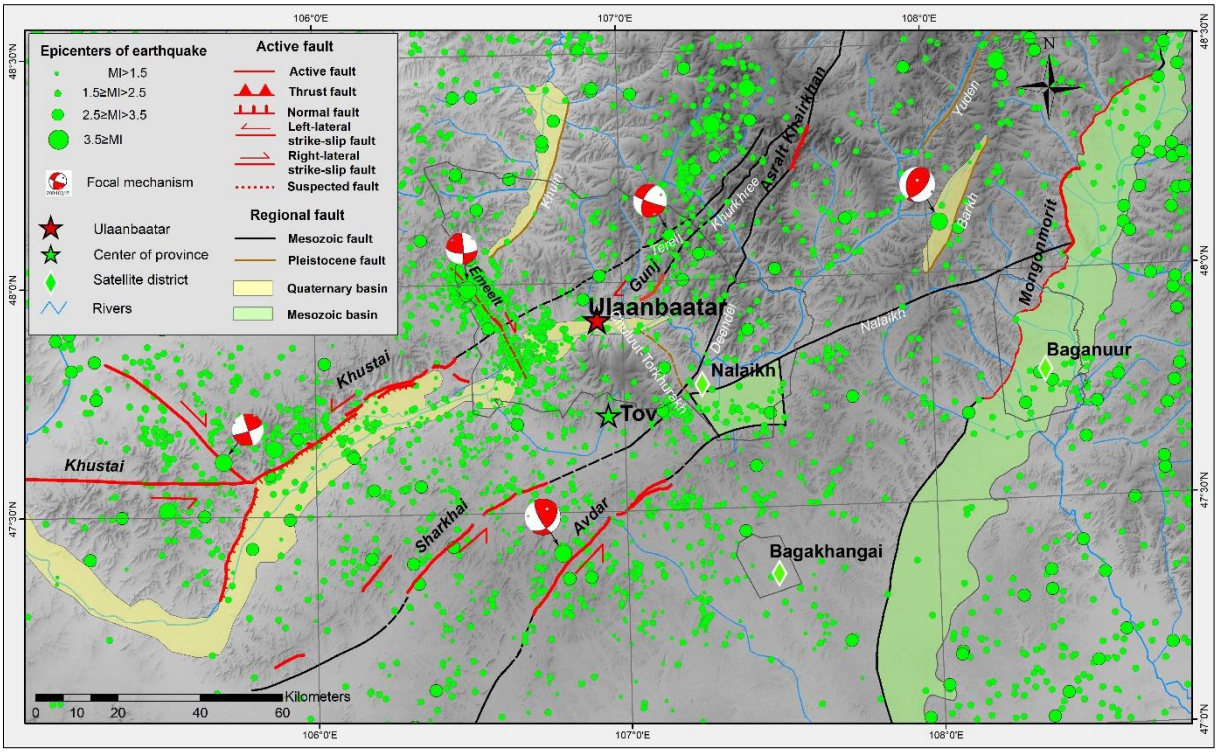

Figure 42. Seismotectonic map in Ulaanbaatar city and its surroundings. The red lines demonstrate the active faults. The black lines show the Paleozoic faults, whereas the Pleisctocene faults are marked by the golden lines. (After Odonbaatar et al., 2015)

Microseismic activity is not specifically correlated to these faults except along the Emeelt fault. Available focal mechanisms are showing various kinematics but are not very well constrained. The regional faults are usually found along ancient geological boundaries and are NE-SW oriented. The active faults are inherited from Mesozoic structures. Önödelger and Banzragch, (1993) interpreted the Paleozoic rocks in Ulaanbaatar and its suburbs as associated to the closure of the Mongol-Okhotsk Sea defining anticlines and synclines with northeastern folding axes.

In summer 2017, scientists from Hiroshima and Nagoya Universities of Japan carried out a morphological and paleoseismological study along NW-SE trending Ulaanbaatar fault, which is crossing the Ulaanbaatar city, and interpreted it as an active fault Suzuki et al. (2020). This fault had been regarded so far as an ancient geological fault by previous studies (Önödelger and Banzragch, 1993; Takeuchi et al., 2012; Odonbaatar et al., 2015). From their study, Suzuki et al. (2020) interpreted the kinematics of the Ulaanbaatar fault to be left-lateral and reverse. Consequently, the Earthquake Research Sector of the Institute of Astronomy and Geophysics of Mongolian Academy of Sciences has been investigating the fault since 2019 in the framework of "Studying the seismic activities in the Ulaanbaatar and its surroundings" project.

5.2 Morphotectonics

Japanese researchers first detected the Ulaanbaatar fault (UB fault) by satellite images with the help of DEM Viewer. And in addition, they interpreted the fault-related landforms on the stereoscopic Corona images, which were taken by a satellite in 1960-1972 (Suzuki et al., 2020). The fault stretches for more than 50 km between the western foot of Mount Tolgoit where it is located at northwest of the city and southeast of Mount Bogd Khan where it is located at the south of the city (Figure 43).

After their mapping of fault scarp features all along the fault, Suzuki et al (2020) divided the fault trace into three main sections: Naran fault, Ulaanbaatar Central Fault, and Bumbat fault (Figure 43). The fault scarps are generally northeast facing along the Naran fault and southwest facing in the Bumbat fault. In their fault map, they marked the Ulaanbaatar Central Fault with a dashed line where it crosses a densely populated area with a large number of buildings, and where the original ground surface in clearly invisible.

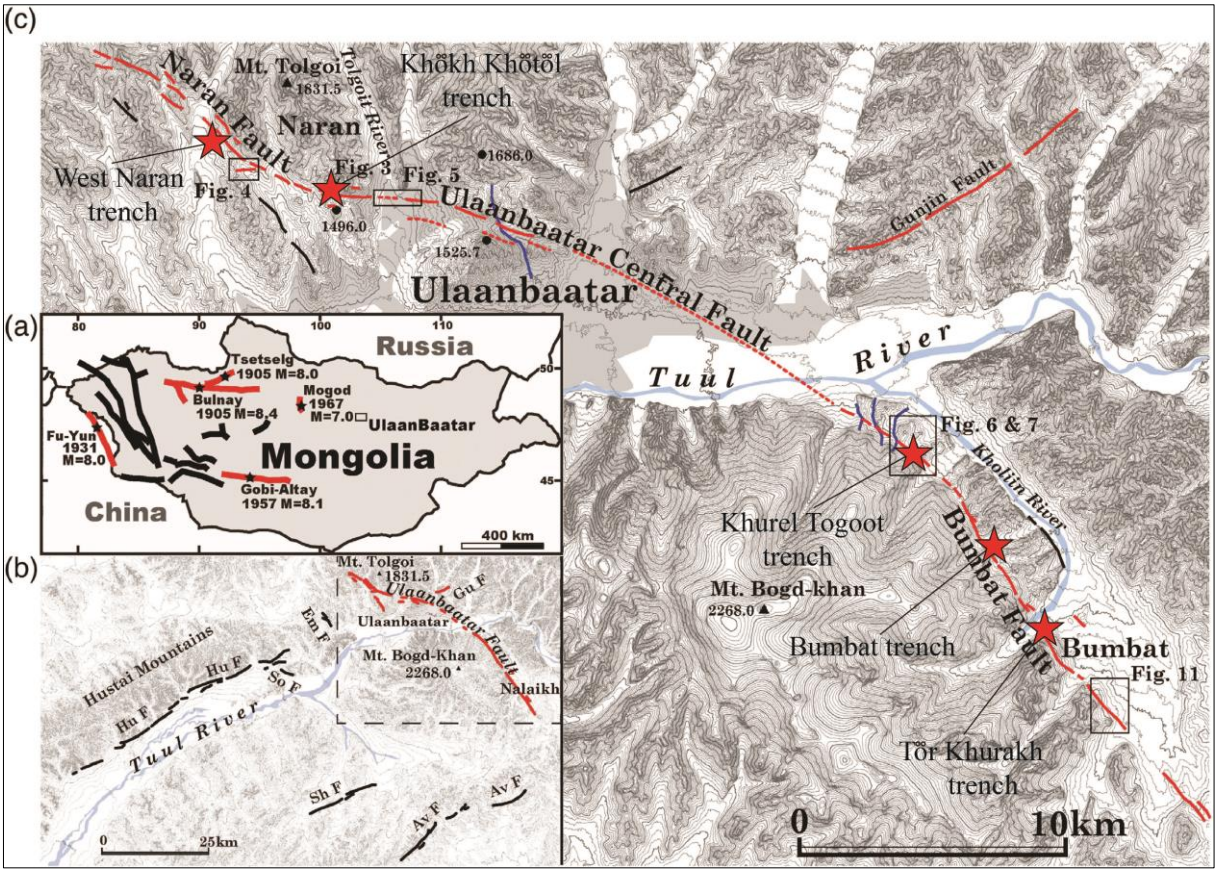

Figure 43. Sketch map of the Ulaanbaatar fault (after Suzuki et al., 2021). A: location map. B: The Ulaanbaatar (red) and the other faults around Ulaanbaatar city. C: Detailed map of the Ulaanbaatar and other faults. The red stars display the trenching sites West Naran, Khökh Khötöl, Khürel Togoot, Bumbat, and Tör Khurakh.

In summer 2020, during a field survey along the fault, I observed that the geomorphological features at Shajin Khurakh and Shirdegtiin Bogino valleys, along the east and northeast flank of Bogd Khan Mountain respectively were the most notable areas and look like active tectonic features (Figure 44). There, the fault defines a counter-slope scarp with the northwestern block uplifted relatively to the southeastern one. At one point, the northern block looks like displaced left-laterally (Figure 44-C). However, it also clearly appears to me that the Ulaanbaatar fault scarp features clearly are located along an ancient geological boundary (see Takeuchi et al., 2012), and that differential erosion processes may have influenced the occurrence of the fault scarps.

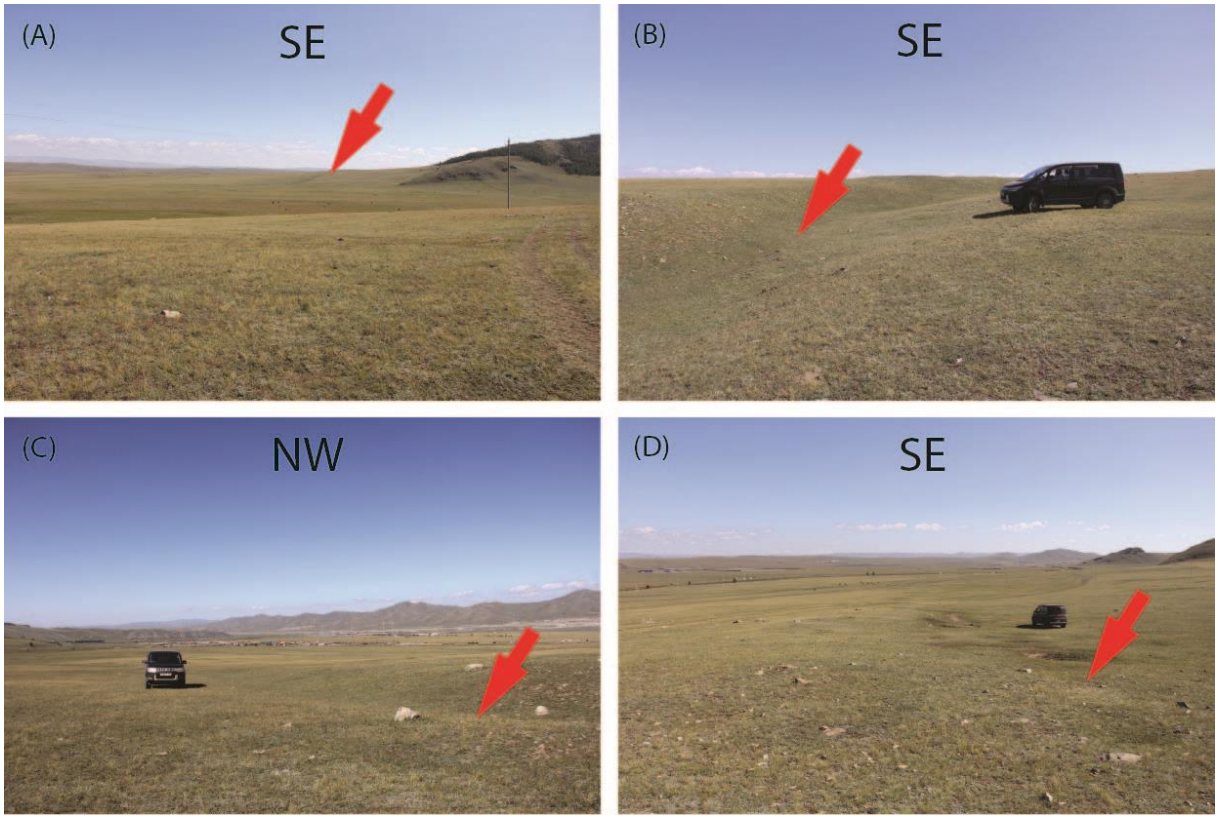

Figure 44. Field view of the Ulaanbaatar fault scarps nearby the Shajin Khurakh and Shirdegtiin Bogino valleys along Mount Bogd Khan. A: Far distance southeastern view of the fault scarp east of the Shajin Khurakh Valley. B-C: Detailed views of the counter-fault scarp at the eastern side of the Shajin Khurakh Valley. D: Southeastern view of the counter fault scarp at the western side of the Shirdegtiin Bogino Valley.

5.3 Paleoseismological investigation

5.3.1 The Khürel Togoot trench

The Khürel Togoot trench is the largest trench (10 m wide, 37 m long, and 7 m deep) ever dug in Mongolia for paleoseismological investigation (Figure 4). It was excavated under the

direction of Mongolian-Japanese joint scientific team in June 2019. Prior to that, in 2018, the Japanese researchers first excavated a small trench (9 m long x 3 m wide x 4 m deep) at the same site of and discovered a black colored formation that was deformed by the faults. The trench was excavated across a smooth counter-slope scarp along the Ulaanbaatar fault within the northeast flank of Mount Bogd Khan (Figure 45).

This paleoseismological study aimed at analyzing the fault kinematics and determining the timing of past ground-rupturing earthquakes to estimate a mean recurrence interval and assess the risk of a future major earthquake along the fault. In order to excavate the trench as deep as possible, we made a bench at a depth of ~3 m. A large number of people were involved for cleaning the trench walls. Then a cubic reference grid of 1 x 1 m was constructed on both walls of the trench, which were logged at the scale of 1/20.

Figure 45. Northeastern view of the Khürel Togoot trench (on the left-hand side standing Pr. Nakata in profile and Battogtokh on the right, picture taken during summer of 2019).

5.3.1.1 Stratigraphy

5.3.1.1.1 Description of the units of the Khürel Togoot trench

The Khürel Togoot trench is very interesting because it shows different geological formations of different ages with different structures: a deformed metamorphic unit capped by an ancient

shear zone, gradually tilted sedimentary layers (clay and clasts), eolian sands (Figure 46 to Figure 49).

I documented and logged both walls of the trench (Figure 46 to Figure 49). The two walls have similar stratigraphy thus I mainly focus on the eastern wall when I describe the units.

- U300. A bedrock unit composed mainly of feldspar-quartzite described as massive sandstone in Takeushi et al. (2002) is observed in the northernmost part of the trench. It is capped by a dark fragmented folded fault shear zone. The bedrock is strongly weathered and fragmented near the surface. As it deepens, the texture of the unit becomes firmer and we notice a slight folding mimicking the fold shape observed within the black shear zone unit (U210). The contact with the black shear zone appears severely affected by friction and is fragmented and the color becomes dark gray and black. Within the shear zone, the brecciated and mylonitized parts of the bedrock show a shearing fabric with "fish-like" structures. The petrographic analysis of a bedrock sample collected from a coring survey (see in the drilling section) allows defining its lithology as sandstone-alevrolite.
- U210. Dark-fragmented-shear-zone showing a sub-horizontal geometry in the northern part of the trench, then undergoing a southwards folding to become a steep 80° northeastward shear zone. It is 1-1.5 m thick and contains strongly brecciated bedrock fragments. A more recent fault plane separates the bedrock caped by the folded shear zone from the reddish-brownish sedimentary layers to the southwest. Thick fault gouges with various types of colors are common along ancient fault zones in Mongolia. Notably, a similar thick gouge was observed by Ishikova et al (2014) in the Median Tectonic Line in Japan.
- U200. Black organic rich horizon partly folded with a turf-like texture (peat) strongly eroded. Note that there is no bedrock clasts or cobbles in this unit.

SEDIMENTARY UNITS

In the southwestward part of the trench, accumulated in a depression between the bedrock, gouge and paleosoil units (U300, U210 and U200, respectively) and the northward slope of Mount Bogd. These sedimentary layers consist of clay with various colors (brown, red, and pink) likely due to variations of the climatic conditions during their deposition. Almost all of these units contain large and small size of pink granite fragments from the Bogd granitic massif. It is clear therefore that these granite fragments were transported from Mount Bogd in the south of the trench. Two outstanding features characterize these clayey units: 1) They show a progressive and downward tilting from the horizontal (U20-U30) to a dip of more than 60° to the SW (U170-U190); 2) All the units show also a rapid thickening towards the SW. These features suggest that the deposition of these units was controlled by an underlying sliding NE dipping plane moving with a normal kinematic. However, the section exposed in the trench is not dip enough to enable the observation of this NE dipping sliding plane. Another interesting feature is that the strata are also affected by reverse faulting along a one steep brecciated

contact-unit along the shear-zone unit 210 and also within the like which are farther south from the fault zone, are formed, although the sections of the strata bordering the fault plane can be pulled up, and deformed and lifted upwards. Also, some units, such as U120, U110 and U100, are thicker to the south. These multi-colored sedimentary layers are covered with a fairly thick layer of sand on the top.

5.3.1.1.2 Description of the sedimentary units:

- **U190.** The lowest layer of the trench contains dark reddish-brown clayey layer on top, slightly darker than the U170. The U190 and U170 layers are separated by a brown layer labeled U180. Fine grained slightly angular gravels are widespread within the U190 unit. Among them, most of the larger pebbles are almost vertically oriented. This is a type of clay that is very hard when dry and soft when it is wet. This layer borders directly with the dark colored fault plane.
- **U180.** A thin brown clayey layer located between the lower U190 and upper U170 units. This layer is more noticeable on the western wall of the trench (see Figure 48 and Figure 49).
- **U170.** Dark-reddish-brown colored unit. Angular gravels are widespread. Hard when dry and soft when wet.
- **U160.** Dark-brown clayey unit. Contains less gravel compared to the lower U170 unit. This unit forms an individual layer between U170 and U150 units on the western wall (see Figure 48), but is mapped on the left wall as thin lens sandwiched between these layers. This unit becomes hard when dry.
- **U150.** A reddish-brown clayey unit. This unit is mapped as thin lens between U160 and U140 units on the left wall of the trench, but illustrated as relatively independent unit on the western wall (see Figure 48 and Figure 49). The unit contains vertically oriented gravels.
- **U140.** Brown clayey unit. Contains lesser amount of gravels compared to U190, U180, U170, U160 and U150 units. This layer is drawn continuously to the right wall of the trench to the fault zone (see Figure 48 and Figure 49).
- **U130.** Carbonate rich light-gray unit. This may be the downward continuation of carbonate alteration in the upper U120 unit. This unit forms conformity with the below and above units. Occasionally contains scattered small-grained gravels.
- **U120.** Gray-reddish-orange clayey unit. It contains fine-grained gravels. The unit is wider at the bottom of the trench, gradually narrows to the upward direction, deforms vertically, and incised by the fault. The boundaries of relatively thick bottom part are dipped approximately by 30˚ compared to the horizontal level.
- **U110.** A gray clayey unit. This unit contains relatively large granite boulders, size of up to 24x35 cm. These boulders have a 30° dipping angle relative to the horizontal layers. This means that during the tectonic events the original horizontal layer may have tilted with 30˚ angle. This unit also contains brown mud lenses with the same characteristics as the U100 unit.

- **U100.** Brown clay unit. Solid when dry and soft when wet. This unit contains angled gravels of various sizes. Some pebbles along the boundary with unit U110 have same 30˚ dipping angle, similar to the boundaries of the two units.
- **U90.** The brown-gray clayey unit. The unit contains angular gravels of various sizes.
- **U80.** Brown clayey unit. Japanese researchers suggested that the "flame structure" is formed in this layer due to the earthquake shaking.
- **U70.** Red-pinkish clayey unit. There are almost no small-sized gravels, however occasionally contains relatively large granite boulders of up to 30x50 cm in size. It deforms around the fault zone forming vertical dip and tilted almost upright. It also contains 2 large vertical granite boulders with height up to 15x30 cm placed in the deformed belt. This implies that the layer is strongly affected and deformed by tectonic process.
- **U60.** Sandy unit with occasional boulders and gravels. On the bordering area with the fault zone, it is also deformed in an inclined direction, and the large boulders contained in the fault zone almost vertically followed the deformation direction of the bearing layer. This layer is placed between the lower U70 and the upper U50 units. The colors are very different from the two-neighboring reddish and pinkish layers. This unit is sampled for “OSL” analysis in order to determine the age of the quartz grains.
- **U50.** Red-pinkish clayey unit. Contains small number of cobbles and pebbles. Narrow dark stripes are observed through the lower part of this layer, as well as through the main bodies. This dark material may be transported from the major fault zone (the dark gouge) and piled up here.
- **U40.** Unit with reddish colored and small-grained gravels. Occasionally contains small number of boulders.
- **U30.** Thick sandy layer. Well sorted, fine-grained aeolian sand. The color is light-yellow-brownish-gray according to the Soil Color Chart. Occasionally contains small number of gravels, cobbles and boulders. OSL samples are collected from this unit in order to determine the age of this layer.
- **U20.** Fine-grained sandy layer. It contains less gravels although there is no a sharp boundary with the lower U30 unit. The boundaries of this layer are mapped roughly.
- **U10.** Surface soil (brown turf). Relatively thicker on the sedimentary deposit section south of the fault zone. It is thinly distributed over the top of the bedrock scarp, north of the fault zone. This could also be explained by the relatively larger accumulation of materials in the depressive section enclosed by the fault scarp.

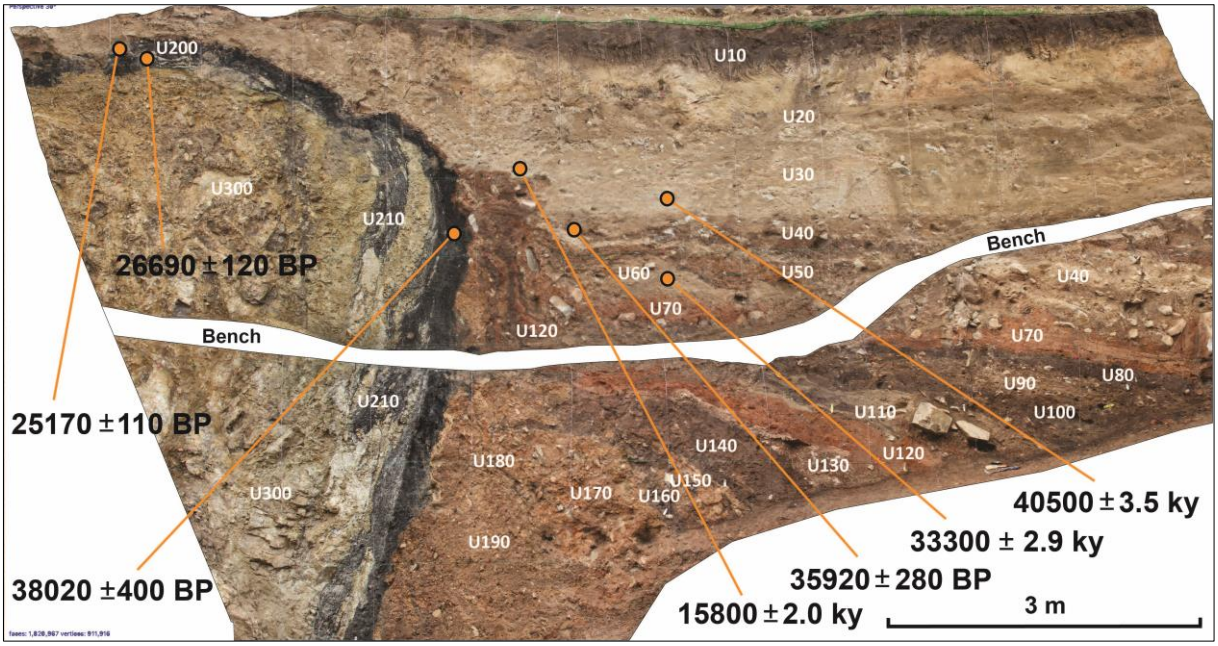

Figure 46. Photomosaic of the east wall of the Khürel Togoot trench. The layers and rocks on the east wall of the Khürel Togoot trench and their respective ages (BP and ky).

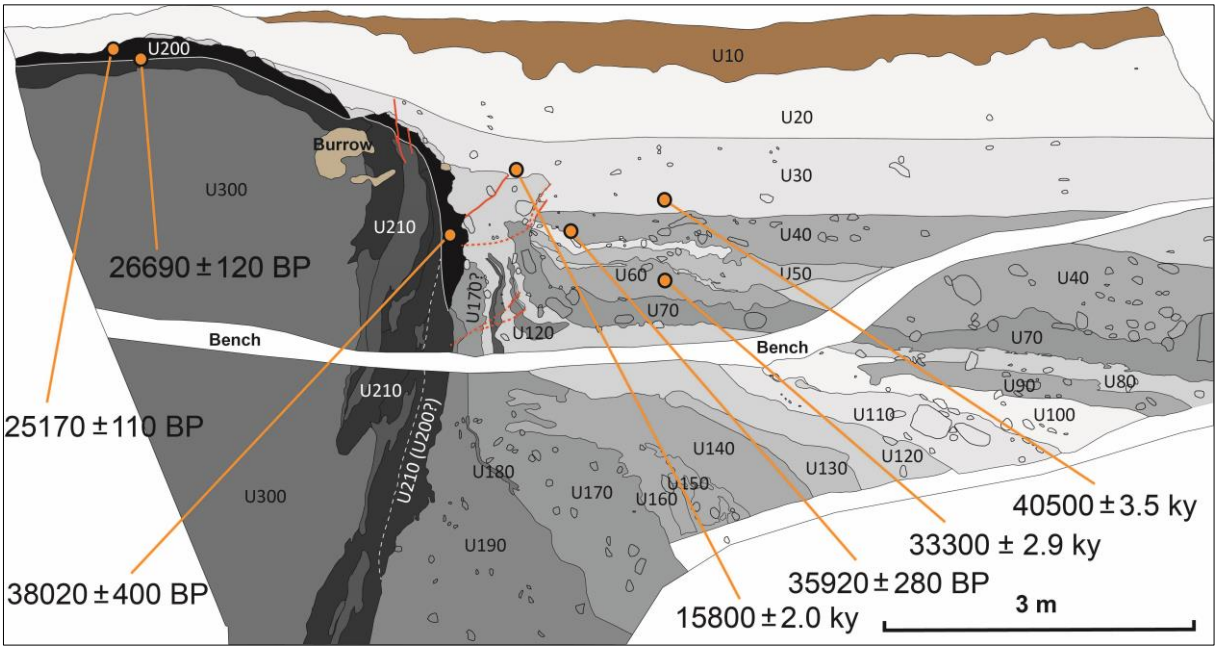

Figure 47. The documentation and logging of the units on the east wall of the Khürel Togoot trench.

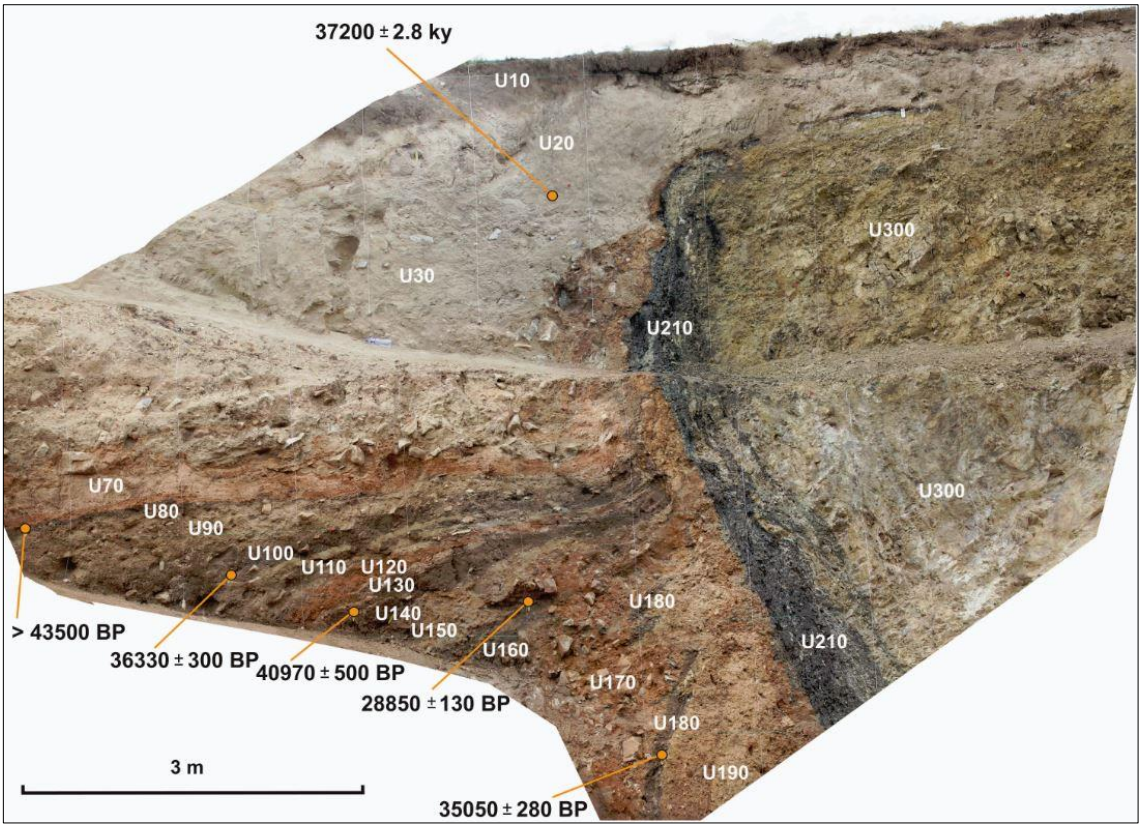

Figure 48. Photomosaic of the west wall of the Khürel Togoot trench.

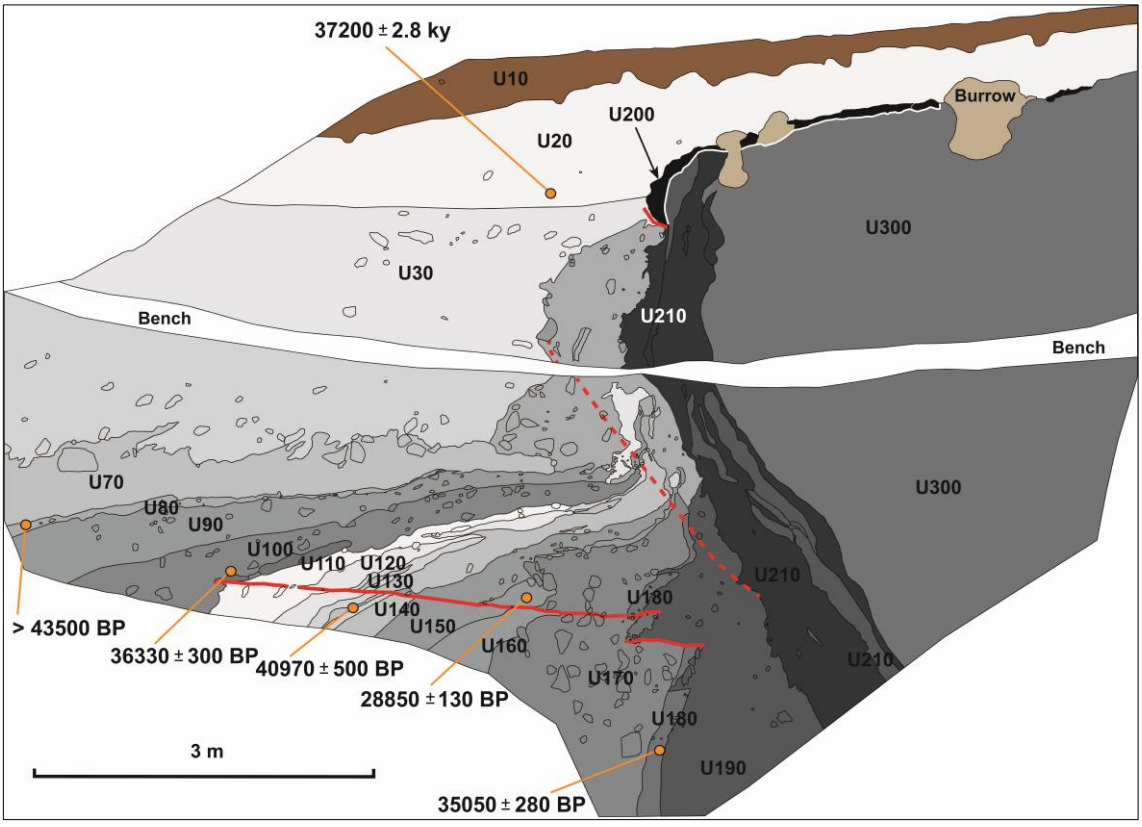

Figure 49. Western wall of the trench showing the progressive southwards tilting and thickening of the sedimentary units, and the two main reverse faults that affect them.

5.3.1.2 Dating results

As noted above, the radiocarbon samples were collected in order to determine the ages of the sedimentary layers that were discovered in the trench walls. The samples were analyzed at "Beta Analytic" radiocarbon dating laboratory, funding by researchers from the Universities of Nagoya and Hiroshima of Japan who cooperated with us (Institute of Astronomy and Geophysics of Mongolian Academy of Sciences) on this project. The results of the samples are shown in Table 4.

We sampled OSL tubes from the thick sand deposits. And those samples were processed and dated in the Department of Geography of the University of Sheffield in the UK. The dating results are shown below in Table 4.

Radiocarbon analysis of samples collected from each stratigraphic units showed age results of 35050 ± 280 BP, 28850 ± 130 BP, 40970 ± 500 BP, 36330 ± 300 BP, > 43500 BP in the right wall from bottom to top, respectively. The age results of sample collected from the young stratigraphic unit in the left wall was 35920 ± 280 BP that was covered with multi-colored sedimentary layers.

The OSL samples collected from the sand units yielded 37200 ± 2.8 ky from unit U20 on the right wall, 33300 ± 2.9 ky from unit U60 on the left wall, 35920 ± 280 ky from unit U40, 40500 ± 3.5 ky and 15800 ± 2.0 ky from unit U30 (Figure 46 to Figure 49).

The age of some units of the right and left walls differs from the deposited sequence. However, the minimum value is ~28850 BP, the maximum value is ~43500, and the average value is ~36175, and the left wall showed a minimum value of ~15800 BP, a maximum value of ~40500 BP, and the average value of ~28150 BP.

Table 4. The dating results of the samples collected from the Khürel Togoot trench.

Stratigraphy	Age constraints	Description
U20	37200 ± 2.8 KY	West wall. OSL sample.
U30	15800 ± 2.0 KY	East wall. OSL sample.
U30	40500 ± 3.5 KY	East wall. OSL sample.
U40	35920 ± 280 BP	East wall
U60	33300 ± 2.9 KY	East wall. OSL sample.
U80	>43500 BP	West wall
U100	36330 ± 300 BP	West wall
U130	40970 ± 500 BP	West wall
U160	28850 ± 130 BP	West wall
U180	35050 ± 50 BP	West wall
U200	38020 ± 400 BP	East wall
U210	26690 ± 120 BP	East wall
U210	25170 ± 110 BP	East wall

5.3.1.3 Interpreting the deformation observed in the Khürel Togoot trench (the eastern wall)

Given the strong and continuous tilting observed within units U190-U40, it is clear that either many deformational events or a continuum of deformation (rather) occurred around ~25 ka or just after. We gave credit to the radiocarbon ages obtained for the organic rich unit U200, which is predating units U190-U30, and we interpret the ages obtained on the later units as corresponding to the ages of detritic elements that were washed from the northeastern flank of the Bogd mountain upslope and get trapped with the clayed units. Note that this interpretation is consistent with the fact that we observe some kind of stratigraphic inversion in the radiocarbon ages in units U190-U30. This a classic feature observed in trenches when analysing scarp derived colluvions originated from a location located upslope the studied site and where organic-rich material as forest or human settlements existed (see for instance Philip et al., 2001).

As already pointed out above (see the documentations) , this southwards tilting together with the fact that the units are thickening towards the south and contain detritic elements from the slope situated above (i.e granitic cobbles from the Bogd massif and charcoals etc.) involves that a fault - not observed in the trench - must exist below to control this sedimentary and structural pattern. This is the only way to explain the occurrence of the tilting and the thickening of units U190-U30 towards the south.

Thus we explain the rapid clockwise tilting (in a ~7 m long section only) of the clayed trapped units U190-U40, by the normal movement along a listric fault that produced a roll over process within the hanginwall. The question is now to determine whether this deformation corresponds to a gravitational collapse located along the ancient Bogd fault zone or if it is the result of an extensional tectonic phase with several normal fault events localised in time. Note that the few reverse faults that are affecting the clayed units are interpreted as contemporenaous features simply due to the volumetric compensation inside the sedimentary units trapped between the hanging wall quartzites to the north and the Bogd granites to the South.

It is clear that many paleo-earthquakes (perhaps in Paleozoic and Cenozoic) had happened along the dark large fault plane (U200 and U210), to form this wide shear zone. However, it is still questionable to determine the timing of the latest tectonic events along the UB fault. The latest fault traces in the east wall may represent the events that displaced units U30 and U40 (Figure 50).

There are no well constrained data about the ages of the units. Radicarbon dating results and OSL ages are mixed up stratigraphically, and there are no arguments to pick one instead another.

The only robust argument to bracket is to take the ages about radiocarbon-rich unit U210 (where the 14C data is convincing to be consistent around 25-28 ka) and imply that the other units are younger given that they are deposited above.

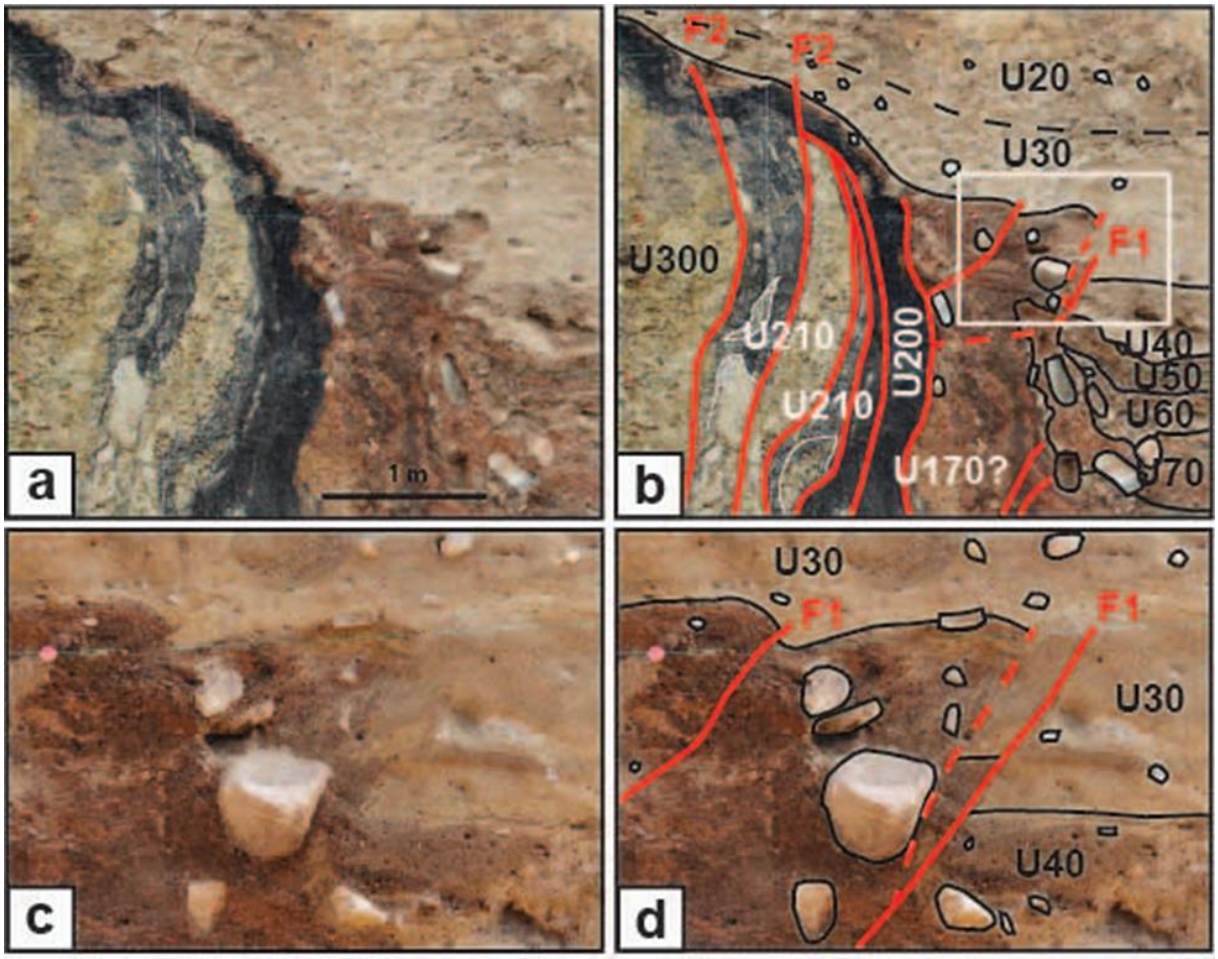

Figure 50. The latest faults that deformed and displaced the units in the east wall.

5.4 Discussion

This studied site being located next to the Ulaanbaatar city brought the Khürel Togoot paleoseismological investigation site to the interest of a large community with discussion between Mongolian and foreign experts. Among them, Dr J-F Ritz's report is regarded to be significant interpretation for the Khürel Togoot paleoseismological site (Figure 51). The occurrence of the gouge involves at least a first intense and localized deformation stage probably during the Paleozoic times (Takeuchi et al., 2012). The fact that the gouge is folded and thrusted over younger deposits involves a second deformation stage. Although this stage seems compressional (at a first glance) as interpreted by Suzuki et al. (2020) – making the UB

fault an active transpressional feature. (Suzuki et al also interpreted a strike-slip component in the morphology) - a careful structural analysis allows proposing that the observed features correspond in fact to some rotational deformation associated with the normal movement along an hidden fault (a fault not observed in the trench, but which should correspond very likely to the ancient Paleozoic fault zone described in Takeuchi et al, 2012, putting the alevrolite in contact with the granites of the Bogd massif).

The fact that the sedimentary sequence (for example, set of clayey units, rich in iron oxide, containing granitic colluvium from Mount Bogd) shows an increase of the amount of clasts, and an increase of their size towards the SW, as well as a fan-shaped sedimentation away from the gouge zone (U200), suggests strongly that a syn-tectonic sedimentation episode occurred.

Therefore, the simplest interpretation is that 2 main deformation episodes occurred:

1) Post-sandstone-alevrolite compression (Paleozoic) putting the sandstone-alevrolite in contact with granite of Mount Bogd Khan along the earlier UB fault zone (Takeuchi et al., 2012). The fault gouge observed in the trench is either inherited from this episode or from an older episode (The fault gouge corresponds to a secondary tectonic feature within a broader UB fault zone).
2) Late Cenozoic reactivation of the ancient UB fault zone contacts as a NE-dipping normal fault leading to the formation of a syn-tectonic detritic gutter along the UB fault (The main fault that controls this syn-tectonic sedimentation is not observed in the trench).

It seems that no other deformation occurred since the deposition of unit U20 which is sealing the deformation observed in units U190-U30. Two important questions remain to be answered: 1) determine whether this episode of deformations (~25 ka) corresponds to the expression of some tectonic activity, in other words the reactivation of the Bogd shear zone as normal fault or if it corresponds simply to some localized gravitational collapse (in time and space). 2) determine if this deformation (tectonic or slope process) can still be activated.

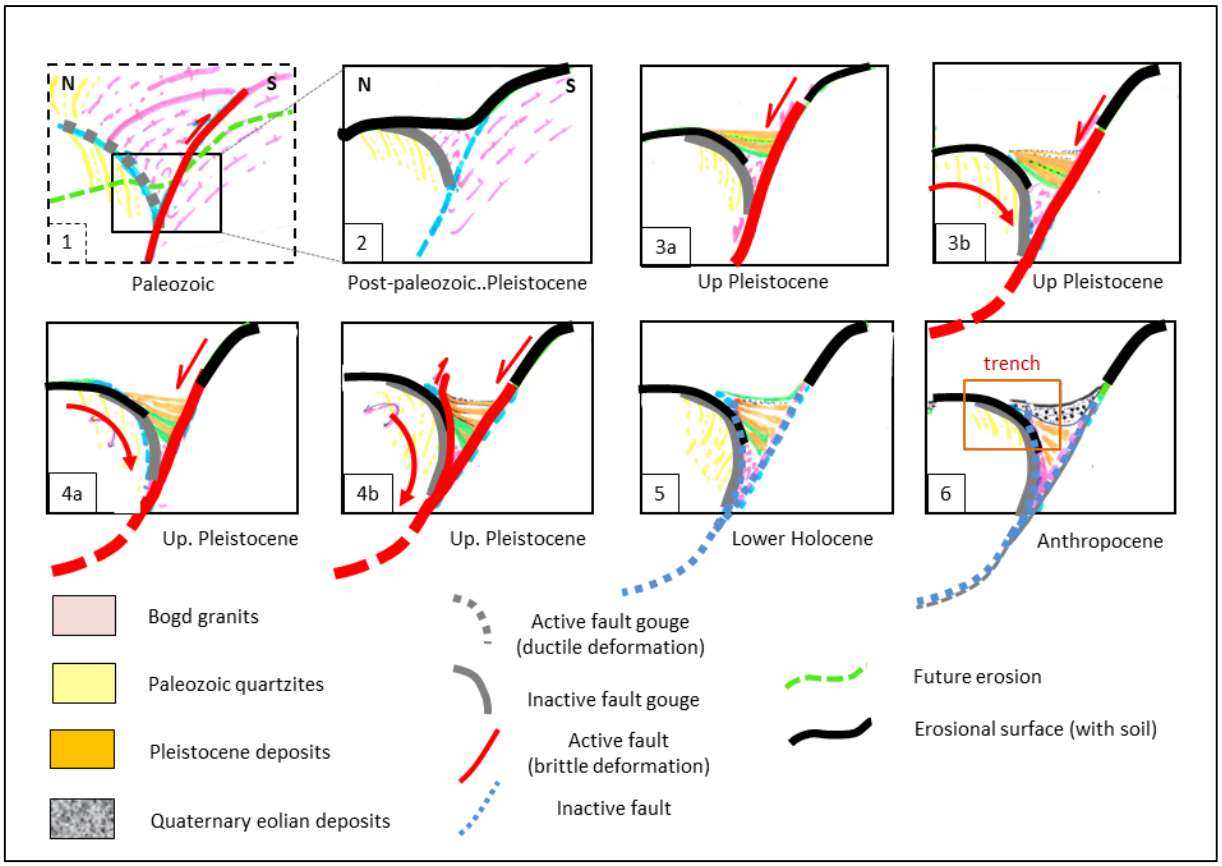

Figure 51. Interpretative scenario to explain the deformation observed in the Khürel Togoot trench. Modified from J-F Ritz, internal report for IAG, MAS.

About the second question, no historic observations of the Ulaanbaatar area are available to either support or negate this hypothesis. There are no seismicity records along the UB fault.

5.5 The other trenches along the Ulaanbaatar fault

5.5.1 The West Naran trench

The exploration traversing and paleoseismological survey by the Mongolian-Japanese joint research team was executed on the UB fault for 14 days starting from 5 May, 2019. In the first 2 days, we conducted the exploration traverses along the fault and selected a site for trenching.

The trenching site (N47°58'46.5'', E106°43'57.0'') where the fault is clearly identifiable on the ground surface was selected and excavated and the location was in ~15 km NW from Sukhbaatar Square central point of Ulaanbaatar city (Figure 52).

The trench was excavated perpendicular to the fault strike, stripping the top soil to check in details that the fault outcrop and Holocene deposits were affected by the fault. Despite the fact that the fault has the identifiable scarp on the surface, there were not enough characteristics of

active faulting to the depth. Therefore we scratched the surface to shallow depth at the 2-3 points to optimize the location, and then excavated the main trench. On the trench wall, the ancient geological fault plane was observed, but we closed the trench due to absence of the recent active fault signs.

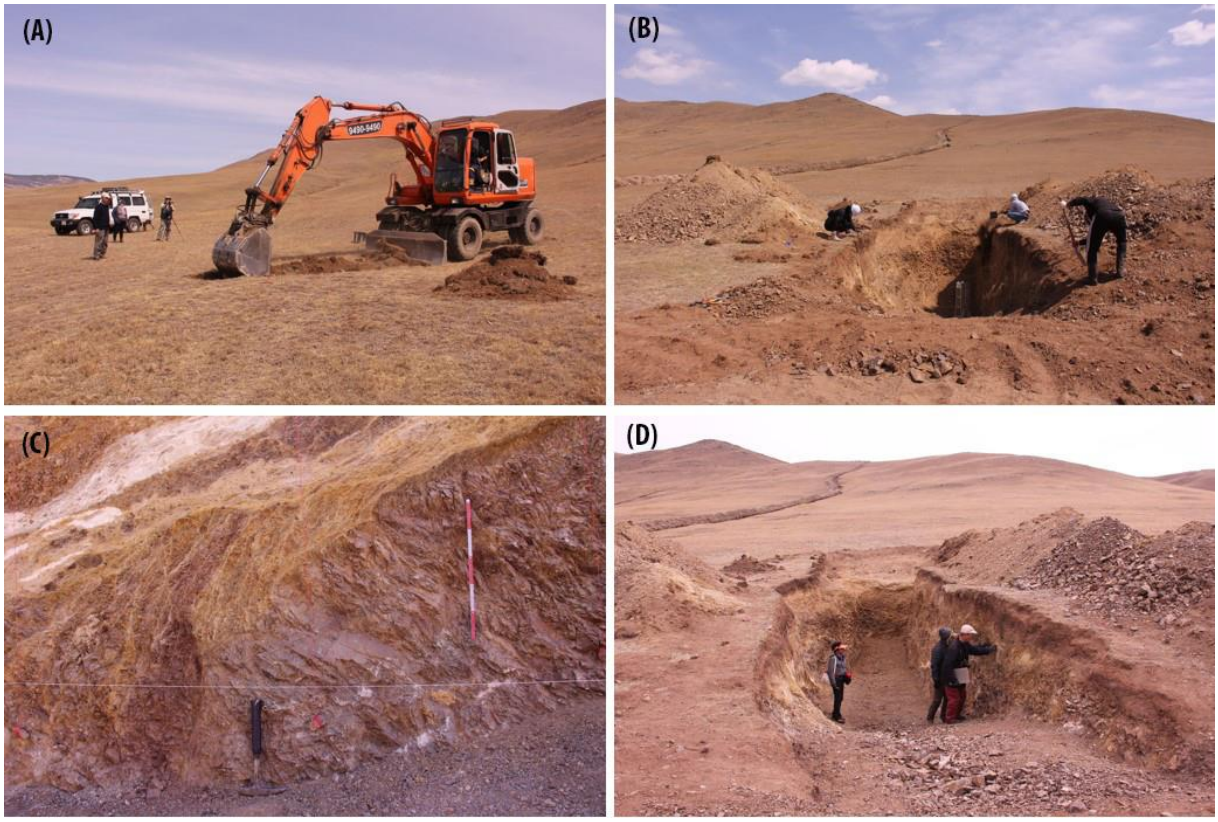

Figure 52. The West Naran trench (N47°58'46.5'', E106°43'57.0''). (A)-The trench was excavated across the clear fault scarp on the ground surface, (B)-The wall cleaning and preparation process for the investigation, (C)-The visibility of some parts of the trench where the ancient fault plane was exposed, (D)-The researchers who are Nakata, Watanabe and Bayasgalan are looking for faulting in Holocene deposits on the east and west walls of the trench.

5.5.2 The Bumbat trench

The joint team of Mongolian-Japanese researchers executed a trenching study in the Bumbat section of the UB fault at Mount Bogd Khan on August 2019 (Figure 53).

The main purpose of the study was to confirm an activity of the UB fault and to detect a similar phenomenon as the deformation in the Khürel Togoot trench.

We excavated two trenches in the Bumbat Valley of Mount Bogd Khan. The first trench was excavated across a fault scarp which displays a linear feature on the satellite image (Figure 53 and Figure 54).

Figure 53. The locations of the two trenches in the Bumbat Valley of Mount Bogd Khan. The trenching locations were selected on the "open cracks" that might be tectonic related landforms. Trench 1: N47˚50'1.62", 107˚06'50.77"; Trench 2: N47˚49'58.1", E107˚06'53.3".

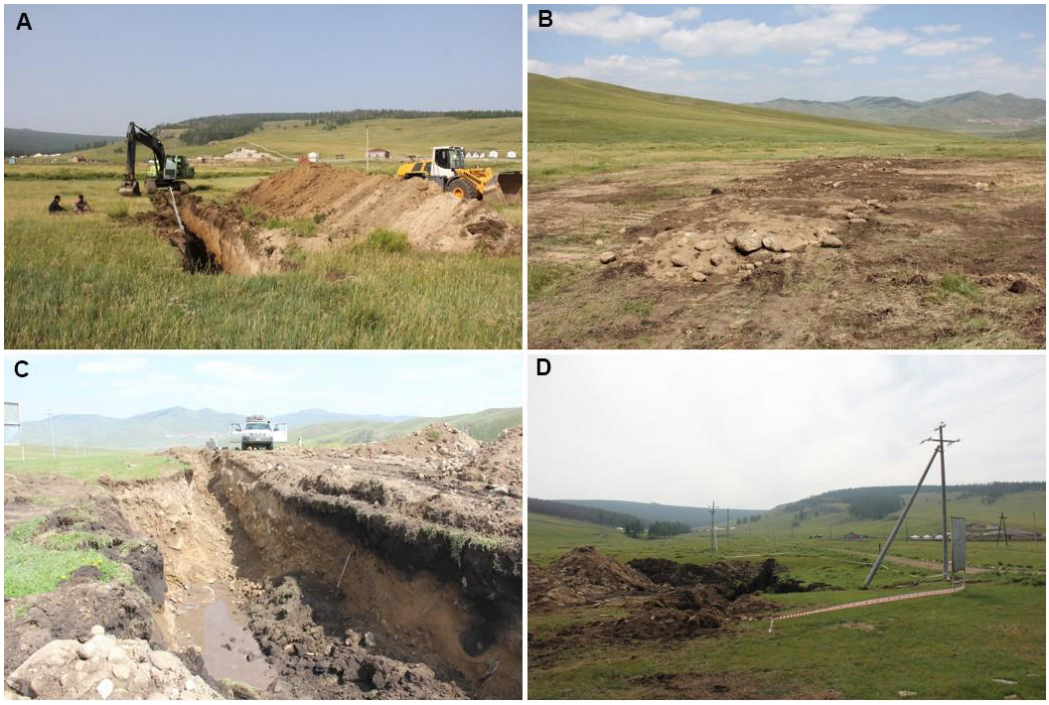

Figure 54. The view of the trenches in the Bumbat Valley of Mount Bogd Khan.

There were no signs of an earthquake, so the trench was refilled and rehabilitated (Figure 54-A-B). The next trenching site was selected on the small depression that might have been formed tectonic related forces and it was excavated to a length of ~ 40 m (Figure 54-C-D). The area was mountainous with nearby rivers and swamps causing water to rise from a depth of ~2 m and permafrost, making it impossible to deepen more. When the excavated areas were cleared and studied, no traces of the earthquakes were investigated.

5.5.3 The Chuluut trench

The research team of IAG, MAS conducted route and paleoseismological study along the UB fault from August 28 to September 12, 2020.

A small trench was dug ~50 m east of the Khürel Togoot trench by crossing the fault scarp (Figure 55). The trench was located at N47˚51′56.4″, E107˚04′38.9″ as 2 m deep, 1.5 m wide and 10 m long.

No faults were discovered in the Holocene fluffy sediment near the surface, but at a depth of 1.9 m, the black materials similar to those found in the Khürel Togoot trench were discovered and sampled to determine its structure, composition and age (Figure 55-D).

Figure 55. The trench that was dug for the paleoseismological investigation in the Chuluut Valley of Mount Bogd Khan. The location of the trench: N47˚51′56.4″, E107˚04′38.9″.

5.5.4 The Tör Khurakh trench

The 3 locations were selected for the paleoseismological investigations at the east side of the Tör Khurakh Valley in Mount Bogd Khan. Those sites that are represented by indistinct lineaments on the satellite images might be either fault scarps or washout ravines.

It was not possible to dig deep trenches by hand-excavation due to numerous numbers of large boulders in the study area. An excavation of 0.9 m high, ~2 m long trench at 47˚47'55''N, 107˚08'47''E revealed no faults in the clayey and gravelly deposits below the ground surface (Figure 56-A).

We cleaned the walls along the ditches at the side of the railway where the surface geo-morphologies exist. Moreover, the two locations at 47˚47'56''N, 107˚08'47''E; 47˚47'56''N, 107˚08'49''E were deepened and checked. Nevertheless, no faults affecting the loose sediments were discovered (Figure 56-B-C-D).

Figure 56. The trenches in the Tör Khurakh Valley of Mount Bogd Khan. The paleoseismological survey was conducted by the selecting 3 points on the satellite images that could be either the indistinct fault scarps or washout ravines (A, B, and D). (C)-the investigation process of the ditch walls.

5.6 The Drilling Report at the Khürel Togoot trench

In the framework of "Studying seismic activities in Ulaanbaatar city and its vicinity" project, the Joint-Team of IAG of MAS and Hiroshima and Nagoya Universities of Japan excavated the Khürel Togoot trench at Mount Bogd Khan along the UB fault in 2019 and performed the paleoseismological investigation on it.

The main purpose of the paleoseismological investigation was to discover the faulted and deformed zone beneath the surface, to map the units which were displaced by faults, and to identify the latest strong earthquake along the UB fault. Even though the trench was the largest for paleoseismological investigation that ever dug under direction of researchers in Mongolia, drilling was required to better determine the depth structure of the units.

We executed the drilling on November 3, 2021. The drilling was carried out by a high-capacity SANDVIK drill that is manufactured in Australia. The drilling diameter was HQ (Borehole diameter was 75 mm).

The first 90˚ vertical drilling hole was drilled through the sedimentary layers and bedrock with a depth of 35.5 m below the surface (Figure 57 and Figure 59). The drilling hole number is BK21_01 and geographical coordinates are N47˚51'57.1", E107˚04'37.8". The drilling cut the 2-3 m thick sand that was exposed at the trench wall and then it went through the brown colored clayey unit for 23-30 m, and it crossed through the bedrock at ~ 30 m of depth. Just to confirm the bedrock, we drilled 5.5 m more and stopped the drilling (Table 5 and Table 6).

The next drilling was drilled to Mount Bogd with 70˚ of dip angle in order to cross through the black gouge at 10-11 m. The drilling hole number is BK21_02 and geographical coordinates are N47˚51'57.3", E107˚04'38.0". And the length of the drilling hole was 13.5 m. The borehole penetrated the exposed bedrock on the north block and crossed through the black gouge with 85˚ of dip angle at 10-11 m and drilled 2 m more and stopped it (Figure 59).

The 1st borehole drilled the total of 35.5 m. And the sampled core length were 17.6 m and the core loss were 17.9 m because the soft sedimentary deposits were washed by the drilling liquid. The 2nd borehole drilled the total of 13.5 m. And the sampled core length were 5.8 m and core loss were 7.7 m (Table 5 and Table 6).

The drilling result: The vertical borehole core samples show that the sedimentary units are considerably thick that are ~30 m depth until the bedrock. At a depth of 19.8 m in the vertical borehole where the orange colored clay was contaminated with a black material of 8 cm. It is

assumed that it was re-deposited from the black gouge along the fault plane. In particular, no black gouge-like materials were found along the entire vertical drilling process except the black material of 8 cm that (It is described as the black material because it is not like the black unit which was exposed in the trench. The black material that was discovered by the drilling is more like black clay. And it is solid) is described above. The vertical drilling proves that the thick black unit is not present in the south block of the fault plane. The bedrock begins at a depth of ~ 30 m (Table 5 and Table 6).

Based on the 70˚ drilling samples, the fault gouge (or the black thickness) keeps its dip angle of 85˚ at 10-11 m depth. And the black thickness of 25 cm was discovered at 10.9-11.15 m depth. This may suggest that the black thickness has the tectonics origin (Table 5 and Table 6).

The following three samples were selected from the drilling cores and sent them to the Central Geological Laboratory of Mongolia for the Complete Petrographic Analysis in order to describe their rock type.

The sample of light-colored granite (BK21_01, 8.5 m) in the vertical drilling that is contained in 8.5 m depth of the clayey sediment was analyzed to determine the composition of the granite (Figure 60 and Figure 61). This type of granites are very common in the clayey units of the trench. According to the analysis, Kalishpat 64-65%, Quartz 15-20%, Biotite 10-15%, Plagioclase 3-5% and the rock type is described as small-to-medium-grained alkaline-feldspar-biotite-quartzite-syenite (Figure 61). This type of the rocks are exposed on the Bogd Khan Mountain and they are accumulated by the gravity transport.

The sample of the bedrock (BK21_01, 32.5 m) in the vertical drilling was analyzed for the petrographic record. And it contains such as 40-45% sericite, 30-35% quartz, 15-20% pelite, 5-10% feldspar, and 0.5% ore minerals (Figure 62). And the rock type is described as strongly-silicated-feldspar-quartz-sericite-schist. Considering the appearance and microsection of the samples, the bedrock is likely to be the schist from igneous rock.

The sample (BK21_02, 3-5.5 m) in ~3-5.5 m depth of the 70 degrees drilling contains feldspar 40%, quartz 20-25%, mafic intrusive 5%, cement 25-30%, pelite and others 5% respectively and it is microscopically described as brecciated, irregular-grained sandstone-alevrolite (Figure 63).

To conclude based on the description of the above samples, the bedrocks of the northern and southern blocks of the fault plane in the Khurel Togoot trench are two different types of rocks

with different compositions and origins. Therefore, it is clear that the fault plane is the boundary between two different types of rocks.

Figure 57. The vertical 90˚ drilling in ~5 m distance the eastern side of the east wall of the Khürel Togoot trench. November 3, 2021. Mount Bogd Khan, Ulaanbaatar.

Figure 58. The drilling process. Researcher-geologist D. Battogtokh works on the first 10-20 meters deep core samples of the vertical drilling. Mount Bogd Khan, Ulaanbaatar.

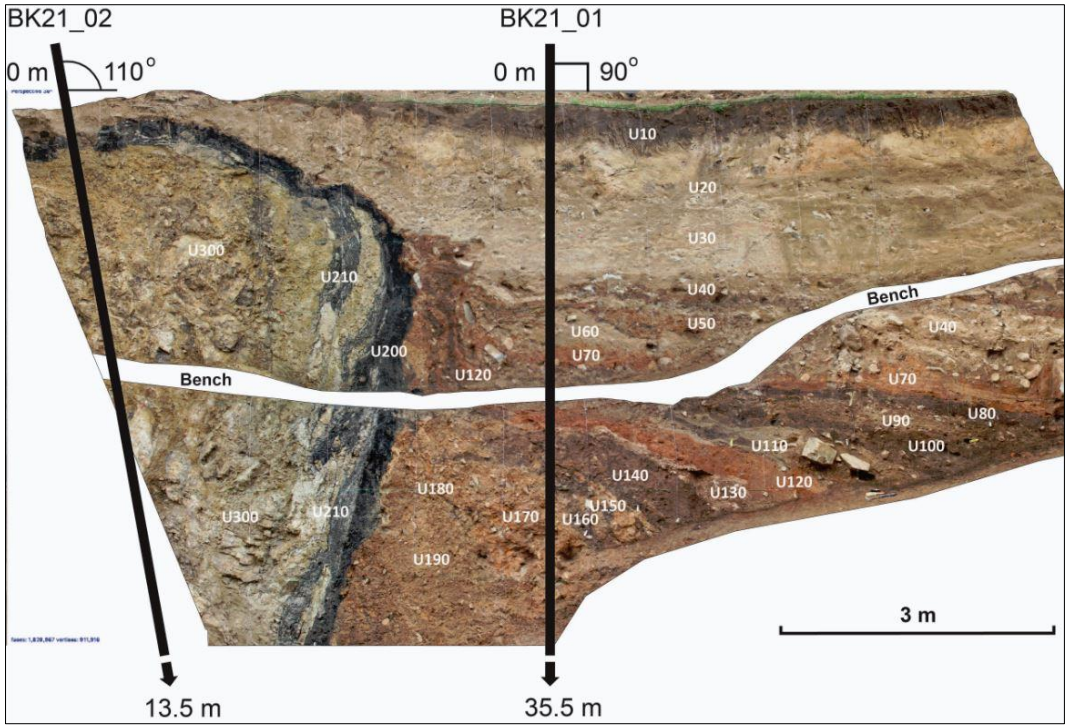

Figure 59. Schematic of BK21_01 and BK21_02 boreholes where we drilled in ~5 m distance beyond the east wall of the Kürel Togoot trench. BK21_01 borehole is vertical of 90˚ degree and it was drilled to the 35.5 m. BK21_02 borehole was drilled to the depth of 13.5 m to Mount Bogd Khan.

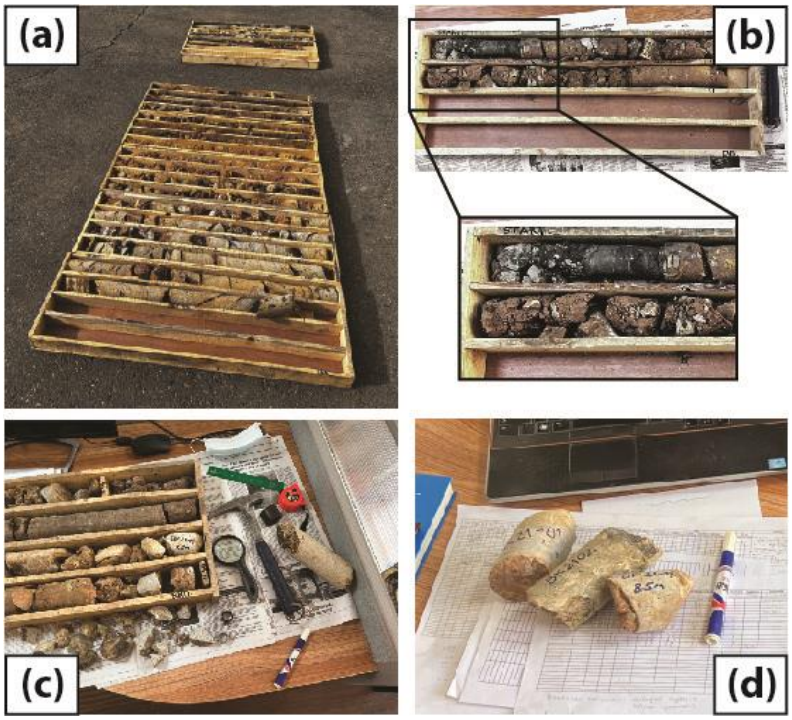

Figure 60. The drilling samples. Total of 7 boxes cores were sampled from BK21_01 and BK21_02 boreholes, (b) the black thickness which was detected at a depth of 10-11 meters of BK21_02, (c) the core samples those were from 0-11.5 m deep of BK21_01 and a granitic sample found at a depth of 8.5 meters were analyzed by the full petrographic record, (d) the 3 samples were performed by the petrographic record analyzes in the Central Geological Laboratory of Mongolia (BK21_01 (8.5 m and 32.5m), BK21_02 (3-5.5 m)).

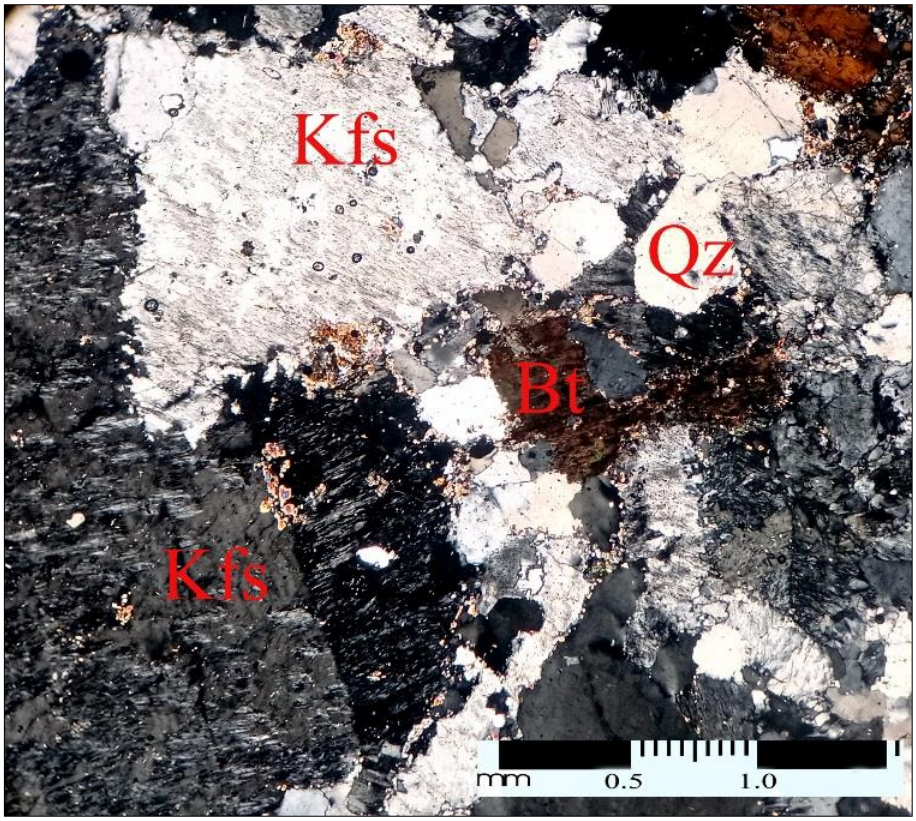

Figure 61. Microsection of the BK21_01, 8.5 m sample. Multiplication 40^{x}. Nicole II. Small-medium-grained alkalic feldspar, biotite-quartzite syenite. (Kfs)-Kalishpat, (Qz)-Quartz and (Bt)-Biotite.

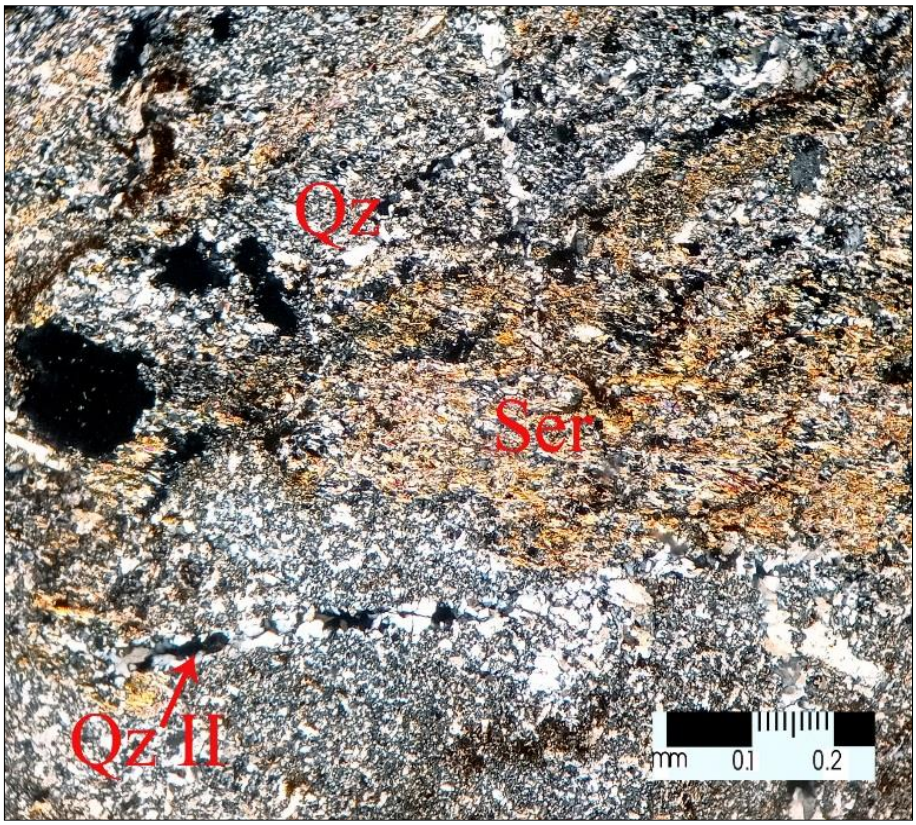

Figure 62. Microsection of the BK21_01, 32.5 m sample. Multiplication 100^{x}. Nicole II. Strongly silicate feldspar-quartz-sericite schist. (Qz)-Quartz, (Ser)-Sericite and (QII)-Late Stage Quartz.

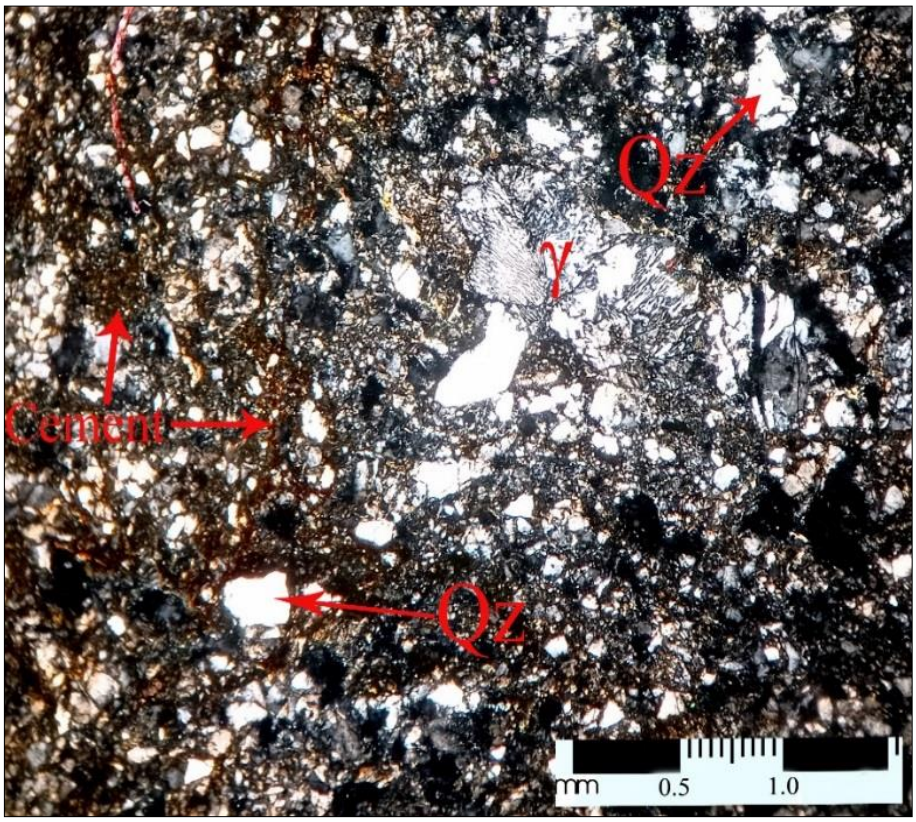

Figure 63. BK21_02, 3-5.5 m sample cut drawing. Increase 40^{x}. Nicole II. Brecciated irregular-grained sandy-alevrolite. (Qz)-Quartz fragments, (ϒ)-Mafic intrusive fragments, (Cement)-Cement.

Table 5. Geotechnical sheet of BK21_01 and BK21_02 drilling holes.

Drillhole Number	Depth		Run Number	Core			RQD (%)	Hard-ness
	From (m)	To (m)		Length(m)	Loss (m)	Length (>0.1 m)		
BK21_01	0	3	1	0.3	2.7	-	10	-
	3	5.5	2	0.5	2.0	-	20	1
	5.5	8.5	3	2.3	0.7	1.3	76.6	1
	8.5	11.5	4	1	2.0	0.35	33.3	1
	11.5	14.5	5	0.6	2.4	0.2	20	1
	14.5	17.5	6	1.7	1.3	1.3	56.6	1
	17.5	20.5	7	3	0	1.6	100	1
	20.5	23.5	8	1.1	1.9	0.2	36.6	1
	23.5	26.5	9	1.2	1.8	-	40	3
	26.5	29.5	10	0.9	2.1	-	30	3
	29.5	32.5	11	2	1	0.5	66.6	3
	32.5	35.5	12	3	0	2	100	3
BK21_02	0	3	1	0.3	2.7	-	10	-
	3	5.5	2	1.9	0.6	0.4	76	3
	5.5	8.5	3	1.8	1.2	0.15	60	3
	8.5	11.5	4	0.7	2.3	0.6	23.3	1
	11.5	13.5	5	1.1	0.9	0.6	55	1

Note: RQD means Run Quality Description. Hardness (Clay = 1 and Bedrock = 3).

Table 6. Lithological sheet of BK21_01 and BK21_02 drilling holes.

Drilling Hole Number	From (m)	To (m)	Lithology	Description
BK21_01	0	3	Gray sand	Upper sandy thickness.
	3	7.9	Black-brown clay	Compacted clay.
	7.9	17.7	Brown clay	The clay bears white-gray colored granite clasts.
	17.7	23.2	Orange clay	There is a black colored clay of 8 cm thick in 19.8 m depth.
	23.2	~30	Orange clay and green-gray schist	Upper part of the bedrock.
	~30	35.5	Green-gray schist	The bedrock that is the schist. There are two separate quartz veins in 30.8-31 m (~20 cm) and 32-32.1 m (~10 cm) respectively those are weakly iron oxidized.
BK21_02	0	3	Gray soil	Upper part.
	3	8.5	Green Alevrolite	Altered green alevrolite that is silicated and chloritized.
	8.5	10.9	Core Loss	It is considered to be that because the black thickness directly connects with the brown clay unit.
	10.9	11.15	The black thickness	
	11.15	13.5	Brown clay	The brown clay contains gray-colored silica-rich clasts (20% of total).

5.7 Conclusions

The UB fault follows an ancient fault zone. In other words, it is located at the contact between different geological formations (Takeuchi et al., 2012).

Suzuki et al (2021) mapped the UB fault between southeast of Mount Bogd and northwest of Mount Tolgoit for ~56 km. The section around Bayankhoshuu and Mount Tolgoit as well as the section to the east and northeast of Mount Bogd, have linear scarps which are clearly visible on the surface. However, the fault scarps in the central part of the city are invisible because of the constructions. Thus, they tentatively connected the segments of Mount Bogd and Mount Tolgoit and marked by the dashed lines.

Most of the fault scarps are mapped along the ancient geological boundaries between the different rock formations thus differential erosion rates may have influenced for the exposures of the mapped fault scarps.

Based on the drilling, the bedrocks of the northern and southern blocks of the fault plane in the Khurel Togoot trench are two different types of rocks with different compositions and origins. Therefore, it is clear that the fault plane is the boundary between two different types of rocks (Figure 64).

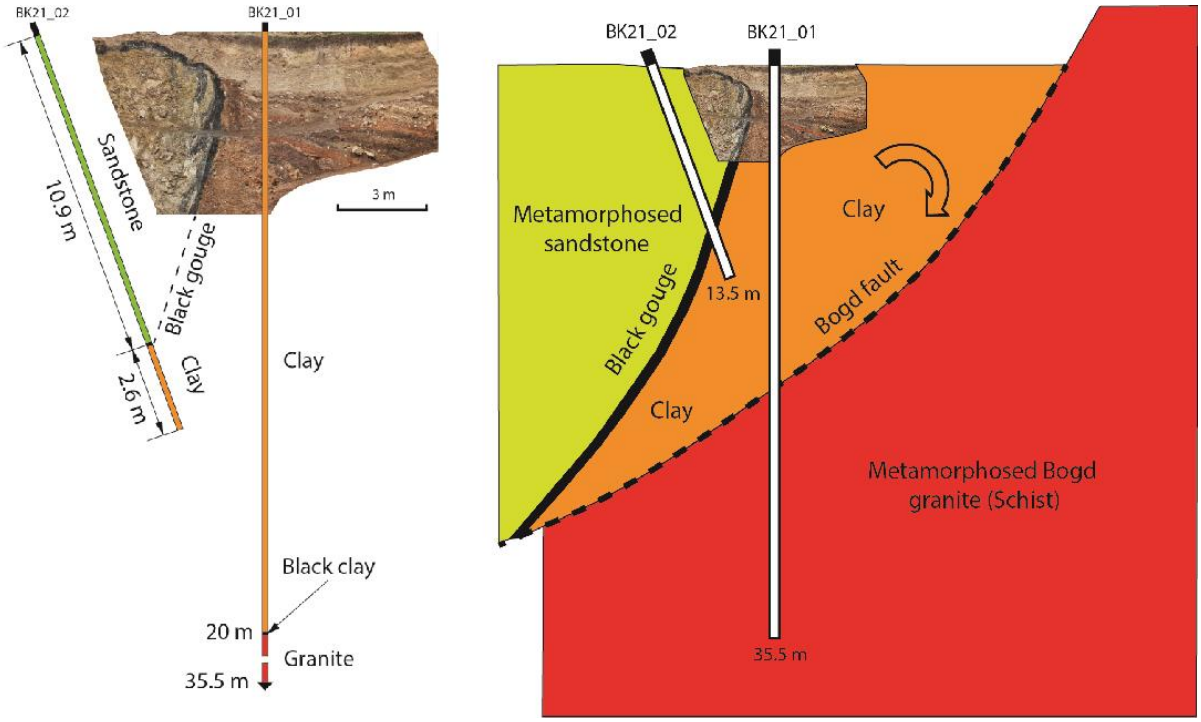

Figure 64. The interpretive scenario based on the trench walls (bedrock, fault gouge, and syntectonic sedimentation) and drilling cores.

In the trench walls, the thick black gouge unit (U210) with the anticlinal folded structure covering decomposed and deformed sandstone-alevrolite unit (U300) seems to be thrusted over the sedimentary sequences (U190-U30) to the southwest.

Looking at the thickening of the sedimentary layers in front of the black fault gouge towards Mount Bogd side, and the tilting of the sedimentary layers we interpret a main structure below the units (not observed in the trench but supposedly corresponding to the units drilled within BK21-01 found around ~ 20 m (see Table 6 and Figure 64)).

According to the paleoseismological studies of the Khürel Togoot trench, the last deformation episode along the UB fault may have occurred in Late Pleistocene, between 40,500 and ~15,800 years BP considering the all obtained ages (preferably around ~25,000 years BP ka which is the age of the paleosoil unit (U200) that is below the clayey units U190-U30 stratigraphically.

The other excavations along the Ulaanbaatar fault do not provide evidence of Holocene or Late Pleistocene seismic activity. It seems therefore that the deformations observed within the Khürel Togoot trench may well correspond to features associated to a local gravitational collapse located along the ancient Paleozoic Bogd fault. Therefore, the Ulaanbaatar fault needs to be further investigated.

ACKNOWLEDGEMENTS

The research involved large number of personnel. The authors thank R.Sarangua, D.Altangerel and Kh. Ölziisaikhan staff from IAG, Mongolian Academy of Sciences, drivers B. Zagdsuren and Ts. Shijirbaatar, B. Khos-Erdene a teacher of Ulaanbaatar State University, students O. Vanchig, B. Davaakhüü and A. Namjildorj. We are also grateful to S. Battulga the Director of the School of International Relations and Public Administration of the National University of Mongolia, as well as thank to Tomoru Yamanaka a researcher at the Hiroshima University, and the staff of the JICA Mongolian office for visiting and cooperating with us.

In addition, we acknowledge Alain Chauvet, a researcher at the Geosciences Montpellier in France, Yann Klinger, head of the Department of Tectonics at the Institute of Global Physics in Paris, and we would like to thank S. Khishigsüren a lecturer at the School of Geology and Mining at the Mongolian University of Science and Technology for sharing their valuable ideas and suggestions. Also, we would like to thank Antoine Schlupp, a researcher at the University of Strasbourg, for sharing his views on the field study for the Ulaanbaatar fault zone on the northeast side of Mount Bogd. We thank to Richard Walker and his two PhD students, Chia-Hsin Tsai and Roberta Wilkinson of the University of Oxford and also Andrew Ivester of the University of Sheffield for processing and dating for the OSL tubes. We also would like to thank the State Agency of Emergency for its technical assistance in excavating the Khürel Togoot Trench.

Finally, we express our gratitude to the Bogd Khan Uul Strictly Protected Area Administration for the opportunity to conduct our research.

5.8 References

Al-Ashkar, A., Schlupp, A., Ferry, M., & Munkhuu, U. (2022). Tectonic Geomorphology and Paleoseismology of the Sharkhai fault: a new source of seismic hazard for Ulaanbaatar (Mongolia). *Solid Earth, 13*, 761-777. https://doi.org/10.5194/se-13-761-2022

Calais, E., & Amarjargal, S. (2000). New constraints on current deformation in Asia from continuous GPS measurements at Ulaanbaatar, Mongolia. *Geophysical Research Letter*, 545-550 p.

Ishikawa, T., Hirono, T., Matsuta, N., Kawamoto, K., Fujimoto, K., Kameda, J., … Honda, G. (2014). Geochemical and mineralogical characteristics of fault gouge in the Median Tectonic Line, Japan: evidence for earthquake slip. Sprinter, Earth, Planets and Space.

Molnar, P., & Tapponnier, P. (1975). Cenozoic tectonics of Asia: Effects of a continental collision. *Science, 189*(4201), 419-426. https://doi.org/10.1126/science.189.4201.419

Odonbaatar, Ch., Ulziibat, M., Battogtokh, D., … Dugarmaa, T. (2015). Micro-zoning map (1:10,000 scale) of Ulaanbaatar city and its satellite districts (in Mongolian). The Institute of Astronomy and Geophysics of Mongolian Academy of Sciences.

Philip, H., Avagyan, A., Karakhanian, A., Ritz, J.-F., & Rebai, S. (2001). Estimating slip rates and recurrence intervals for strong earthquakes along an intracontinental fault: example of the Pambak-Sevan-Sunik fault (Armenia). *Tectonophysics, 343*, 205-232.

Suzuki, Y., Nakata, T., Watanabe, M., Battulga, S., Enkhtaivan, D., Demberel, S., Odonbaatar, C., Bayasgalan, A., & Badral, T. (2020). Discovery of Ulaanbaatar fault: A New Earthquake Threat to the Capital of Mongolia. *Seismological Research Letters*, XX, 1-11. https://doi:10.1785/0220200109

Takeuchi M., Tsukada K., Suzuki T., Nakane Y., Sersmaa G., Manchuk N., Kondo T., Matsuzawa N., Bacht N., Khishigsuren S., Onon G., Katsurada Y., Hashimoto M., Yamasaki S., Matsumoto A., Oyu-Erdene B., Bulgantsetseg M., Kundyz S., Enkhchimeg L., Ganzorig R., Myagmarsuren G., Jamiyandagva O., Molomjamts M. (2012). Stratigraphy and geological structure of the Paleozoic system around Ulaanbaatar, Mongolia. *Bulletin of the Nagoya University Museum, 28*, 1-18.

Önödelger, T., & Banzragch, B. (1993). Report of the hydrogeological survey (aerophotogeology, geophysics, and geochemistry) carried out in 1990-1992 in the vicinity of Ulaanbaatar. UGF. #4718.

Zonenshain, L. P., & Savostin, L. A. (1981). Geodynamics of the Baikal rift zone and plate tectonics of Asia. *Tectonophysics, 76*(1981), 1-45.

CHAPTER 6

This paper benefited from several contributions; In terms of field analysis, I participated to the paleoseismic investigations, which have been carried out during summer 2019 under the supervision of J-F Ritz. I wrote the first draft concerning these investigations including the analysis of the data and its interpretations. I also wrote an introduction and a tectonic setting that have been revised by J-F Ritz. The section about the morphotectonic analysis is based on the Master thesis of Clément Boivin (Géosciences Montpellier, 2019) about the morphological analysis of the Möngönmorit fault, carried out under the supervision of Matthieu Ferry and J-F Ritz. The results of Boivin's work has been synthetized and translated in English by J-F Ritz and I modified some figures.

6. ANALYSING THE KINEMATICS AND PALEOSEISMOLOGY OF THE MÖNGÖNMORIT FAULT (KHENTII DÔME, NE MONGOLIA)

Davaasambuu Battogtokh [1,2], Jean-Francois Ritz [1], Matthieu Ferry [1], Clement Boivin [3], Munkhuu Ulziibat [2] and Adya Munkhsaikhan [2]

[1]Geosciences Montpellier, University of Montpellier, CNRS, France

[2]Department of Earthquake Research, Institute of Astronomy and Geophysics, Mongolian Academy of Sciences

[3]University of Strasbourg

6.1 Abstract

The Möngönmorit active fault is located at the southern edge of the Khentii Dôme, in north-eastern Mongolia, 100 km eastward the capital city of Ulaanbaatar. The fault has been described as a potential reverse active fault from preliminary GPS data and paleoseismic investigations. However, the region of Ulaanbaatar and its surrounding is known to correspond to a transtensional deformational context. Moreover the fault is situated on top of the Khentii Dôme.

This raises the question whether the preliminary statement about its kinematics is correct. To go further in the characterization of seismotectonic characteristics of the fault (geometry, length, segmentation, kinematics, potential magnitude and recurrence intervals of events) we carried out a morphotectonic and paleoseismological study. Our morphological analysis, based on remote sensing data show that the fault can be subdivided into two main sections, themselves subdivided in several segments. The northern section (~70 km) appears more active than the southern one (90 km). Within the northern section, the Möngönmorit fault appears very sinuous with an eastwards dip of ~20° making it a shallow dipping normal fault, at least near the surface. Paleoseismological investigations confirm the gentle eastwards dipping of the fault in surface, and allow bracketing the ages of the most recent and penultimate surface rupturing events between 4893 and 6609 cal BP and between 8052 and 8571 cal BP, respectively. This yields an interval between these two last events of 2560 ± 1117 years, while the time elapsed since the last surface rupturing event reaches 5ka. The minimum vertical offset observed in the morphology associated with the gentle dip of the fault suggest that the fault is capable of producing Mw 7 + event, and shows that the Möngönmorit fault represent a non-negligible seismic hazard not only for the close Möngunmörit village (~3000 peoples) and Baganuur town (~30,000 peoples), but also for the Mongolian capital where ~1.6 million peoples are living.

6.2 Introduction and Tectonic setting

The active tectonics in Mongolia is controlled by two geodynamic processes: the SSW-NNE India-Eurasian collision and the WNW-ESE extension of the Baikal rift system (e.g. Molnar & Tapponnier, 1975; Calais et al., 2003; Ritz et al., 2003; Arjannikova et al., 2004; Lukhnev et al., 2010; Ritz et al., 2018). Due to the SSW-NNE collision, transpressional deformations are observed in western Mongolia within the Altai and Gobi-Altai mountain ranges, which are respectively characterized by large-scale right-lateral and left-lateral strike-slip faulting, both associated with secondary reverse faulting (e.g., Tapponnier & Molnar, 1979; Khilko et al., 1985; Baljinnyam et al., 1993; Ritz et al., 1995; 2003; 2006; Vassallo et al., 2006; Ulziibat, 2006; Walker et al., 2006; Nissen et al., 2009; Frankel et al., 2010; Rizza et al., 2011; Gregory, 2012). Due to the WNW-ESE extension of the Baikal rift system, transtensional deformations are observed within the Darkhad and Lake Khövsgöl regions, both characterized by oblique normal faulting along ~NS fault systems associated with right-lateral movements. These transtensional deformations are also observed further to the southeast within both the western-central and the southeastern central parts of the Khangai and the Khentii dome, respectively,

where normal faulting or strike-slip faulting combined with normal faulting are observed along NE-SW structures (e.g., Walker et al., 2007; 2008; Al-Ashkar, 2015, Al-Ashkar et al., 2022; Walker et al., 2015).

These two strain regime are consistent with GPS measurements, which show that western Mongolia is submitted to a north-northeasternward compression at a rate of 5 mm/yr, which is accommodated by large right-lateral NW-SE trending strike-slip faults associated to secondary reverse faults and the anticlockwise rotation of the crustal blocks between these faults, while southern, central and eastern Mongolia are moving eastward-southeastward with an average rate of ~4 mm/year with respect to the Baikal rift (e.g., Calais & Amarjargal, 2000; Calais et al., 2003).

Compared to western Mongolia, eastern Mongolia corresponds to a low seismic active region. It is only recently that active faulting along faults as the Möngönmorit, Avdar, Sharkhai, or Khustai faults has been described from morphological and paleoseismological studies (e.g., Imaev et al., 2012; Smekalin et al., 2016; Al-Ashkar, 2022). Currently, the Möngönmorit fault is considered as the easternmost active fault in Mongolia. Beyond the fault, eastwards, the reliefs decreases joining the Great Steppe and Plateau of Dornod.

The Möngönmorit fault is located in the southwestern Khentii region in north-central Mongolia and is considered as an active fault capable of producing surface-rupturing events. Situated 100 km to the east of Ulaanbaatar, it represents therefore a potential seismic hazard for the Mongolian capital with 6 other faults situated in its vicinity (i.e. situated in a 100 km radius around the city; Figure 65). The Möngönmorit fault corresponds to the furthest (100 km) among the Avdar (42 km), Sharkhai (42 km), Khustai (35 km), Emeelt (23 km), Günj (12 km), and Ulaanbaatar (1.6) faults, but it is the longest one with length of 80 km. Avdar and Sharkhai correspond to NE-SW trending faults and are located ~40 km southwest of Ulaanbaatar, with lengths of 47 km and 40 km, respectively (Al Ashkar, 2015, Al Ashkar et al., 2022). These faults have been defined as left-lateral strike-slip faults with a normal component. The Khustai fault has the same orientation (NE-SW), and is located on the southern foothills of the Khustai Mountains, west of Ulaanbaatar. It is also characterized by a left-lateral sense of motion with a normal component (Ferry et al., 2010). The NS trending Emeelt fault, situated to the NW is described as essentially a normal fault (Dujardin et al., 2014; Odonbaatar et al., 2015). These four faults and their kinematics are consistent with the GPS velocity field in the area, which -

although still poorly defined - show that the region is deforming under an E-W transtensional regime (Calais et al., 2003).

However, other studies on other faults in the same region suggested in contrary that the region is characterized by transpressional deformation. For instance, Imaev et al. (2012) described the NE-SW trending Günj fault situated northwards of Ulaanbaatar as corresponding to a dextral strike-slip fault with a reverse component. Recently, Suzuki et al., (2021) described the NW-SE trending Bogd fault, a structure crossing the city of Ulaanbaatar and inherited from the Paleozoic orogenesis, as left-lateral reverse fault. Concerning the Möngönmorit fault, Smekalin et al. (2016) concluded that it corresponds to a NNE-SSW reverse fault from paleoseismological investigations.

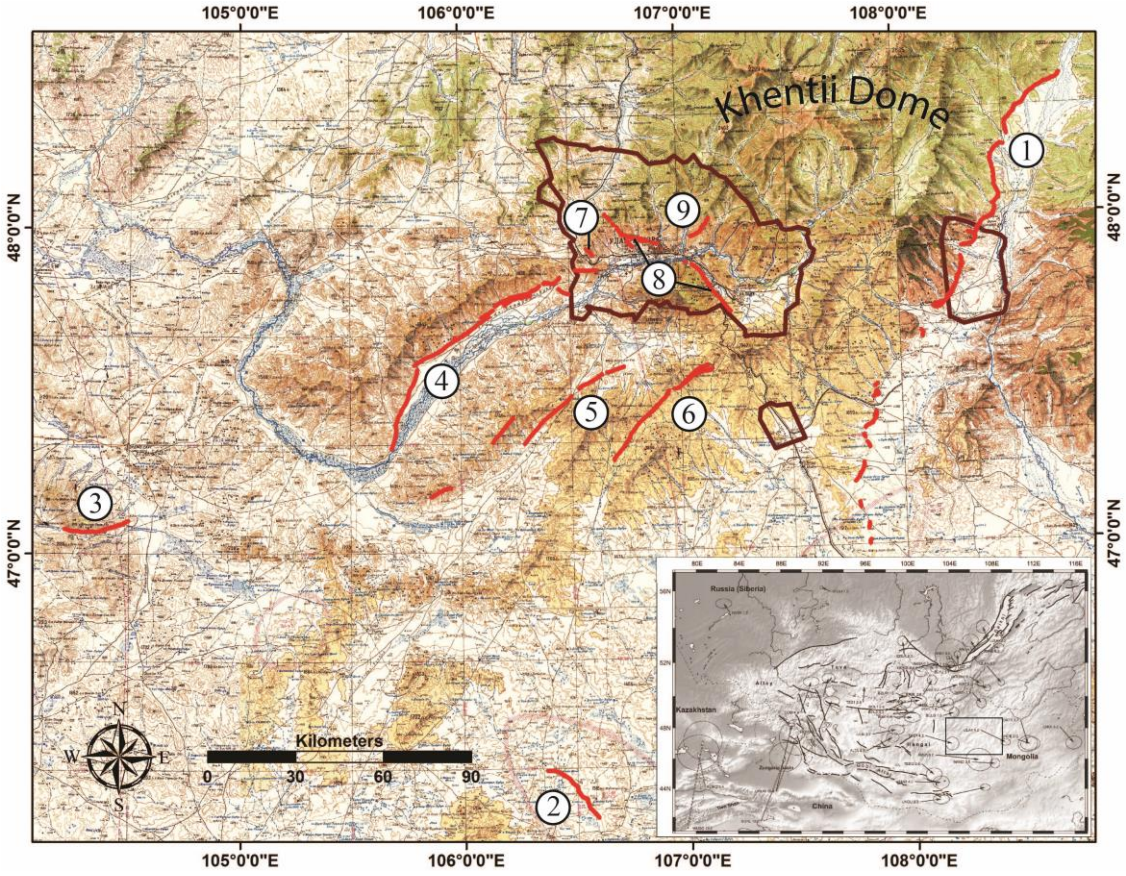

Figure 65. 1:500,000 scale topographic map of the southwestern Khentii Dome in central Mongolia showing the main faults considered as active in the region: (1) Möngönmorit, (2) Deren, (3) Agit, (4) Khustai, (5) Sharkhai, (6) Avdar, (7) Emeelt, (8) Ulaanbaatar, and (9) Günj. The polygons show the urban area of Ulaanbaatar city and its satellite districts. The inset map represents Mongolia with its main active faults and GPS velocities field (after Calais et al., 2003). The black rectangle in the inset map corresponds to the base map.

In this paper, on the base of new observations from both morphotectonic and paleoseismological investigations, we determine the seismotectonic characteristics of the Möngönmorit fault (geometry, length, segmentation, kinematics, potential magnitude and

recurrence intervals of past events). We then discuss its meaning in the framework of the Mongolia-Baikal regional geodynamics.

6.3 Analyzing the morphotectonic features along the Möngönmorit fault

The Möngönmorit active fault is located at the southern central part of the Khentii Dôme. A swath topographic profile made across the area shows that the fault is located in the center of the dome.

To go further in the characterization of the fault, we mapped it using web-based Google Earth, as well as “Pleiades” and “TanDEM” satellite images. The Google Earth offered the advantage of zooming in and out easily over small and large areas. It also allows detecting and mapping the fault scarps and tectonic-related geomorphological features. In parallel, Pleiades images with ground resolution of 0.5 m allowed visualizing the fault scarps in great details. TanDEM digital elevation data (12 m resolution) were useful for 3D viewing of the fault scarp in the landscape, mapping it at a broad scale and quantifying the vertical displacements.

Our morphotectonic study mainly relied on the comparison between high resolution Digital Terrain Models (DTM) from TanDEM-X and drone data, high-resolution ortho-rectified images of Pleiades and drone data, and spectral analyzes of Sentinel-2 images. The combination of these three families of data helped to accurately map the fault surface rupture (Figure 66 and Figure 67). In a second step, the DEMs combined with the ortho-rectified images allowed determining the dip direction and dip value of the fault and therefore its kinematics.

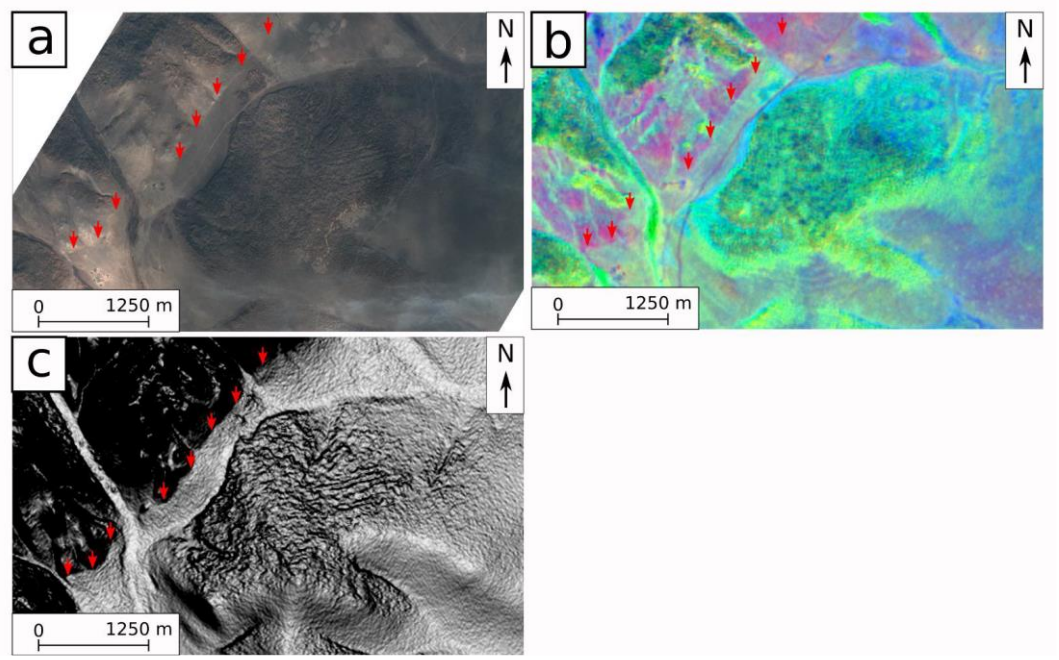

Figure 66**.** Section of the Möngönmorit surface rupture pointed out on (a) Pleiades high-resolution image, (b) Sentinel-2 spectral image, (c) TanDEM-X DTM.

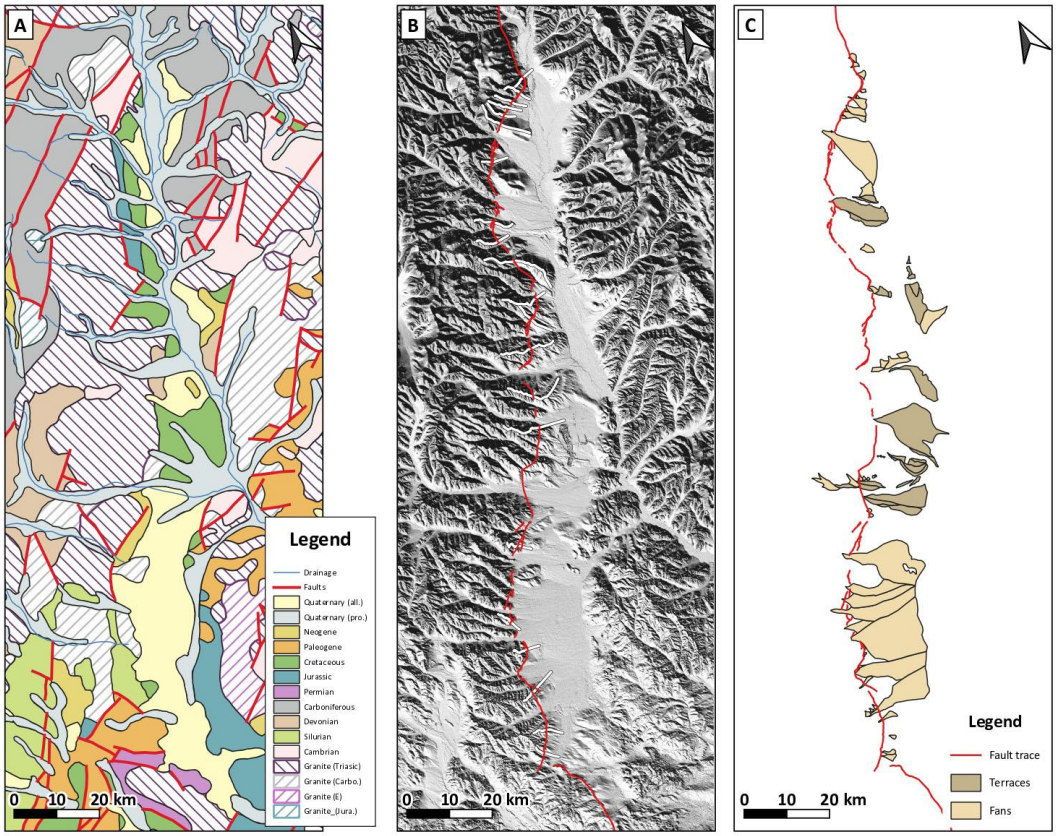

Figure 67**.** (A) Geological map of the Möngönmorit fault and surrounding geological units showing Mesozoic inherited structures; (B) Map of the Möngönmorit surface ruptures associated with quaternary activity from Google Earth, Pleiades and Tandem images. Locations of the vertical cumulative displacement profiles across the fault as shown Figure 9. (C) Map of the geomorphological features of the Kherlen Valley and the Möngönmorit fault.

DTMs are 3D models representing the vertical data (altitude) of the topography, according to a defined horizontal resolution and vertical precision. With this type of data several analyzes are possible, ranging from the identification and mapping of geomorphological markers; the measurements of displacement related to the fault activity. Here, we mainly relied on the high-resolution DEM from the TanDEM-X satellite, with a vertical accuracy of 2 m and a horizontal resolution of 12 m. Having a sufficiently fine resolution to identify the surface rupture of the fault as well as the geomorphological objects such as the valleys, the alluvial fans, the terraces, etc. We used DEMs with higher vertical precision to measure vertical displacements lower than 2 m. To complete the observations, 7 high-resolution digital surface models (DSM) were obtained by photogrammetric calculations from the images acquired with a drone during the summer 2018. The resolution of the data is 10 cm (Figure 68).

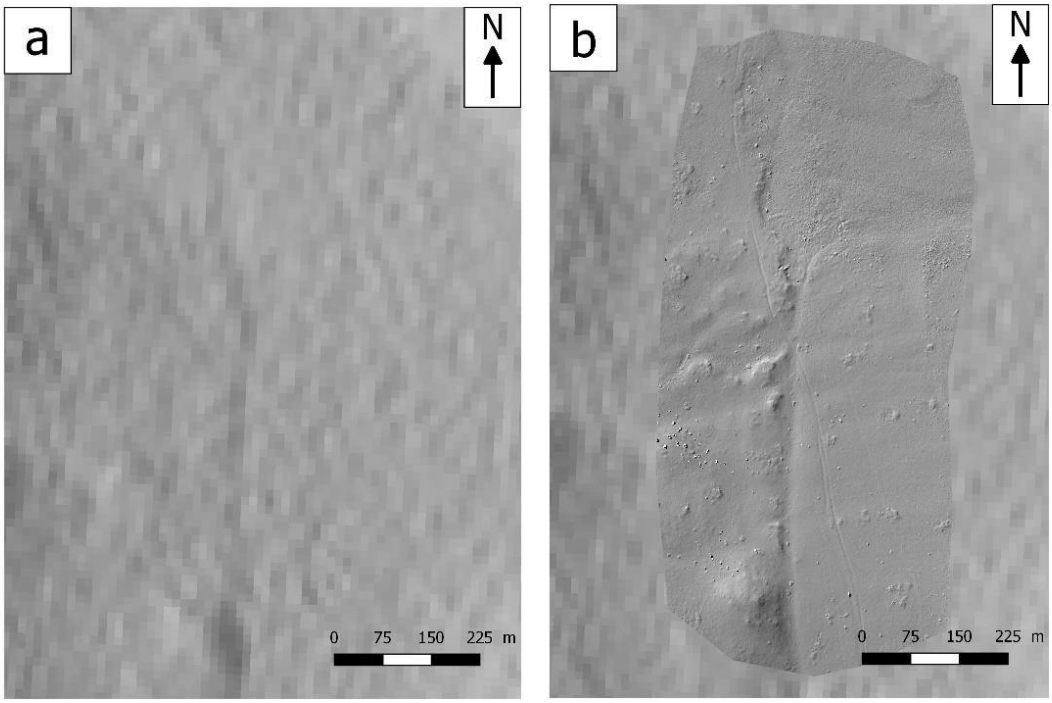

Figure 68**.** Comparison between DEMS obtained from a TanDEM-X image (a) and a drone survey (b) (NB: the height of the fault scarp is lower than 1 m).

To characterize the main kinematics of the fault, we first determined the dip direction of the fault and its angular value. The surface rupture corresponding to the intersection of the fault plane with the topographic surface, we analyzed the direction pointed out by the "V" and the "inverted V" that the surface rupture was forming when crossing the valleys or when crossing the interfluve, respectively (Figure 69). The surface rupture is discontinuous and less clear in the southern section than in the northern section of the fault, and we could determine the dip direction and its angular value only along the northern section. The high-resolution DEM

provided by the TanDEM-X satellite, allowed determining the value with an uncertainty of ± 0.5°. The average azimuth of the fault is N025°E and its average dip is 18° ± 5° towards the E/SE. This clearly shows that the Möngönmorit fault corresponds to a shallow normal fault dipping to the East.

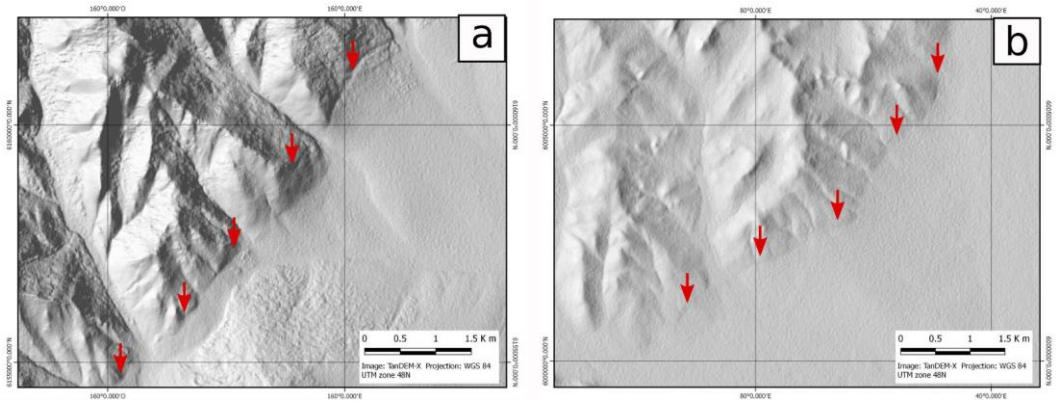

Figure 69. DEMs tandem-X images allowing pointing out the fault scarp (red arrows) along the Möngönmorit fault within the northern (a) and southern (b) sections. In both cases, the southeastwards concave arcuate shape of the scarp within the interfluves, between rivers, allows calculating the dip of the fault.

Within the northern section, the Drone data allowed us analyzing the smaller offsets along the fault. 11 profiles across the fault scarp were performed and led results comprised between 0.5 m and 7.3 m (Figure 70).

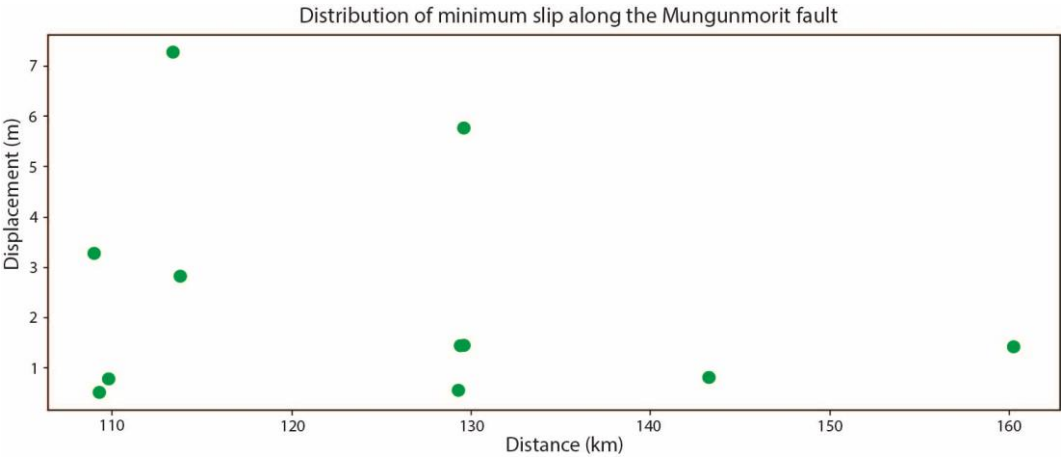

Figure 70**.** Smallest vertical offsets measured along the Möngönmorit within the area survey with the drone (northern section).

CUMULATIVE NORMAL DISPLACEMENT

We estimated the total cumulative displacement associated to the normal movement along the Mungunmorit fault and analyzed its distribution by means of a series of topographic sections (see Figure 71). To achieve this analysis, we selected piercing lines such offset ridge-crest lines between rivers (e.g. Ritz et al., 2012) (Figure 72).

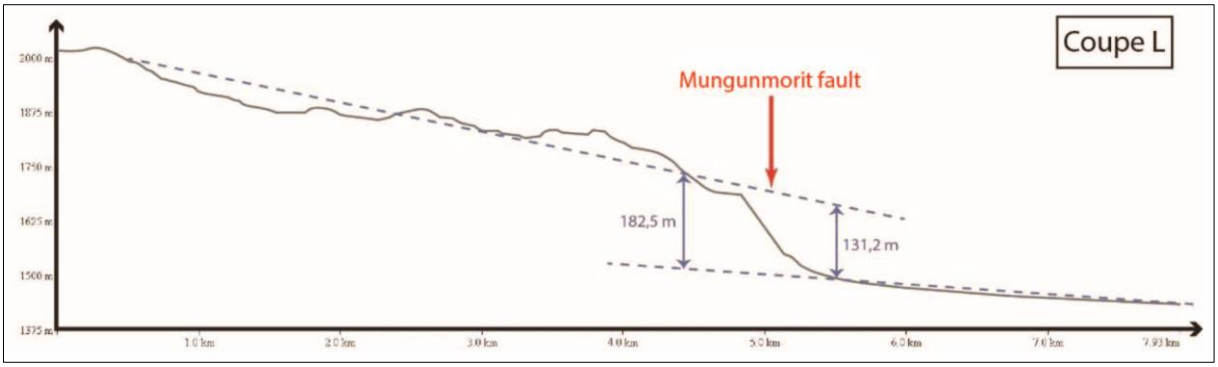

Figure 71**.** Example of a topographic profile across the Möngönmorit fault allowing estimating the cumulative displacement along the fault. Note that the two dashed piercing lines are not parallel leading to determining a maximum (182.2 m) and minimum (131.2 m) values.

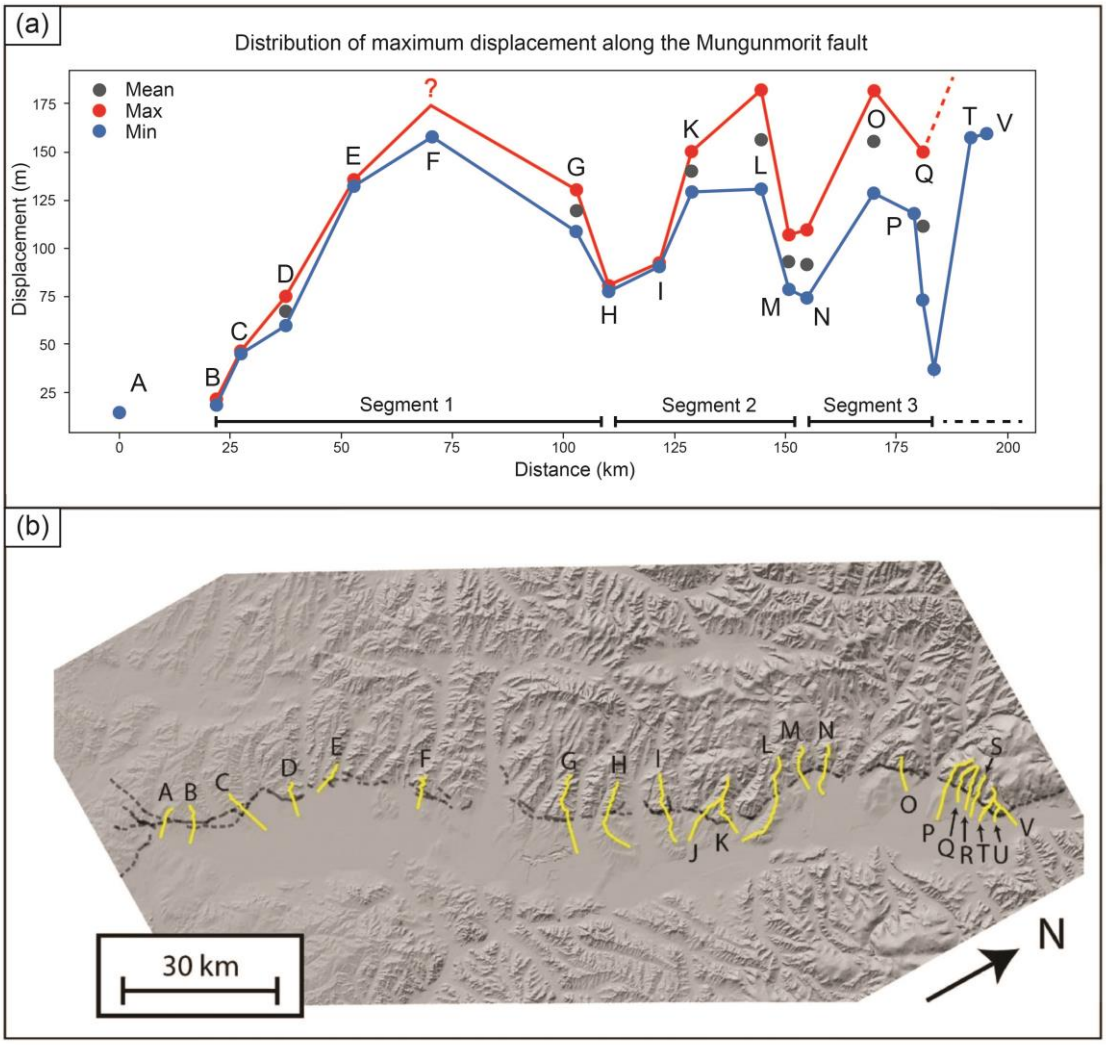

Figure 72**.** (a) Distribution of the total vertical cumulative displacement along the Möngönmorit fault (b) Locations of the profiles along the fault.

Figure 72 shows 22 offset measurements along the Möngönmorit fault which allows estimating an average cumulative vertical displacement comprised between 170 m and 130 m. The distribution of data suggests that at least 3 fault segments can be distinguished. Segment 1 with

a first homogeneous lobe between profiles A and H, corresponds to the southern section of the fault with a length of about 90 km. The distribution of the cumulative displacement along the northern section appears more complex. At least, two shorter segments seem to be distinguished between profiles H and N, and between profiles N and S, with lengths of 40 and 30 km, respectively.

6.4 Analysing the paleoseismology along the Möngönmorit fault

We excavated three trenches across the Möngönmorit fault, 5.5 km to the southwest of the Möngönmorit village. The trench 1 was dug across a clear fault scarp feature affecting the ground surface at the foothills of which flat morphology suggested trapped sedimentary deposits (Figure 73). The site where we dug trench 2 corresponds also to a clear fault scarp feature. It not only shows a sequence of sedimentary accumulation, but allows also observing the fault plane affecting the bedrock. Trench 3 was excavated on an antithetic fault to the east of the main fault.

Figure 73**.** Field picture of trench 1 (T1); researchers are cleaning and brushing the trench walls before photographing, logging and sampling (photo by D. Battogtokh, July 2019).

Trenches 1 and 2 were dug across the main fault, and are 24-30 m long, 1.5 m wide and 2-3 m deep. They are separated by a distance of 200 m. Trench 3, ~10 m long, ~1 m wide and ~2 m deep and was excavated across an antithetic fault about ~200 m to the east of the main fault

(Figure 74). The trench walls were scraped and cleaned before setting up a 1x1 m string grid in order to log the trench at the scale of 1/20. All walls of the trenches were photographed and the photos then assembled into mosaics. Stratigraphic units were characterized, named, and logged in a coherent way between the 3 trenches. Stratigraphic and structural relationships were then described and logged onto millimeter tracing papers.

SAMPLES

In order to estimate the timing of the past surface rupturing earthquakes along the Möngönmorit fault, we collected total of 8 samples from the three trenches for radiocarbon dating. All the samples are bulk. The samples were processed and dated in Poznan Radiocarbon Laboratory in Poland. Ages of samples range between 2960±30 BP and 14690±150 BP. The laboratory dating results were calibrated on OxCal using the methodology developed by Christopher Bronk Ramsey (2009). All radiocarbon dates of 8 samples are in well stratigraphic order and consistent over the 3 trenches (Figure 80). Despite the fact that some samples were not used directly to determine the timing of earthquakes, they were used to identify the relative ages of the host layers and also it yielded the absolute ages of other units (Table 7).

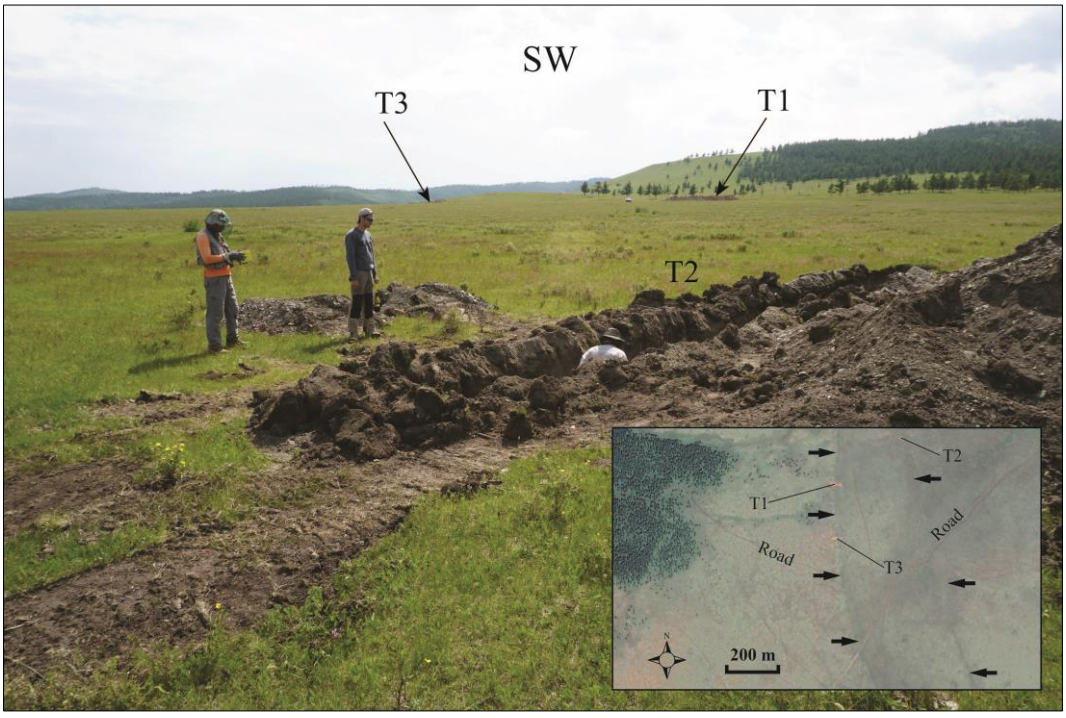

Figure 74. Field picture of trench T2 dug across a secondary antithetic fault of the Möngönmorit fault. T1 and T3 dug across the main fault scarp are pointed out with arrows in the background. The inset map shows the locations of the trenches. The black arrows indicate the main normal fault with dipping to the east, while the antithetic fault is dipping to the west. The coordinates of T1, T2, and T3 are 48˚9'49.7"N, 108˚26'27.6"E; 48˚9'54.8"N, 108˚26'38.5"E; and 48˚9'43.6"N, 108˚26'27.8"E, respectively (photo by C. Boivin, July 2019).

Table 7. Radiocarbon dating from the 3 trenches (T1, T2 and T3).

Sample Name[a]	Lab. Number[b]	Radiocarbon Age[c]	Calibrated Ages (Calendric)
BA19-C1	Poz-121148	5390 ± 40 BP	6130 – 6264 Cal BP
BA19-C2	Poz-121149	2960 ± 30 BP	3088 – 3196 Cal BP
BA19-C3	Poz-121150	6170 ± 50 BP	7006 – 7148 Cal BP
BA19-C4	Poz-121151	14690 ± 150 BP	17605 – 18381 Cal BP
BA19-C5	Poz-121152	7730 ± 60 BP	8453 – 8571 Cal BP
BA19-C6	Poz-121153	7320 ± 80 BP	8052 – 8248 Cal BP
BA19-C7	Poz-121154	5730 ± 50 BP	6471 – 6609 Cal BP
BA19-C8	Poz-121081	4380 ± 40 BP	4893 – 5021 Cal BP

Note: [a]Samples were labelled BA19 to mean that they were collected in the region of the Baganuur district during the year 2019. [b]Laboratory sample codes. All samples have been dated by the Poznan Radiocarbon Laboratory. [c]Radiocarbon years (BP) are counted respect to 1950 AD.

INTERPRETING THE LOGS

The logging of the trench both is the field and with the use of photomosaics, allowed interpreting the paleoseismicity in terms of past-surface rupturing events produced by the Möngönmorit fault. The illustrations presented hereafter on which we reported the ages of the collected samples synthetize our interpretations (Figure 80).

ANALYSING TRENCH 1 (T1)

Trench T1 is 24 m long and 1.5 m wide with a depth comprised between 2 and 3 m. The sedimentary units observed in the trench were numbered from U10 (modern soil unit) to U80 (the oldest, respectively) and differentiated from their nature, their grain-size and colors:

- U10 is the organic-rich brown-colored surface soil.
- U20 is a brown-colored sub-soil unit, coarser than U10 and containing some gravels.
- U30 is a brown-grayish-colored, small-sized-gravels bearing layer.
- U40 is a light-yellow-colored clayish-gravelly layer.
- U50 is a greyish-colored clayish-gravelly layer.
- U60 is an orange-colored clayish layer that bears small-sized angular gravels.
- U70 corresponds to green-colored clays. It occupies a large portion of the trench wall from 7th column to 24th columns in the log. This clayish layer contains boulders of various sizes (the largest is 30-40 cm).
- - U80 corresponds to the bedrock unit and can be observed between columns 0 and 9 at the bottom of the trench.

The most recent event MRE (most recent event) E1 is observed in the northern wall of the trench between columns 7 and 10 in the log (Figure 75). This section, logged in details (Figure

12A), is located just below the topographic scarp. The main fault defines a gently dipping abnormal contact between U80 (bedrock) at the bottom of the trench and the above-lying units, notably unit U70 which is affected by plastic deformation interpreted as liquefaction features associated with shearing along the fault contact. The unit is affected by secondary fault features at several areas. Some of these features show clear normal fault displacements.

From this main contact several fissures, cracks and secondary faults affect all the above-lying sedimentary units until U20. The fault F1 for instance displaced units U70 to U30, and is sealed by unit U20. In order to constrain the age of this MRE, we collected samples in the predating unit U30 (BA19-C1) and the postdating unit U20 (BA19-C2). Radiocarbon ages allow bracketing the MRE (event 1) between 3142 ± 54 Cal BP and 6197 ± 67 Cal BP (see Table 7).

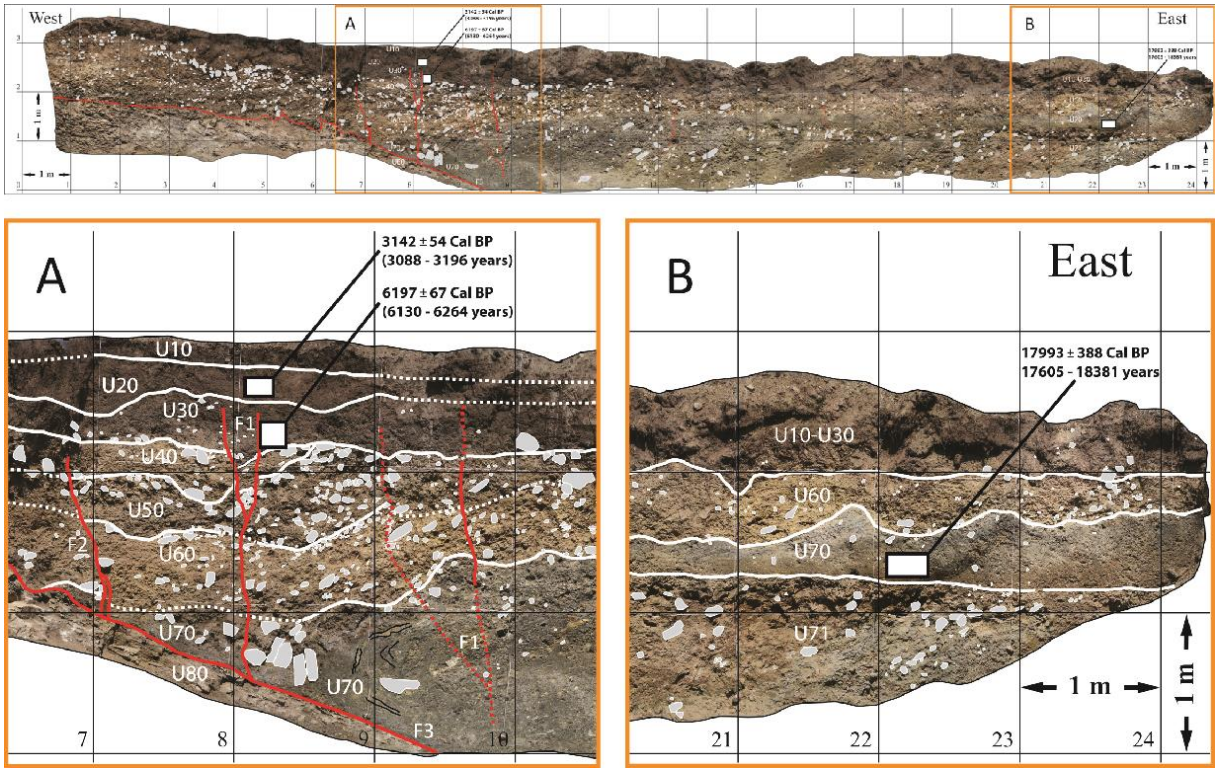

Figure 75**.** Paleoseismological log of trench T1 northern wall. The uppermost figures show the general photomosaic of the T1 north wall and its corresponding log in superposition. The larger clasts are represented by grey polygons with their actual shapes and locations. The faults are shown by the red colored lines. (A) and (B) shows the detailed sections of log with superposition of the logs and photomosaics.

We could not log in details the southern wall of trench T1 due to the lack of time, but we could make some interesting observations that complete the analysis of the northern wall (Figure 76). Within the central section of the southern wall, we evidence for the most recent event with a clear small normal fault affecting unit 30 and 40. Radiocarbon dating of bulk sample (BA19-

C3) collected in the pre-dating unit 30 allows to give an age of 7077 ± 71 yrs cal BP for the most recent event.

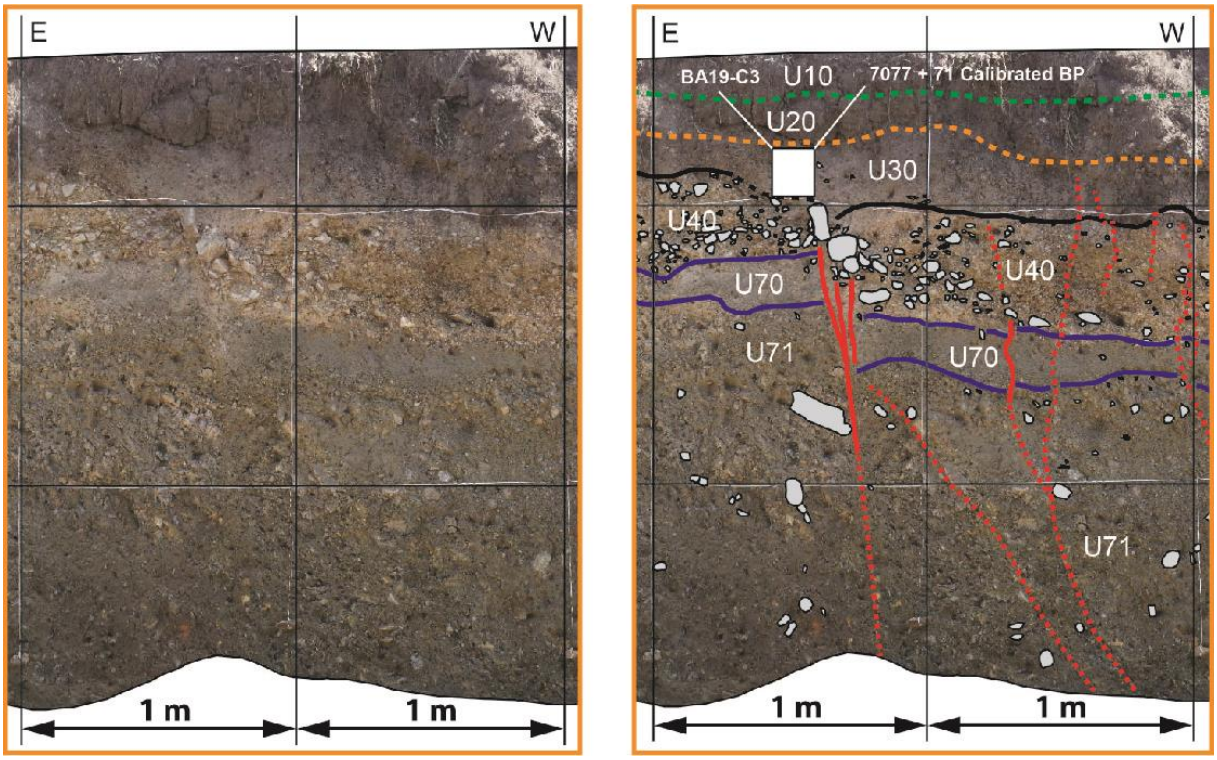

Figure 76**.** Detailed sketch log of normal fault associated with the most recent event observed within the southern wall of trench T1. These 2 columns are located at the center of the south wall. The east image displays the photomosaic, whereas the west image represents the illustrations of the units and faults.

An earlier event (E3) can be deduced from the clayey unit U70. This unit corresponding to low-energy ponded sediments against the fault scarp, with boulders of various sizes in it, suggests that it might correspond to post-event deposits. We collected a sample from the unit in the eastern part of the trench (column 23, Figure 75-B). Its analysis yielded a radiocarbon age of 17605-18381 Cal BP, meaning it was deposited during the end of the last glacial period.

ANALYZING TRENCH 2 (T2)

Trench T2 was excavated in the secondary branch (antithetic fault). It has smaller dimensions (5 m long, 1 m wide, 2 m high). Clayey sediments bearing various sizes and angles of gravels and boulders define most of the trench stratigraphy (U30). The upper part of the trench corresponds to a 30-50 cm thick layer (U20) covered by a soil horizon (U10). A main fault/shear zone is observed between columns 3 and 5, and affects the entire gravel section (Figure 77 and Figure 78). It terminates within a V-shape fissure sealed by U20. The gravels at the bottom of the fissure are oriented and vertical along the fault suggesting they were taken in the deformation, and do not correspond to post-event fissure filling.

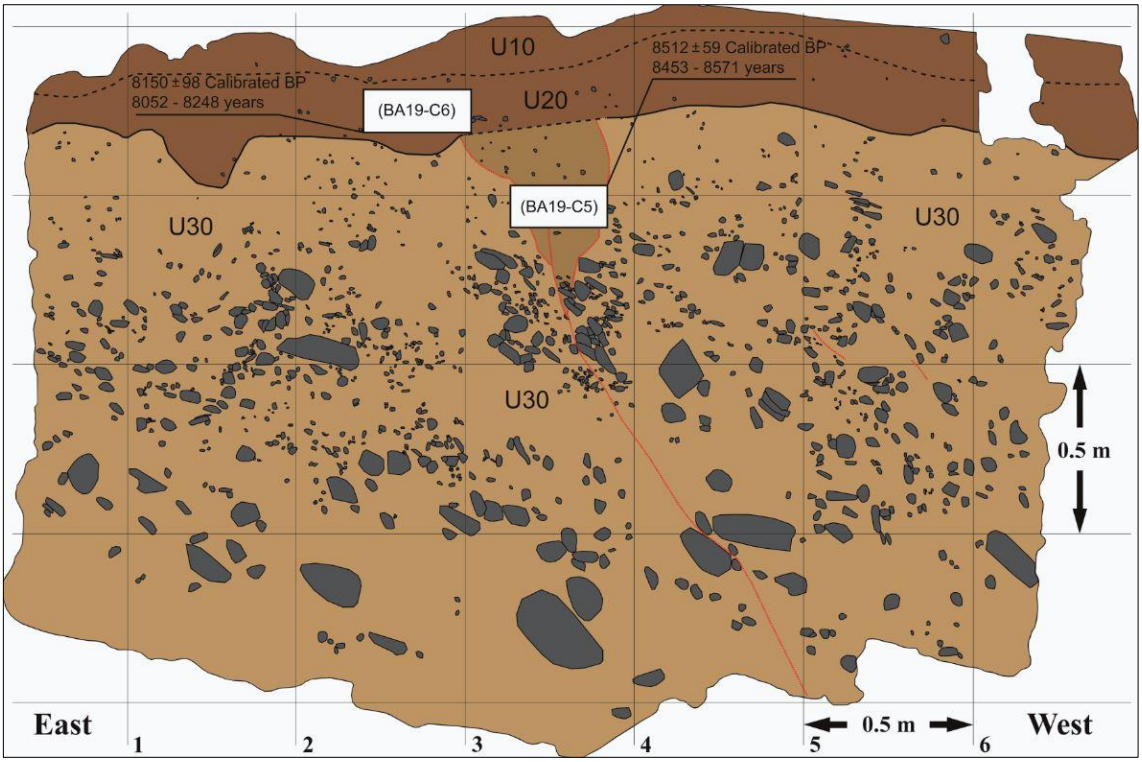

Figure 77**.** Sketch log of the trench T2.

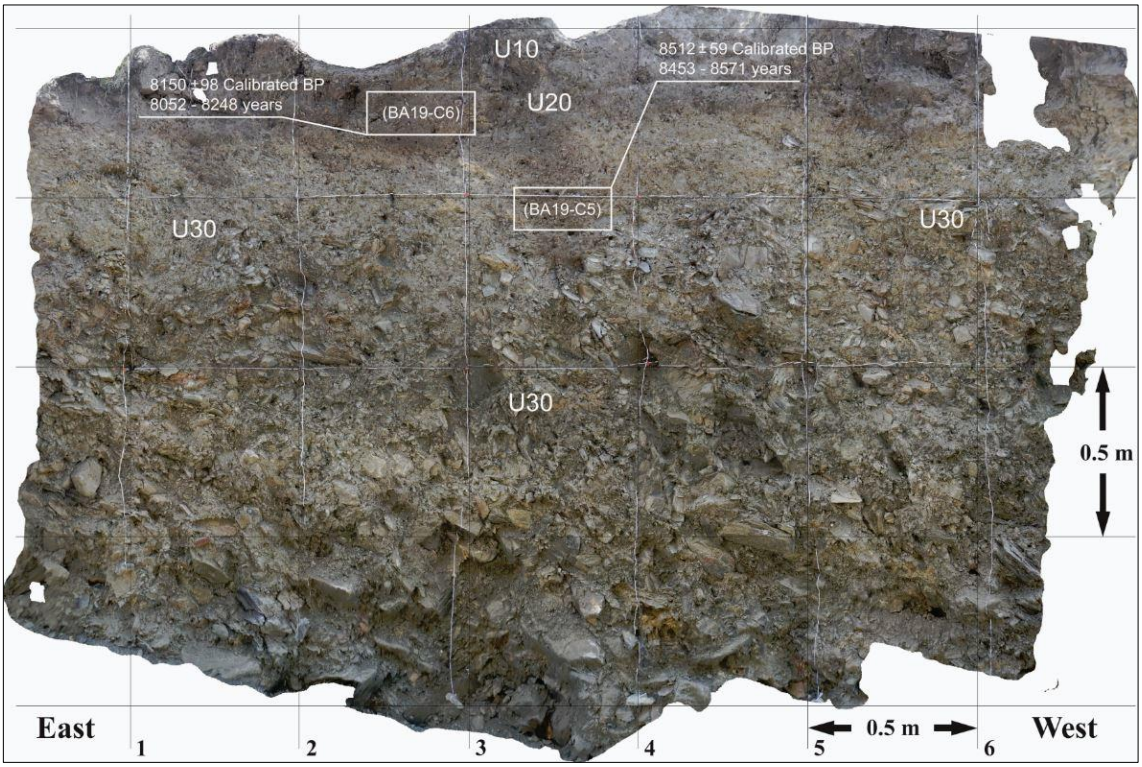

Figure 78. Photomosaic of the trench T2.

In order to date the surface-rupture, we collected two bulk samples, in the fissure and in the overlying unit U20, respectively. The radiocarbon analysis of the samples allows bracketing the event between 8453-8571 Cal BP and 8052-8248 Cal BP (Figure 77 and Table 7). Given

the antithetic nature of this secondary fault and its distance (200 m) with respect to the main fault - involving that it necessarily moves contemporaneously with the main fault – these results imply that a penultimate event (PE) or event 2 occurred between 8150±98 Cal BP and 8512±59 Cal BP along the Möngönmorit fault. These results also imply that the antithetic fault ruptured during the PE but not during the MRE.

ANALYSING TRENCH 3 (T3)

T3 trench was opened across the main fault, ~200 m southward trench T1. It shows similar stratigraphy to T1. The bedrock (U80) in the bottom of the trench is covered by the green-colored fine-grained clay U70. The green sediments are overlain by clayish-gravelly units (U30-U50). At the top, these units (U30-U50) are covered by brown thick soil horizon turf (U10 and U20).

We could not log trench T3 in details due to the lack of time, but we managed to carry out a quick analysis that we completed with field photographs. As observed in trench T1, unit U30 is faulted by the MRE, and sealed by unit U20 (Figure 79). A sample collected in U30 yielded an age of 6540±69 Calibrated BP, while the sample collected in U20 yielded an age of 4957±67 Calibrated BP (Figure 79 and Table 7). Thus trench T3 allows tightening the MRE between 4957±64 Cal BP and 6540±69 Cal BP.

Our paleoseismological investigations along the Möngönmorit fault allow us interpreting 2 surface-rupturing events having occurred in the past 8400 years. Figure 80 synthetizes the results obtained within the 3 trenches. The most recent event (E1) occurred between 4893 and 6609 Cal BP. A penultimate event (E2) occurred between 8052 and 8571 Cal BP. During this penultimate event, both the main fault (F1) and its conjugated antithetic one (F2) moved contemporaneously. A last, a third event (E3) can be interpreted from the occurrence of the clayey lacustrine sediments of unit U70 that are trapped against the fault scarp. The age of the unit suggests that this earlier event occurred not long before 17.6 ka.

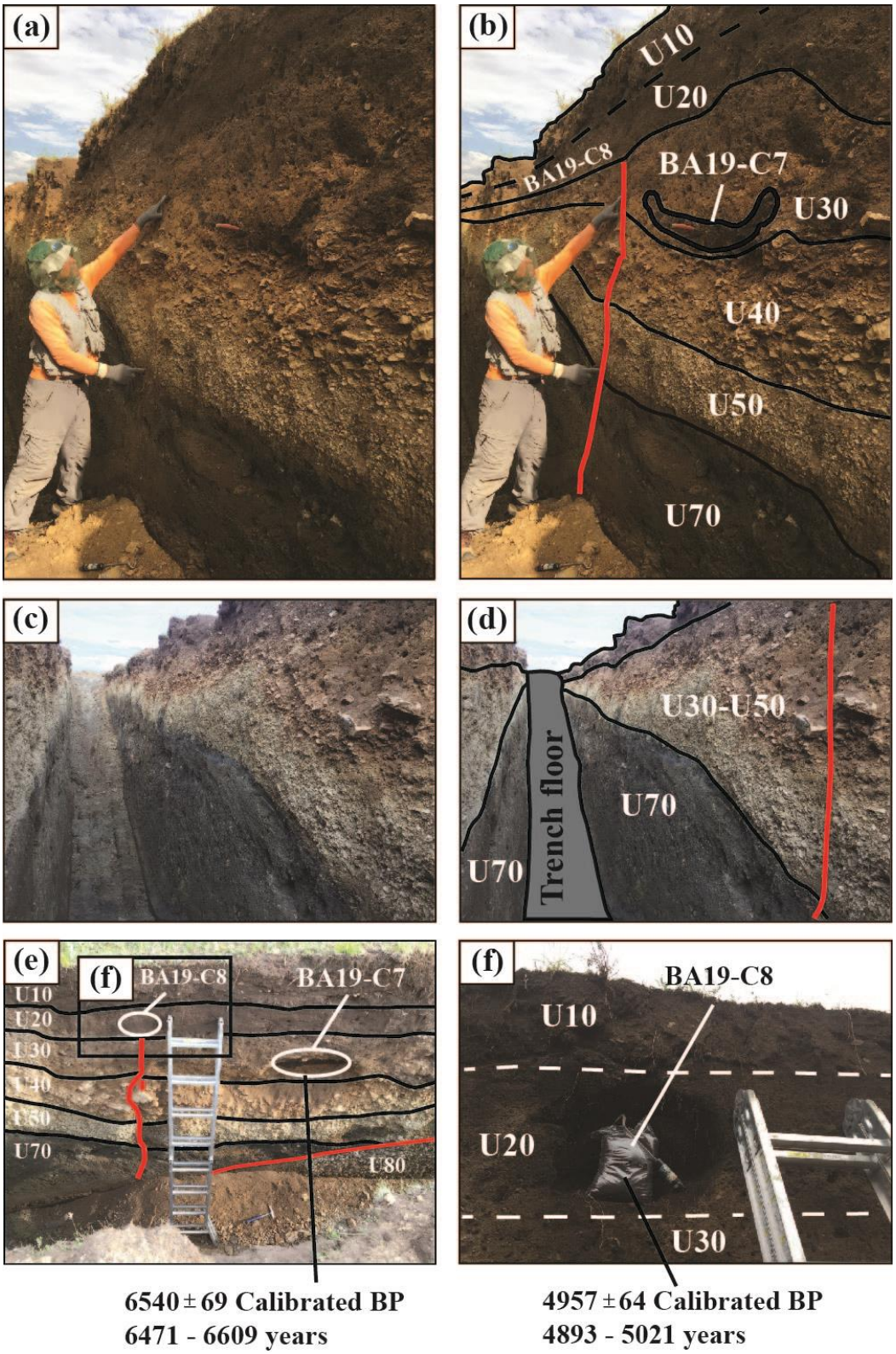

Figure 79**.** Trench T3 field photos and interpretation. (a) Battogtokh points out the fault exposure on the trench wall (photo by J. Ritz, July 2019). (b) Interpretation of the photo. (c) General eastwards view of the trench. (d) Interpretation of the photo C. (e) Interpretation of the main deformed zone. Note that the fault (vertical red line) is the fault pointed in A and B. The gentle dipping fault overlying U80 is the basic normal fault as observed in trench T1. (f) Enlarged section on the photo F represents the sampling procedure BA19-C8.

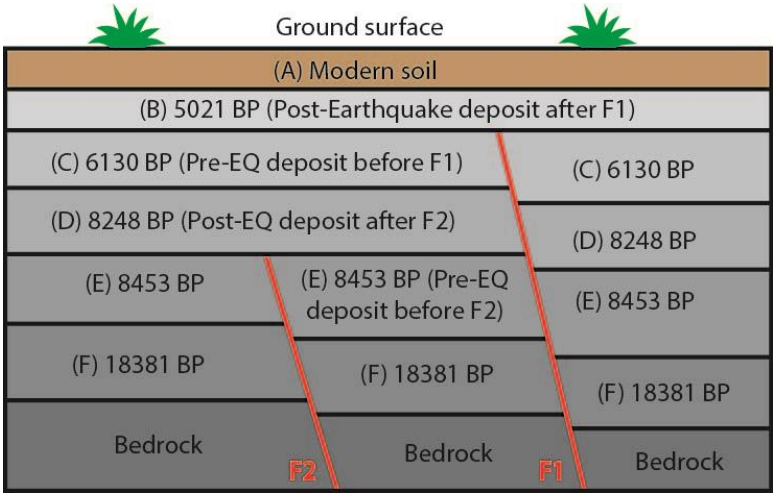

Figure 80. Sketch diagram synthetizing the chronology of the 3 past surface rupturing events having occurred along the Möngönmorit fault during the last 18 ka near the Möngönmorit Village.

6.5 Discussion and Conclusion

Our morphotectonic and paleoseismological study along the Möngönmorit fault shows that it corresponds to an active gently eastwards dipping normal fault, at least in sub-surface. From this kinematical point of view, this result confirms that the southwestern Khentii region is undergoing active extensional strain regime, which is consistent with the E-W transtensional regime observed in the Ulaanbaatar region immediately to the South-West. This transtensional/extensional regime seems to be correlated to the strain regime of the Baikal rift, and would be controlled the uplift of the asthenosphere in the area. From the point of view of paleoseismology, our investigations allow characterizing the occurrence of two surface-rupturing events since 8.4 ka. If we extend the time window of our observations, it seems that at least one more strong event occurred not long after 18 ka.

The paleoseismological data concerning the two last events suggest a mean recurrence period of surface rupturing events comprised between 3000 and 5000 years. The latest earthquake along the fault having occurred 5 ka ago, yields an elapsed time equal to the maximum bound of the recurrence interval. Although this statement is based only on the 2 past events, and despite the fact that a possible earlier event at ~18 ka increases the recurrence time (~10 ka), the question of the seismic hazard associated to the Möngönmorit fault is clearly posed.

Moreover, despite the co-seismic slip associated with the different events observed in the trenches could not been determined (observed co-seismic feature corresponding mainly to secondary small scale normal faults or fissures), other features as the minimum vertical offset observed in the morphology (i.e. 0.5 m, see section 3), associated with the very gentle dip (~20°)

of the fault, its total length (~160 km) and the length of its different segments (90-30 km) show the possibility of surface-rupturing events reaching easily Mw 7 after Wells and Coppersmith (1994)'s scaling functions, linking co-seismic slip, rupture length and moment magnitude.

In conclusion, the Möngönmorit fault represents a non-negligible seismic hazard for the southern Khentii region notably for the Möngönmorit village and its ~3000 inhabitants, as well as for the city of Baganuur where ~30,000 peoples are living. Even for Ulaanbaatar, situated ~100 km westwards, the Möngönmorit fault represents a seismic hazard which must be taken into account given the ~1.6 million citizens who live in the Mongolian capital.

ACKNOWLEDGMENTS

This work benefited from the Fund of Science & Technology of Mongolia, and the support of the "SEISMONG" INSU-CNRS PICS program (PI J-F Ritz). We thank Coopérant Matthieu Morel who helped during the 2019 field work.

6.6 References

Al-Ashkar, A. (2015). Active tectonics of the Ulaanbaatar region, Mongolia. Morphotectonic and paleoseismological analysis of the active faults of Sharkhai and Avdar. PhD thesis. *University of Strasbourg.*

Arjannikova, A., Larroque, C., Ritz., J.-F., Deverchere, J., Stephan, J. F., Arjannikov, S., & Sankov, V. (2004). Geometry and kinematics of recent deformation in the Mondy-Tunka area (south-westernmost Baikal rift zone, Mongolia-Sibirea). Terra Nova, 16(5), 265-272. https://doi.org/10.1111/j.1365-3121.2004.00565.x

Baljinnyam, I., Bayasgalan, A., Borisov, B. A., Cisternas, A., Dem'yanovich, M. G., Ganbaatar, L., … Vashchilov, Y. Y. (1993). Ruptures of major earthquakes and active deformation in Mongolia and its surroundings. Geological Society of America, Memoir, 181, 62. https://doi.org/10.1130/MEM181-p1

Bayasgalan, A., Jackson, J., & McKenzie, D. (2005). Lithosphere rheology and active tectonics in Mongolia: Relations between earthquake source parameters, gravity and GPS measurements. Geophysical Journal International, 163, 1151-1179. https://doi.org/10.1111/j.1365-246X.2005.02764.x

Calais, E., & Amarjargal, S. (2000). New constraints on current deformation in Asia from continuous GPS measurements at Ulan Baatar, Mongolia. Geophysical Research Letter, 27(10). https://doi.org/10.1029/1999GL005444

Calais, E., Vergnolle, M., San'kov, V., Lukhnev, A., Miroshnitchenko, A., Amarjargal, S., & Deverchere, J. (2003). GPS measurements of crustal deformation in the Baikal-Mongolia area (1994-2002): Implications for current kinematics of Asia. Journal of Geophysical Research, 108(B10), 2501. https://doi.org/10.1029/2002JB002373

Dujardin, J.-R., Bano, M., Schlupp, A., Ferry, M., Munkhuu, U., Tsend-Ayush, N., & Enkhee, B. (2014). GPR measurements to assess the Emeelt active fault's characteristics in a

highly smooth topographic context, Mongolia. Geophysical Journal International. https://doi.org/10.1093/gji/ggu130

Ferry, M., Schlupp, A., Ulzibat, M., Munschy, M., Fleury, S., Baatarsuren, G., … Ankhtsetseg, D. (2010). Tectonic Morphology of the Hustai fault (Northern Mongolia): A Source of Seismic Hazard for the city of Ulaanbaatar. Geophysical Research Abstracts, 12. EGU General Assembly, Vienna, Austria.

Frankel, K. L., Wegmann, K. W., Bayasgalan, A., Carson, R. J., Bader, N. E., Adiya, T., … Gregory, L. (2010). Late Pleistocene slip rate of the Höh Serh-Tsagaan Salaa fault system, Mongolian Altai and intracontinental deformation in central Asia. Geophysical Journal International, 183, 1134-1150. https://doi.org/10.1111/j.1365-246X.2010.04826.x

Gregory, L. C. (2012). Active faulting and deformation of the Mongolian Altay Mountains. PhD thesis. University of Oxford.

Imaev, V. S., Smekalin, O. P., Strom, A. L., Chipizubov, A. V., & Syas'ko, A. A. (2012). Seismic-hazard assessment for Ulaanbaatar (Mongolia) on the basis of seismogeological studies. Russian Geology and Geophysics, 53(2012), 906-915.

Khilko, S. D., Kurushin, R. A., Kochetkov, V. M., Misharina, L. A., Melnikova, V. I., Gilyova, N. A., … Monkhoo, D. (1985). Earthquakes and the bases of the seismic zoning of Mongolia. The Joint Soviet-Mongolian Scientific-Research Geological Expedition, Transactions (Volume 41).

Lukhnev, A. V., San'kov, V. A., Miroshnichenko, A. I., Ashurkov, S. V., & Calais, E. (2010). GPS rotation and strain rates in the Baikal-Mongolia region. *Russian Geology and Geophysics, 51*, 719-727. https://doi:10.1016/j.rgg.2010.06.006

Molnar, P., & Tapponnier, P. (1975). Cenozoic tectonics of Asia: Effects of a continental collision. *Science, 189*(4201), 419-426. https://doi.org/10.1126/science.189.4201.419

Nissen, E., Walker, R., Bayasgalan, A., Carter, A., Fattahi, M., Molor, E., … Xu, S. (2009). The late Quaternary slip-rate of the Har-Us-Nuur fault (Mongolian Altai) from cosmogenic ^{10}Be and luminescence dating. *Earth and Planetary Science Letters, EPSL-09924*, 12 p. https://doi:10.1016/j.epsl.2009.06.048

Odonbaatar, Ch., Ulziibat, M., Battogtokh, D., … Dugarmaa, T. 2015. Micro-zoning map (1:10,000 scale) of Ulaanbaatar city and its satellite districts (in Mongolian). The Institute of Astronomy and Geophysics of Mongolian Academy of Sciences. Ulaanbaatar.

Ramsey, C. B. (2009). Bayesian analysis of radiocarbon dates. *Radiocarbon, 51*(1), 337-360.

Ritz, J.-F., Arzhannikova, A., Vassallo, R., Arzhannikov, S., Larroque, C., Michelot, J.-L., & Massault, M., (2018), Characterizing the present-day activity of the Tunka and Sayan faults within their relay zone (western Baikal rift system, Russia). Tectonics, 37, 1376-1392. https://doi.org/10.1002/2017TC004691

Ritz, J.-F., Bourles, D., Brown, E. T., Carretier, S., Chery, J., Enhtuvshin, B., … Yiou, F. (2003). Late Pleistocene to Holocene slip rates for the Gurvan Bulag thrust fault (Gobi-Altay, Mongolia) estimated with ^{10}Be dates. Journal of Geophysical Research, 108(B3), 2162. http://doi:10.1029/2001JB000553

Ritz, J. F., Brown, E. T., Bourles, D. L., Philip, H., Schlupp, A., Raisbeck, G. M., … Enkhtuvshin, B. (1995). Slip rates along active faults estimated with cosmic-ray-

exposure dates: Application to the Bogd fault, Gobi-Altai, Mongolia. *Geology*, *23*(11), 1019-1022.

Ritz, J.-F., Nazari, H., Balescu, S., Lamothe, M., Salamati, R., Ghassemi, A., … Saidi, A. (2012). Paleoearthquakes of the past 30,000 years along the North Tehran fault (Iran). Journal of Geophysical Research, 117(B06305). https://doi.org/10.1029/2012JB009147

Ritz, J.-F., Vassallo, R., Braucher, R., Brown, E. T., Carretier, S., & Bourles, D. L. (2006). Using in situ-produced ^{10}Be to quantify active tectonics in the Gurvan Bogd mountain range (Gobi-Altay, Mongolia). *Geological Society of America, Special Paper, 415*, 87-110. http://doi:10.1130/2006.2415(06)

Rizza, M., Ritz, J.-F., Braucher, R., Prentice, C., Mahan, S., McGill, S., … Bourles, D. (2011). Slip rate and slip magnitudes of past earthquakes along the Bogd left-lateral strike-slip fault (Mongolia). *Geophysical Journal International*. https://doi:10.1111/j.1365-246X.2011.05075.x

Smekalin, O. P., Chipizubov, A. V., & Imaev, V. S. (2016). Seismogeology of Verkhnekerulen basin (Khentei, Northern Mongolia). Geodynamics & Tectonophysics, 7(1), 39-57. http://dx.doi.org/10.5800/GT-2016-7-1-0196

Suzuki, Y., Nakata, T., Watanabe, M., Battulga, S., Enkhtaivan, D., Demberel, S., … Badral, T. (2021). Discovery of Ulaanbaatar Fault: A New Earthquake Threat to the Capital of Mongolia. Seismological Research Letters, 92, 437-447. http://doi:10.1785/0220200109

Tapponnier, P., & Molnar, P. (1979). Active faulting and Cenozoic tectonics of the Tien Shan, Mongolia, and Baykal regions. Journal of Geophysical Research, 84(B7), 3425-3459. https://doi.org/10.1029/JB084iB07p03425

Ulziibat, M. (2006). The 2003 Chuya sequence (North Altay range): tectonic context and seismological study. PhD thesis. University of Nice Sophia Antipolis.

Walker, R. T., Bayasgalan, A., Carson, R., Hazlett, R., McCarthy, L., Mischler, J., … Tsolmon, G. (2006). Geomorphology and structure of the Jid right-lateral strike-slip fault in the Mongolian Altay mountains. *Journal of Structural Geology*, *28*, 1607-1622. https://doi:10.10106/j.jsg.2006.04.007

Walker, R. T., Molor, E., Fox, M., & Bayasgalan, A. (2008). Active tectonics of an apparently aseismic region: distributed active strike-slip faulting in the Hangay Mountains of central Mongolia. *Geophysical Journal International*. https://doi:10.1111/j.1365-246X.2008.03874.x

Walker, R. T., Nissen, E., Molor, E., & Bayasgalan, A. (2007). Reinterpretation of the active faulting in central Mongolia. Geology, 35(8), 759-762. https://doi:10.1130/G23716A.1

Walker, R. T., Wegmann, K. W., Bayasgalan, A., Carson, R. J, Elliott, J., Fox, M., … Wright, M. (2015). The Egiin Davaa prehistoric rupture, central Mongolia: a large magnitude normal faulting earthquake on a reactivated fault with little cumulative slip located in a slowly deforming intraplate setting. Geological Society, London, Special Publications, 432. https://doi.org/10.1144/SP432.4

Wells, D. L., & Coppersmith, K. J. (1994). New empirical relationships among magnitude, rupture length, rupture width, rupture area, and surface displacement. Bulletin of the Seismological Society of America, 84(4), 974-1002.

CHAPTER 7

7. DISCUSSIONS AND CONCLUSIONS

The vast territory of Mongolia is under the influence of two different geodynamic environment in terms of active tectonics: the Altai and Gobi-Altai Mountains are under transpressive regimes associated with the India-Eurasia collision, whereas the Sayan and Khentii Mountains are influenced by the extension of the Baikal-Khövsgöl rift (Figure 81). Moreover, most of the territory of Central Mongolia is in a transtensional regime possibly related to the movement of the North China block (locally Amur micro-block) to the east.

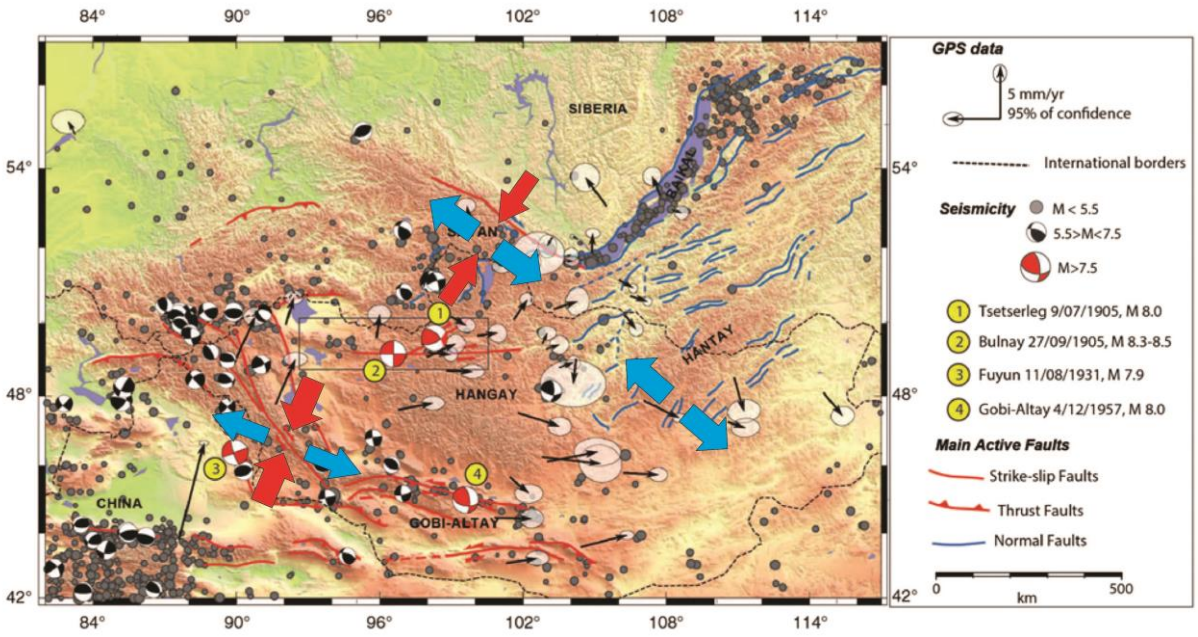

Figure 81. Regional kinematics of Mongolia. The Altai region represents transpressive regime (in red arrows). Normal-dextral Khövsgöl fault suggests that the regime changes from extensive to transtensive (in blue arrows) as observed in southwest Baikal region. Pure-normal Möngönmorit fault demonstrate the extensive regime (in blue arrows) in southeast of the territory. Seismotectonic map from Rizza et al (2015).

My research was performed in areas located in different regions of tectonics and geographical boundaries as well as climate and topography/relief: the Khovd fault in the Altai Mountains, the Khövsgöl fault in the Sayan Mountains, and the Möngönmorit fault in the Khentii Mountains, that are hundreds of kilometers apart.

Thus, I am going to describe the kinematics of the faulting in two types of regions. Research works of active faults are also important in answering where compression and extension start

and end. For example, by studying the kinematics of the Khovd fault, it allows to determine the deformation of the Altai Mountains, and the mapping and paleoseismological investigations of the Möngönmorit fault confirmed that the fault is normal that means the Baikal-Khövsgöl extension is taking place there. The study of the focal mechanism solutions for the 2021 Mw 6.7 Khankh earthquake answered the question "What is the current kinematics in the Khövsgöl rift?". In addition, my research gives an input for solving practical problems for seismic hazard such as discovering locations of active faults, determining potential magnitudes of large earthquakes, and estimating recurrence periods of large earthquakes. However, on the other hand, we study the kinematic environments of the regions, the deformation of crust, mountain-building, and geomorphology – surface processes in scientific aspect.

In this study, the following methods for studies of active faults were used. These include fault mapping based on satellite images and field routes, paleoseismological investigation to determine the ages and recurrence period of large earthquakes along the faults, drilling research to identify the deep structure of the fault, radiocarbon dating method to determine the timing of surface-rupturing earthquakes, and petrographic and mineralogical studies of the rocks that were displaced by fault plane.

7.1 The Ar-Khötöl surface rupture (Khovd Fault, Altai Mountains)

The Ar-Khötöl surface rupture is the central part of the main Khovd fault that is the longest strike-slip fault of the 5 major faults in the Altai Mountain Range. In this sense, it can be reckoned that the Ar-Khötöl surface rupture is the most prominent representation of the modern kinematics in the Altai Mountains.

I mapped the Ar-Khötöl surface rupture using satellite data such as Sentinel-2, TanDEM, Google Earth, and Pleiades with the resolutions of 0.5 – 15 m. The rupture itself exhibits a length of 238.5 ± 0.5 km and displays well defined changes in strike, faulting style and complexity generally associated with relay zones that may play a role in the propagation of the rupture (e.g. Harris & Day, 1993; Wesnousky, 2008; Choi et al., 2018). On that basis, we propose a structural segmentation model that separates the fault into 11 segments (S1 to S11) displaying homogeneous characteristics. The central segments S7 and S8 reach lengths of ~ 50 km while the remaining segments reach lengths ranging from 7 km (S5) to 23 km (S3). The northern end of the surface rupture is near the Khongo River, south of Mount Tsambagarav.

Therefore, the Tsambagarav massive could be the most prominent barrier for propagation of the fault. Cunningham (2005) considers that the Tsambagarav is a restraining bend. Although the Ar-Khötöl surface rupture terminates just before the restraining bend, there is an active fault scarp along the west flank of the mountain range which is the part of the Khovd master fault. The southernmost tip of the surface rupture to be fresh tension gashes and mole tracks was checked on the ground at N46°33′1.60″, E92°26′55.60″. From this point, the Ar-Khötöl surface rupture disappears in 2.7 km to the south near Bodonch and Khujirt River Valleys. If the ~3 km long parallel segment where it is located at ~2 km to the east of the main strand is considered to be as the part of the Ar-Khötöl surface rupture, those termination sections represent the typical horse-tale structures of strike-slip faults (Choi et al., 2012).

The Ar-Khötöl surface rupture follows the geological faults or the contact between two different geological formations that are Paleozoic intrusive rocks and Ordovician marine sediments. The rupture is consisted of 3 of determinant linkages and 11 segments based upon the mapping of the rupture traces, the abrupt changes of azimuth and geological maps of the area. Moreover the 3 junction zones are strictly controlled by the structural boundaries in the base geology. The 3 linkages are North Ulaan Bulag, South Ulaan Bulag and Khökh Öndör. The latest fault traces (the Ar-Khötöl surface rupture) along the Khovd fault always follow the western geological faults at the each junctions. Although there are patterns of earthquakes of late Quaternary along the eastern geological faults, the Ar-Khötöl fault doesn't run along it for a long distance. All the three relay zones are concentrated on the junctions with two geological faults which bound both flanks of the mountains.

The southernmost segment that it runs from Khökh Öndör junction to the south occurred on a relative young fault compared to the main middle segments of the fault or eastern fault which is the general Khovd fault. There are virtually no big cumulative displacements in this segment. It shows that the Khovd fault creates a new segment to the south. In other words, the Ar-Khötöl surface rupture did not follow the previously existing Myangan Ugalzat fabric, instead of that, it broke along the new branch in the direction of the Bayan Salaa segment to the south. This findings gives an input for the view of anticlockwise vertical axis rotations in the Altai from the previous researchers (Baljinnyam et al., 1993; Cunningham et al., 1996; Bayasgalan et al., 1999). Consequently, we found that the Ar-Khötöl fault follow the regime either the inherited preexisting structure or the fault steps due to the kinematics.

Previous researchers (Khilko et al., 1985; Baljinnyam et al., 1993) mapped tentatively the Ar-Khötöl surface rupture but not in detail and only document 6-7 offset features. I mapped the Ar-Khötöl surface rupture in detail, and measured about 200 right-lateral displacements based on satellite imageries and field surveys. 105 of these are 1-10 meters of offsets, and this data was used to produce the slip distribution envelope of the Ar-Khötöl surface rupture and derive a segmentation model. According to our research, the average co-seismic offset that was caused by the latest large earthquake along the Ar-Khötöl surface rupture is ~2-3 m, maximum co-seismic offset is 4.8 ± 0.5 m located near the center of the rupture. The remaining 100 values are cumulative displacements ranging from 10 meters to 5 km. Notably there are 3 large valleys with 2-8 km of right-lateral displacements along the Ar-Khötöl fault.

The co-seismic slip curve displays a series of slip envelopes consistent with individual segments and suggests a broader model with only 6 well-defined segments. The Northernmost segment (S1+S2+S3), the Khoid Tsenkher segment (S7), the Goo Mountains segment (S8) and the Southernmost segment (S9+S10+S11) reach lengths ranging from 45 km to 51 km. The Buyant segment (S4) and Ar-Khötöl segment (S5+S6) only reach 20 km and 23 km, respectively. It should be noted that the central segment (Khoid Tsenkher) displays the largest co-seismic slip value (4.8 ± 0.5 m) as well as two well-defined cumulative curves suggesting previous events were recorded at the same segments.

My produced slip distribution and envelope model for the Ar-Khötöl surface rupture is comparable with Willemse's model although the fault types and lengths of comparing two models are totally different. The Ar-Khötöl fault has a length of 238 km whereas the Bishop Tuff exposure is only 650 m. In addition, the Ar-Khötöl is a strike-slip fault and the Bishop Tuff is a normal fault. The marginal segments of the Ar-Khötöl fault are asymmetric and the maximum displacement is towards the center of the fault. Also, the central segments can be relatively symmetrical, and the maximum displacement along the fault is 4.8±0.5 m on the central segment. Considering general scaling relationships established by Wells & Coppersmith (1994) for strike-slip faults (with a = 5.16 ± 0.13 and b = 1.12 ± 0.08), we may derive a moment magnitude of 7.8 ± 0.3.

The paleoseismological study conducted in the Marmot Creek trench identified the large earthquake on the Ar-Khötöl fault as 1280-1640 CE. Considering the ~4 m of horizontal displacement caused by the latest large earthquake on the Ar-Khötöl fault, with a slip rate of ~1 mm/year, the recurrence period of the fault is ~4000 years. In the 20th century, three large

earthquakes of magnitude 8 occurred on the territory of Mongolia. Nevertheless, modern GPS surveys, geological slip-rate research, and paleoseismological investigations suggest that the territory of Mongolia is being deformed at a very low rate. Then, why 3 large earthquakes with magnitude 8 occurred in just 100 years of time span despite the fact that those faults are considered to have the recurrence periods of 3000-5000 years? If we consider all the earthquakes with magnitude 6-8, there are about 20 moderate and large earthquakes in Mongolia including Fu-Yun and Chuya earthquakes that occurred in neighboring countries near the border of Mongolia.

As far as we know, in the last ~300 years, major faults in Altai, Khangai, Gobi-Altai, Sayan Mountains such as Tsetserleg, Bulnai, Fu-Yun, Sayan-Tunka, and Khövsgöl have ruptured.

The large earthquakes that occurred in Mongolia and its neighboring countries within similar time span may have triggered each other. If it is considered to be triggered earthquakes, the large earthquake between 1280-1640 CE that occurred along the Ar-Khötöl fault in the Altai Mountains may be the first. Then, there was the Fu-Yun earthquake in the Altai Mountains in 1931, then the Tsetserleg and Bulnai earthquakes in the Khangai in 1905, and then the Great Bogd earthquake in Gobi-Altai in 1957, and so on.

Furthermore, earthquakes in Mongolia may break in the form of earthquake clustering with a similar recurrence period. The paleoseismological studies also confirm this idea. Rizza et al. (2015) concluded that two earthquakes prior to the 1905 have recurrence intervals of ~2700-4000 years. In addition, Ritz et al (2003) and Kurtz (2017) noted that magnitude 7.6-8 earthquakes are likely to occur along the West Bogd fault and the Valley of Lake fault every 3000-4000 years.

7.2 The Khankh earthquake & Khövsgöl fault (Sayan Range)

The magnitude 6.7 Khankh earthquake of January 12, 2021 was an opportunity to understanding the modern kinematic processes of the Khövsgöl rift. The location, azimuth, dip and depth of this earthquake defined by the moment tensor solutions calculated by the international seismological centers and the analysis of InSAR interferograms and field observations. The projected intersections of the east-dipping nodal planes with the surface for GCMT, JAJ and IPGP focal mechanism solutions correlate relatively well with the mapped strike and location of the old tectonic scarp of the Khövsgöl fault although we have not

discovered any primary co-seismic surface rupture. Apparently, the Khövsgöl fault is a transtentional fault with combined right-lateral strike-slip and normal components.

The InSAR interferogram displays a strong deformation in the area of 20 x 30 km^2 in the Doloon Uul peninsula and the northwestern part of the Doloon Uul. The south and east sides of the Doloon Uul are covered by the deep water of Lake Khövsgöl, thus they cannot be seen in the interferogram.

Since the Mw 6.7 main shock, there have been ~80,000 weak aftershocks recorded by the seismic network, among which ~200 are magnitude 3.5 and above. The epicenters of those earthquakes are located on the Doloon Uul half-island of Lake Khövsgöl, under the water in the south of the Doloon Uul, and in the vicinity of the Mungarag and Khodon Rivers. In other words, the epicenters of those aftershocks coincide with well defined dense fringes and deformations of the InSAR interferogram. The fringes on the interferogram also coincides with the tectonic scarp of the northern segment of the Khövsgöl fault. Continuous preexisting tectonic scarps and right-lateral cumulative displacements are visible around the Khongor Böösh river valley (around 51˚35′05″ N, 100˚09′11″ E) southwest of Emeel Mountain on Landsat 8, Google Earth and Bing Map. As mentioned above, any fresh surface rupture was not discovered along the segment on KOMPSAT imagery acquired after the earthquake and during my winter and summer field expeditions that crossed the Khövsgöl fault on 2-3 localities but the site effects and small cracks due to the moderate earthquake are discovered in the epicenter area.

The moderate earthquake of magnitude 6.7 can produce a surface rupture up to ~25 km long, but the surface rupture is not detected on the ground surface, indicating that on the one hand, the main surface rupture is likely to be under Lake, and on the other hand, the deformation displayed in the InSAR interferogram may have spread over a large area without producing a surface rupture.

7.3 The Ulaanbaatar fault (Central Mongolia)

The Ulaanbaatar fault follows an ancient fault zone and marks the boundary between different geological formations (Takeuchi et al., 2012). Suzuki et al (2021) mapped the Ulaanbaatar fault between southeast of Mount Bogd and northwest of Mount Tolgoit for ~56 km. The section around Bayankhoshuu and Tolgoit Mountains as well as the section to the east and northeast of Mount Bogd, have linear scarps which are clearly visible on the surface. However, because the

urban area of the Ulaanbaatar city has been actively constructed, the fault scarps in the central part of the city are not visible. Thus, they tentatively connected the segments of Mount Bogd and Mount Tolgoit and marked by the dashed lines.

Most of the fault scarps are mapped along the ancient geological boundaries between the different rock formations thus differential erosion rates may have influenced for the exposures of the mapped fault scarps. Based on a cored drill I carried out, the bedrocks of the northern and southern blocks of the fault plane in the Khürel Togoot trench are two different types of rocks with different compositions and origins. Therefore, it is clear that the fault plane is the boundary between two different types of rocks.

In the trench walls, the thick black gouge unit (U210) with the anticlinal folded structure covering decomposed and deformed sandstone-alevrolite unit (U300) is observed to be thrusted over the sedimentary sequences (U190-30) to the southwest. Looking at the thickening of the sedimentary layers in front of the black fault gouge towards Mount Bogd side, the sedimentary layers are likely to be rotated between the two faults (an undetected fault in the trench walls not far away south of the trench).

According to the paleoseismological studies of the Khürel Togoot trench, the last deformation episode along the UB fault may have occurred in Late Pleistocene, between 40,500 and ~15,800 years BP considering all obtained ages (preferably around ~25,000 years BP which is the age of the paleosoil unit (U200) that is below the clayey units U190-U30 stratigraphically.

The other excavations along the Ulaanbaatar fault do not provide evidence of Holocene or Late Pleistocene seismic activity. It seems therefore that the deformations observed within the Khürel Togoot trench may well correspond to features associated to a local gravitational collapse located along the ancient Paleozoic Bogd fault. Therefore, the Ulaanbaatar fault needs to be further investigated.

7.4 The Möngönmorit fault (Khentii Dome)

Our morphotectonic and paleoseismological study along the Möngönmorit fault shows that it corresponds to an active gently (~20°) eastward-dipping normal fault, at least in the sub-surface. Its total length (~160 km) and the length of its different segments (90-30 km) show the possibility of surface-rupturing events reaching easily Mw7 after Wells and Coppersmith's (1994) scaling laws.

From a kinematical point of view, this result confirms that the southern Khentii region is undergoing active extension, which is consistent with the E-W transtensional regime observed in the Ulaanbaatar region immediately to the South-West. This transtensional/extensional regime seems to be correlated to the strain regime of the Baikal rift, and would be controlled by the uplift of the asthenosphere in the area.

From the point of view of paleoseismology, our investigations allow characterizing the occurrence of two surface-rupturing events since 8.4 ka. If we extend the time window of our observations, it seems that at least one more strong event occurred not long after 18 ka. The paleoseismological data concerning the two last events suggest a mean recurrence period of surface rupturing events comprised between 3000 and 5000 years. The latest earthquake along the fault having occurred 5 ka ago, yields an elapsed time equal to the maximum bound of the recurrence interval. Although this statement is based only on the 2 past events, and despite the fact that a possible earlier event at ~18 ka increases the recurrence time (~10 ka), the question of the seismic hazard associated to the Möngönmorit fault is clearly posed.

7.5 Conclusions

Mongolia is a high active seismic zone from the research conducted in 3 different geographical locations. While a ~240 km-long surface rupture is documented in the Altai Mountains, recently in 2021, a moderate earthquake with a magnitude of 6.7 occurred in the Khövsgöl basin. To the east, there is a more than 100 km-long active fault in the Khentii Mountains.

The effects of deformations are expressed by right-lateral strike-slip faults in the Altai Mountains of Western Mongolia, transtensional faults in the Khövsgöl Mountains, and normal faults in the Khentii Mountains. This indicates that the region is in two different tectonic regimes.

The Ar-Khötöl fault in the Altai and the Möngönmorit fault in the Khentii are located along ancient geological faults between two different geological formations. This means that the deformation under the influence of neotectonic forces is taking place in a way of re-activating the paleo-faults.

In terms of orography and relief, the faults that were activated in the late Cenozoic give a certain influence on the current appearance of the Altai, Sayan, and Khentii Mountains. For example, the accumulated horizontal displacements along the Ar-Khötöl fault are 2-8 km in the large

river valleys, which are considerable effects on the changes of the landscape. The cumulative horizontal displacement along the Khövsgöl fault is ~0.5 km and the fault has a dominant influence on expansion of the basin. The Khövsgöl basin is a half-graben structure controlled by the Khövsgöl fault on the right. The Möngönmorit fault has a main influence on the current landform of the Kherlen river valley because the river valley is controlled only by the Möngönmorit fault on the west, and there is no mapped active fault on the east.

In terms of fault lengths, whereas the longest rupture of ~240 km is mapped in the Altai Mountains, ~60 km fault is mapped in the Khövsgöl and ~90 km fault in the Khentii Mountains. Even in terms of the magnitudes of the earthquakes, magnitude ~8 earthquakes are likely to occur in the Altai, whereas moderate earthquake with magnitude 6.7 took place in the Khövsgöl. It is estimated that a strong earthquake of magnitude ~7 may occur on the Möngönmorit fault.

As for the recurrence period of the faults, it is 3000-4000 years in the Altai Mountains and 3000-5000 years in the Khentii Mountains.

In terms of seismic hazard assessment, almost half of the Mongolian total population of ~3.5 million live in the capital city of Ulaanbaatar. Therefore, Central Mongolia is the most densely populated, along with it, there are many buildings and strategic objects. The Möngönmorit fault is located 100 km east of Ulaanbaatar city, and the latest earthquake occurred on the fault between 4893 and 6609 calibrated BP, the recurrence period of the fault is 3000-5000 years, thus it may be a danger for the capital city and its satellite districts. The Mw 6.7 earthquake in the Khövsgöl region caused relatively little damage. This earthquake may have had a passable influence because it was a sparsely populated and rural area. Nevertheless, it cannot be ruled out that earthquakes similar to the earthquake on the Khövsgöl fault may occur on the other faults in the Khövsgöl region. The Ar-Khötöl section of the Khovd fault in the Altai Mountains released its some stress few centuries ago between 13-17th centuries. If the recurrence period of the fault is 3000-4000 years, it can be considered that there is less danger for a large earthquake from the Ar-Khötöl section in the towns in the Altai. On the contrary, it cannot be ruled out that a large earthquake with a magnitude of ~8 may be caused by the other major strike-slip faults in the Altai Mountains. Therefore, the towns in the Altai Mountains should improve the qualities of their buildings and construct buildings in accordance with the codes of constructions located in seismic active areas.

In Mongolia, where infrastructures, industries, and buildings are being built in large numbers, urban settlements are expanding, and people from scattered nomadic lives are moving to a more densely settled lifestyles in the towns. At the same time, many active faults have been discovered and mapped in the regions. It conveys us to be prepared for the potential seismic hazard.

7.6 References

Baljinnyam, I., Bayasgalan, A., Borisov, B. A., Cisternas, A., Dem'yanovich, M. G., Ganbaatar, L., … Vashchilov, Yu. Ya. (1993). Ruptures of major earthquakes and active deformation in Mongolia and its surroundings. *Geological Society of America*.

Bayasgalan, A., Jackson, J., Ritz, J. F., & Carretier, S. (1999). Field examples of strike-slip fault terminations in Mongolia and their tectonic significance. *Tectonics, 18*, 394-411.

Cunningham, W. D. (2005). Active intracontinental transpressional mountain building in the Mongolian Altai: Defining a new class of orogen. *Earth and Planetary Science Letters*, 436-444.

Choi, J. H., Jin, K., Enkhbayar, D., Davaasambuu, B., Bayasgalan, A., & Kim, Y. S. (2012). Ruptures propagation inferred from damage patterns, slip distribution, and segmentation of the 1957 M_w8.1 Gobi-Altay earthquake rupture along the Bogd fault, Mongolia. *Journal of Geophysical Research, 117*, B12401. https://doi:10.1029/2011JB008676

Choi, J. H., Klinger, Y., Ferry, M., Ritz, J. F., Kurtz, R., Rizza, M., & Demberel, S. (2018). Geologic inheritance and earthquake rupture processes: The 1905 M≥8 Tsetserleg-Bulnay strike-slip earthquake sequence, Mongolia. *Journal of Geophysical Research: Solid Earth, 123*. https://doi.org/10.1002/2017JB013962

Cunningham, W. D., Windley, B. F., Dorjnamjaa, D., Badamgarav, G., & Saandar, M. (1996). A structural transect across the Mongolian Western Altai: Active transpressional mountain building in central Asia. *Tectonics, 15*, 142-156.

Harris, R. A., & Day, S. M. (1993). Dynamics of Fault Interaction: Parallel Strike-Slip Faults. *Journal of Geophysical Research, 98*(B3), 4461-4472.

Khil'ko, S. D., Kurushin, R. A., Kochetkov, V. M., Baljinnyam, I., & Munkhuu, D. (1985). Strong earthquakes, paleoseismogeological and macroseismic data, in earthquakes and the bases for seismic zoning of Mongolia. The joint Soviet-Mongolian scientific geological research expedition. *Nauka*, Moscow.

Kurtz, R. (2017). Late-Pleistocene to Holocene spatio-temporal evolution of the seismic deformations in the Gobi-Altay mountain range, Mongolia: morphotectonical and paleoseismological approaches. PhD Thesis. The Geosciences Montpellier of the University of Montpellier.

Ritz, J.-F., Bourles, D., Brown, E. T., Carretier, S., Chery, J., Enhtuvshin, B., … Yiou, F. (2003). Late Pleistocene to Holocene slip rates for the Gurvan Bulag thrust fault (Gobi-Altay, Mongolia) estimated with ^{10}Be dates. Journal of Geophysical Research, 108(B3), 2162. http://doi:10.1029/2001JB000553

Suzuki, Y., Nakata, T., Watanabe, M., Battulga, S., Enkhtaivan, D., Demberel, S., … Badral, T. (2021). Discovery of Ulaanbaatar Fault: A New Earthquake Threat to the Capital of Mongolia. Seismological Research Letters, 92, 437-447. http://doi:10.1785/0220200109

Takeuchi, M., Tsukada, K., Suzuki, T., Nakane, Y., Gonchigdorj, S., Nuramkhaan, M., … Munkhjargal, M. (2012). Stratigraphy and geological structure of the Paleozoic system around Ulaanbaatar, Mongolia. *Bulletin of the Nagoya University Museum, 28*, 1-18.

Wells, D. L., & Coppersmith, K. J. (1994). New empirical relationships among magnitude, rupture length, rupture width, rupture area, and surface displacement. *Bulletin of the Seismological Society of America, 84*(4), 974-1002.

Wesnousky, S. G. (2008). Displacement and Geometrical Characteristics of Earthquake Surface Ruptures: Issues and Implications for Seismic-Hazard Analysis and the Process of Earthquake Rupture. *Bulletin of the Seismological Society of America, 98*(4), 1609-1632. http://doi:10.1785/0120070111

Willemse, J. M. (1997). Segmented normal faults: Correspondence between three-dimensional mechanical models and field data. Journal of Gephysical Research. https://doi.org/10.1029/96jB01651